

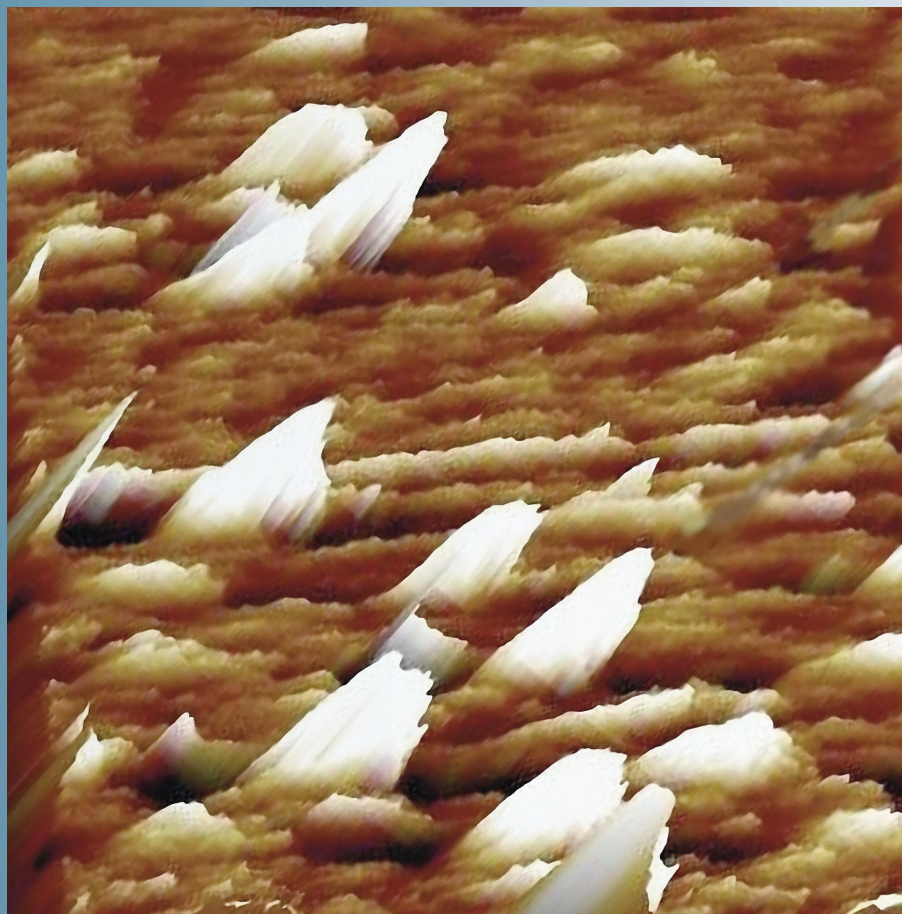


ISSN 1028-8546

Volume XVII, Number 2  
Section: En  
March, 2011

# Azerbaijan Journal of Physics

# Fizika



[www.physics.gov.az](http://www.physics.gov.az)

G.M. Abdullayev Institute of Physics  
Azerbaijan National Academy of Sciences  
Department of Physical, Mathematical and Technical Sciences

# *Azerbaijan Journal of Physics*

# *Fizika*

*G.M.Abdullayev Institute of Physics*  
*Azerbaijan National Academy of Sciences*  
*Department of Physical, Mathematical and Technical Sciences*

## HONORARY EDITORS

**Arif PASHAYEV**

**Mahmud KERIMOV**

## EDITORS-IN-CHIEF

Arif HASHIMOV  
Chingiz QAJAR

## SENIOR EDITOR

Talat MEHDIYEV

## INTERNATIONAL REVIEW BOARD

Ivan Scherbakov, Russia  
Kerim Allahverdiyev, Turkey  
Mehmet Öndr Yetiş, Turkey  
Gennadii Jablonskii, Buelorussia  
Rafael Imamov, Russia  
Vladimir Man'ko, Russia  
Eldar Salayev, Azerbaijan  
Dieter Hochheimer, USA  
Victor L'vov, Israel  
Vyacheslav Tuzlukov, South Korea  
Majid Ebrahim-Zadeh, Spain

Firudin Hashimzadeh, Azerbaijan  
Anatoly Boreysho, Russia  
Mikhail Khalin, Russia  
Hasan Bidadi, Tebriz, East Azerbaijan, Iran  
Mamed Emin Shahtakhtinskii, Azerbaijan  
Maksud Aliyev, Azerbaijan  
Bahram Askerov, Azerbaijan  
Vali Huseynov, Azerbaijan  
Javad Abdinov, Azerbaijan  
Bagadur Tagiyev, Azerbaijan  
Tayar Djafarov, Azerbaijan

Natiq Atakishiyev, Mexico  
Talat Mehdiyev, Azerbaijan  
Nazim Mamedov, Azerbaijan  
Emil Guseynov, Azerbaijan  
Ayaz Bayramov, Azerbaijan  
Tofiq Mammadov, Azerbaijan  
Salima Mehdiyeva, Azerbaijan  
Shakir Naqiyyev, Azerbaijan  
Rauf Guseynov, Azerbaijan  
Almuk Abbasov, Azerbaijan  
Yusif Asadov, Azerbaijan

## TECHNICAL EDITORIAL BOARD

senior secretary

Elmira Akhundova, Narmin Babayeva, Nazli Guseynova,  
Sakina Aliyeva, Nigar Akhundova, Elshana Tarlanova

## PUBLISHING OFFICE

33 H.Javid ave, AZ-1143, Baku  
ANAS, G.M.Abdullayev Institute of Physics

Tel.: (99412) 439-51-63, 439-32-23  
Fax: (99412) 447-04-56  
E-mail: [joph@physics.ab.az](mailto:joph@physics.ab.az); [jophphysics@gmail.com](mailto:jophphysics@gmail.com)  
Internet: [www.physics.gov.az/journals](http://www.physics.gov.az/journals)

It is authorized for printing: 06.30.2011

Published at: "ŞƏRQ-QƏRB"  
17 Ashug Alesger str., Baku  
Typographer :Aziz Gulaliyev

Sent for printing on: \_\_\_ 07.2011  
Printing approved on: \_\_\_ 07.2011  
Physical binding: \_\_\_\_\_  
Number of copies: \_\_\_ 200  
Order: \_\_\_\_\_

## CURRENT-VOLTAGE (I-V) AND CAPACITANCE-VOLTAGE (C-V) CHARACTERISTICS OF $\text{Bi}_4\text{Ti}_3\text{O}_{12}$ AMORPHOUS FILMS

**Şemşettin ALTINDAL, Adem TATAROĞLU**

*Physics Department, Faculty of Arts and Sciences, Gazi University, 06500, Teknikokullar,  
Ankara, Turkey*

**A.A. AGASIYEV, M.Z. MAMEDOV, E.M. MAGERRAMOV,  
J.G. JABBAROV, Kh.O. QAFAROVA**

*Institute for Physical Problems, Baku State University, Baku, 370145, Azerbaijan*

The current-voltage ( $I$ - $V$ ), capacitance-voltage ( $C$ - $V$ ) and conductance-voltage ( $G$ - $V$ ) characteristics were measured at room temperature and obtained experimental results are comparable in detail to the others measured value for  $\text{Bi}_4\text{Ti}_3\text{O}_{12}$  films in the literature. Inspite of the apparently symmetric capacitor structure but current-voltage ( $I$ - $V$ ) measurements showed rectifying behaviors. These results indicate structural disordering and the interface states in the BTO capacitors and existence polarization. The characteristics parameters of the interface states are derived from the  $I$ - $V$  measuremets as a function of  $E_c$ - $E_{ss}$  at room temperature. The density of states distribution profiles of the sample obtained from the  $I$ - $V$  measurements and the mean of interface state  $N_{ss}$  estimated about  $2 \times 10^{11} \text{ eV}^{-1}\text{cm}^{-2}$ . The ideality factor  $n$  was found 1.5 at forward bias from  $I$ - $V$  measurements. In addition to series resistance  $R_s$  was found at room temperature  $350 \Omega$  from the measured conductance in the strong accumulation region.

### 1. INTRODUCTION

When a metal is brought into intimate contact with a semiconductor, a barrier is formed at the metal-semiconductor (MS) interface [1]. In 1938 Schottky suggested that the rectifying behaviors could arise from a potential barrier as a result of the stable space charges in the semiconductor. This model is known as the Schottky Barrier (SB). Metal-semiconductor device can also be no rectifying: that is, the contact has a negligible resistance regardless of the polarity of the applied voltage. Such a contact is called an ohmic contact. The height of potential barrier can be determined by the difference in the work function of the metal ( $\phi_m$ ) and electron affinity ( $\chi_s$ ) or work function of semiconductor ( $\phi_s$ ). The work function is the energy difference between the vacuum level and Fermi level ( $E_f$ ).  $q\chi_s$  is the electron affinity measured from the bottom of the conduction band  $E_c$  to the vacuum level. When a forward bias voltage  $V_a$  is applied to the junction the effective barrier height in the semiconductor becomes  $q(V_D - V_a)$  and the electron flow from the semiconductor into the metal is enhanced by a factor  $\exp(qV_a/kT)$ . Experimentally obtained barrier height deviate from this rule and the basic mechanism of the Schottky Barrier formation are still a field of intensive research. Bismuth titanite ( $\text{Bi}_4\text{Ti}_3\text{O}_{12}$ ) amorphous films, the simplest an well known compound among the bismuth layer-stuctured ferroelectrics is particularly interesting because of its pepeculiar switching behavior resulting from a small  $c$ -axis component of the spontaneous polarization and a small coercive force [2,3].  $\text{Bi}_4\text{Ti}_3\text{O}_{12}$  is a typical ferroelectrics material with useful properties optical memory, piezoelectric, and electro-optic devices [4].  $\text{Bi}_4\text{Ti}_3\text{O}_{12}$  amorphous films have been extensively studied during the last few decades [5-9].

In this study, we were aimed particularly at investigating the role of interface states and series resistance on the current-voltage ( $I$ - $V$ ), capacitance-voltage ( $C$ - $V$ ) and conductance-voltage ( $G$ - $V$ ) characteristics. Because the interface states cannot follow the a.c. signal in the high frequency, the situation may be different at low and intermediate frequencies. It is

therefore important to include the effect of the frequency and series resistance and investigate in detail the frequency dispersion of capacitance in the forward  $C$ - $V$  and  $G$ - $V$  characteristics.

### 2. EXPERIMENTAL

The  $\text{Bi}_4\text{Ti}_3\text{O}_{12}$  (BTO) thin films obtained by a hot compacting of  $\text{Bi}_4\text{Ti}_3\text{O}_{12}$  powder of a stoichiometric composition was used a target. The mixture of Ar and O<sub>2</sub> was used a working medium. The structure of the obtained BTO thin films obtained by dc magnetron sputtering was used investigation. The chemical composition of films was determined by local X-ray spectral method on scanning electron microscope REM-101M by comparison of spectral line intensity relations for films and standard sample. The gold top electrodes, with the thickness of about 2000Å and diameter of 2,5 mm were deposited using a shadow-mask at room temperature by rf. sputtering. The electron diffraction pattern of  $\text{Bi}_4\text{Ti}_3\text{O}_{12}$  films with thickness of  $\sim 2\mu\text{m}$  obtained by magnetron sputtering on crystal substrate at temperatures of  $\sim 700^\circ\text{C}$ . The measurements of capacitance vs. voltage ( $C$ - $V$ ) and conductance vs. voltage ( $G$ - $V$ ) characteristics the BTO capacitors were performed by using a Hewlett-Packard HP 4192 A LF impedance analyzer (5 Hz-13 MHz) at various frequencies (1 kHz-5 MHz). The current voltage ( $I$ - $V$ ) characteristics of the BTO capacitors were measured using a Keithley model 614 electrometer and 220 programmable constant current sources at room temperature. The samples (BTO) was mounted on a cooper holder in a box and the electrical constant were made to the upper gold electrodes by the use of tiny silver coated wires with silver paste.

### 3. RESULTS AND DISCUSSIONS

#### 3.1. Current-Voltage Characteristics

The most common theory of Schottky barrier diode is based on the thermionic emission (TE) and according to this model the current-voltage ( $I$ - $V$ ) relationship is given by,

$$I = I_S \left[ \exp\left(\frac{qV_B}{kT}\right) - 1 \right] \quad (1)$$

Where  $q$  is the electronic charge,  $k$  is the Boltzman constant,  $T$  is the absolute temperature,  $V_B$  is the voltage across the junction and  $I_S$  is the reserve saturation current and described by (1),

$$I_S = AA^* T^2 \exp(-q\phi_B/kT) \quad (2)$$

Where  $A$  is area of diode,  $A^*$  is modified Richardson constant and  $\phi_B$  is the effective metal to semiconductor barrier height. The  $I_S$  was found 6,13,10-15A by extrapolating the linear mid bias region of the curve to zero applied voltage axis and the ideality factor  $n$  was found 1,5 from the slope this linear region.

For a real Schottky diode having interface states  $N_{ss}$  in equilibrium with the semiconductor, the ideality factor  $n$  becomes greater than unity as proposed by Card and Rhoderick [10] and is given by

$$n = 1 + \frac{\delta}{\varepsilon_i} \left( \frac{\varepsilon_s}{W_D} + qN_{ss} \right) \quad (3)$$

Where  $\varepsilon_s$  and  $\varepsilon_i$  are the permittivity of semiconductor and interfacial layer, respectively,  $W_D$  is the space charge

width and  $N_{ss}$  is the density of interface states. The substituting in Eq. (3) the values of ideality factor  $n$  related to forward bias  $V$  obtained from experimental data of  $I$ - $V$  in Fig. 1 and space charge width  $W_D$  calculated from  $C$ - $V$  vs.  $V$  characteristics (Fig. 5) and taking  $\varepsilon_s$  (BTO)=118 $\varepsilon_0$ ,  $\varepsilon_i$  (SnO<sub>2</sub>)=7 $\varepsilon_0$  and  $\varepsilon_0=8,85 \times 10^{-14}$  F/cm, the values of  $N_{ss}$  as a function of  $V$  were obtained and are given in table 1.

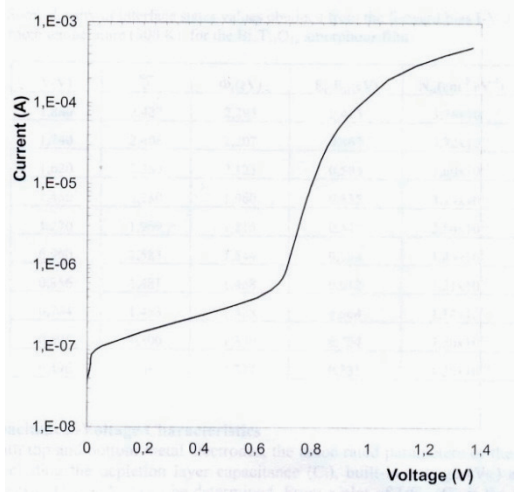


Fig. 1. Forward bias Current-Voltage ( $I$ - $V$ ) characteristics at room temperatur (300K) for the  $\text{Bi}_4\text{Ti}_3\text{O}_{12}$  amorphous film.

Some density of interface states values obtained from the forward bias  $I$ - $V$  data at room temperature (300K) for the  $\text{Bi}_4\text{Ti}_3\text{O}_{12}$  amorphous film.

| $V(V)$ | $n$   | $\Phi_e(eV)$ | $E_c-E_{ss}(eV)$ | $N_{ss}(cm^{-2}, eV^{-1})$ |
|--------|-------|--------------|------------------|----------------------------|
| 1,880  | 2,427 | 2,295        | 0,415            | $3,78 \times 10^{11}$      |
| 1,740  | 2,408 | 2,207        | 0,467            | $3,72 \times 10^{11}$      |
| 1,620  | 2,359 | 2,123        | 0,503            | $3,60 \times 10^{11}$      |
| 1,450  | 2,180 | 1,960        | 0,535            | $3,14 \times 10^{11}$      |
| 1,270  | 1,969 | 1,815        | 0,545            | $2,54 \times 10^{11}$      |
| 0,960  | 1,583 | 1,544        | 0,584            | $1,49 \times 10^{11}$      |
| 0,856  | 1,481 | 1,468        | 0,612            | $1,21 \times 10^{11}$      |
| 0,764  | 1,453 | 1,428        | 0,664            | $1,14 \times 10^{11}$      |
| 0,606  | 1,300 | 1,330        | 0,724            | $7,20 \times 10^{10}$      |
| 0,496  | 1,082 | 1,227        | 0,731            | $1,25 \times 10^{10}$      |

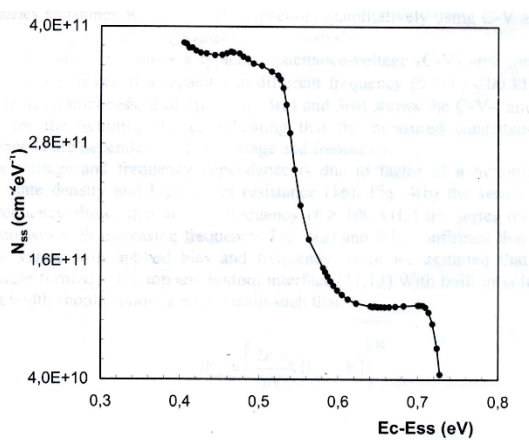


Fig. 2. Density of interface states  $N_{ss}$  as a function of  $E_c - E_{ss}$  deduced from the I-V data at 300K for the  $\text{Bi}_4\text{Ti}_3\text{O}_{12}$  amorphous film.

In a  $n$ -type semiconductor Schottky diode, the energy of interface states,  $E_{ss}$  with respect to the bottom of the semiconductor is given by [1, 11, 12].

$$E_c - E_{ss} = q(\phi_e - V) \quad (4)$$

where

$$\phi_e = \phi_B + \left[ 1 - \frac{1}{n} \right] (V - IR_s) \quad (5)$$

Eq. (3)-(5), along with the forward bias  $I$ - $V$  characteristics can be used for the determination of interface states density as a function interface states energy  $E_{ss}$  with respect to the bottom of the conduction band. Fig. 2 show the resulting dependence of  $N_{ss}$  as a function of  $E_{ss}$  using Eq. (3) and (4) at room temperature

(300K). As can be seen Fig. 2 and Table 1, the value of interface states  $N_{ss}$  are adequately high and increases towards the conductance band.

### 3.2. Capacitance-Voltage Characteristics

With top and bottom metal electrodes, the assoc rated parameters of the Schottky diode, including the depletion layer capacitance ( $C_i$ ), built-in voltage ( $V_{bi}$ ) and space charge density ( $N_D$  or  $N_A$ ) can be determined. From a plot of  $I/C_m$  ( $C_m$  is the measured capacitance) versus  $d_m$  ( $d_m$  is measured thickness), at various bias voltage. In this section we will show efforts to determine the build in voltage  $V_{bi}$ , space charge density  $N_D$  and series resistance  $R_s$  of the BTO capacitors quantitatively using  $C-V$  and  $G/\omega -V$  measurements and a detailed equivalent circuit analysis.

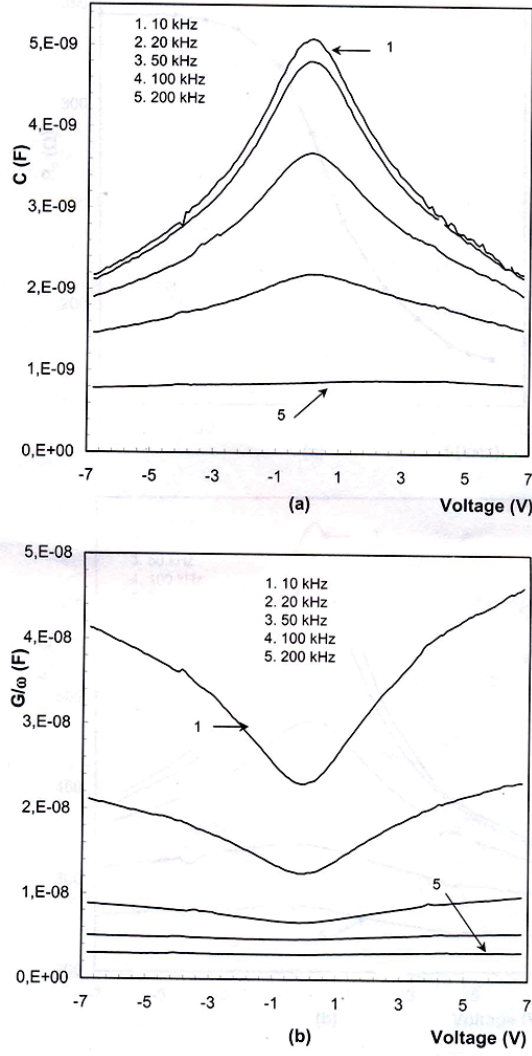


Fig. 3. Measured capacitance ( $C$ ) and conductance ( $G/\omega$ ) vs. gate bias at room temperatur (300K) for the  $\text{Bi}_4\text{Ti}_3\text{O}_{12}$  amorphous film at five different frequencies.

Fig. 3 (a) and fig. 3 (b) shows a typical capacitance-voltage ( $C-V$ ) and conductance-voltage ( $G/\omega -V$ ) curves of a capacitor at different frequence (5 kHz - 200 kHz) whose BTO layer has a thickness,  $d$  of  $2\mu\text{m}$ . Fig 3(a) and 3(b) shows the  $C-V-f$  and  $G/\omega -f$  response for the Schottky diode, indicating that the measured capacitance

$C$  and conductance  $G$  are dependent on bias voltage and frequency.

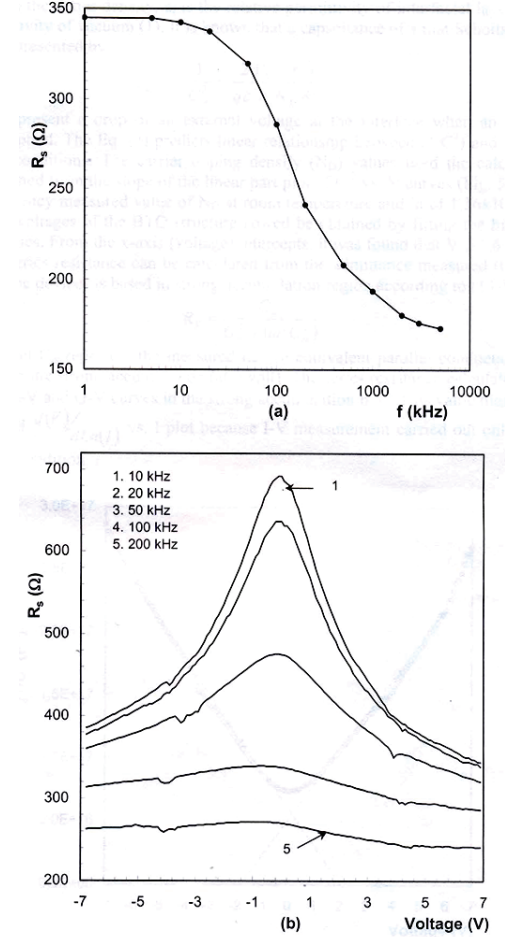


Fig. 4. Frequency and voltage dependence of series resistance ( $R_s$ ), respectively, at 300K for the  $\text{Bi}_4\text{Ti}_3\text{O}_{12}$  amorphous film.

The voltage and frequency dependence is due to factor of a Schottky barrier, interface state density and high series resistance [16]. Fig. 4(b) the series resistance versus frequency shows that at high frequency ( $f \geq 100$  kHz) the series resistance of diode decreases with increasing frequency. Fig. 4(a) and 4(b) confirmed that the series resistance varies with applied bias and frequency. Here we assumed that Schottky barriers were formed at the top and bottom interface [11, 13]. With build in voltage  $V_{bi}$ , a depletion width should follow a relationship such that

$$W_D = \left[ \frac{2\epsilon_i\epsilon_0}{qN_D}(V_{bi} - V) \right]^{1/2} \quad (6)$$

Where  $N_D$  is the donor density,  $\epsilon_i$  is the relative permittivity of interfaciallayer and  $\epsilon_0$  is the permittivity of vacuum (1). It is known that a capacitance of a that Schottky diode (1) can be represented by

$$\frac{1}{C_m^2} = \frac{2(V_{bi} - V_i)}{q\epsilon_s\epsilon_0 N_D A^2} \quad (7)$$

Where  $V_i$  represent a drop of an external voltage at the interface when an external voltage is applied. The eq. (7) predicts linear relationship between  $(1/C^2)$  and  $V$  under

strong bias conditions. The carrier doping density ( $N_D$ ) values used the calculations were determined from the slope of the linear part plot of  $C^2$  vs.  $V$  curves (Fig. 5).

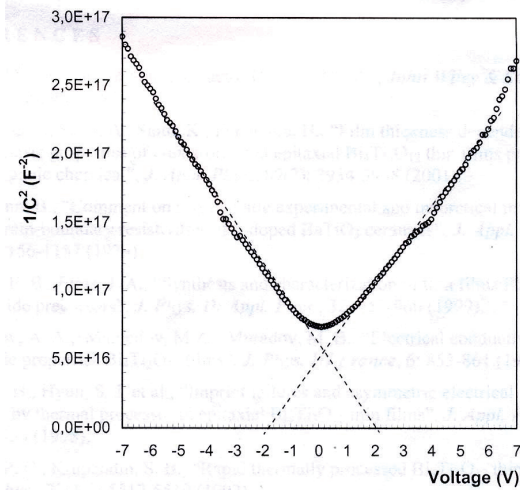


Fig. 5. Plot of  $1/C^2$  vs. at 300K for the  $\text{Bi}_4\text{Ti}_3\text{O}_{12}$  amorphous film at frequency of 50 kHz.

In the 50 kHz frequency measured value of  $N_D$  at room temperature and in of  $1.36 \times 10^{15} \text{ cm}^{-3}$ .

The built in voltages of the BTO structure could be obtained by fitting the high field with linear lines. From the x-axis (voltage) intercepts, it was found that  $V_b=1.6$  Volt. In addition to series resistance can be calculated from the admittance measured ( $C-V$  and  $G-V$ ) when the device is based in strong accumulation region according to [14-17].

$$R_s = \frac{G_m}{G_m^2 + (\omega^2 C_m^2)} \quad (8)$$

Where  $G_m$  and  $C_m$  represent the measured device equivalent parallel conductance and capacitance in the strong accumulation (at 6 volt). The series resistance

calculated  $\sim 350\Omega$  from the  $C-V$  and  $G-V$  curves in the strong accumulation bias. This value higher than from obtained  $\frac{d(V)}{d\ln(I)}$  vs.  $I$  plot because  $I-V$  measurement carried out only under forward bias condition.

### 3. CONCLUSION

A small signal of 40 mV amplitude and 50 kHz frequency was applied bias across the sample while bias was swept from -7V to +7V. There was a decrease in the capacitance at strong bias and this reduction in the capacitance may be attributed to increased conductivity at strong dc bias. The ideality factor  $n$  was found 1.5 at forward bias from  $I-V$  measurements. In addition to series resistance  $R_s$  was at room temperature  $350\Omega$  from the measured conductance in the strong accumulation region. The higher value the ideality factor  $n$  may be attributed to a structural disordering of the film also point to thickness of the film layer and surface charge density.  $C-V-f$  and  $G/\omega-V-f$  measurements confirmed that the measured capacitance  $C$  and conductance  $G$  strongly depend on applied bias voltage and frequency. This dependence is due to the presence of Schottky barrier, doping concentration ( $N_A$  or  $N_D$ ), density of interface states ( $D_{it}$ ) and series resistance ( $R_s$ ). Because the interface states cannot follow the a.c. signal in the efficient high frequency ( $f \geq 500$  kHz), the situation may be different at low and intermediate frequencies. The density of states distribution profiles of the sample obtained from the  $I-V$  measurements and obtained these results indicates the reliability of the others measured value for  $\text{Bi}_4\text{Ti}_3\text{O}_{12}$  films in the literature [18-20]. It is therefore important to include the effect of the frequency and series resistance and investigate in detail the frequency dispersion of capacitance in the forward  $C-V$  and  $G-V$  characteristics.

**Acknowledgments:** This work was supported by the Gazi University Scientific Research Project (BAB), FEF.05/2002-46 and Turkish of Prime Ministry State Planning Organization Project Number 2001K20590.

- 
- [1] S.M. Sze. "Physics of Semiconductor Devices 2nd ed.", John Wiley and Sons, New York, 362-390 (1981).
  - [2] T. Watanabe, A. Saiki, K. Saito, H. Funakubo. J. Appl. Phys., 2001, 89(7), 3934-3938.
  - [3] B. Hoffmann. J. Appl. Phys., 1979, 50(2), 1156-1157.
  - [4] E.B. Araujo, J.A. Eiras. J. Phys. D: Appl. Phys., 32, 1999, 957-960.
  - [5] A.A. Agashev, M.Z. Mamedov, M.B. Muradov. J. Phys. III France, 6: 1996, 853-861.
  - [6] B.H. Park, S.J. Hyun et al. J. Appl. Phys., 84(8), 1998, 4428-4435.
  - [7] P.C. Joshua, S.B. Krupandin. J. Appl. Phys., 72(11), 1992, 5517-5519.
  - [8] L. Pintilie, I. Pintilie et.al. Appl. Phys. A, 69, 1999, 105-109.
  - [9] L. Fu, K. Liu, et.al. Appl. Phys. Lett., 72(14), 1998, 1784-1786.
  - [10] H.C. Card, E.H. Rhoderick. J. Phys. D., 4, 1971, 1589-1601.
  - [11] P. Cova, A. Singh. Solid –State Electronics. 33(1), 1990, 11-19.
  - [12] A. Singh. Solid –State Electronics. 28(3), 1985, 223-232.
  - [13] A.G. Milnes and D.L. Feucht. "Heterojunctions and Metal-Semiconductor Junctions", Academic Press, New York, 1972, 362-390.
  - [14] A. Tataroğlu, Ş. Altindal, S. Karadeniz, N. Tuğluoğlu. Microelectronic Journal, 34(11), 2003, 1043-1049.
  - [15] Ş. Altindal, S. Karadeniz, N. Tuğluoğlu, A. Tataroğlu. Solid –State Electronics. 47, 2003, 1847-1854.
  - [16] S. Özdemir, Ş. Altindal. Doğa-Tr. J. Of physics, 17, 1993, 838-846.
  - [17] E.H. Nicollian and J.R. Brews. "MOS Physics and Technology", John Wiley and Sons, New York, 1982, 40-175.
  - [18] J. Yu, H. Wang et.al. Solid –State Electronics. 45, 2001, 411-415.
  - [19] S.K. Kim, M. Miyayama, H. Yanagida. Materials Research Bulletin. 31(1), 1996, 121-131.
  - [20] T. Kolodiaznyi, A. Petric, G.P. Johari. J. Appl. Phys., 89(7), 2001, 3939-3946.

Received: 14.04.10

## PICOSECOND DISTRIBUTED FEEDBACK DYE LASER EXCITED WITH DIODE-PUMPED SOLID-STATE MICRO LASER

T.Sh. EFENDIEV<sup>1</sup>, V.M. KATARKEVICH<sup>1</sup>,

<sup>1</sup>*B.I.Stepanov Institute of Physics, National Academy of Sciences of Belarus  
68 Nezavisimosti Ave., 220072, Minsk, Belarus*

Ch.O. QAJAR<sup>2</sup>, R.A. KARAMALIYEV<sup>2,3</sup>

<sup>2</sup>*G.H. Abdullayev Institute of Physics, Azerbaijan NAS, Az-1143, H. Javid av., 33, Baku,  
3<sup>3</sup>Baku, AZ-1148, Baku State University, Z. Khalilov str., 23*

The realization of a compact and highly stable tunable picosecond laser system based on a distributed feedback (DFB) dye laser and subnanosecond ( $\tau_{0.5} \approx 0.5$  ns) diode-pumped solid-state (DPSS) Nd-LSB micro laser ( $\lambda = 531$  nm) as the pump source is reported. It is shown, that using an ethanol solution of Rhodamine 6G ( $C = 2 \times 10^{-4}$  M) as an active medium (length of the excited zone  $L_{DFB} \sim 12$  mm), a DFB laser, pumped as high as 2.25 times above the threshold by a micro laser, provides generation of single ( $\tau_{0.5} \sim 55$  ps;  $P \sim 2.4$  kW) transform-limited ( $\Delta\nu_{0.5} \cdot \tau_{0.5} \sim 0.4$ ) picosecond pulses tunable in the spectral range of 543 – 604 nm. At energy stability of pump pulses of ~0.4% (RMS) energy stability of the emitted by a DFB dye laser single picosecond pulses was not worse than ~1%.

**Keywords:** distributed-feedback (DFB) dye laser, picosecond pulse, diode-pumped solid-state (DPSS) micro laser, Rhodamine 6G, energy stability.

**PACS:** 42.55.Mv; 42.55.-f; 42.60.By

### 1. INTRODUCTION

The search and development of the compact and cost-effective tunable laser sources, suitable for a wide range of scientific and practical applications, is a very important and urgent problem of the modern laser physics and engineering. One of the possible ways to solve this problem is the use of distributed-feedback (DFB) dye lasers in conjunction with diode-pumped solid-state (DPSS) microchip (or micro) lasers as the pump sources.

At present, much progress toward investigation and development of DFB dye lasers has been achieved. A variety of optical schemes of such lasers have been realized and their advantages, such as a small spectral linewidth, a wide tuning range, a high efficiency and the possibility of picosecond and femtosecond pulse generation under both picosecond and nanosecond excitation, have been demonstrated [1-19]. It should be noted that the indicated lasers are also simple-design, adaptable to the streamlined production, and convenient in service. Thanks to its simplicity and rather high output characteristics, DFB dye lasers realized seem to be very promising ones for application in spectroscopy, medicine, biology and ecology [20-24]. Expanding the possibilities of using DFB dye laser in these areas is related to the issue of improving the stability of parameters of generated radiation. A considerable progress in the manufacturing of the DPSS micro lasers with their remarkable performance characteristics opens cardinally new possibilities for the construction of efficient tunable dye laser devices.

In this work a simple and efficient tunable laser system based on DFB dye laser and sub-nanosecond DPSS micro laser as a pump source is reported.

### 2. EXPERIMENTAL SETUP

For the excitation of a DFB dye laser we made use of a DPSS Nd-LSB micro laser “STA-01SH” commercially available from the “Standa Ltd.”

(Lithuania) [25]. Such a laser provides 2-nd harmonics generation ( $\lambda = 531$  nm) with a pulse width of  $\tau_{0.5} \sim 0.5$  ns, a pulse energy of ~50  $\mu\text{J}$ , the energy stability of ~0.4 % (RMS), beam quality  $M^2 \leq 1.2$  and a pulse repetition rate up to 1 kHz. The measurements were performed using an experimental setup outlined in fig.1.

Herein an optical scheme of a DFB dye laser is presented as well. In this scheme vertically polarized input pump beam is focused into a horizontal stripe by a cylindrical lens  $CL$  and than divided with a beamsplitter  $BS$  into the two partial beams  $I$  and  $II$  of nearly equal intensities. With the help of the mirrors  $M_1$  and  $M_2$  the beams  $I$  and  $II$  are brought together symmetrically on a face of a prism  $P$  which is in contact with the dye solution in a cell  $DC$ . The interfering beams are absorbed in a thin layer of dye solution at the face of the prism  $P$  and form a periodic spatial grating which is responsible for the DFB laser operation. When the pump energy  $E_p$  is higher than its threshold value  $E_{thr}$ , a narrow-linewidth lasing in a view of the two symmetrical output beams appears. The lasing wavelength of the device  $\lambda_L$  is defined by the expression

$$\lambda_L = \frac{n_s \lambda_p}{n_{pr} \sin \theta} \quad (1)$$

(where  $n_s$  is the refractive index of the dye solution at the lasing wavelength,  $n_{pr}$  is the refractive index of the prism material at the pumping wavelength  $\lambda_p$ ,  $\theta$  is the angle of the pumping beam incidence on the prism-solution interface) and can be conveniently tuned by changing the convergence angle  $2\theta$  of the exciting beams. The last is reached by simultaneous turning mirrors  $M_1$  and  $M_2$ . To adjust the pump power in a continuous manner, a rotatable half-wave plate  $\lambda/2$  in combination with a linear polarizer 8 (Glan prism) is employed. The length of the

excited zone in dye solution  $L_{DFB}$  is controlled by the width of a vertical slit diaphragm  $SD$  located in front of the beam-splitter  $BS$ .

In the course of experiments the pump and the DFB laser energies were measured by calibrated FD-24K photodiodes and an ADC-20M/10-2 two-channel analog-to-digital converter (ADC). The spectral characteristics were determined with a fiber-coupled automated S 3804 spectrograph (resolution of  $\sim 0.01$  nm) and an IT 51-30 Fabry-Perot interferometer. The temporal behavior of lasing intensity was monitored by an Agat-SF3 streak camera with a time resolution as high as  $1.9$  ps. Both the streak camera and ADC were triggered by an electronic circuit based on a KT-342 hf transistor operating in the avalanche mode. To provide scanning rate calibration a part of the light beam entering the input slit of the camera was temporary delayed while passing through a 6 cm-thick plane-parallel glass plate installed before the camera input objective. Both the streak camera traces and Fabry-Perot interferometer images were captured with a "Canon Power Shot SX 100 IS" digital photo camera, operating in RAW format.

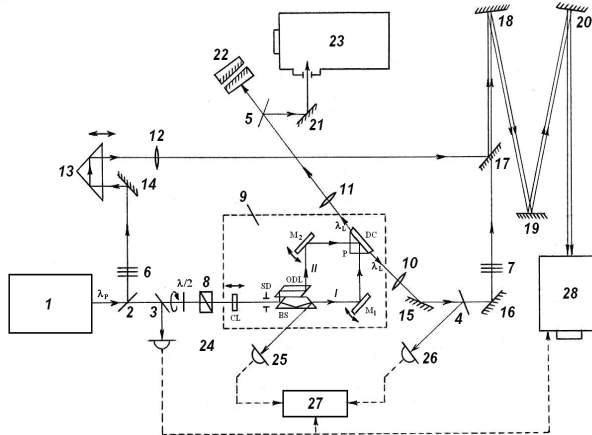


*Fig.1.* Schematic diagram of the apparatus: 1- Nd:LSB microlaser; 2-5 – beam splitters; 6-7 – optical filters; 8 – Glan prism; 9 – DFB dye laser (CL – cylindrical lens; SD – slit diaphragm; BS – beam splitter; ODL – optical delay line; M<sub>1</sub> – M<sub>2</sub> - mirrors; P – prism; DC – dye cell); 10 – 12 – collimating lenses; 13 – quartz prism; 14 -21- rotatable mirrors; 22 – IT 51-30 Fabry- Perot interferometer; 23 – S 3804 diffraction spectrograph; 24 – KT-342 avalanche transistor; 25 - 26 - FD-24K silicon photodiode; 27 - analog to digital converter; 28 - Agat-SF3 streak camera.

### 3. EXPERIMENTAL RESULTS

The investigations were carried out using an ethanol solution of Rhodamine 6G (concentration  $C = 2 \times 10^{-4}$  M) as the active medium of a DFB laser. Since the DFB laser characteristics depend directly on those of the pump source, some of the DPSS micro laser output parameters have been previously investigated in more details.

As an example Fig.2 shows an interferogram of the "STA-01SH" micro laser emission (a), as well as the intensity temporal profile of its pulse (b). Single rings in the interferogram as well as smooth pulse profile make evidence on the single-mode operational regime of the device. The laser linewidth and pulse duration (FWHM)

calculated from the series of measurements were determined to be  $\Delta\lambda_{0.5} \leq 0.003$  nm and  $\tau_{0.5} \sim 0.48$  ns, respectively.

Using a dye solution mentioned above a DFB laser pumped by full power of a micro laser provided a narrow-band emission ( $\Delta\lambda < 0.1$  nm) tunable in the spectral range of 543 – 604 nm. In such regime of operation the conversion efficiency of the pump energy into the DFB output energy was as high as  $\sim 43\%$ . The dependence of the DFB laser output characteristics on the experimental conditions was investigated in details for the case when lasing wavelength was adjusted to be in the vicinity of the gain profile of an active medium.

As a result of the measurements of the temporal characteristics of a DFB laser, it was found that, generally, when a DFB laser is pumped well above the threshold, a train of picosecond pulses is generated. In this case, both the total width and a number of pulses in the train depend on the pumping level  $\gamma = E_p/E_{thr}$  decreasing with lowering the  $\gamma$  value. At pumping levels  $\gamma$  not very far from the threshold single picosecond pulses are emitted by a DFB laser.

As a result of the measurements of the temporal characteristics of a DFB laser, it was found that, generally, when a DFB laser is pumped well above the threshold, a train of picosecond pulses is generated. In this case, both the total width and a number of pulses in the train depend on the pumping level  $\gamma = E_p/E_{thr}$  decreasing with lowering the  $\gamma$  value. At pumping levels  $\gamma$  not very far from the threshold single picosecond pulses are emitted by a DFB laser.

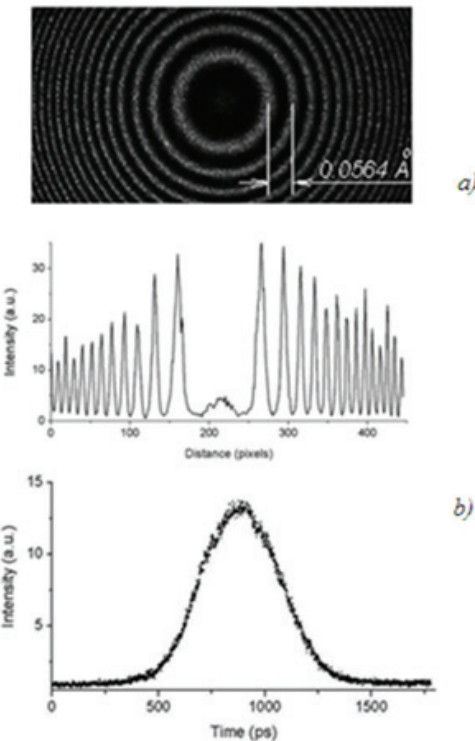


*Fig.2.* The output emission spectrum (a) and the temporal intensity profile (b) of the DPSS micro laser STA-01SH.

As an example, the temporal intensity profiles of the DFB laser emission registered at different pumping levels

$\gamma$  are presented in Fig. 3 ( $\lambda_L = 569 \text{ nm}$ ;  $L_{DFB} \approx 12 \text{ mm}$ ;  $E_{thr} \approx 2.5 \mu\text{J}$ ).

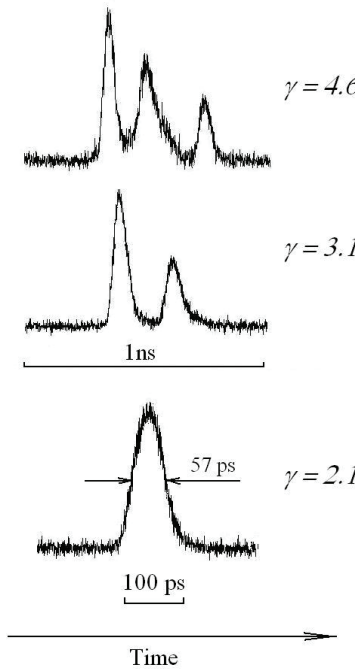


Fig.3. Temporal intensity profiles of the DFB laser output at different pumping levels  $\gamma$ :  $L_{DFB} \approx 12 \text{ mm}$ ;  $\lambda_L = 569 \text{ nm}$ .

It is seen that at  $\gamma \approx 4.6$  a DFB laser emits a train of three picosecond pulses with a total width of  $\sim 550 \text{ ps}$ . When the excitation power is lowered to  $\gamma \approx 3.1$ , a number of the generated pulses is reduced to two and their overall length becomes about  $440 \text{ ps}$ . At the pumping level  $\gamma \approx 2.1$  a DFB laser produces a single picosecond pulse with duration  $\tau_{0.5} \approx 57 \text{ ps}$ .

During the measurements it was installed that single pulse duration is a function of the pump level  $\gamma$  and tends to lengthen with decreasing the  $\gamma$  value. As was proposed in ref. [3], the duration of a single pulse may be defined as the duration of the first DFB laser pulse taken at the pumping level  $\gamma$  when the second pulse just reaches the threshold. With regard to the experimental conditions mentioned above the pumping level, at which the second pulse tends to appear in the DFB laser output, was close to  $\gamma \approx 2.25$ . Single pulse duration registered for this case was measured to be  $\tau_{0.5} \approx 55 \text{ ps}$ .

The spectrum of a DFB laser operating in the regime of single picosecond pulses was found to be in a view of the single narrow line (Fig.4), whose width  $\Delta\lambda_{0.5}$  reduces with decreasing the excitation power.

For example, when the pumping power was maintained at the levels  $\gamma$  equal to 2.2, 1.7 and 1.3 a DFB laser delivered the output emission with a linewidth of  $\sim 0.008$ ,  $\sim 0.007$  and  $\sim 0.005 \text{ nm}$ , respectively. The duration of single picosecond pulses  $\tau_{0.5}$ , corresponding to these pumping conditions, was measured to be  $\sim 57$ ,  $\sim 67$  and  $\sim 83 \text{ ps}$ , respectively. Taking into account these data, we have found that the time-bandwidth product  $\Delta\nu_{0.5}\tau_{0.5}$  for single pulses is  $\sim 0.4$ . This makes evidence on the transform-limited character of single picosecond

pulses generated by a DFB dye laser under the DPSS Nd-LSB micro excitation.

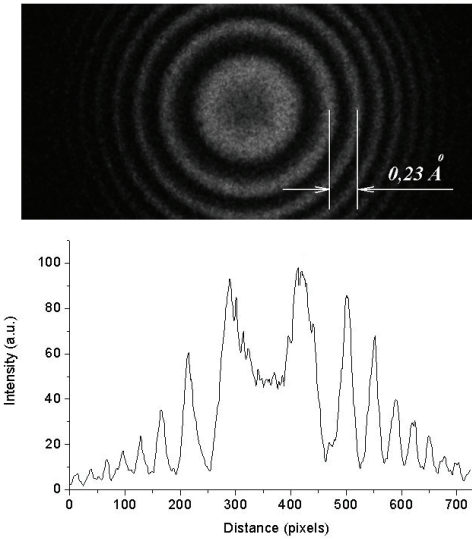


Fig.4. The output emission spectrum of a DFB dye laser in the regime of single picosecond pulses:  
 $\lambda_L = 569 \text{ nm}$   $\gamma \approx 1.7$ ;  $\tau_{0.5} \approx 67 \text{ ps}$ .

The experimentally measured dependence of the single pulse energy on the pump energy is presented in fig.5. It is seen that this dependence is of nonlinear character and near the second pulse threshold ( $E_p \sim 5.6 \mu\text{J}$ ) the single pulse energy  $E_L$  reaches  $\sim 0.13 \mu\text{J}$ . Taking into account single pulse duration of  $\sim 55 \text{ ps}$  registered for this case, the peak power of single pulse  $P_L$  is estimated to be  $\sim 2.4 \text{ kW}$ . At the pumping level  $\gamma \approx 2.1$  the energy stability of single picosecond pulses produced by a DFB dye laser was not worse than 1%.

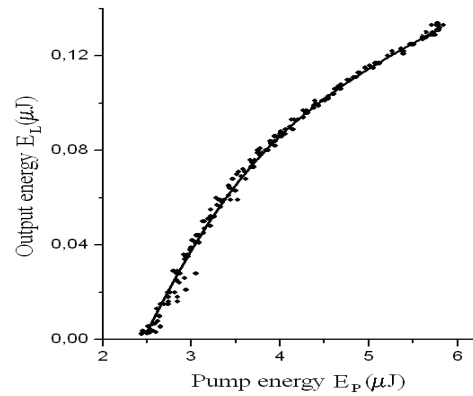


Fig.5. The dependence of the single picosecond pulse energy on the pump energy.

#### 4. CONCLUSION

In conclusion, a compact and highly stable tunable picosecond laser system based on a DFB dye laser pumped with a subnanosecond DPSS Nd-LSB micro laser has been realized. To our knowledge, both the pumping level  $\gamma \approx 2.2$  (at which a DFB laser is still able to generate single picosecond pulses without an external quenching of the gain medium), and  $\leq 1\%$  single picosecond pulse energy fluctuation, have been demonstrated in this work

are among the best values of such parameters ever reported for DFB dye lasers pumped with comparatively long (subnanosecond) pulses. Since only a small part of the DPSS micro laser energy is required for a DFB dye laser to operate in the regime of single picosecond pulses, the rest of the micro laser power may be used for the

synchronous pumping the amplifier based on the similar active medium. In such a way the energy of single picosecond pulses produced by a DFB “generator” may be noticeably increased thus expanding the range of practical use of the device.

- 
- [1] *C.V. Shank, J.E. Bjorkholm, H. Kogelnik.* Tunable distributed feedback dye laser. *Appl. Phys. Lett.* 1971, v.18, p.395-396.
  - [2] *T.Sh. Efendiev, A.N. Rubinov.* Tunable dfb dye laser with narrow emission line. *Zh. Prikl. Spektr.* V.21, №3 (1974) 526-528.
  - [3] *Zs. Bor.* Tunable picosecond pulse generation by a N2 laser pumped self Q-switched distributed feedback dye laser. *IEEE J. Quantum Electron.*, 1980, v.QE-16, №5, p.517.
  - [4] *A.N. Rubinov, T.Sh. Efendiev.* Holographic DFB dye laser. *Optica Acta*, 1985, v.32, №9/10, p.1291.
  - [5] *T.Sh. Efendiev, V.M. Katarkevich, A.N. Rubinov.* Generation of Tunable Picosecond Pulses in a Simple Distributed Feedback Dye Laser Under N<sub>2</sub> - Laser Pumping. *Optics Communs.* 1985. V.55, №5. P.347- 352.
  - [6] *G.M. Gale, B. Pedersen and P. Schanne.* Kilohertz picosecond distributed-feedback dye laser system. *Optics Communications.* Volume 76, Issue 2, 15 April 1990, Pages 138-142.
  - [7] *V M. Katarkevich, V.Yu. Kurstak, Anatolii N. Rubinov and T.Sh. Efendiev.* Lasing and amplified luminescence kinetics for a distributed-feedback dye laser with subnanosecond pumping. *Sov. J. Quantum Electronics* V. 22 №5. 1992. P.458.
  - [8] *Y. Cui, T.N. Ding, D.L. Hatten, W.T. Hill 111 and J. Goldhar.* Frequency tuning of a distributed feedback dye laser with two transmission gratings. *APPLIED OPTICS / Vol. 32, No. 33 / 20 November 1993.* P.6602-6606.
  - [9] *V.M. Katarkevich, V.Yu. Kurstak, A.N. Rubinov, T.Sh. Efendiev,* "Kinetics of the operation of a distributed-feedback dye laser with nanosecond excitation". *Sov. J. Quantum Electron.* 1996, V.26 №12, 1061–1064.
  - [10] *M. Basheer Ahamed, P.K. Palanisamy.* Nd:YAG laser pumped energy transfer distributed feedback dye laser in Rhodamine 6G and Acid blue 7 dye mixture. *Optics Communications* 213 (2002) 67–80.
  - [11] *C.Ye, J. Wang, L. Shi, D. Lo.* Polarization and threshold energy variation of distributed feedback lasing of oxazine dye in zirconia waveguides and in solutions. *Appl. Phys. B* 78, 189–194 (2004).
  - [12] *S. Balslev, T. Rasmussen, P. Shi, A. Kristensen.* Single mode solid state distributed feedback dye laser fabricated by grey scale electron beam lithography on dye doped SU-8 resist. *J. Micromech. Microeng.*, 2005, v.15, p.2456
  - [13] *Zhenyu Li, Zhaoyu Zhang, Axel Scherer, and Demetri Psaltis.* Mechanically tunable optofluidic distributed feedback dye laser. *Optics Express*, Vol. 14, Issue 22, pp. 10494-10499 (2006).
  - [14] *R. Sailaja, P.B. Bisht.* Tunable multiline distributed feedback dye laser based on the phenomenon of excitation energy transfer. *Organic Electronics*, 2007, v.8, p.175
  - [15] *F. Chen, D. Gindre, J.-M. Nunzi.* First-order distributed feedback dye laser effect in reflection pumping geometry. *Opt. Lett.*, 2007, 32(7): 805-7 17339943
  - [16] *Y. Chen, Zh. Li, Zh. Zhang, D. Psaltis, A. Scherer.* Nanoimprinted Circular Grating Distributed Feedback Dye Laser. *Appl. Phys. Letts.*, 2007, v.91, p.051109-1
  - [17] *T.Sh. Efendiev, V.M. Katarkevich, Ch.O. Kajar, R.A. Karamaliev, A.Ch. Izmailov.* Transactions of Azerbaijan Academy of Sciences, series of physical- mathematical and technical sciences, Physics and Astronomy, 2009, 29, №5, c. 67-73.
  - [18] *D.Q. Hoa, P. Long, T. Imasaka.* A self-quenching picosecond distributed feedback dye laser pumped by a picosecond laser pulse. *Appl Phys B* (2010) 101: 571–574
  - [19] *K.Yamashita, N.Takeuchi, K.Oe, H.Yanagi.* Simultaneous RGB lasing from a single-chip polymer device. *Optics Letters*. 2010. V.35, №14. P. 2451.
  - [20] *P.P. Yaney, D.A.V. Kliner, P.E. Schrader, R.L.Farrow.* Distributed-feedback dye laser for picosecond ultraviolet and visible spectroscopy. *Rev. Sci. Instrum.*, 2000, v.71, p.1296.
  - [21] *N. Khan, A. Idrees.* Overexposure analysis of pulsed distributed feedback laser source. *J. of Biomed. Opt.*, 2001, v.6, p.86.
  - [22] *N. Takeyasu, T. Deguchi, M. Tsutsumikawa, J. Matsumoto, T. Imasaka.* A tunable picosecond dye laser for use in dioxin analysis. // *Anal. Sci.*, 2002, v.18. p.243.
  - [23] *P. Cacciania, F. Brandib, J.P. Sprengersb, A. Johanssonc, A. L'Huillierc, C.-G. Wahlström, W. Ubachs.* Predissociation of the 4ppL1P Rydberg state of carbon monoxide. *Chemical Physics* 282 (2002) 63–73.
  - [24] *T. Ushimura, S. Kawanabe, Y. Maeda, T. Imasaka.* Fluorescence Lifetime Imaging Microscope Consisting of a Compact Picosecond Dye Laser and a Gated Charge-Coupled Device Camera for Applications to Living Cells Anal. *Sci.*, 2006, v.22, p.1291.
  - [25] [http://www.standa.lt/products/catalog/lasers\\_laser\\_accessories.item=190&prod=diode\\_pumped\\_nd\\_ls\\_b\\_solid\\_state\\_micro\\_laser&print=1](http://www.standa.lt/products/catalog/lasers_laser_accessories.item=190&prod=diode_pumped_nd_ls_b_solid_state_micro_laser&print=1).

Received: 12.04.2011

## LUMINESCENT PROPERTIES OF (Ba,Ca)Ga<sub>2</sub>(S,Se)<sub>4</sub> CHALCOGENIDE SEMICONDUCTORS DOPED WITH RARE EARTHS

**V.Z. ZUBIALEVICH, E.V. LUTSENKO, M.S. LEANENIA, E.V. MURAVITSKAYA,  
G.P. YABLONSKII, A.M. PASHAEV<sup>1,2</sup>, B.G. TAGIEV<sup>1,2</sup>, O.B. TAGIEV<sup>1,3</sup>,  
S.A. ABUSHOV<sup>1</sup>**

*Institute of physics of NAS of Belarus, Nezalezhnasci ave. 68, 220072 Minsk, Belarus;  
tel.: +375172840428, e-mail: g.yablonskii@ifanbel.bas-net.by*

<sup>1</sup>*G.M. Abdullayev Institute of physics of NAS of Azerbaijan, G. Javid ave. 33, AZ-1143 Baku,*

<sup>2</sup>*National Academy of Aviation, Bina, 25<sup>th</sup> km, AZ-1045 Baku, Azerbaijan*

<sup>3</sup>*Branch of Moscow State University in Baku, F. Agayev str. 9, AZ-1141 Baku, Azerbaijan*

Photoluminescence properties of (Ba,Ca)Ga<sub>2</sub>(S,Se)<sub>4</sub> chalcogenide semiconductors doped with Eu or/and Ce were studied. Barium and calcium thiogallates were found to have more efficient luminescence in comparison with selenogallates. The (Ba,Ca)Ga<sub>2</sub>S<sub>4</sub> semiconductors co-doped with europium and cerium show a high thermal stability of luminescence characteristics in the range of 10-300 K. Both thio- and selenogallates activated with Eu or/and Ce demonstrate a considerable PL efficiency droop at high excitation levels exceeding 10<sup>4</sup> W/cm<sup>2</sup>. A photon assisted de-excitation due to absorption from excited states of the rare earths mainly by the exciting radiation and a following nonradiative relaxation of the electrons is proposed as a mechanism of the droop.

Anti-stokes luminescence of Er-Yb pairs in barium thiogallate has been obtained for the first time. Room temperature excitation intensity dependence of BaGa<sub>2</sub>S<sub>4</sub>:Er,Yb anti-stokes luminescence is studied in the range of 0.5–125 W/cm<sup>2</sup> (976 nm) and discussed.

**Keywords:** Photoluminescence, barium thiogallate, barium selenogallate, europium, cerium, luminophore

**PACS:** 78. 20. – e. 7840 Fy

### 1. INTRODUCTION

Ternary chalcogenide semiconductors of II-III<sub>2</sub>-VI<sub>4</sub>-type doped with rare earths are attracting materials for electroluminescent panels [1-4], as phosphors [5-8], anti-stokes phosphors [9-11] and laser media [12-14]. Europium and cerium ions are radiative centers emitting in the visible spectral range when incorporated in the ternary chalcogenide hosts. For example, BaAl<sub>2</sub>S<sub>4</sub> PL properties of some of the materials doped with Eu<sup>2+</sup> and Ce<sup>3+</sup> were studied before in respect of dependencies of their photoluminescence (PL) on temperature [15,16] and on rare earth concentrations [6]. One of the possible applications of the phosphors is using them in white LEDs. Easy dimming of LED emission intensity is an important advantage over fluorescent lamps. Phosphors used in white LEDs should have stable spectral characteristics and constant quantum yield of luminescence in respect of excitation power density level to avoid dependence of LED chromaticity and color rendering index on dimming factor. Recently, excitation intensity dependencies of luminescent properties of BaGa<sub>2</sub>S<sub>4</sub> [17] and BaGa<sub>2</sub>Se<sub>4</sub> [18] doped with Eu or/and Ce were explored for the first time. It was found that PL efficiency of the phosphors droops at excitation power densities above 10<sup>4</sup> W/cm<sup>2</sup> and it seems to be common feature of the ternary chalcogenide semiconductors doped with Eu or/and Ce. The review of previous and new results concerning BaGa<sub>2</sub>S<sub>4</sub>, BaGa<sub>2</sub>Se<sub>4</sub> as well as CaGa<sub>2</sub>S<sub>4</sub> and CaGa<sub>2</sub>Se<sub>4</sub> doped with Eu or/and Ce are presented in this work.

Ability to convert invisible radiation (UV, IR) in a variety of wavelengths in the visible light (0.38-0.76 nm) lies at the heart of their visualization. For the range of 0.9-1.0 μm has been developed and used anti-stokes phosphors based on La<sub>2</sub>O<sub>2</sub>S and Y<sub>2</sub>O<sub>2</sub>S with erbium and ytterbium as a sensitizer and activator, respectively

[19,20]. In this paper, the anti-stokes luminescence of BaGa<sub>2</sub>S<sub>4</sub>:Er,Yb, recently obtained for the first time [21] is investigated depending on the level of excitation at room temperature (RT).

### 2. EXPERIMENTAL

(Ba,Ca)Ga<sub>2</sub>(S,Se)<sub>4</sub> samples were synthesized from pure barium, calcium and gallium sulphides or selenides as precursors by solid-phase reaction. Synthesis was carried out in one-temperature furnace during 4 hours at 1000-1300°C. Post-synthesis 4 hour annealing at 900-1000°C in atmosphere of H<sub>2</sub>S was applied. The additional synthesis and doping details are presented elsewhere [22]. Polycrystalline ceramics samples were prepared for measurements by milling into powder to avoid sample inhomogeneity. Then samples were compacted in 100-200 μm layers on silicon plates. BaGa<sub>2</sub>S<sub>4</sub>:Eu<sup>2+</sup>,Ce<sup>3+</sup> was doped with 3 at.% of each ions. All others were doped with 5 at.% of REE.

Radiation of a xenon lamp (cw) monochromated and chopped was used for measurements of PL and PL excitation (PLE) spectra. For registration a monochromator equipped with a photomultiplier and a lock-in multiplier was applied. A close-cycle helium cryostat was employed for temperature-resolved measurements (10 – 300 K). Radiations of an InGaN laser diode (cw, 405 nm), a HeCd laser (cw, 325 nm), and an N<sub>2</sub> laser (8 ns, 337.1 nm) were used for excitation intensity resolved PL measurements. Integral PL intensities were measured by power meter Thorlabs PM-120 (at cw excitation) and by radiometer LaserProbe RM-3700 (at pulse excitation). The PL spectra were taken off by a CCD-spectrograph. E-gun Radan-2250 (250 keV) was applied as excitation source for cathodoluminescence (CL) measurements. GaInAsP IR-laser diode (cw, 972 nm) was used for excitation of anti-stokes

luminescence. Time-resolved measurements were carried out using N<sub>2</sub> laser radiation. The PL transients were registered from a fast photodiode by a digital oscilloscope with time resolution of about 1 ns.

### 3. PL AND PL EXCITATION SPECTRA AT RT

Room temperature PL properties of (Ba,Ca)Ga<sub>2</sub>(S,Se)<sub>4</sub> doped with Eu or/and Ce were studied. Eu doped samples excepting barium selenogallate have one ion-related band in emission spectra (Eu: 4f<sup>6</sup>5d→4f<sup>7</sup>). The band position depends on matrix and for the studied compounds it lies in the “green-yellow” spectral range. Additional wide PL band of BaGa<sub>2</sub>Se<sub>4</sub>:Eu located near 685 nm originates from matrix since it is only composes the emission spectrum of not doped material. The PL excitation (PLE) spectra were measured at detected wavelengths corresponding to the maxima of the ion related PL bands (Eu: 4f<sup>6</sup>5d→4f<sup>7</sup>). As it is seen from Fig. 1, all of the doped with europium compounds excepting BaGa<sub>2</sub>Se<sub>4</sub> have the PLE spectra convenient for excitation by blue emission of InGaN-chips (near 450 nm).

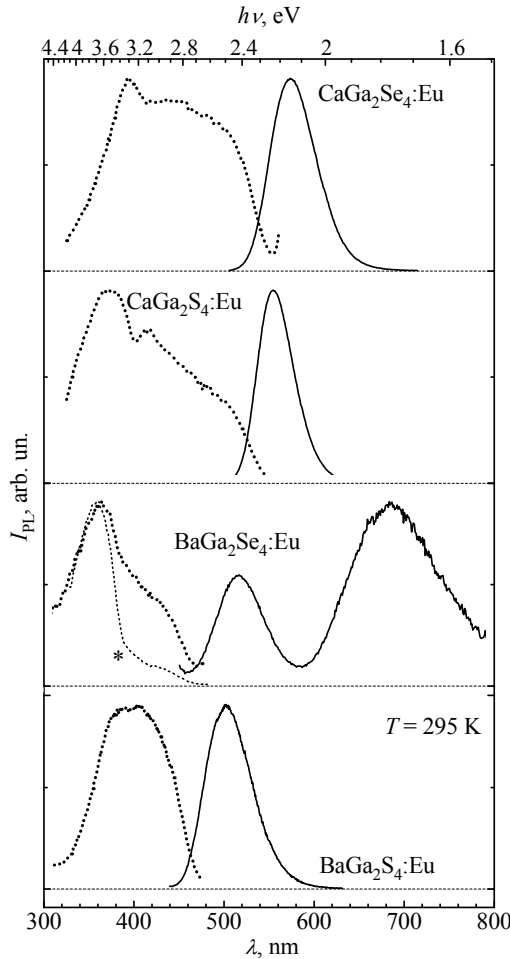


Fig. 1. Normalized PL (solid) and PLE spectra (dot) of (Ba, Ca)Ga<sub>2</sub>(S, Se)<sub>4</sub>:Eu measured at RT. PLE spectrum marked with “\*” is measured for the matrix related PL band of BaGa<sub>2</sub>Se<sub>4</sub>:Eu ( $\lambda_{\text{reg}} = 680$  nm).

PL spectra of the samples are compared in Fig. 2. All measurements were done at proper excitation

wavelengths under the same other conditions. The resulting spectra were reduced to equal  $\lambda_{\text{exc}} = 450$  nm by multiplying factors according to the corresponding PLE spectra. One can see that the thiogallates have more efficient PL. Most probably it is caused by higher band-gaps of the thiogallates than those of the selenogallates [23,24]. Low efficiency of the BaGa<sub>2</sub>Se<sub>4</sub>:Eu photoluminescence in addition to relatively narrow band-gap is determined by energy loss from ions to deep levels in the matrix. It is supported by presence of an ion-related wing in the PLE spectrum of the matrix-related PL band (the curve marked with “\*” in Fig. 1).

The samples doped with cerium have two bands in their PL spectra corresponding to 5d→<sup>2</sup>F<sub>5/2</sub> and 5d→<sup>2</sup>F<sub>7/2</sub> transitions in Ce<sup>3+</sup> ions. PL efficiencies of Ce-doped samples are typically by 10-20 times lower than those of Eu-doped ones. However the co-doping with both ions leads to nearly doubling (relative to Eu-doped sample) the value of BaGa<sub>2</sub>S<sub>4</sub> PL efficiency and to fivefold increase of the BaGa<sub>2</sub>Se<sub>4</sub> PL efficiency. This is known to be due to resonant energy transfer from excited Ce<sup>3+</sup> ions to Eu<sup>2+</sup> ones [6,22,25]. However, for calcium selenogallate the co-doping oppositely worsens PL efficiency about one order of its magnitude. Probably a reverse transfer of excitation energy (from excited Eu<sup>3+</sup> ions to Ce<sup>2+</sup> ones) occurs in the matrix. This supposition could explain the observed PL efficiency decrease since as it was noted before Ce-doped calcium selenogallate has lower PL efficiency in comparison with Eu-doped one.

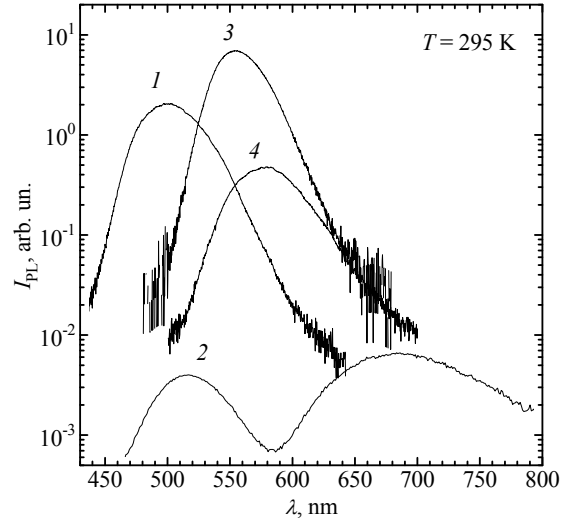


Fig. 2. PL spectra of BaGa<sub>2</sub>S<sub>4</sub>:Eu (1), BaGa<sub>2</sub>Se<sub>4</sub>:Eu (2), CaGa<sub>2</sub>S<sub>4</sub>:Eu (3) and CaGa<sub>2</sub>Se<sub>4</sub>:Eu (4) measured at low level excitation ( $\lambda = 450$  nm, cw)

The obtained data on PL spectra positions  $\lambda_{\text{PL}}$ , optimal wavelengths of excitation  $\lambda_{\text{PLE}}$  of studied phosphors and types of corresponding electron transitions are summarized in the Table 1. The ranges of effective excitation wavelengths instead of PLE spectrum maximum positions are given in the corresponding column of the table in the cases of absence or insufficiently well-resolved maxima of PLE spectra. The range of the effective excitation wavelengths of a certain phosphor is determined as a wavelength interval where its PL signal is higher than half of its maximal value.

Table 1.

Wavelengths of characteristic electron transitions.

| Compound                                 | $\lambda_{\text{PLE}}$ , nm   | Transition in absorption   | $\lambda_{\text{PL}}$ , nm | Transition in emission  |
|--|-------------------------------|--|----------------------------|---|
| BaGa <sub>2</sub> S <sub>4</sub> :Eu     | 352<br>-448                   | Eu: 4f <sup>7</sup> →4f <sup>6</sup> 5d  | 502                        | Eu: 4f <sup>6</sup> 5d→4f <sup>7</sup>  |
| BaGa <sub>2</sub> S <sub>4</sub> :Ce     | 392<br>300                    | Ce: 2F <sub>5/2</sub> →5d <sup>1</sup><br>Ce: 2F <sub>5/2</sub> →5d <sup>2</sup>   | 442<br>497                 | Ce: 5d <sup>1</sup> →2F <sub>5/2</sub><br>Ce: 5d <sup>1</sup> →2F <sub>7/2</sub>                            |
| BaGa <sub>2</sub> S <sub>4</sub> :Eu,Ce  | 335<br>-449<br>300            | Eu: 4f <sup>7</sup> →4f <sup>6</sup> 5d,<br>Ce: 2F <sub>5/2</sub> →5d <sup>1</sup><br>Ce: 2F <sub>5/2</sub> →5d <sup>2</sup> | 501                        | Eu: 4f <sup>6</sup> 5d→4f <sup>7</sup>  |
| BaGa <sub>2</sub> S <sub>4</sub> :Er,Yb  | 976                           | Yb: 2F <sub>7/2</sub> →2F <sub>5/2</sub>   | 645-675<br>515-560         | Er: 4F <sub>9/2</sub> →4I <sub>15/2</sub><br>Er: 2H <sub>11/2</sub> , 4S <sub>3/2</sub> →4I <sub>15/2</sub> |
| BaGa <sub>2</sub> Se <sub>4</sub>        | < 380                         | band-to-band   | 685                        | deep levels   |
| BaGa <sub>2</sub> Se <sub>4</sub> :Eu    | < 380<br>winning near 400–455 | band-to-band,<br>Eu: 4f <sup>7</sup> →4f <sup>6</sup> 5d   | 685<br>515                 | deep levels<br>Eu: 4f <sup>7</sup> →4f <sup>6</sup> 5d  |
| BaGa <sub>2</sub> Se <sub>4</sub> :Ce    |                               |  | 507                        | 5d <sup>1</sup> →2F <sub>7/2</sub> , 2F <sub>5/2</sub>  |
| BaGa <sub>2</sub> Se <sub>4</sub> :Eu,Ce | 323<br>-448                   | band-to-band,<br>Eu: 4f <sup>7</sup> →4f <sup>6</sup> 5d   | 685<br>515                 | deep levels<br>Eu: 4f <sup>6</sup> 5d→4f <sup>7</sup>   |
| CaGa <sub>2</sub> S <sub>4</sub> :Eu     | 302<br>-470<br>352<br>, 398   | Eu: 4f <sup>7</sup> →4f <sup>6</sup> 5d  | 554                        | Eu: 4f <sup>6</sup> 5d→4f <sup>7</sup>  |
| CaGa <sub>2</sub> Se <sub>4</sub> :Eu    | 339<br>-520                   | Eu: 4f <sup>7</sup> →4f <sup>6</sup> 5d  | 577                        | Eu: 4f <sup>6</sup> 5d→4f <sup>7</sup>  |
| CaGa <sub>2</sub> Se <sub>4</sub> :Ce    | 460<br>391                    | Ce: 2F <sub>5/2</sub> →5d <sup>1</sup><br>Ce: 2F <sub>5/2</sub> →5d <sup>2</sup>   | 570<br>507                 | Ce: 5d <sup>1</sup> →2F <sub>7/2</sub><br>Ce: 5d <sup>1</sup> →2F <sub>5/2</sub>                            |
| CaGa <sub>2</sub> Se <sub>4</sub> :Eu,Ce | 340<br>-480                   | Eu: 4f <sup>7</sup> →4f <sup>6</sup> 5d  | 578                        | Eu: 4f <sup>6</sup> 5d→4f <sup>7</sup>  |

#### 4. THERMAL STABILITY OF PL

For many applications it is important to know thermal PL quenching and spectrum change of phosphor

to predict possibility of using it in conditions of variable temperatures.

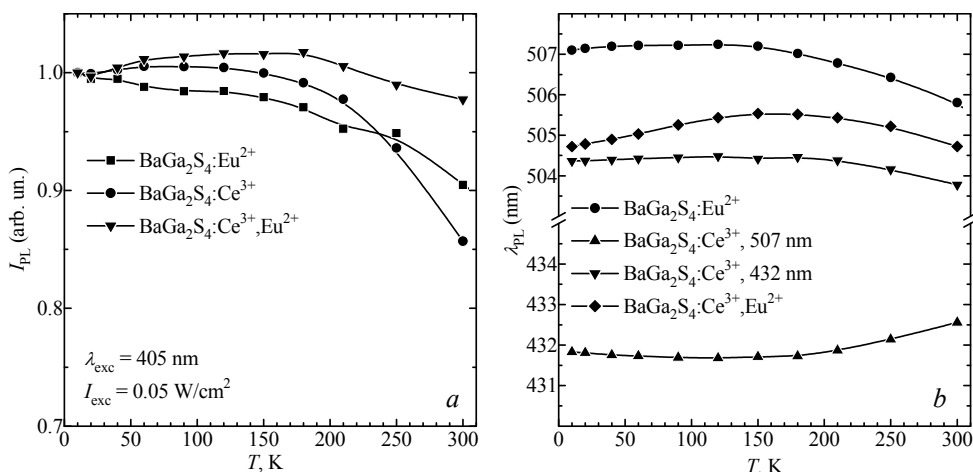


Fig. 3. Integral PL intensities (a) and PL positions (b) of BaGa<sub>2</sub>S<sub>4</sub> doped with Eu, Ce and co-doped with Eu and Ce as functions of temperature.

Temperature dependence of PL in the range of 10–300 K was studied for the barium thiogallates. It was found that the integral PL efficiency decreases only by 10, 15 and 4% at the temperature rise from 10 K to RT (Fig. 3, a). The observed temperature PL quenching of the  $\text{BaGa}_2\text{S}_4:\text{Eu}$  PL is only a half of previously reported value for a sample with lower content of europium [15]. Positions of the ions related PL bands of barium thiogallates shift by less than 2 nm within the studied temperature interval (Fig. 3, b).

## 5. PL AT DIFFERENT EXCITATION LEVELS

Our study shows that the thiogallates and selenogallates are characterized by a very stable PL position of the ion-related bands in a wide range of excitation levels. For example, several PL spectra of the barium thiogallate co-doped with Eu and Ce are presented in Fig. 4. As it is seen from the figure the PL spectra do not demonstrate any significant shift over more than nine orders of excitation power density. This may indicate a fine solubility of rare earths in the matrixes and a formation of isolated radiative centers.

The selenogallates doped with Eu and co-doped with Ce demonstrate a similar behaviour of PL positions (Fig. 5, a). However the short-wavelength PL band of  $\text{BaGa}_2\text{S}_4:\text{Ce}$  corresponding to  $5d \rightarrow ^2F_{5/2}$  transition of  $\text{Ce}^{3+}$  ions suffer from a significant high energy shift in contrast to the  $5d \rightarrow ^2F_{5/2}$ -related band.

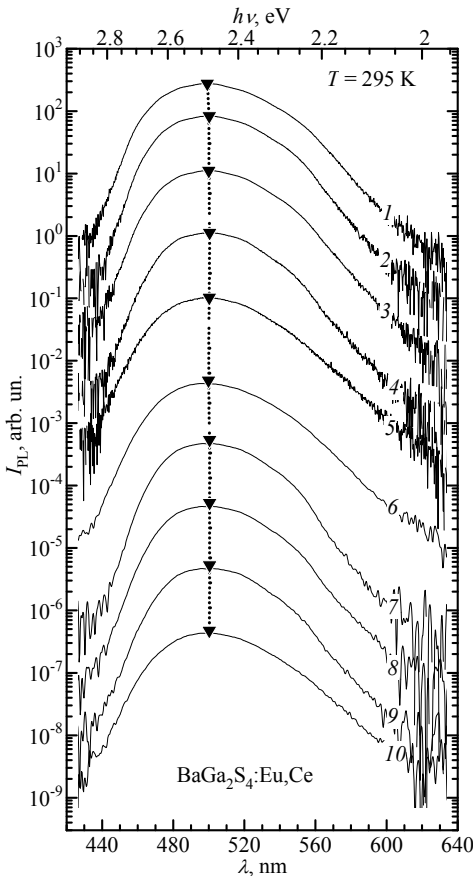


Fig. 4. PL spectra of  $\text{BaGa}_2\text{S}_4$  co-doped with Eu and Ce at different levels of excitation,  $\text{W}/\text{cm}^2$ : pulse (8 ns):  
1 –  $1.25 \cdot 10^6$ , 2 –  $1.25 \cdot 10^5$ , 3 –  $1.25 \cdot 10^4$ ,  
4 –  $1.25 \cdot 10^3$ , 5 –  $1.25 \cdot 10^2$ ; cw: 6 – 10, 7 – 1,  
8 – 0.1, 9 –  $10^{-2}$ , 10 –  $10^{-3}$ .

The PL efficiencies of some studied samples determined as ratio between integral PL intensity and corresponding power density of exciting radiation are presented in the Fig. 5, b. One can see that PL efficiencies of barium thiogallates independently on doping type are constant up to  $20 \text{ kW}/\text{cm}^2$ . This property of  $\text{BaGa}_2\text{S}_4$  allows to compare PL efficiencies of barium selenogallates at high ( $\text{N}_2$  laser) and low (Xe lamp) levels of excitation.

One can see from Fig. 5, b that barium selenogallates doped with Eu and co-doped with Eu and Ce do not satisfy requirements of constant luminescent quantum yield. Their PL efficiencies at  $I_{\text{exc}} \sim 10^4 \text{ W}/\text{cm}^2$  are several times higher than that at low Xe lamp excitation level. The Eu-related bands of  $\text{BaGa}_2\text{Se}_4:\text{Eu}$  and  $\text{BaGa}_2\text{Se}_4:\text{Eu,Ce}$  rise with excitation level faster than the matrix-related ones. Thus the increase of the PL efficiencies occurs most probably due to saturation of channels of radiative relaxation of excited ions via deep levels of matrix.

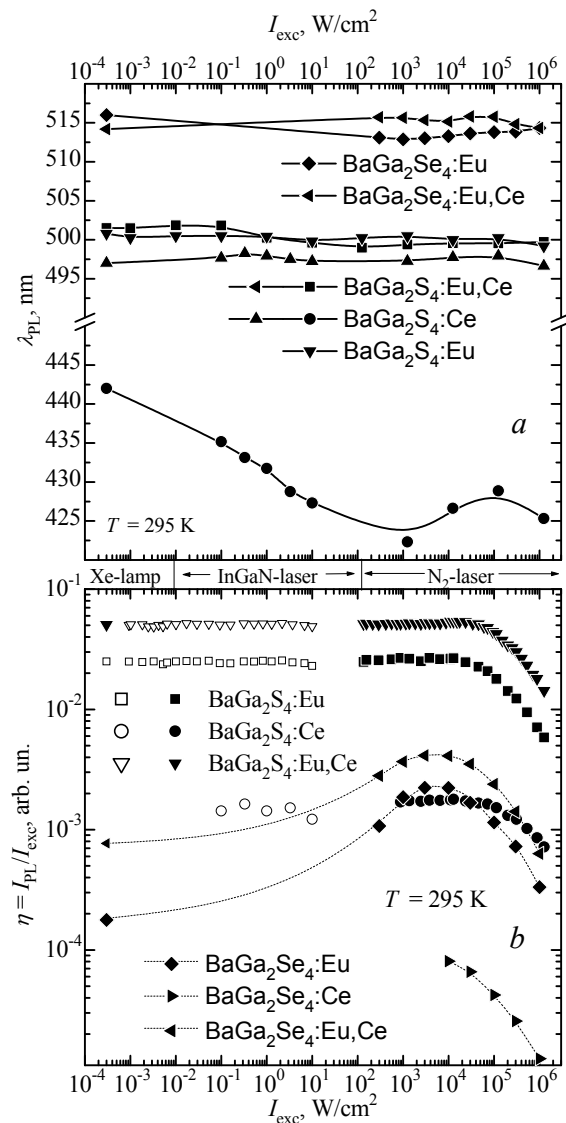


Fig. 5. Integral PL intensities (a) and PL positions (b) of  $\text{BaGa}_2(\text{S}, \text{Se})_4$  doped with Eu, Ce and co-doped with Eu and Ce as functions of excitation level.

PL efficiencies of all studied samples decrease at excitation intensity are higher than 10<sup>4</sup> W/cm<sup>2</sup>. Excited Eu<sup>2+</sup>-ion concentration at 10<sup>4</sup> W/cm<sup>2</sup> of pulse (8 ns) excitation corresponds to that at about 270 W/cm<sup>2</sup> (cw) taking into account the lifetime of excited Eu<sup>2+</sup> of about 300 ns (see below). This level is not reached even in the most bright state-of-the-art LEDs, and the observed PL efficiency droop is not an obstacle for using the phosphors as a component of white LEDs. However the phenomenon is interesting in itself.

Degradation of material, heating and corresponding temperature PL quenching, absorption saturation, absorption from excited state may be proposed as mechanisms of the observed PL efficiency droop.

It was found that a decrease of the excitation intensity from 1 MW/cm<sup>2</sup> (the level at which the PL efficiency droop is essential) to 10 kW/cm<sup>2</sup> leads to the total recovery of the PL efficiency. This observation allows ruling out the degradation as a possible mechanism.

High temperatures of material during exciting pulse should be considered to explain the droop by heating taking into account a relatively weak temperature PL quenching of BaGa<sub>2</sub>S<sub>4</sub>:Eu at above RT range [15]. Moreover the droop occurs also at low temperatures at which PL efficiency of doped BaGa<sub>2</sub>S<sub>4</sub> extremely weakly depends on temperature (see Fig. 3, a). Obviously temperature PL quenching of less than 10% (at temperature rise from 10 to 300 K) cannot lead to PL efficiency droop of several times.

Laser line of nitrogen laser used for high excitation has photon energy (3.68 eV) less than the BaGa<sub>2</sub>S<sub>4</sub> band-gap value ( $\approx$  3.94 eV при 300 K [23]) and thus it is too low for band-to-band excitation of BaGa<sub>2</sub>S<sub>4</sub>. The absorption of nitrogen laser emission by BaGa<sub>2</sub>S<sub>4</sub>:Eu, therefore, is due to the rare earth ion absorption which can be in principle saturated at high levels of excitation. However even the maximal energy (10 mJ/cm<sup>2</sup>) of excitation pulse can excite all ions in only 600 nm of material doped up to 5 at.% of Eu or/and Ce. Thus, one should conclude that absorption saturation in the thin surface layer cannot explain the observed droop since layers of phosphors were about 100-200  $\mu$ m.

At high pumping levels, when concentration of excited ions is high, encounter probability of a photon emitted inside the material with an excited ion ceases to be negligible. This should lead to nonlinear effects. For example, leaving the material luminescence photons can induce an electron from an excited state to radioactively relax to its ground state. However the emission stimulation will not lead the PL efficiency droop. Other possibility is excitation of a previously excited ion by a luminescence or exciting radiation photon to higher levels of the ion or in the conduction band of the matrix. In the first case of de-excitation we lose a luminescence photon and an excited ion (potential photon). In the second case an exciting photon would be spent not only on excitation of an ion in its ground state, but also on de-excitation of a previously excited one. Both cases lead to a decrease of the external quantum yield value, because, as expected, the matrixes have a large number of defects and nonradiative recombination in it is a more probable process than the radiative recombination or electron

transfer back to the excited level of the ion. This photon-assisted de-excitation can, in principle, be responsible for the observed PL efficiency droop of BaGa<sub>2</sub>(S,Se)<sub>4</sub> doped with the rare earths.

From the standpoint of laser properties of the materials, the de-excitation by pumping radiation complicates amounting to the level of excitation sufficient for lasing threshold in the medium. However, the de-excitation by intrinsic luminescence AES of the ions generates a more serious obstacle to lasing. A luminescent photon meeting an excited ion may interact with it: either be absorbed by it or stimulate the ion to relax to the ground state with emission of the same photon (optical gain). In other words, the absorption of the luminescence photons from excited state (AES) of ions competes with their stimulated radiative relaxation. It is obvious that the optical gain in the material would be impossible if the rare earth AES cross-section for the luminescence photons is larger than the cross section of their photostimulated radiative relaxation. Thus, it is important to know how effective AES of own luminescence photons is in the considered materials to predict their application as laser media.

## 6. ACCOUNTING FOR THE OWN EMISSION AND EXTERNAL RADIATION AES

To quantify the intrinsic emission AES of Eu<sup>2+</sup> in BaGa<sub>2</sub>S<sub>4</sub> on the effectiveness of its luminescence, we need to solve the following rate equation:

$$\frac{dn(t)}{dt} = -A \cdot n(t) - B \cdot n(t) - B_A \cdot n(t) \cdot A \cdot n(t), \quad (1)$$

with initial condition  $n(0) = n_0$ , where  $n_0$  is an excited ion concentration just after end of short exciting pulse.

Summand  $A \cdot n(t)$  on the right of (1) corresponds to the spontaneous radiative transition of electrons of the ground state,  $B \cdot n(t)$  – to their nonradiative relaxation, and  $B_A \cdot n(t) \cdot A \cdot n(t)$  – AES of own emission. Clearly, the probability of the latter process is proportional to the concentration of excited ions  $n(t)$  and flux of luminescence quanta, which, in turn, is proportional to the rate of spontaneous radiative transitions –  $A \cdot n(t)$ . Equation (1) is simply integrated:

$$n(t) = \frac{n_0 \cdot e^{-t \cdot A/\eta}}{1 + \eta \cdot B_A \cdot n_0 \cdot (1 - e^{-t \cdot A/\eta})}, \quad (2)$$

where  $\eta = A/(A+B)$  is luminescence efficiency at low excitation levels, when  $B_A \cdot n(t) \ll 1$ . It may be shown that the quantum efficiency of luminescence  $\eta_L$  (ratio of difference between number of ions relaxing radiatively and number of photons losing on ion AES to the initial number of excited ions  $n_0$ ) is expressed by:

$$\eta_L = \left( 1 + \frac{1}{\eta} \right) \cdot \frac{\ln(1 + \eta \cdot B_A \cdot n_0)}{B_A \cdot n_0} - 1. \quad (3)$$

It is noteworthy that the quantum yield of luminescence is found to be independent on the probability of spontaneous radiative relaxation time (the lifetime of the excited state of the ion), except through  $\eta$

and, hence, (3) applies to any rare earths, which have AES of own radiation.

Concentration  $n_0$ , achieved in the material by the end of the pump pulse, linearly depends on excitation pulse energy if its duration  $\tau$  is much shorter than the lifetime  $\eta/A$  of the excited state of ions and its intensity ( $I_{\text{exc}}$ ,  $\text{cm}^{-2} \cdot \text{s}^{-1}$ ) is low:  $n_0(I_{\text{exc}}) = k \cdot I_{\text{exc}} \cdot \tau$ , where  $k$  – coefficient of absorption. However, the dependence of  $n_0(I_{\text{exc}})$  can become sublinear due to AES of ions at sufficiently high levels. Measured in the experiment efficiency  $\eta_{\text{exp}}$  is the product of the excitation efficiency  $\eta_{\text{exc}}$ :

$$\eta_{\text{exc}} = n_0(I_{\text{exc}})/(k \cdot I_{\text{exc}} \cdot \tau) \quad (4)$$

and luminescence efficiency  $\eta_L$  since the ion de-excitation by its own emission and by pump radiation can be separated in time in the case of short excitation pulses. To determine the dependence of  $n_0(I_{\text{exc}})$ , one need to solve the following rate equation:

$$\frac{dn(t)}{dt} = I_{\text{exc}} \cdot B_{G+} \cdot (N - n(t)) - I_{\text{exc}} \cdot B_{G-} \cdot n(t), \quad (5)$$

where  $B_{G+}$  – photon absorption cross section of an ion from its ground state,  $B_{G-}$  – photon absorption cross section ion from its excited state,  $N$  – the total concentration of ions (doping level). Terms  $A \cdot n(t)$  and  $B \cdot n(t)$  responsible for the radiative and nonradiative relaxation as well as term  $B_A \cdot n(t) \cdot A \cdot n(t)$  responsible for luminescence AES of the ions are neglected in (5) since  $\tau \ll \eta/A$ . The solution of equation (5) has the next form:

$$n(t) = \frac{1 - e^{-t \cdot I_{\text{exc}} \cdot (B_{G+} + B_{G-})}}{(B_{G+} + B_{G-})} \cdot N \cdot B_{G+}. \quad (6)$$

From this expression we can determine the concentration of excited carriers by the end of the pump pulse  $n_0 = n(t)|_{t=\tau}$ , as a function of  $I_{\text{exc}}$ :

$$n_0 = \frac{1 - e^{-\tau \cdot I_{\text{exc}} \cdot B_{G+} \cdot (1+\zeta)}}{(1+\zeta)} \cdot N, \quad (7)$$

where  $\zeta = B_{G-}/B_{G+}$ . Taking into account (7), the expression (4) for excitation efficiency is:

$$\eta_{\text{exc}} = \frac{n_0}{k \cdot I_{\text{exc}} \cdot \tau} = \frac{(1 - e^{-\tau \cdot I_{\text{exc}} \cdot B_{G+} \cdot (1+\zeta)})/(1+\zeta)}{\tau \cdot I_{\text{exc}} \cdot B_{G+}}, \quad (8)$$

where  $k = B_{G+} \cdot N$  (absorption only by ions). Finally, the experimentally determined efficiency  $\eta_{\text{exp}}$  being as discussed above the product of  $\eta_{\text{exc}} \cdot \eta_L$  taking into account (3), (7) and (8) can be written as following:

$$\begin{aligned} \eta_{\text{exp}} &= \frac{(1+1/\eta)}{B_A \cdot \tau \cdot I_{\text{exc}} \cdot B_{G+} \cdot N} \times \\ &\times \ln \left( 1 + \eta \cdot B_A \cdot \frac{1 - e^{-\tau \cdot I_{\text{exc}} \cdot B_{G+} \cdot (1+\zeta)}}{(1+\zeta)} \cdot N \right) - \\ &- \frac{1 - e^{-\tau \cdot I_{\text{exc}} \cdot B_{G+} \cdot (1+\zeta)}}{\tau \cdot I_{\text{exc}} \cdot B_{G+} \cdot (1+\zeta)}. \end{aligned} \quad (9)$$

Figure 6 shows the experimental dependence points  $\eta_{\text{exp}}(I_{\text{exc}})$  and lines – curves calculated using (9). Curves “calculation 1” and “calculation 2” differ in that the first of these is a free approximation in respect of all parameters, and the second one is a fitting in which  $B_A$  is fixed at a small value so that the  $B_A \cdot n_0 \ll 1$ . In the first case de-excitation of the ion by luminescence composes of about a quarter of the overall PL efficiency droop, while the second one the de-excitation by own emission is practically absent ( $\eta_L \approx \eta$ ).

As it is seen from the small difference in the solid and dashed curves in Fig. 6, the formula (9) alone and its approximation of  $\eta_{\text{exp}}(I_{\text{exc}})$  can not answer the question of the contribution of luminescence AES of ions in the droop of  $\eta_{\text{exp}}$ . Therefore, some additional criteria are required to elucidate it. It was found that analysis of kinetics of luminescence decay may help here.

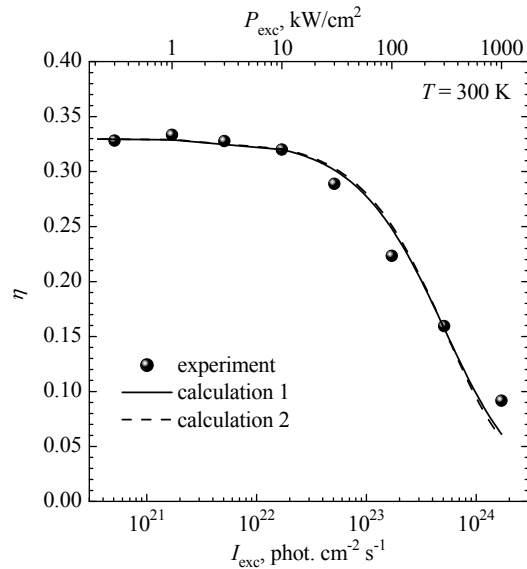


Fig. 6. Experimental (points) and calculated (lines) PL efficiencies of BaGa<sub>2</sub>S<sub>4</sub>:Eu at different excitation levels. Calculation 1 – free fitting with (9), calculation 2 – fitting with fixed at a low value of  $B_A$ , practically fully excluding the ion de-excitation by luminescence.

## 7. PL KINETICS AT OWN AND EXCITING RADIATION AES OF IONS

From general consideration it is clear that the kinetics of luminescence at high excitation levels should not differ from monoexponential decay (characteristic of low-intensity excitation) if the experimentally observed decrease in the efficiency is determined solely by the dependence  $\eta_{\text{exc}}(I_{\text{exc}})$ . Otherwise, at high pump level, at least the initial part of the luminescence kinetics is determined not only by spontaneous relaxation of the excited ions, but also by their nonradiative de-excitation with the loss of photons on AES of the rare ions. This should lead to a suppression of the luminescence signal, its downward deviation from the monoexponential decay curve signal.

Based on (1) and its solutions (2) one can obtain an expression for kinetics of luminescence  $I_{\text{PL}}(t)$ . The number of generated per unit volume per unit time of photons is equal to  $A \cdot n(t)$ , the number of photons that are

lost in the de-excitation per unit volume per unit time is equal to  $B_A \cdot n(t) \cdot A \cdot n(t)$ , therefore, per unit of time material will leave the number of photons  $I_{PL}(t)$ , proportional to  $A \cdot n(t) \cdot B_A \cdot n(t) \cdot A \cdot n(t)$ , where  $n(t)$  is given by (2). Then, after substituting (2) in this expression and simple transformations, the kinetics of the luminescence can be represented as:

$$I_{PL}(t) = An_0 e^{-\frac{t}{\eta}} \frac{\left(1 + \eta B_A n_0 \left(1 - \left(1 + \frac{1}{\eta}\right) e^{-\frac{t}{\eta}}\right)\right)}{\left(1 + \eta B_A n_0 \left(1 - e^{-\frac{t}{\eta}}\right)\right)^2}, \quad (10)$$

where  $n_0$  is given by (7). The above mentioned features of the PL kinetics in cases of different contribution of own emission to the de-excitation of ions are easily visible from (10). Difference from the monoexponential decay in the case of any breach of  $B_A \cdot n_0 \ll 1$  condition will be the stronger, the more  $B_A \cdot n_0$  is and, therefore, the greater contribution of luminescence efficiency  $\eta_L$  gives to the overall droop of experimental PL efficiency  $\eta_{exp}(I_{exc})$ .

The PL kinetics (10) for the parameters of  $B_A$ ,  $\eta$ ,  $\zeta$ ,

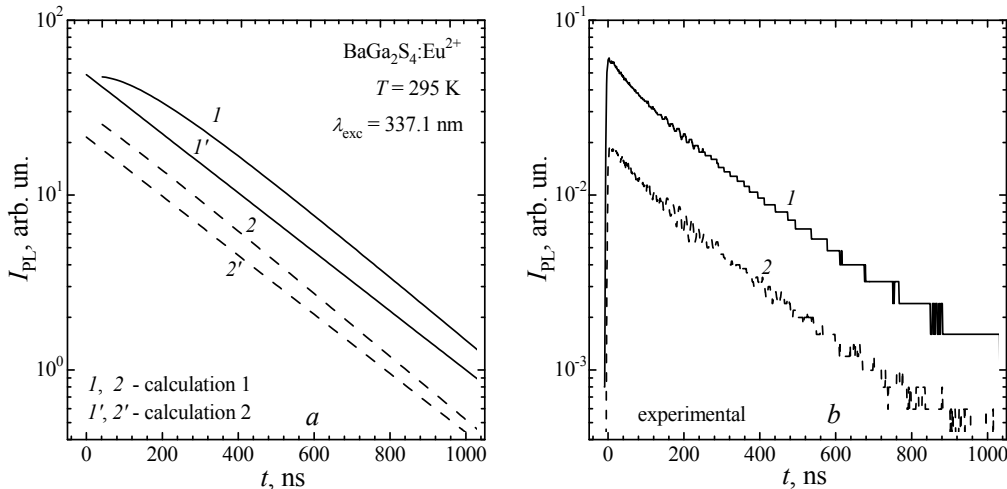


Fig. 7. Calculated (a) and measured (b) luminescence kinetics: 1, 1' –  $P_{exc} = 1 \text{ MW/cm}^2$ , curves 2, 2' –  $P_{exc} = 0.1 \text{ MW/cm}^2$ . 1, 2 – (10) with parameters from “calculation 1”, 1', 2' – (10) with parameters from “calculation 2”.

## 8. CATHODOLUMINESCENCE OF BaGa<sub>2</sub>(S,Se)<sub>4</sub> DOPED WITH Eu OR/AND Ce

All studied samples show also an intensive luminescence at e-beam excitation. CL spectra of some of the studied samples are presented in Fig. 8 (only doped with europium are shown). The main relationships between luminescence intensities at this type of excitation correlate with those at optical excitation. Spectra positions are the same independently on type of excitation. However full widths at half maximum of CL spectra of the samples with relatively high efficiency is significantly less than widths of their PL spectra (compare curves 1 and 1' in Fig. 8, for example). The difference between spectra can, in principle, be determined by higher depth of penetration of exciting electrons (in comparison with photons). As a result the whole material is the origin of emission in the case of e-beam excitation, while in the case of optical excitation only surface layer of material is considered to be excited and emit.

$B_G$ , received in fittings "calculation 1" and "calculation 2" and for two excitation intensities equal to the power densities of  $0.1 \text{ MW/cm}^2$  (dashed lines) and  $1 \text{ MW/cm}^2$  (solid line) are presented in the Fig. 7.

PL kinetics at the excitation levels  $P_{exc}$  equal to the calculated values  $I_{exc}$  ( $P_{exc} = I_{exc} \cdot h\nu \cdot e$ , where  $h\nu$  – photon energy of exciting radiation,  $e$  – electron charge) were measured to derive the realized in the present phosphor mechanism. As it is seen from Fig. 7, b, where experimental PL kinetics are presented, no suppression of the luminescence signal at the initial stage is observed even at the highest level of excitation. This fact suggests the complete absence of the nonradiative ion de-excitation by own emission. More over, the upward deviation of the measured PL kinetics from monoexponential decay in the initial stage (see Fig. 7, b) may indicate not only on compensation of AES by optical gain, but even on its excess over AES. This, in turn, suggests that lasing can be achieved in the studied materials in the form of microscopic crystals, bulk single crystals or epitaxial layers.

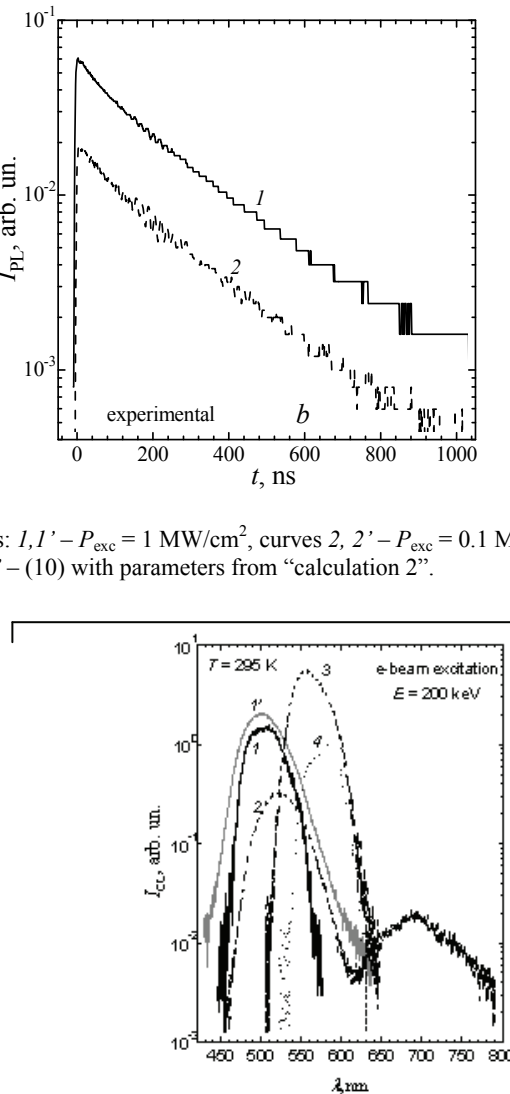


Fig. 8. CL spectra of BaGa<sub>2</sub>S<sub>4</sub>:Eu (1), BaGa<sub>2</sub>Se<sub>4</sub>:Eu (2), CaGa<sub>2</sub>S<sub>4</sub>:Eu (3) and CaGa<sub>2</sub>Se<sub>4</sub>:Eu (4) and PL spectrum of BaGa<sub>2</sub>S<sub>4</sub>:Eu (1').

Though this explanation do not give answer on the questions why low energy wings of spectra suffer from the transformation and why the observed spectrum narrowing occurs only in the samples with relatively high efficiencies ( $\text{BaGa}_2\text{S}_4:\text{Eu}$ ,  $\text{BaGa}_2\text{S}_4:\text{Eu,Ce}$ ,  $\text{BaGa}_2\text{Se}_4:\text{Eu,Ce}$ ,  $\text{CaGa}_2\text{S}_4:\text{Eu}$ ,  $\text{CaGa}_2\text{S}_4:\text{Eu}$ ) and is absent in weaker emitting samples ( $\text{BaGa}_2\text{S}_4:\text{Ce}$ ,  $\text{BaGa}_2\text{Se}_4:\text{Eu}$ ,  $\text{BaGa}_2\text{Se}_4:\text{Ce}$ ,  $\text{CaGa}_2\text{Se}_4:\text{Ce}$ ,  $\text{CaGa}_2\text{Se}_4:\text{Eu,Ce}$ ). Other explanation can be development of a stimulated emission in the corresponding phosphors at a high level of the e-beam excitation. However no significant shortening of CL kinetics relative to PL kinetics being expected was observed.

## 9. ANTI-STOKES LUMINESCENCE OF BARIUM THIOGALLATE CO-DOPED WITH ERBIUM AND YTTERBIUM

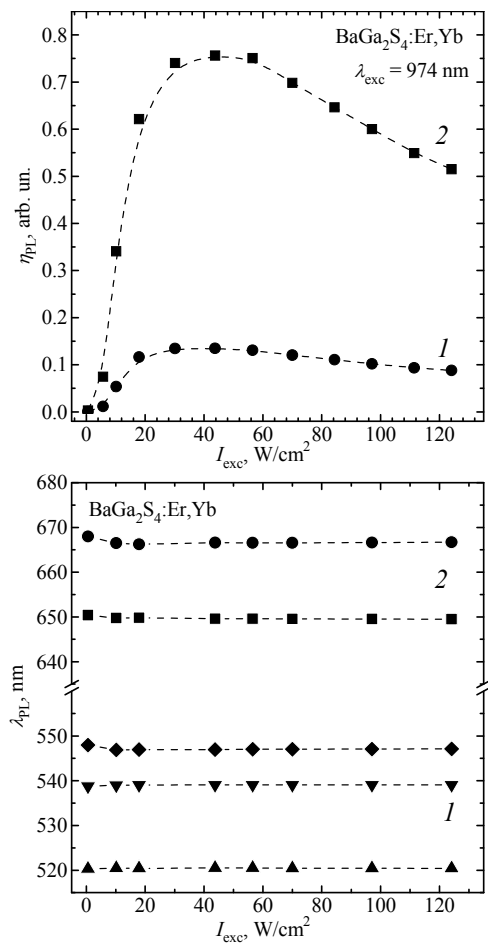


Fig. 9. Integral efficiencies (a) and separate lines positions (b) of green (1) and red (2) bands of anti-stokes luminescence of  $\text{BaGa}_2\text{S}_4:\text{Er,Yb}$ .

The  $\text{BaGa}_2\text{S}_4$  doped with only erbium studied here has no anti-stokes luminescence. This is usually explained by the small absorption cross section of the ground state of  $\text{Er}^{3+}(\text{I}_{15/2})$ . Co-doping of barium thiogallate with erbium and ytterbium has allowed obtaining luminescence in the visible spectral range at excitation by IR radiation. The 972 nm emission of a laser diode was used for the measurements. Two main groups of lines were detected in the emission of  $\text{BaGa}_2\text{S}_4:\text{Er}^{3+},\text{Yb}^{3+}$ : PL band with a

complex structure in the region of 500-560 nm corresponding to the transitions from the  $^2\text{H}_{11/2}$ ,  $^4\text{S}_{3/2}$  levels of erbium ion, and PL band in the range of 640-680 nm ( $^4\text{F}_{9/2} \rightarrow ^4\text{I}_{15/2}$ ). The  $^2\text{H}_{11/2}$ ,  $^4\text{S}_{3/2}$  and  $^4\text{F}_{9/2}$  levels of  $\text{Er}^{3+}$  ion are excited via level  $^4\text{F}_{7/2}$ , which in turn is excited by resonant energy transfer from two close ytterbium ions, as in other matrices. The cross section of absorption from the ground state of  $\text{Yb}^{3+}$  ion ( $^2\text{F}_{7/2}$ ) is significantly higher than that of  $\text{Er}^{3+}$  ( $^4\text{I}_{15/2}$ ).

It was found that that the efficiency of conversion "IR radiation  $\rightarrow$  visible radiation" has a bell-shaped dependence on the excitation intensity with a maximum at about 40 W/cm<sup>2</sup> (Fig. 9, a). An initial rise of the efficiency is most probably due to nonlinear dependence of population of erbium  $^4\text{F}_{7/2}$  level on concentration of the excited ytterbium ions. This nonlinearity results from the need to energy transfer to erbium from two excited ions of ytterbium. The decrease of the PL efficiency at high excitation level may be connected also with material heating and heat-induced activation of nonradiative channels of the excited ion relaxation.

There is no significant shift of separate lines composing two bands of anti-stokes luminescence in the whole investigated range of excitation power density. However the most short-wave line of "green" band successfully compete with others lines of the band. Its intensity rises with excitation level faster than others. This may also occur due to thermal carryover of electrons from  $^2\text{H}_{11/2}$ ,  $^4\text{S}_{3/2}$  levels back to  $^4\text{F}_{7/2}$  and may indicate excitation radiation induced heating of material.

## 10. CONCLUSION

Luminescent properties of  $(\text{Ba,Ca})\text{Ga}_2(\text{S,Se})_4$  chalcogenide semiconductors doped with rare earths (Eu, Ce, Er, Yb) has been studied in wide ranges of temperature and excitation intensity. Doped with Eu barium and calcium thiogallates can be effectively excited by blue emission of LEDs. High thermal stability of PL efficiency was observed for barium thiogallate co-doped with europium and cerium. Thiogallates were found to have luminescence efficiencies almost independent on excitation power density at levels below  $10^4 \text{ W/cm}^2$ . All samples were determined to demonstrate a significant PL efficiency droop at higher levels of excitation. AES of rare earth ions was proposed to be responsible for the droop.

Kinetics following from the solution of balance equations describing own luminescence and external exciting radiation AES of rare earth were compared between each other and with experimental ones. From the comparison was found that luminescence is not involved in the nonradiative deexcitation what suggests the potential prospects of using these compounds as laser media on the visible spectrum.

Anti-stokes luminescence (510-560 and 640-680 nm) in erbium and ytterbium co-doped barium thiogallate was obtained and investigated in respect of dependence of excitation level of IR radiation (972 nm). It was ascertained that the dependence of anti-stokes luminescence has a bell-shaped form and the optimal excitation power density is about 40 W/cm<sup>2</sup>.

- [1] N. Miura, M. Kawanishi, H. Matsumoto and R. Nakano. Jpn. J. Appl. Phys., 38, L1291 (1999).
- [2] W. Barou, R. Corvet, E. Dickey, C. King. A New Class of Blue TFEL phosphors with application to VGA Full – Color Display. SID Digest, Washington, 1993, p.761 – 764.
- [3] A.N. Georgobiani , B.G. Tagiev, O.B. Tagiev, R.B. Jabbarov, N.N. Musayeva, U.F. Kasumov. Jpn. J. Appl. Phys., 39, 434 (2000).
- [4] P. Benalloul, C. Barthou, J. Benoit. Appl. Phys. Lett., 63, 154 (1993).
- [5] P. Benalloul, C. Barthou, C. Fouassier, A.N. Georgobiani, L.S. Lepnev, Y.N. Emirov, A.N. Gruzintsev, B.G. Tagiev, O.B. Tagiev, and R.B. Jabbarov. J. Electrochem. Soc., 150, G62 (2003).
- [6] H.S. Yoo, W.B. Im, S. Vaidyanathan, B.J. Park, and D.Y. Jeon. J. Electrochem. Soc., 155, J66 (2008).
- [7] B.G. Tagiyev, R.B. Jabbarov, N.N. Musayeva. JPS, 262 (1999).
- [8] T. Prters, J. Bagio. J. Electrochem. Soc, 119, 230 (1972)
- [9] A.N. Georgobiani, B.G. Tagiev, O.B. Tagiev, R.B. Dzhabbarov, S.A. Abushov, F.A. Kazymova, C. Barthou, P. Benalloul and V.M. Salmanov. J. Appl. Spectr., 74, 369 (2007).
- [10] C. Barthou, P. Benalloul, B.G. Tagiev, O.B. Tagiev, S.A. Abushov, F.A. Kazymova, A.N. Georgobiani. J. of Physics: Condensed matter. 2004, 16, p.8075-8084.
- [11] M. Tsuda, K. Soga, H. Inoue, A. Maishima. J. of Appl. Phys., 85, 29 (1999).
- [12] S. Iida, T. Matsumoto, N.T. Mamedov, G. An, Y. Maruyama, A.I. Bairamov, B.G. Tagiev, O.B. Tagiev and R.B. Dzhabbarov. Jap. J. Appl. Phys. 36, L857 (1997).
- [13] M.C. Nostrand, R.H. Page, S.A. Payne, W.F. Krupke, and P.G. Schunemann. Opt. Lett. 24, 1215 (1999).
- [14] S. Iida. Ternary and multinary Compounds in the 21<sup>st</sup> Century, IPAP Books, 1, 302(2001).
- [15] R.B. Jabbarov, C. Chartier, B.G. Tagiev, O.B. Tagiev, N.N. Musayeva, C. Barthou, P. Benalloul. J. Phys. Chem. Sol., 66, 1049 (2005).
- [16] B.G. Tagiev, S.A. Abushov and O.B. Tagiev. J. Appl. Spectr., 76, 101 (2009).
- [17] V.Z. Zubelevich, E.V. Lutsenko, A.V. Danilchik, E.V. Muravitskaya, G.P. Yablonskiy, A.M. Pashaev, B.G. Tagiyev, O.B. Tagiyev, S.A. Abushov. JPS, 78, 154 (2011).
- [18] G.P. Yablonskii, V.Z. Zubialevich, E.V. Lutsenko, A.M. Pashaev, B.G. Tagiev, O.B. Tagiev, S.A. Abushov. Accepted to Jap. J. Appl. Phys., (2011).
- [19] A.V. Kurochkin, L.M. Maylibaeva, O.Ya Manashirov, D.K. Sattarov, V.B. Smirnov. А.В. Курочкин, Л.М. Майлибаева, О.Я. Манаширов, Д.К. Саттаров, В.Б. Смирнов Курочкин, А.В. Антистоксова люминесценция La<sub>2</sub>O<sub>2</sub>S:Er<sup>3+</sup>,Yb<sup>3+</sup> в составе триплексов при возбуждении в областях 0.93, 1.06, 1.53 и 1.59 мкм // Оптика и спектроскопия, 73, 741(1992). ??????
- [20] I. Hyppänen, J. Hölsä, J. Kankare, M. Lastusaari and L. Pihlgren. Optical Materials, 31, 1787 (2009).
- [21] V.Z. Zubelevich, E.V. Lutsenko, A.V. Danilchik, A.M. Pashaev, B.G. Tagiyev, O.B. Tagiyev, S.A. Abushov. Kvantovaya elektronika: tezisi dokl. mejdunar. nauch.-prakt konf., Minsk, BGU, 46(2010).
- [22] A.N. Georgobiani, B.G. Tagiev, S.A. Abushov, O.B. Tagiev, Z. Xu, and S. Zhao: Inorg. mat., 44, 110 (2008).
- [23] M.-Y. Kim, S.-J. Baik, W.-T. Kim, M.-S. Jin, H.-G. Kim, S.-H. Choe, and C.-S. Yoon. J. Korean Phys. Soc. 43, 128 (2003).
- [24] S.-H. Choe, M.-S. Jin, W.-T. Kim. J. Korean Phys. Soc. 47, 866 (2005).
- [25] M. Marceddu, A. Anedda, R. Corpino, A.N. Georgobiani, P.C. Ricci. Mat. Sci. Eng., 146, 216(2008).

Received: 28.03.2011

# **$SU(3)_C \times SU(3)_L \times U(1)_X$ MODEL OF ELECTROWEAK INTERACTION AND ELECTRIC CHARGE QUANTIZATION**

**O.B. ABDINOV, F.T. KHALIL - ZADE, S.S. RZAEVA**

*Laboratory of High Energy Physics*

*G.M. Abdullayev Institute of Physics NAS of Azerbaijan Republic,  
AZ143, Baku, G. Javid avenue, 33*

Basing on the general photon eigenstate and anomaly cancellation, it is shown that the electric charge quantization in  $SU(3)_C \times SU(3)_L \times U(1)_X$  model with exotic particles can be obtained independently on parameters  $\alpha$  and  $\beta$ . The fixation of hypercharges of fermions fields by the Higgs fields and dependence of the electric charges quantization conditions from the hypercharges of Higgs fields leads to the fact that the electric charge in the considered model can be quantized and fixed only in the presence of Higgs fields. In addition, we have shown that in the considered model the classical constraints following from the Yukawa interactions are equivalent to the conditions following from the P – invariance of electromagnetic interaction. The most general expressions for the gauge bosons masses, eigenstates of neutral fields and the interactions of leptons and quarks with gauge bosons have been derived in the arbitrary case.

**Keywords:** Extensions of electroweak gauge sector, Gauge Models, Electroweak interaction, Electric charge quantization, Higgs fields.

**PACS:** 12.10. Dm; 12.10.-g; 12.15.-y; 14.80.-Bn; 11.15.-q

## 1. INTRODUCTION

Standard Model (SM) of strong and electroweak interaction well describing existing experimental data involves several unanswered questions. Within SM have not been solved such problems as existence of three families [1, 2], mass hierarchy problem [1, 2], electric charge quantization etc. Solution of mentioned theoretical problems can be achieved either by introduction of additional particles or by enlargement of symmetry group. For instance, the  $SU(5)$  grand unification model [3] can unify the interactions and predicts the electric charge quantization, while the models based on  $E_6$  group can also unify the interactions and might explain the masses of the neutrinos [4].

Interesting alternative to explain the origin of generations comes from the cancellation of chiral anomalies [5]. In particular, the models with gauge group  $SU(3)_C \times SU(3)_L \times U(1)_X$  [6-9], (called 3-3-1 models) arise as a possible solution to this puzzle, since some of such models require the three generations in order to cancel chiral anomalies completely [9-11]. An additional motivation to study this kind of models comes from the fact that in these models there are some progress in investigations of such problems as neutrino mass [12], P – parity violation in nuclear transitions [13] and etc. Electric charge quantization in two model based on the  $SU(3)_C \times SU(3)_L \times U(1)_X$  gauge group, namely in the minimal model and in the model with right-handed neutrino has been considered in [14]. Authors have shown, that electric charge quantization is not dependent on the classical constraints on generating mass to the fermions, is related closely with the generation number problem and is a direct consequence of the fermion content under the anomaly free conditions.

It should be noted that the electric charge quantization problem considered in [14] has been derived for the concrete values of parameters  $\alpha$  and  $\beta$ . Besides in these type models based on  $SU(3)_C \times SU(3)_L \times U(1)_X$  group

symmetry [5-14], the expressions for the masses of neutral gauge bosons and eigenstates of neutral fields have been obtained in particular case.

It has been shown [15, 16] that photon eigenstate depends from the hypercharges of Higgs fields (see, also [14]), that leads to necessity of more detailed research of electric charge quantization in gauge theories. This work is devoted to investigation of electric charge quantization in  $SU(3)_C \times SU(3)_L \times U(1)_X$  model with exotic particles independent of parameters  $\alpha$  and  $\beta$ .

## 2. MODEL STRUCTURE

The electric charge is defined in general as a linear combination of the diagonal generators of  $SU(3)_C \times SU(3)_L \times U(1)_X$  group

$$\hat{Q} = \alpha \hat{T}_3 + \beta \hat{T}_8 + X \hat{I}, \quad (1)$$

with  $T_3 = \text{diag}(1, -1, 0)/2$  and  $T_8 = \text{diag}(1, 1, -2)/2\sqrt{3}$ , where the normalization chosen is  $\text{Tr}(T_\alpha T_\beta) = \delta_{\alpha\beta}/2$  and  $I = \text{diag}(1, 1, 1)$  is the identity matrix. The value of the parameters  $\alpha$  and  $\beta$  determines the fermion assignment and it is customary to use this number to classify the different models (see, for example [17]).

The hypercharges of fermions (as well as the Higgs) fields causing interaction with Maxwell field, is defined as

$$\hat{Y} = \beta \hat{T}_8 + X \hat{I}. \quad (2)$$

Note that as the aim of this paper is the study of electric charge quantization, the expressions of electric charge (1) and hypercharge (2) further are not used.

Let's consider the case when symmetry is broken by the Higgs fields

$$\langle \chi \rangle = \frac{1}{\sqrt{2}} \begin{pmatrix} 0 \\ 0 \\ V \end{pmatrix}, \quad \langle \rho \rangle = \frac{1}{\sqrt{2}} \begin{pmatrix} 0 \\ v \\ 0 \end{pmatrix}, \quad \langle \eta \rangle = \frac{1}{\sqrt{2}} \begin{pmatrix} u \\ 0 \\ 0 \end{pmatrix}. \quad (3)$$

The part of interaction Lagrangian responsible for the Higgs fields looks like

$$V_{kin} = (D_\mu \chi)^+ (D_\mu \chi) + (D_\mu \eta)^+ (D_\mu \eta) + (D_\mu \rho)^+ (D_\mu \rho). \quad (4)$$

The covariant derivative  $D_\mu$  is given by

$$D_\mu = \partial_\mu - ig T_a W_{a\mu} - ig' T_9 X B_\mu, \quad (5)$$

where  $T_a$  ( $a = 1, \dots, 8$ ) are the  $SU(3)_L$  generators, and  $T_9 = \text{diag}(1, 1, 1)/\sqrt{6}$  are defined as  $\text{Tr}(T_a T_b) = \delta_{ab}/2$ , ( $a, b = 1, 2, \dots, 9$ );  $g$  and  $g'$  – coupling constants.

To keep consistency with the effective theory, the VEVs in the model satisfy the constraint:  $V \gg v \gg u$  (similarly to papers [7]).

For lepton and quark fields we choose the flowing representations (we will consider one family of leptons and quarks without mixing):

$$\psi_{eL} = \begin{pmatrix} v_e \\ e^- \\ N \end{pmatrix}_L \sim (1, 3, y_{eL}), \quad \psi_{eR} = e_R \sim (1, 1, y_{eR}), \quad \psi_{NR} = N_R \sim (1, 1, y_{NR}),$$

$$\psi_{uL} = \begin{pmatrix} u \\ d \\ U \end{pmatrix}_L \sim (3, 3, y_{uL}), \quad \psi_{uR} = u_R \sim (3, 1, y_{uR}), \quad \psi_{dR} = d_R \sim (3, 1, y_{dR}), \quad \psi_{UR} = U_R \sim (3, 1, y_{UR}). \quad (6)$$

### 3. MASSES OF GAUGE BOSONS

The gauge bosons of this model form an octet  $W_{a\mu}$  and singlet  $B_\mu$  associated with  $SU(3)_L$  and  $U(1)$  accordingly. It is easy to see that the massless gauge bosons associated with  $SU(3)_C$  group decouple from the neutral bosons mass matrix and are not considered late. The masses matrix of gauge bosons arises from the

$$P_\mu = \frac{g}{2} \begin{pmatrix} W_{3\mu} + \frac{W_{8\mu}}{\sqrt{3}} + \sqrt{\frac{2}{3}} t X B_\mu & \sqrt{2} W_\mu^+ & \sqrt{2} X_\mu'^0 \\ \sqrt{2} W_\mu^- & -W_{3\mu} + \frac{W_{8\mu}}{\sqrt{3}} + \sqrt{\frac{2}{3}} t X B_\mu & \sqrt{2} Y_\mu'^- \\ \sqrt{2} X_\mu'^* & \sqrt{2} Y_\mu'^+ & -\frac{2W_{8\mu}}{\sqrt{3}} + \sqrt{\frac{2}{3}} t X B_\mu \end{pmatrix}, \quad (8)$$

where  $t = g'/g$  and

$$W_\mu^\pm = \frac{W_{1\mu} \mp i W_{2\mu}}{\sqrt{2}}, \quad Y_\mu'^\mp = \frac{W_{6\mu} \mp i W_{7\mu}}{\sqrt{2}}, \quad X_\mu'^0 = \frac{W_{4\mu} - i W_{5\mu}}{\sqrt{2}}. \quad (9)$$

In this case taking into account (3), (8) and (9) in (4) for the masses of gauge bosons we have

$$L_{mass} = M_X^2 X_\mu'^0 X_\mu'^0 + M_W^2 W_\mu^+ W_\mu^- + M_Y^2 Y_\mu'^+ Y_\mu'^- + \frac{g^2 u^2}{8} \left( W_{3\mu} + \frac{1}{\sqrt{3}} W_{8\mu} + \sqrt{\frac{2}{3}} t X_\eta B_\mu \right)^2 + \frac{g^2 v^2}{8} \left( -W_{3\mu} + \frac{1}{\sqrt{3}} W_{8\mu} + \sqrt{\frac{2}{3}} t X_\rho B_\mu \right)^2 + \frac{g^2 V^2}{8} \left( -\frac{2}{\sqrt{3}} W_{8\mu} + \sqrt{\frac{2}{3}} t X_\chi B_\mu \right)^2, \quad (10)$$

where

$$M_W^2 = \frac{g^2}{4} (v^2 + u^2), M_Y^2 = \frac{g^2}{4} (V^2 + v^2), M_X^2 = \frac{g^2}{4} (V^2 + u^2). \quad (11)$$

Note that as far as the masses (11) and interactions of gauge bosons (9) are not the subject of this paper we will not discuss them later. Discussion of these problems can be found in [5-14].

The interactions lagrangian, containing the mass of the neutral gauge bosons in this case, looks like:

$$L_{mass}^{NG} = \frac{1}{2} V^T M_0^2 V, \quad (12)$$

where  $V^T = (W_{3\mu}, W_{8\mu}, B_\mu)$  and

$$M_0^2 = \frac{g^2}{4} \begin{pmatrix} m_{11} & m_{12} & m_{13} \\ m_{12} & m_{22} & m_{23} \\ m_{13} & m_{23} & m_{33} \end{pmatrix}, \quad (13)$$

here

$$\begin{aligned} m_{11} &= (u^2 + v^2), \quad m_{12} = \frac{I}{\sqrt{3}} (u^2 - v^2), \quad m_{13} = \frac{2}{\sqrt{6}} t (u^2 X_\eta - v^2 X_\rho), \quad m_{22} = \frac{I}{3} (4V^2 + u^2 + v^2), \\ m_{23} &= \frac{2}{3\sqrt{2}} t (u^2 X_\eta + v^2 X_\rho - 2V^2 X_\chi), \quad m_{33} = \frac{2}{3} t^2 (u^2 X_\eta^2 + v^2 X_\rho^2 + V^2 X_\chi^2). \end{aligned} \quad (14)$$

The eigenvalues of the mass matrix (13) are the roots of equation

$$M^3 - \chi_1 M^2 + \chi_2 M - \chi_3 = 0, \quad (15)$$

where  $M = 4M_0^2/g^2$  and

$$\begin{aligned} \chi_1 &= \frac{2}{3} \left[ 2(u^2 + v^2 + V^2) + t^2 (u^2 X_\eta^2 + v^2 X_\rho^2 + V^2 X_\chi^2) \right], \\ \chi_2 &= \frac{4}{3} \left[ u^2 V^2 + v^2 V^2 + u^2 v^2 \right] + \frac{2t^2}{3} \left[ u^2 V^2 (X_\eta^2 + X_\chi^2 + X_\eta X_\chi) + v^2 V^2 (X_\rho^2 + X_\chi^2 + X_\rho X_\chi) + u^2 v^2 (X_\eta^2 + X_\rho^2 + X_\eta X_\rho) \right], \\ \chi_3 &= \frac{8}{9} u^2 v^2 V^2 t^2 (X_\eta + X_\rho + X_\chi)^2. \end{aligned} \quad (16)$$

In general case the eigenvalues of mass matrix corresponding to the masses of neutral gauge bosons can be real and differ from zero. In the case when the roots of equation (15) satisfy condition  $M_1^2 \gg M_2^2 \gg M_3^2$  (that is in agreement with experimental data [19]), we have

$$\begin{aligned} M_{Z_1}^2 &\approx \frac{g^2 V^2}{6} (2 + t^2 X_\chi), \quad M_2^2 \approx \frac{g^2 v^2}{6} \cdot \frac{3 + 2t^2 (X_\rho^2 + X_\chi^2 + X_\rho X_\chi)}{2 + t^2 X_\chi}, \\ M_{Z_3}^2 &\approx \frac{g'^2 u^2}{2} \cdot \frac{(X_\eta + X_\rho + X_\chi)^2}{3 + 2t^2 (X_\rho^2 + X_\chi^2 + X_\rho X_\chi)}. \end{aligned} \quad (17)$$

In our case ( $V \gg v \gg u$ ) the easiest mass in (17) can be identified with photon mass ( $M_3^2 = M_\gamma^2$ ) only under the condition

$$X_\eta + X_\rho + X_\chi = 0. \quad (18)$$

Notice that this condition also follows from the electric charge conservation [14]. In this case for the masses of neutral bosons we have

$$M_{\gamma}^2 = 0, \quad M_{Z_{1,2}}^2 \approx \frac{g^2}{8} \left[ \chi_1 \pm \sqrt{\chi_1^2 - 4\chi_2} \right]. \quad (19)$$

The easiest of massive neutral vector bosons (19), can be identified with SM  $Z$ -boson  $M_{Z_2} \equiv M_Z$ .

#### 4. ELECTRIC CHARGE QUANTIZATION

Transformation of neutral fields  $W_{3\mu}, W_{8\mu}, B_\mu$  to the physical photon field, can be written in the form

$$A_\mu = a_1 W_{3\mu} + a_2 W_{8\mu} + a_3 B_\mu. \quad (20)$$

The eigenstate with zero eigenvalue follow from the equation

$$M_0^2 \begin{pmatrix} a_1 \\ a_2 \\ a_3 \end{pmatrix} = 0. \quad (21)$$

It can be checked that (taking into account (18)) the matrix  $M_0^2$  has a non-degenerate zero eigenvalue and corresponding eigenstate can be identified with physical photon field  $A_\mu$ .

In the considering model for the quantities  $a_i$  ( $i = 1 \div 3$ ) we have

$$\begin{aligned} a_1 &= -\frac{g'}{\sqrt{2}g} (X_\rho - X_\eta), \quad a_2 = \frac{3g'}{\sqrt{6}g} (X_\rho + X_\eta) \\ a_3 &= -\frac{\sqrt{3}g}{g}, \end{aligned} \quad (22)$$

where

$$\bar{g} = g \left[ 3 + 2t^2 (X_\eta^2 + X_\rho^2 + X_\eta X_\rho) \right]^{1/2}. \quad (23)$$

From the expressions (20), (22) and (23) one can see that, the photon eigenstate is independent on VEVs structure. This is a natural consequence of the  $U(1)$  invariance [14-16]. However photon eigenstate depends from the Higgs fields hypercharges. Moreover, to be consistent with the QED based on the unbroken  $U(1)$  gauge group, the photon field has to keep the general properties of the electromagnetic interaction in the framework of the 3-3-1 model, such as the parity invariant nature [20]. These would help us to obtain some consequences related to quantities which are independent on VEVs structure.

At first let us consider interaction of leptons with the electromagnetic field. In the considered model it looks like

$$L_{l\gamma} = Q_\nu \bar{\nu}_e \gamma_\mu (1 + \gamma_5) \nu_e A_\mu + \bar{e} \gamma_\mu (Q_{0e} + Q'_{0e} \gamma_5) e A_\mu + \bar{N} \gamma_\mu (Q_N + Q'_N \gamma_5) N A_\mu, \quad (24)$$

where

$$\begin{aligned} Q_\nu &= \frac{g}{4} [a_1 + \frac{1}{\sqrt{3}} a_2 + \sqrt{\frac{2}{3}} t a_3 y_{lL}], \quad Q_{0e} = \frac{g}{4} [-a_1 + \frac{1}{\sqrt{3}} a_2 + \sqrt{\frac{2}{3}} t a_3 (y_{lL} + y_{eR})], \\ Q'_{0e} &= \frac{g}{4} [a_1 + \frac{1}{\sqrt{3}} a_2 + \sqrt{\frac{2}{3}} t a_3 (y_{lL} - y_{eR})], \quad Q_N = \frac{g}{4} [-\frac{2}{\sqrt{3}} a_2 + \sqrt{\frac{2}{3}} t a_3 (y_{lL} + y_{NR})], \\ Q'_N &= -\frac{g}{4} [-\frac{2}{\sqrt{3}} a_2 + \sqrt{\frac{2}{3}} t a_3 (y_{lL} - y_{NR})]. \end{aligned} \quad (25)$$

Taking into account the parity invariance of the electromagnetic interaction from (24), we have

$$Q_\nu = 0, \quad Q'_{0e} = 0, \quad Q'_N = 0. \quad (26)$$

In the considered case when neutrino has not the right component, the requirement parity invariance of electromagnetic interaction and the condition of neutrino charge equality to zero are equivalent. Besides, from the condition of parity invariance of electromagnetic interaction we have the relations between hypercharges of Higgs and lepton fields

$$y_{lL} = X_\eta, \quad y_{eR} = X_\eta - X_\rho, \quad y_{NR} = X_\eta - X_\chi. \quad (27)$$

Consequently for the electric charges of leptons we have

$$Q_\nu = 0, \quad Q_{0e} = -Q_e, \quad Q_N = -Q_e \frac{2X_\eta + X_\rho}{X_\eta - X_\rho}, \quad (28)$$

where

$$Q_e = \frac{gg'}{\sqrt{2}g} (X_\eta - X_\rho). \quad (30)$$

In the considered model the Yukawa interactions which induce masses for the leptons can be written as

$$L_Y^l = f_e \bar{\psi}_{IL} \rho \psi_{eR} + f_N \bar{\psi}_{IL} \chi \psi_{NR} + h.c. \quad (31)$$

From (31) under the U (1) invariance we also have conditions (27). As a result we can conclude that conditions following from the P-invariance of electromagnetic interaction are equivalent to the conditions following from the Yukawa interactions which induce masses for the leptons. The equations (27) are the fixing condition for the hypercharges of the leptons fields by the Higgs fields and further it will be shown that they are also the conditions of electric charge quantization of leptons.

Let's consider interaction of quarks with electromagnetic field. In the considered model it looks like

$$L_{q\gamma} = \bar{u} \gamma_\mu (Q_u + Q'_u \gamma_5) u A_\mu + \bar{d} \gamma_\mu (Q_d + Q'_d \gamma_5) d A_\mu + \bar{U} \gamma_\mu (Q_U + Q'_U \gamma_5) U A_\mu, \quad (32)$$

where

$$\begin{aligned} Q_u &= \frac{g}{4} [a_1 + \frac{1}{\sqrt{3}} a_2 + \sqrt{\frac{2}{3}} t a_3 (y_{QL} + y_{uR})], \quad Q'_u = \frac{g}{4} [a_1 + \frac{1}{\sqrt{3}} a_2 + \sqrt{\frac{2}{3}} t a_3 (y_{QL} - y_{uR})], \\ Q_d &= \frac{g}{4} [-a_1 + \frac{1}{\sqrt{3}} a_2 + \sqrt{\frac{2}{3}} t a_3 (y_{QL} + y_{dR})], \quad Q'_d = \frac{g}{4} [-a_1 + \frac{1}{\sqrt{3}} a_2 + \sqrt{\frac{2}{3}} t a_3 (y_{QL} - y_{dR})], \\ Q_U &= \frac{g}{4} [-\frac{2}{\sqrt{3}} a_2 + \sqrt{\frac{2}{3}} t a_3 (y_{QL} + y_{UR})], \quad Q'_U = \frac{g}{4} [-\frac{2}{\sqrt{3}} a_2 + \sqrt{\frac{2}{3}} t a_3 (y_{QL} - y_{UR})]. \end{aligned} \quad (33)$$

Similarly to the of leptons case taking into account P-invariance of electromagnetic interaction from (32) and (33) we have conditions

$$Q'_u = 0, \quad Q'_d = 0, \quad Q'_U = 0. \quad (34)$$

These conditions lead to the following relations between hypercharges of Higgs and quarks fields

$$y_{QL} - y_{uR} = X_\eta, \quad y_{QL} - y_{dR} = X_\rho, \quad y_{QL} - y_{UR} = X_\chi. \quad (35)$$

The expressions (35) fix the left and right hypercharges difference of quarks fields are also the conditions of quarks electric charge quantization. Equations (35) also follow from the Yukawa interactions which induce masses for the quarks

$$L_Y^q = f_u \bar{\psi}_{QL} \eta \psi_{uR} + f_d \bar{\psi}_{QL} \rho \psi_{dR} + f_U \bar{\psi}_{QL} \chi \psi_{UR} + h.c., \quad (36)$$

Similarly to the leptons case we can conclude that conditions following from the P-invariance of electromagnetic interaction are equivalent to the conditions following from the Yukawa interactions which induce masses for the quarks. (See also [15, 16]). Taking into account (35), (22) and (18) in (33) for the quarks electric charges we have

$$Q_u = Q_e \frac{X_\eta - y_{QL}}{X_\eta - X_\rho} \quad Q_d = Q_e \frac{X_\rho - y_{QL}}{X_\eta - X_\rho} \quad Q_U = Q_e \frac{X_\chi - y_{QL}}{X_\eta - X_\rho} \quad (37)$$

The obtained expressions (28) and (37) can be considered as the evidence of electric charge quantization of leptons and quarks. However these expressions do not define numerical values of electric charges of leptons and quarks (in terms of electron charge). For obtaining of the numerical values for the leptons and quarks electric charges, it is necessary to have the additional relations between fermions field hypercharges. Such of relations can be obtained from the conditions of cancellations of gauge [5, 21] and mixed gauge-gravitational anomalies [22]. In the considered model we have

$$\begin{aligned}
 y_{IL} + 3y_{QL} &= 0, \\
 3y_{QL} - y_{uR} - y_{dR} - y_{UR} &= 0, \\
 3y_{IL} + 9y_{QL} - 3(y_{uR} + y_{dR} + y_{UR}) - y_{eR} - y_{NR} &= 0, \\
 3y_{IL}^3 + 9y_{QL}^3 - 3(y_{uR}^3 + y_{dR}^3 + y_{UR}^3) - y_{eR}^3 - y_{NR}^3 &= 0.
 \end{aligned} \tag{38}$$

From the first equation (38) (with taken into account (27)) we have:

$$y_{QL} = -\frac{1}{3}X_\eta, \quad y_{uR} = -\frac{4}{3}X_\eta \quad y_{dR} = -\frac{1}{3}X_\eta - X_\rho, \quad y_{UR} = -\frac{1}{3}X_\eta - X_\chi. \tag{39}$$

Taking into account (35) from the second and third equations (38) we have expression (18). Fourth equation (38) leads to:

$$X_\eta = -X_\rho. \tag{40}$$

Consequently for the hypercharges of fermions fields we have:

$$\begin{aligned}
 y_{IL} &= X_\eta, & y_{eR} &= 2X_\eta & y_{NR} &= X_\eta. \\
 y_{QL} &= -\frac{1}{3}X_\eta, & y_{uR} &= -\frac{4}{3}X_\eta, & y_{dR} &= \frac{2}{3}X_\eta, & y_{UR} &= -\frac{1}{3}X_\eta.
 \end{aligned} \tag{41}$$

This leads to the electric charge quantization

$$Q_v = 0, \quad Q_e = \frac{\sqrt{2}gg'X_\eta}{\left(3+2X_\eta^2t^2\right)^{1/2}}, \quad Q_N = -\frac{1}{2}Q_e, \quad Q_u = \frac{2}{3}Q_e, \quad Q_d = -\frac{1}{3}Q_e, \quad Q_U = \frac{1}{6}Q_e, \tag{42}$$

Similar expressions can be written for other fermions. Conditions (27) and (35) fix the hypercharges of fermions fields. The conditions following from the anomalies cancellations (taking into account (27) and (35)), fix hypercharges of all remained fields. Thus, if there are no conditions (27) and (35) it is obvious that to solve the equations following from the anomalies cancellations is impossible and consequently there are not electric charge quantizations, hence, these conditions are electric charge quantization ones. However these conditions depend from the hypercharges of Higgs fields, so these facts can be interpreted as a presence of influence of Higgs fields on the electric charge quantization.

It is necessary to note that unlike results of work [14] in which authors have shown that electric charge quantization does not depend on the classical constraints on generating mass to the fermions in the considered case the conditions following from the Yukawa interactions are equivalent to the conditions following from the P – invariance of electromagnetic interaction. Equivalence of conditions following from the P – invariance of electromagnetic interaction and from the classical

---

constraints on generating mass to the fermions in the SM and  $SU(3)_C \times SU(3)_L \times U(1)_X \times U'(1)_{X'}$  model has been shown in [15,16]. This fact may be useful for the explanation of the P – invariance of electromagnetic interaction.

#### 4. CHARGED AND NEUTRAL CURRENTS

For the eigenstate with nonzero eigenvalue we have

$$\begin{aligned}
 Z_{1\mu} &= b_1 W_{3\mu} + b_2 W_{8\mu} + b_3 B_\mu, \\
 Z_{2\mu} &= c_1 W_{3\mu} + c_2 W_{8\mu} + c_3 B_\mu,
 \end{aligned} \tag{43}$$

where

$$b_1 = \frac{\sqrt{2}g'\mathcal{A}_1}{g_Z}, \quad b_2 = \frac{\sqrt{6}g'\mathcal{A}_2}{g_Z}, \quad b_3 = -\frac{\sqrt{3}g\mathcal{A}_3}{g_Z}. \tag{44}$$

Here (in the case of arbitrary Higgs field hypercharges)

$$\mathcal{A}_I = (u^2 X_\eta - v^2 X_\rho)(4V^2 - \frac{12M_{Z_I}^2}{g^2}) + 2u^2 v^2 (X_\eta - X_\rho) + 2V^2 (u^2 - v^2) X_\chi,$$

$$\begin{aligned} \mathcal{A}_2 &= 2u^2 v^2 (X_\eta + X_\rho) - 2V^2 (u^2 + v^2) X_\chi - \frac{4M_{Z_1}^2}{g^2} (v^2 X_\rho + u^2 X_\eta - 2V^2 X_\chi), \\ \mathcal{A}_3 &= -4V^2 (u^2 + v^2) + \frac{16M_{Z_1}^2}{g^2} (u^2 + v^2 + V^2) - \frac{48M_{Z_1}^2}{g^4}, \quad \bar{g}_Z = \left[ 3g^2 \mathcal{A}_3^2 + 2g'^2 (\mathcal{A}_1^2 + 3\mathcal{A}_2^2) \right]^{1/2}. \end{aligned} \quad (45)$$

The magnitudes  $c_i$  ( $i = 1 \div 3$ ) can be found from the appropriate expressions  $b_i$  by substitution  $Z_1 \rightarrow Z_2$ .

In the most general form the interaction lagrangian of fermions with gauge bosons has the following form:

$$L_{int} = i\bar{\psi}_{fL} \gamma_\mu (\partial_\mu - ig \sum_{a=1}^8 T_a W_{a\mu} - ig' T_9 X B_\mu) \psi_{fL} + i\bar{\psi}_{fR} \gamma_\mu (\partial_\mu - ig' X B_\mu) \psi_{fR}, \quad (46)$$

where  $\psi_{fL}$ ,  $\psi_{fR}$  – are left and right fermions fields.

Taking into account (43) and (46) we have

$$L_{int} = L_f^{CC} + L_f^{NC}, \quad (47)$$

where

$$L_f^{CC} = \frac{g}{\sqrt{2}} (\bar{v}_e W_\mu e_L + \bar{N}_L Y'_\mu e_L + \bar{v}_N X'_\mu N_L + \bar{d}_L W_\mu u_L + \bar{U}_L Y'_\mu d_L + \bar{u} X'_\mu U_L + h.c.). \quad (48)$$

$$L_f^{NC} = \frac{g}{4} \sum_f \bar{f} \gamma_\mu (g_{V_1}^f + g_{A_1}^f \gamma_5) f Z_{1\mu} + \frac{g}{4} \sum_f \bar{f} \gamma_\mu (g_{V_2}^f + g_{A_2}^f \gamma_5) f Z_{2\mu}, \quad (49)$$

where  $f$  takes values  $\nu_e, e, N, d, u, U$ . For the coupling constants we have:

$$g_{V_1}^l = k_1^l b_1 + \frac{k_2^l}{\sqrt{3}} b_2 + \sqrt{\frac{2}{3}} t b_3 (y_{lL} \pm y_{lR}), \quad g_{V_1}^q = k_1^q b_1 + \frac{k_2^q}{\sqrt{3}} b_2 + \sqrt{\frac{2}{3}} t b_3 (y_{qL} \pm y_{qR}), \quad (50)$$

where upper signs relate to victories coupling constants and lower signs relates to axial ones. Besides:

$$\begin{aligned} \text{for } l = \nu &\quad k_1^\nu = k_2^\nu = 1; \quad y_{\nu R} = 0; \quad \text{for } l = e & k_1^e = -1, \quad k_2^e = 1; \quad \text{for } l = N & \quad k_1^N = 0, \quad k_2^N = -1; \\ \text{for } q = u &\quad k_1^u = k_2^u = 1; \quad \text{for } q = d & k_1^d = -1, \quad k_2^d = 1; \quad \text{for } q = U & \quad k_1^U = 0, \quad k_2^U = 1. \end{aligned}$$

Note that the expression of magnitudes  $g_{V_2}^f$  и  $g_{A_2}^f$  – can be obtained from appropriate expressions (50) by the substitution  $b_i \rightarrow c_i$ .

- 
- |  |  |
|--|--|
| <ul style="list-style-type: none"> <li>[1] P. Laugacker, Phys. Rev., 72, p.185, 1981.</li> <li>[2] P. Fayet, hep-ph/9812300, 1998; S.Harfin. hep-ph/9709356, H. Green, J. Schwars and E. Witten. Superstring theory. Cambridge University Press, 1987.</li> <li>[3] H. Georgi and S.L. Glashow. Phys.Rep.Lett.,32, p.438, 1974; H. Georgi, H. R. Quinn and S. Weinberg. Phys. Rev., Lett. 33, p.451, 1974;</li> <li>[4] F. Gürsey, P. Ramond, and Sikivie, Phys. Lett., B 60, p.177, 1975; F. Gürsey and M. Serdaroglu, Lett. Nuovo Cimento Soc. Ital. Fis, 21, p.28, 1978; H. Fritzsch and P. Minkowski, Phys. Lett., B63, p.99, 1976.</li> </ul> | <ul style="list-style-type: none"> <li>[5] C. Bouchiat, J. Iliopoulos and Ph. Meyer. Phys. Lett., B 38, p.519, 1972; H.Georgi and S. L. Glashow. Phys. Rev., D 9, p.416, 1974; D. Gross and R. Jackiv. Phys. Rev., D6, p.477, 1972 .</li> <li>[6] F. Pisano and V. Pleitez, Phys. Rev., D46, p.410, 1992; P. H. Frampton, Phys. Rev. Lett., 69, p.2889, 1992; R. Foot et al, Phys. Rev., D47, p.4158, 1993.</li> <li>[7] M. Singer, J.W.F. Valle and J. Schechter, Phys. Rev., D22, p.738, 1980; R. Foot, H. N. Long and Tuan A. Tran, Phys. Rev., D50, p.34, 1994; J.C. Montero, F. Pisano and V. Pleitez, Phys.</li> </ul> |
|--|--|

**SU(3)<sub>C</sub> × SU(3)<sub>L</sub> × U(1)<sub>X</sub> MODEL OF ELECTROWEAK INTERACTION AND ELECTRIC CHARGE QUANTIZATION**

- Rev., D47, p.2918, 1993; Phys. Rev., D54, p.4691, 1996.
- [8] *H.N. Long*, Phys. Rev., D53, p.437, 1996.
- [9] *W.A. Ponce, D.A. Gutierrez and L.A. Sanchez*. Phys. Rev. D 69, p.055007, 2004; *A.G. Dias and V. Pleitez*, Phys. Rev. D 69, p.077702, 2004.
- [10] *W.A. Ponce, D.A. Gutierrez and L.A. Sanchez*. hep – ph/031243v3, 2004.
- [11] *W.A. Ponce, J.B. Flores and L.A. Sanchez*. hep – ph/0103100v2, 2001.
- [12] *H.N. Long*. hep – ph /9603258v1, 1996; hep – ph/9504274v2, 1995.
- [13] *P.V. Dong, H.N. Long and D.T. Nhun*. hep – ph /0604199v2, 2006.
- [14] *P.V. Dong and H. N. Long*. hep – ph/0507155v1, 2005.
- [15] *O.B. Abdinov, F.T. Khalil-zade and S.S. Rzaeva*. hep – ph/0807.4359v1, 2008; *O.B. Abdinov, F.T. Khalil-zade and S. S. Rzaeva*. Fizika, c. XV, №2, p76, 2009.
- [16] *O.B. Abdinov, F.T. Khalil-zade and S.S. Rzaeva*. Fizika, c. XV, №1, p.24, 2009.
- [17] *R.A. Diaz, R.A. Martinez and F. Ochoa*. hep – ph/0309280v2, 2004.
- [18] *P.V. Dong and H.N. Long*, Eur.Phys. J.C42, 2005; hep – ph /060022.
- [19] Particle Data Group. Phys., Lett. B, v667, issues 1 – 5, 2009.
- [20] *T.D. Lee and C.N. Yang*. Phys.Rev.,104, p. 254, 1956; *A. Salam*. Nuovo Cimento, 5, p.299, 1957; *V. Kobzarev, L. Okun and I. Pomeranchuk*. Sov. J. Nucl. Phys., 3, p.837, 1966.
- [21] *S.L. Adler*. Phys.Rev, 177, p2426, 1968, *J.S. Bell and R. Jackiw*. Nuovo Cimento 60A, p.69, 1969; *S.L. Adler and W. Bardeen*. Rhys. Rev. 182, p.1517, 1969.
- [22] *R. Delbourgo and A. Salam*. Phys. Lett., B40, p.381, 1972; *T. Eguchi and P. Freund*. Phys. Rev. Lett., 37, p.1251, 1776; *L. Alvares – Gaume and E. Witten*. Nucl. Phys., B234, p. 269, 1983.

Received: 11.04.11

## GROWTH InGaN DIODE STRUCTURE AND DOUBLE EMISSION $(\text{Ca}_{1+x-y}\text{Eu}_y)\text{Ga}_2\text{S}_{4+x}$ PHOSPHOR FOR WHITE LEDs

**R. JABBAROV<sup>1</sup>, N. MUSAYEVA<sup>1</sup>, S. ABDULLAYEVA<sup>1</sup>, F. SCHOLZ<sup>2</sup>,  
T. WUNDERER<sup>2</sup>, P. BENALLOUL<sup>3</sup>, C. BARTHOU<sup>3</sup>, C. LAURENT<sup>3</sup>**

<sup>1</sup>*G.M. Abdullayev Institute of Physics, Azerbaijan NAS, Baku, Azerbaijan*

<sup>2</sup>*Institut für Optoelektronik, Ulm University, Ulm, Germany*

<sup>3</sup>*Institut de NanoSciences de Paris (INSP), UMR CNRS–Université Pierre et Marie Curie*

In the present work we report the growth of InGaN light emitting diode structure on c-plane sapphire substrate and preparation bicolor phosphor for creating phosphor converted white light emitting diode. Their optical characteristics have been investigated. It is shown that, although thermal quenching is observed, the room temperature luminescence intensity curve before and after heating process of the samples is almost identical, which indicates the thermal quenching is recoverable or no thermal degradation. It is very important aspect for pc-white LED, because heat is produced continuously during LEDs operating.

**Keywords:** light emitting diode structure, luminescence.

**PACS:** 535.37; 539.216; 539.22; 538.91-405; 548; 620.18

### 1. INTRODUCTION

White light-emitting diodes (LED) have attracted a great deal of attention in solid-state lighting application. Due to their potential for substantial energy saving, high efficiency and long lifetime, it has been projected that LEDs will broadly replace conventional incandescent and fluorescent lamps for general lighting in the future. In 2020, LED lighting efficiency is expected to be over 200 lm/W. If these goals are reached then 50% of the electrical energy currently used for lighting applications can be saved [1]. But to achieve that, there are many intermediate steps that have to be taken, for example, increasing light extraction from LED devices, improving packaging, finding better infrastructure, and discovering highly efficient LED phosphors.

Two of the key quantities in light source assessment are luminous efficacy of radiation (LER) and color rendering index (CRI). However, a key element associated with the future penetration of LEDs into solid-state lighting market is LER and this parameter is reduced with increasing LED quantity. Main requirements of white LED packaging are high luminous efficiency, high color rendering index, adjustable color stability, low thermal resistance, rapid thermal dissipation, high reliability and low cost. It is not simple task for packaging to satisfy these requirements simultaneously. In general there normally exist some contradictions such as high luminous efficiency and low correlated color temperature (CCT), high performance and low cost. Warm white LED with low CCT needs the addition of longer wavelength phosphor, which will increase the conversion loss and thereby reduce the luminous flux. Light extraction and thermal dissipation are normally interplayed. If more light is extracted, less heat should be dissipated. Low junction temperature will further increase the initial optical power and make the LED brighter. In contrast, if less light is extracted or the junction temperature is too high, there will be a harmful optical-thermal cycle that can damage the chip and cause degradation of material. Packaging design should balance these contradictions and guarantee the most favorable targets.

LED emission spectra are not absolutely stable with temperature and more over change with drive current. The

color rendering depends on the color temperature of the LED and details of the composition of the phosphors. There has extensive research and development for phosphors in LFLs/CFLs, cathode-ray tubes, and X-ray films, but most of these traditional phosphors are not suitable for pc-LED. This is usually because these phosphors do not strongly absorb violet or blue LED radiation, leading to LED package losses from scattering. Also, many traditional phosphor use  $\text{Eu}^{3+}$ ,  $\text{Tb}^{3+}$ , or  $\text{Mn}^{2+}$  activators whose transitions are forbidden with long decay times( $>1\text{ms}$ ), causing phosphor quenching due to saturation from the high LED radiation flux on the phosphor. Generally efficient and stable phosphors are based on an inorganic host, which is doped by  $\text{Eu}^{2+}$  and  $\text{Ce}^{3+}$  ions. They have very short luminescence decay times and saturate only extremely high excitation density.

Obviously, the primary requirement for a phosphor is it converting the radiation from a pump LED into luminescence emission expected from that it absorbs the pump wavelength. Strong absorption can be expected from dipole-allowed electron transitions in dopant ions, if the dopant concentration is high enough. The best known and used examples are  $\text{Ce}^{3+}$  and  $\text{Eu}^{2+}$ , which spectral location of their absorption and emission lines can be shifted due to crystal field, stokes shift may be much less varying. However, only few host materials are known in which the emission from these ions is in the green or red spectral region. In particular, new requirements for color temperature (2700-5000K), color rendering ( $\text{CRI}>75$ ), efficiency, color stability have been introduced. This leads to new challenges for the phosphor in addition to the usual requirements of high absorption, high efficiency and chemical stability. The efficiency should depend as little as possible on temperature, the phosphor must not saturate at high irradiance and the spectral emission must match the particular application. In addition particle size must ensure homogeneous color in all directions. It is not easy task to translate these requirements into phosphor design. For the past decade, there was a great deal of research on the thiogallate and thioaluminate phosphor in applications of inorganic electroluminescent displays (IELDs), field emission displays (FEDs) and white light emitting diodes (white-LEDs). [2,4]. The interest to

binary and ternary compounds such as  $\text{Ca}(\text{Sr},\text{Ba})\text{S}$  and  $\text{Ca}(\text{Sr},\text{Ba})\text{Ga}_2(\text{Al})\text{S}_4$  activated by  $\text{Eu}^{2+}$  and  $\text{Ce}^{3+}$  is start for a realization of multi-color and full color iEL devices. Flat panel displays (FPD) are the one of the most important electronics, not only technologically and scientifically, but also socially and economically. In 1970's, the main research was on multi-color and full color EL (red, green, blue and/or white) [5-7]. This problem was much harder than expected in the beginning. In 1980's, the research was focused exclusively on the development of color EL materials, such as alkaline earth compounds host material ( $\text{CaS}$ ,  $\text{SrS}$ ) with luminescent centers ( $\text{Ce}^{3+}$ ,  $\text{Eu}^{2+}$ ). Subsequently, thiogalates such as  $\text{Sr}(\text{Ca},\text{Ba})\text{Ga}_2\text{S}_4$  doped with  $\text{Eu}^{2+}$  were studied. Finally,  $\text{BaAl}_2\text{S}_4:\text{Eu}^{2+}$  was developed [8], which gave a sufficiently enough blue color available for display use. At present, the technical achievement of inorganic EL display panels is very high, i.e., the size is 30–42 inch, the luminance is enough for TV use, and the color quality is good. In 2005, a new inorganic EL was reported which exhibited very high brightness of 600,000  $\text{cd}/\text{cm}^2$  [9,10]. Finally blue inorganic EL of  $\text{BaAl}_2\text{S}_4:\text{Eu}^{2+}$  was developed, resulting in fullcolor EL-TV using "color by blue" by iFire Technology. Very recently, a new ultra bright inorganic EL of dc driven at lower than 10V has been developed.

In this paper we report a white LEDs phosphor on the base of  $\text{CaGa}_2\text{S}_4$ - $\text{CaS}$  called as composite phosphor, which has many advantages, for example one-step synthesis, double emission bands and excite by n-UV(360-410) and blue (440-480) nm LED chip efficiently.

Many of the needs for new LED phosphors have been met by the discovery and development of new phosphors over the past 10 years. During this time, the field of LED phosphors has moved from a single family of phosphor compositions-the  $\text{Ce}^{3+}$ -doped aluminate garnets-to a variety of silicate, aluminate, nitride, oxynitride, sulfide, and fluoride compositions, leading to commercial LEDs that cover a full range of white CCTs.

## 2. PRINCIPLE OF WHITE LIGHT GENERATING IN LEDs

There are several methods for generating white LEDs [11-12]. Currently, of these, a blue light-emitting diode (LED) coated with a yellow-emitting phosphor has been commercialized because it satisfies both of the following requirements: a high luminous flux and simple structure. In addition, the cost of a white LED of this type is lower than that of white LEDs composed of red, green, and blue LED chips. The main disadvantage of multichip RGB approach is strong temperature dependence of performance and high cost.

The most frequently used yellow emitting phosphor is  $\text{Y}_3\text{Al}_5\text{O}_{12}:\text{Ce}^{3+}$  (YAG:Ce). However, because YAG:Ce emits a greenish-yellow light, the emission from an InGaN-based blue LED coated with YAG:Ce is deficient in the red spectral region and its color rendering property is poor [13]. To improve the color rendering property of white LEDs, Sheu et al. used a near ultraviolet (n-UV) LED [14]. Fabricated with three different phases of phosphors, the n-UV LED-pumped white LEDs lead, firstly, to a decrease in luminous efficiency due to

reabsorption of emissions, and, secondly, also to an increase in manufacturing cost. Won et al. and Kim et al. introduced single-phase full-color-emitting phosphors for an n-UV LED-pumped white LED [15, 16]. Recently, Xie et al. and Kimura et al. reported that high brightness and good color rendering properties were achieved with nitride green/red phosphor-converted (pc) white LEDs [17]. However, both high firing temperature ( $>1600^\circ\text{C}$ ) and high  $\text{N}_2$  pressure ( $>5$  atm) are necessary to synthesize nitride phosphors [18]. In this study, we used white LEDs phosphor  $(\text{Ca}_{1+x-y}\text{Eu}_y)\text{Ga}_2\text{S}_{4+x}$ , which has many advantages, one-step synthesis, double emission bands and excited by n-UV and blue LED chip efficiently and coating technology is simple.

## 3. EXPERIMENTAL

Phosphor  $(\text{Ca}_{1+x-y}\text{Eu}_y)\text{Ga}_2\text{S}_{4+x}$ , were prepared by conventional solid state reaction without the use of any toxic gas. In order to enhance crystallinity and fluorescence radiation, the sample was subjected to post heat-treatment at  $700^\circ\text{C}$  for 6 hours in an evacuated quartz ampoule. The resulting powder samples were characterized by X-ray powder diffraction using X'Pert MRD Philips analytical diffractometer with  $\text{CuK}_\alpha$  ( $\lambda=1.54056\text{\AA}$ ) radiation and scan rate of  $0.01^\circ/\text{sec}$ . The XRD data indicated that the samples obtained consisted of two phases and were in good agreement with data  $\text{CaGa}_2\text{S}_4$  and  $\text{CaS}$ . Excitation spectra were recorded with a Jobin-Yvon spectrophotometer Fluorolog-3 using a Xenon lamp (450W). LEDs used to excite our phosphor were commercial structure emitting at wavelengths 415 and 450 nm. To make white LEDs the phosphor was put in a two component optical gel in liquid phase. Then the chip was covered with this mixture and the gel-phosphor composition was polymerized. The gel-phosphor compositions have been prepared in identical polycarbonate lenses having special cavities to put it. The samples have been prepared with identical phosphor concentration in gel to receive qualitative the same performance of different phosphors used in our experiments. Their optical characteristics have been investigated by exciting them with the different wavelengths provided by the three LED types as described above.

Some of the InGaN light emitting diode structures used to excite the phosphors for these studies grown by low pressure metalorganic vapor phase epitaxy on a c-plane sapphire substrate. A  $2\ \mu\text{m}$  thick undoped GaN buffer layer including a thin in-situ deposited SiN defect reduction layer was grown after AlN nucleation layer. The active region consisted of a single InGaN quantum well grown at about  $800\ ^\circ\text{C}$  with an In content of about 10% covered by a  $10\ \text{nm}$  thick AlGaN electron barrier layer. The structure was finished by a  $200\ \text{nm}$  thick Mg-doped GaN layer. The bare LED structure shows strong electroluminescence at  $415\ \text{nm}$  with a FWHM of  $110\ \text{meV}$  at room temperature.

## 4. RESULTS AND DISCUSSION

Fig.1 presents the excitation spectra at 300K for  $(\text{Ca}_{1+x-y}\text{Eu}_y)\text{Ga}_2\text{S}_{4-x}$ , phosphors at 558 and 680 nm analysis wavelengths.

From the excitation spectra is clearly shown that this composite phosphor can be excited efficiently either by blue or by n-UV light LEDs. According our previous result [19] the emission spectra under different excitation wavelength 360, 400, 430, and 460 nm the two bands correspond to the emission in the ternary  $4f^65d_1(a_1) \rightarrow 4f^7(^8S_{7/2})$  and binary  $4f^65d_1(t_{2g}) \rightarrow 4f^7(^8S_{7/2})$  compounds of transitions of  $\text{Eu}^{2+}$ . Emission spectra of  $(\text{Ca}_{1+x-y}\text{Eu}_y)\text{Ga}_2\text{S}_{4+x}$ , under 415 nm LED excitation measured at different temperature presented in fig.2.

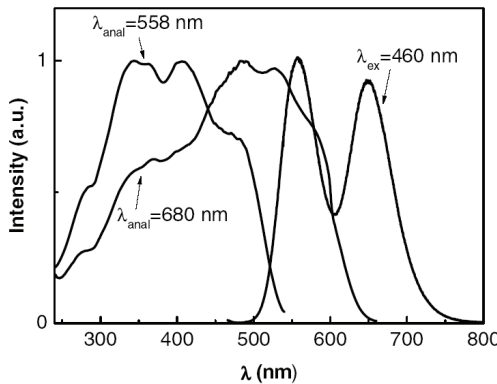


Fig. 1. PLE spectra of phosphor at 300 K.

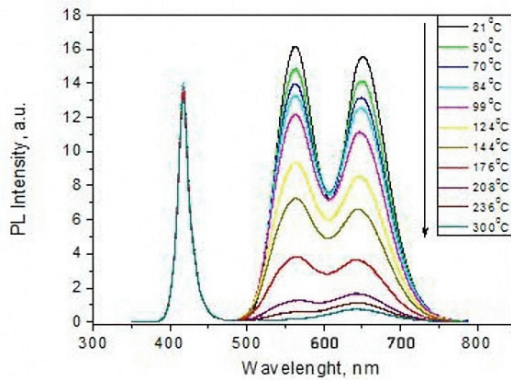


Fig. 2. Emission spectra of phosphor under 415 nm LED excitation with different temperature.

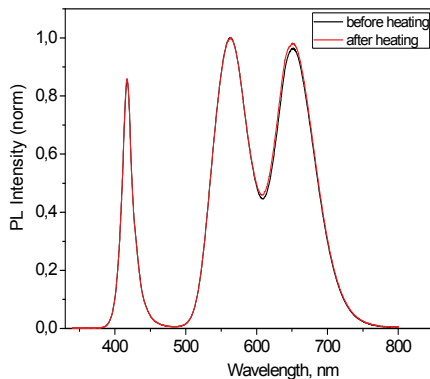


Fig. 3. Luminescence intensity before and after heating of phosphor.

Although thermal quenching is observed, the room temperature luminescence intensity curve before and after heating process of the samples is almost identical, which

indicates the thermal quenching is recoverable or no thermal degradation. (fig.3).

It is very important aspect for pc-white LED, because heat is produced continuously during LEDs operating. In fig.4 shown the spectra of  $(\text{Ca}_{1+x-y}\text{Eu}_y)\text{Ga}_2\text{S}_{4+x}$ , under 415 and 450 nm LED.

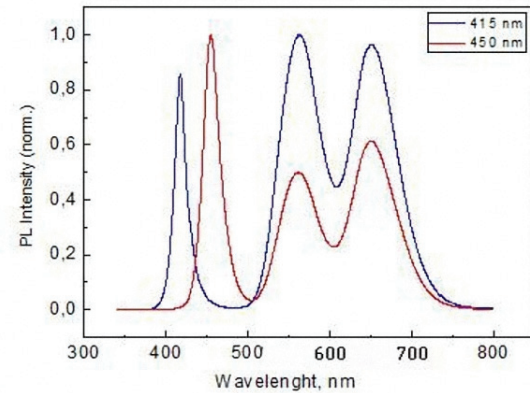


Fig. 4. Normalized spectra of  $(\text{Ca}_{1+x-y}\text{Eu}_y)\text{Ga}_2\text{S}_{4+x}$  under 415 and 450 nm LED excitations.

The best conversion of LED radiation to the phosphor is 415 nm, but the green spectral gap between the LED and phosphor band is narrow for 450 nm LED excitation. Fig.5(a, b) shows EL spectra of white LED under following forward currents of direct current (DC): 10, 20, 30, 40, 50, 60, 70, 80 and 90 mA.

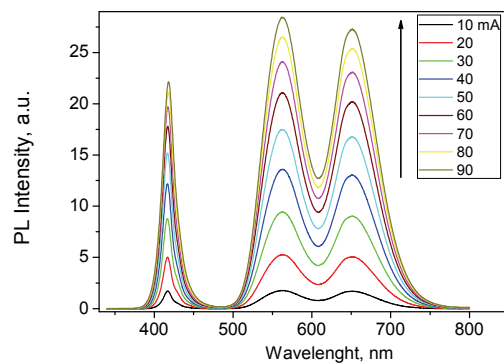


Fig. 5a. EL of 415 nm LED chip with phosphor under different applied current.

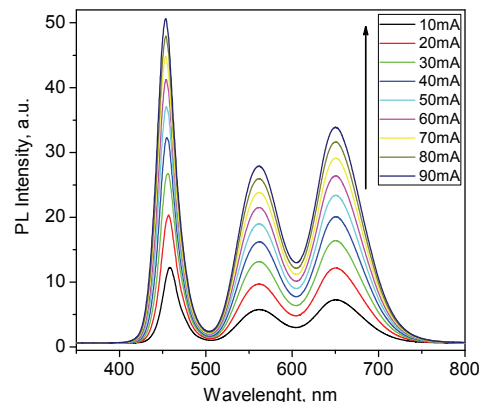


Fig. 5b. EL of 450 nm LED chip with phosphor under different applied current.

Each emitting bands 560 nm and 650nm in this study is showed a superior property whereby the emission intensity increases without saturation as a function of the applied current under 415 and 450 nm LED excitations. The intensity of red band is more higher under 450 nm LED but the green band is narrow for excitation 450 nm

LED and this is influenced to color rendering index.

#### ACKNOWLEDGEMENT

Part of this work have been financially supported by CNRS/ANAS collaboration 0904 project and TWAS research Grant program 09-084 RG/Phys/AS\_G.

- 
- [1] *J.R. Brodrick.* (2003). DOE Solid State Lighting Status and Future, U.S. Dept. of Energy, Office of Energy Efficiency and Renewable Energy. <http://www.netl.doe.gov/ssl/PDFs/DOE%20SPIE%20Presentation%20080304.pdf>
  - [2] *P. Benalloul, C. Barthou, J. Benoit, L. Eichenauer and A. Zeinert.* Appl. Phys. Lett. 63, 1993, 1954.
  - [3] *P. Benalloul, C. Barthou and J. Benoit.* J. Alloys Compounds 275–277, 1998, 709-715.
  - [4] *W.A. Barrow, R.E. Covert, E. Dickey, C.N. King, C. Laakso, S.S. Sun, R.T. Tuenge, R.C. Wentross and J. Kane.* 1993 Digest of Technical Papers of International Symposium, SID (Seattle, Washington). p. 761.
  - [5] *H. Kobayashi.* Proc. SPIE 1910, 15 (1993).
  - [6] *S. Shinoya and S. Kobayashi (eds.),* Electroluminescence (Springer-Verlag, 1998).
  - [7] *Y. Ono (ed),* Electroluminescent display (World Scientific Publishing, 1995).
  - [8] *N. Miura, M. Kawanishi, H. Matsumoto, and R. Nakano,* Jpn. J. Appl. Phys. 38, L1291 (1999).
  - [9] News Release on Kuraray web-page, [http://www.kuraray.co.jp/en/release/2005/051012\\_2.html](http://www.kuraray.co.jp/en/release/2005/051012_2.html), and the related patent: JP 2005-336275A, JP 2005-339924A, JP 2006-199794A.
  - [10] *C. Barthou, R.B. Jabbarov, P. Benalloul, C. Chartier, N. N. Musayeva, B.G. Tagiev, and O.B. Tagiev,* Journal of The Electrochemical Society, 153, (3), G253-G258, 2006.
  - [11] Light Emitting Diodes for General Illumination. Tutorial materials (OIDA), ed. by Jeff I. Tsao (2002). <http://lighting.sandia.gov/>.
  - [12] Strategies in Light 2004, Conf. Proc. (San-Diego, 2004). <strategies-u.com>.
  - [13] *H.S. Jang, W.B. Im, D.C. Lee, D.Y. Jeon, S.S. Kim, J. Lumin.* 126, 371 (2007)
  - [14] *J.K. Sheu, S.J. Chang, C.H. Kuo, Y.K. Su, L.W. Wu, Y.C. Lin, W.C. Lai, J.M. Tsai, G.C. Chi, R.K. Wu,* IEEE Photonics Technol. Lett. 15, 18 (2003).
  - [15] *Y.-H. Won, H.S. Jang, W.B. Im, J.S. Lee, D.Y. Jeon,* Appl. Phys. Lett. 89, 231909 (2006).
  - [16] *J.S. Kim, P.E. Jeon, Y.H. Park, J.C. Choi, H.L. Park, G.C. Kim, T.W. Kim,* Appl. Phys. Lett. 85, 3696 (2004)
  - [17] *R.-J. Xie, N. Hirosaki, N. Kimura, K. Sakuma, M. Mitomo,* Appl.Phys. Lett. 90, 191101 (2007)
  - [18] *R.-J. Xie, N. Hirosaki, M. Mitomo, K. Sakuma, N. Kimura,* Appl. Phys. Lett. 89, 241103 (2006)
  - [19] *R. Jabbarov, N. Musayeva, F. Scholz, T. Wunderer, A. N. Turkin, S. S. Shirokov, and A. E. Yunovich,* Phys. Stat. Solidi A, 206, n.2, 287-292, 2009.

Received: 11.04.2011

## DISPERSION OF OPTICAL PARAMETERS OF $\text{YbBi}_2\text{Te}_4$ AND $\text{YbBi}_4\text{Se}_7$

**M.A. MAKHMUDOVA, N.Z. JALILOV**

*G.M. Abdullayev Institute of Physics of Azerbaijan National Academy of Sciences  
AZ-1143, Baku, H. Javid ave., 33*

The reflection coefficients  $R(E)$  of polycrystalline samples  $\text{YbBi}_2\text{Te}_4$  and  $\text{YbBi}_4\text{Se}_7$  in interval of beam energy 1-6 eV normally falling on the surface have been measured in the work. The optical parameters ( $\varepsilon_2 E$ ,  $\varepsilon_2 E^2$ ,  $n_{\text{ef}}$ ,  $\varepsilon_{0,\text{ef}}$ ) of the given compounds are defined with the help of Kramers-Kronig relations.

**Keywords:** dispersion, optical ytterbium, bismuth, chalcogenide, triple reflections.

**PACS:** 535.3; 539.2/6:539./.04

### INTRODUCTION

The results of optical parameter definition of  $\text{YbBi}_2\text{Te}_4$  and  $\text{YbBi}_4\text{Se}_7$  on the base of measurement of reflection coefficient  $R(E)$  of normally incident beam with the energy 1-6 eV on the sample surface are presented in the present work. The functions of their optical parameters are defined by Kramers-Kronig method. This question in these materials hasn't been investigated yet, whereas the materials of such type are the analogues of  $\text{Ln}_3\text{X}_4$  and  $\text{Ln}_5\text{X}_7$  [1] and have the series of interesting physical properties: the superconductivity and luminescent characteristics are revealed in them. They are also perspective ones for the preparation of thermo-sensitive resistances and thermocouples, gauges in the remote control devices by thermal processes.

From [2] it follows that the section of  $\text{YbTe-Bi}_2\text{Te}_3$  compound is quasi-binary one. Two compounds  $\text{YbBi}_2\text{Te}_4$  and  $\text{YbBi}_4\text{Te}_7$  crystallize in system. The section liquidus consists of primary crystallization branches of  $\alpha$ -solid solutions  $\text{YbTe}$ ,  $\text{YbBi}_2\text{Te}_4$  and  $\text{YbBi}_4\text{Te}_7$  on the basis of bismuth telluride.  $\text{YbBi}_2\text{Te}_4$  compound forms on peritectic reaction  $L + \text{YbTe} \rightleftharpoons \text{YbBi}_2\text{Te}_4$  at 873K temperature. It is established that  $\text{YbBi}_2\text{Te}_4$  has the polymorphous modifications:  $\alpha$  -  $\text{YbBi}_2\text{Te}_4$  at temperature 673K transits into  $\beta$  -  $\text{YbBi}_2\text{Te}_4$ . As it is seen in works [3,4],  $\text{YbBi}_2\text{Te}_4$  compound is isostructurally to  $\text{YbSb}_2\text{Te}_4$  and has the cubic lattice of type  $\text{Th}_3\text{P}_4$  with the elementary cell parameters:  $a=10,48\pm0,01A$ ,  $d_{\text{exp}}=6,35$ ,  $d_{\text{calc}}=6,40\text{gr}/\text{cm}^3$ , the microhardness is  $H\mu=1500\text{MPa}$ .  $\text{YbBi}_2\text{Te}_4$  compound is the semiconductor with narrow forbidden band  $\Delta E=0,34\text{eV}$ .

$\text{YbBi}_4\text{Se}_7$  compound melts without decomposition at temperature 963K. The compound has the dark grey color and is stable in the air. Its picometric density is  $d_{\text{picn}}=6,30\text{gr}/\text{cm}^3$ , the microhardness is  $H\mu=1660\text{ MPa}$ . The structure of  $\text{YbBi}_2\text{Se}_4$  and  $\text{YbBi}_4\text{Se}_7$  single crystals has been studied [5]. The structure of  $\text{YbBi}_4\text{Se}_7$  is related to hexagonal syngony. The elementary cell parameters are:  $a=13,90$ ,  $c=14,384A$ ,  $d_{\text{exp}}=7,45$ ,  $d_{\text{calc}}=7,5430\text{gr}/\text{cm}^3$ . The electric conduction  $\text{YbBi}_4\text{Se}_7$  is  $1,5 \cdot 10^{-4}\text{ Om}^{-1} \cdot m^{-1}$  at 300K, the width of forbidden band is equal to  $\Delta E=0,81\text{eV}$ .

The semiconductor optical spectra are connected with their electronic structures. The material energy level defining their many physicochemical parameters is the one of its main parameters. The knowing of material dispersion allows us to predict the principal possibilities

of definite property realization and its application in semiconductor electronics.

The obtaining and investigation of optical parameter spectra of  $\text{YbBi}_2\text{Te}_4$  and  $\text{YbBi}_4\text{Se}_7$  are the aim o the present work.

### THE EXPERIMENT TECHNIQUE

The synthesis of  $\text{YbBi}_2\text{Te}_4$  and  $\text{YbBi}_4\text{Se}_7$  compounds has been carried out analogically on the synthesis of  $\text{LnBi}_2\text{S}_4$  ( $\text{Se}_4\text{Te}_4$ ) and  $\text{LnBi}_4\text{S}_7(\text{Se}_7\text{Te}_7)$  compounds. The synthesis is carried out from elements bismuth by B-3 cleanliness, ytterbium Ytb-1 cleanliness, tellurium B-3 cleanliness, selenium B-5 cleanliness by ampoule method or by alloying of binary compounds. The synthesis is carried out in the quartz ampoules evacuated (up to  $\sim 10^{-2}\text{Pa}$ ) at temperature 900-1200K in the dependence on the composition.

After compound synthesis finishing the homogenizing annealing during 200h at temperature 100°C has been carried out.

From the obtained materials we have prepared the samples for measurement of reflection coefficient  $R(E)$ . The measurements are carried out by double-beam method in energy range 1-6 eV at normal incidence of light beam on the sample.

As it is known the interaction of light with the substance is described by refractive  $n$  and absorption  $k$  indexes which characterize the phase and dumping of plane wave in the substance. These values can be defined with the help of  $R(E)$  by Kramers-Kronig formula:

$$\theta(E_0) = \frac{E_0}{\pi} \int_0^\infty \frac{\ln R(E)}{E_0^2 - E^2} dE . \quad (1)$$

The optical parameters of the investigated materials are obtained with the help of computer programs applied in refs. [6-9].

### THE RESULTS AND DISCUSSION

In the present work the  $R(E)$  is measured and on its base the optical functions of  $\text{YbBi}_2\text{Te}_4$  and  $\text{YbBi}_4\text{Se}_7$  are defined. Their such parameters as: reflected light phase  $\theta$ , absorption  $k$  and refractive  $n$  indexes, real  $\varepsilon_1$  and imaginary  $\varepsilon_2$  parts of dielectric constants, absorption coefficient  $\alpha$ , the functions of characteristic volume  $-\text{Im}g \varepsilon^{-1}$  and surface  $-\text{Im}g (\varepsilon+1)^{-1}$  electron loss,

## DISPERSION OF $\text{YbBi}_2\text{Te}_4$ AND $\text{YbBi}_4\text{Se}_7$ OPTICAL PARAMETERS

electrooptical differential functions ( $\alpha$ ,  $\beta$ ), optical conduction  $\varepsilon_2 E$ , integral function of bound state density  $\varepsilon_2 E^2$ , effective static dielectric constant  $\varepsilon_{0,\text{ef}}(E)$ , effective number of valence electrons  $n_{\text{ef}}(E)$  taking part in optical transitions up to the given energy  $E$  are obtained.

From them the measurement results of reflection coefficients  $R(E)$  and the functions of their optical

parameters  $\text{YbBi}_2\text{Te}_4$  and  $\text{YbBi}_4\text{Se}_7$  such as coefficient of optical conduction  $\varepsilon_2 E$ , integral function of bound state density  $\varepsilon_2 E^2$ , effective static dielectric constant  $\varepsilon_{0,\text{ef}}(E)$ , effective number of valence electrons  $n_{\text{ef}}(E)$  taking part in optical transitions up to the given energy  $E$  defined on its base, are presented on fig.1-5.

Table

| Samples                    | The band-to-band optical transitions in polycrystalline $\text{YbBi}_2\text{Te}_4$ and $\text{YbBi}_4\text{Se}_7$ in energy range 1÷6 eV. |      |      |      |      |      |      |
|----------------------------|---|------|------|------|------|------|------|
| $\text{YbBi}_2\text{Te}_4$ | 1,15  | 1,49 | 1,94 | 2,14 | 3,26 | 4,13 | 4,95 |
| $\text{YbBi}_4\text{Se}_7$ | 1,94  | 3,44 | 4,42 | 4,5  | 5,17 | 5,39 | -    |

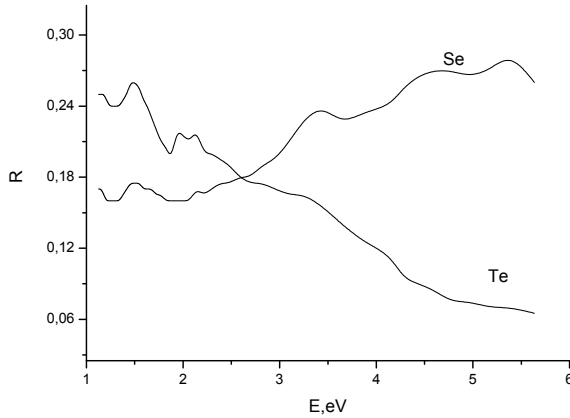


Fig. 1. The reflection coefficient  $R(E)$  spectra:  
 $\text{YbBi}_2\text{Te}_4$  (curve Te) and  $\text{YbBi}_4\text{Se}_7$  (curve Se).

The measurement results of reflection coefficient  $R(E)$  spectra in  $\text{YbBi}_2\text{Te}_4$  and  $\text{YbBi}_4\text{Se}_7$  in beam energy range 1÷6 eV are presented on the fig.1. As it is seen from this figure in  $\text{YbBi}_2\text{Te}_4$  case the reflection coefficient  $R(E)$  decreases with energy, for  $\text{YbBi}_4\text{Se}_7$  its values increase and in the both cases the peaks which are connected with optical transitions in them are observed on the curves.

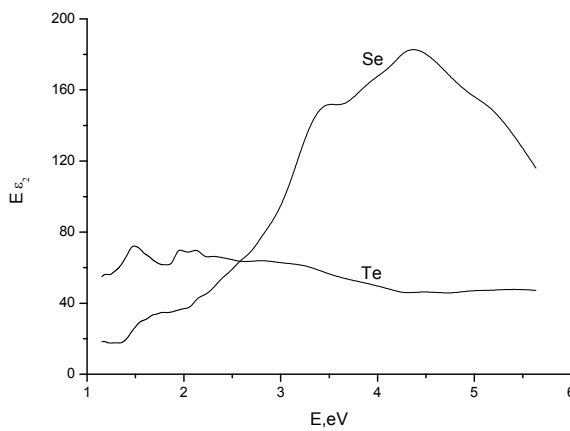


Fig. 2. The spectra of optical conductance  $E\varepsilon_2$ :  
 $\text{YbBi}_2\text{Te}_4$  (curve Te) and  $\text{YbBi}_4\text{Se}_7$  (curve Se).

The calculation results on formula (1) of the spectra of optical conductance  $E\varepsilon_2$  are given in the fig.2. The values

of optical transitions defined by optical conduction peaks are given in the table.

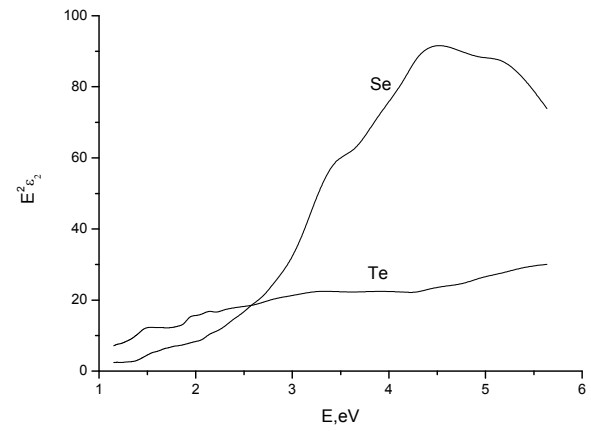


Fig. 3. The spectra of integral functions of bound state density  $\varepsilon_2 E^2$ :  $\text{YbBi}_2\text{Te}_4$  (curve Te) and  $\text{YbBi}_4\text{Se}_7$  (curve Se).

The spectra of integral functions of bound state density  $\varepsilon_2 E^2$  are given on fig.3. The state density is connected with material electronic structure and is the one of its important parameters.

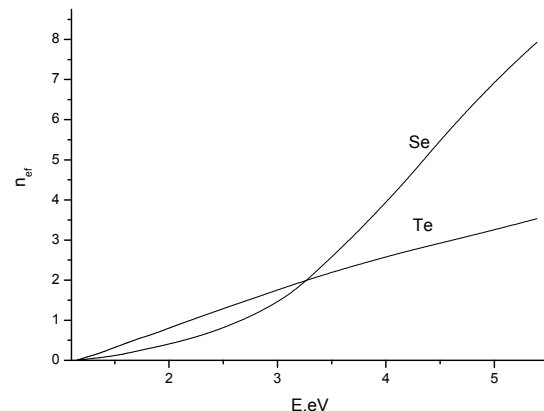


Fig. 4. The spectra of effective number of valence electrons  $n_{\text{ef}}(E)$  taking part in transitions up to the given energy  $E$  for  $\text{YbBi}_2\text{Te}_4$  (curve Te) and  $\text{YbBi}_4\text{Se}_7$  (curve Se).

The values of the number of valence electrons  $n_{\text{ef}}(E)$  taking part in transitions up to the given energy  $E$  for

$\text{YbBi}_2\text{Te}_4$  (curve Te) and  $\text{YbBi}_4\text{Se}_7$  (curve Se) defined on  $(\varepsilon_2)$  are given in fig.4. As it is seen from the figure the values of effective number of valence electrons for  $\text{YbBi}_2\text{Te}_4$  is less than for  $\text{YbBi}_4\text{Se}_7$ . The effective number of valence electrons determines the total force of oscillators in  $(\varepsilon_2)$  spectra.

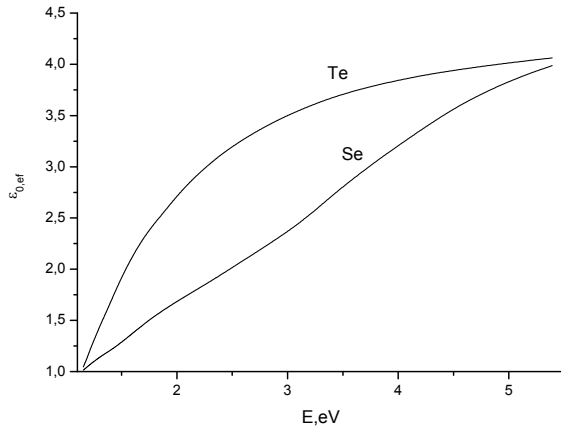


Fig.5. The spectra of effective static dielectric constant  $\varepsilon_{0,\text{eff}}(E)$  of  $\text{YbBi}_2\text{Te}_4$  (curve Te) and  $\text{YbBi}_4\text{Se}_7$  (curve Se).

The spectra of effective static dielectric constant  $\varepsilon_{0,\text{eff}}(E)$  are presented on fig.5. The effective static dielectric constant is connected with electron number taking part in optical transitions at which its values with the energy don't change. In our case this condition isn't carried out, however, for  $\text{YbBi}_2\text{Te}_4$  case this condition is carried out.

As it is shown in [1] the analytic singularity of imaginary part of complex dielectric constant  $\varepsilon_2(E)$  and function of bound state density  $dN/dE$  almost coincide. Moreover the gradient of band-to-band states makes the main contribution into analytic singularity of function  $dN/dE$ :

$$\frac{dN_{ij}}{dE} \sim \int \frac{dS_k}{|\nabla_k E_{ij}|},$$

where  $E_{ij}(k)=E_j(k)-E_i(k)$  is the distance between conduction band and valence band. The values  $dN/dE$  near critic points in  $k$ -space defined by the expression  $|\nabla_k E_{ij}|=0$  and also the position of critic points and transition types can be theoretically calculated from band structures.

The analysis of  $\varepsilon_2(E)$ ,  $dN/dE$  function and reflection coefficient  $R(E)$  shows that the disposition in energy spectrum and peak characters are similar ones or very close to these parameters. That's why the values of corresponding band-to-band intervals and band natures can be defined with the help of the direct comparison of the crystal reflection experimental curves in  $E>E_g$  range with theoretical calculations of  $dN/dE$  function.

As it is mentioned in [9] the state density  $N(E)$  is the conception which is similarly usable one for crystalline and non-crystalline substances. According to experimental data results the speed of state density in non-crystalline substance doesn't strongly differ from corresponding speed of state density in the crystal.

The thin structure in the first case can be lubricated and the local states can appear in forbidden band. The band structure saves at this condition, because it mainly is defined by atom short range ordering.

As it is seen from fig.1 the dependences of reflection coefficients for  $\text{YbBi}_2\text{Te}_4$  and  $\text{YbBi}_4\text{Se}_7$  differ. The reflection coefficients  $R(E)$  for  $\text{YbBi}_2\text{Te}_4$  decreases with energy increase and for  $\text{YbBi}_4\text{Se}_7$  its increase is observed. This fact can be explained by the difference of their electronic structure which depends on the composition, structure and material atomic structure. As it is seen from fig.2-5 the analogous differences are observed in other optical parameters.

Thus, the semiconductor materials  $\text{YbBi}_2\text{Te}_4$  and  $\text{YbBi}_4\text{Se}_7$  are synthesized in the work on the base of the measurement of their reflection coefficient in energy range 1-6 eV, their optical parameters such as  $(\varepsilon_2 E, \varepsilon_2 E^2, n_{\text{ef}}, \varepsilon_{0,\text{eff}})$  are defined.

- 
- [1] Khimiya redkikh elementov. Khalkolantanati redkikh elementov. Moskva «Nauka» 1989, s.288. (in Russian)
  - [2] T.F. Maksudova. Phiziko-khimicheskie osnovi polucheniya troynikh soedineniy v sistemakh Eu(Yb)-Sb(Bi)-X (X=S, Se, Te). Avtoreferat diss. dok. khim. nauk, Baku, 2005, s.47. (in Russian)
  - [3] P.G. Rustamov, T.F. Maksudova, O.M. Aliev. Poluchenie monokristallov  $\text{YbSb}_2(\text{Bi}_2)\text{Te}_4$ ,  $\text{YbSb}_4(\text{Bi}_4)\text{Te}_7$  i ikh svoystva. Tezisi dokl. IV Vses. konf. po troynim poluprovodnikam i ikh primeneniyu. Kishinyov: ShTIINTsA 1983, s.45. (in Russian)
  - [4] O.M. Aliev. Phiziko-khimicheskie osnovi polucheniya troynikh poluprovodnikovikh faz, proizvodnoy strukturi  $\text{Yb}_3\text{S}_4$  i  $\text{Y}_5\text{S}_7$ . Avtoref. diss. dok. khim nauk. Sverdlovsk: IKh UNTsAN SSSR, 1985.47 s. (in Russian)
  - [5] O.M. Aliev, T.F. Maksudova, N.D. Samsonova, L.D. Finkelshteyn, P.G. Rustamov. Neorgan. Materiali. 1986, t.22, № 1, s.29-32. (in Russian)
  - [6] F. Platsman, P. Volf. Volni i vzaimodeystviya v plazme tverdogo tela. Moskva, Mir, 1975, s.436. (in Russian)
  - [7] N.Z. Djalilov, S.I. Mekhtieva, N.M. Abdullayev. Izv. NAN Azerb., seriya fiz.-mat. i tekhn., fiz. i astr., №5, 2007. (in Russian)
  - [8] N.Z. Djalilov, S.I. Mekhtieva, N.M. Abdullayev. NAN Azerb., seriya fiz.-mat. i tekhn., fiz. i astr., Institut Fiziki, Fizika, t. XIII, №4, 2007, s.89-91. (in Russian)
  - [9] N.Z. Djalilov, S.I. Mekhtieva, N.M. Abdullayev, M.I. Veliev. Spektro otrajeniya monokristallov  $\text{Bi}_2\text{Te}_3$ . Akad. H.Abdullayevin 85 illik yubileyine hesr olunmuş konfrans materialları, Fizika, 2003, s. 10. (in Russian)

**DISPERSION OF OPTICAL PARAMETER OF YbBi<sub>2</sub>Te<sub>4</sub> AND YbBi<sub>4</sub>Se<sub>7</sub>**

- [10] *N.Z. Djalilov, S.I. Mekhtieva, N.M. Abdullayev, M.I. Veliev.* Spektri otrajeniya kristallov Bi<sub>2</sub>Te<sub>3</sub> v oblasti 1-6 eV. II Ukrainskaya nauch. konf. po poluprovod., 19-23 sentyabrya, 2004. (in Russian)
- [11] *N.Z. Djalilov, S.I. Mekhtieva, N.M. Abdullayev, M.I. Veliev.* Issledovanie spektrov otrajeniya v monokristalle Bi<sub>2</sub>Te<sub>3</sub>. Izv. NAN Azerb., seriya fiz.-mat. i tekhn., fiz. i astr., 2004, №4, (in Russian)
- [12] *N.Z. Djalilov, S.I. Mekhtieva, N.M. Abdullayev, N.R. Mamedov.* Issledovanie spektra otrajeniya tellurida vismuta. Dokladi NAN Azerb., 2007, LXIII, №4, (in Russian)
- [13] *N.Z. Djalilov, N.M. Abdullayev, N.R. Mamedov.* Koeffitsient otrajeniya plenok sistemi Bi<sub>2</sub>Te<sub>3</sub>-Bi<sub>2</sub>Se<sub>3</sub>. Amorfnie i Mikrokristallicheskie Poluprovodniki. Sb. trudov VI Mejd. konf., Sankt-Peterburg, 2008. (in Russian)
- [14] *N.Z. Djalilov, N.M. Abdullayev, N.R. Mamedov, G.M. Askerov.* Spektri otrajeniya kristallov i plenok Bi<sub>2</sub>Te<sub>3</sub>-Bi<sub>2</sub>Se<sub>3</sub><Tb> i Bi<sub>2</sub>Te<sub>3</sub>-Bi<sub>2</sub>Se<sub>3</sub><Cl>. Fizika, 2008, XIV, №3, (in Russian)
- [15] *N.Z. Djalilov, G.M. Damirov.* Opticheskie parametri amorfnykh tverdikh rastvorov sistemi Se-S. Trudi X Mejd. konf. «Opto-nanoelektronika, nanotekhnologii i mikrosistemi». Ulyanovsk, 2008. (in Russian)
- [16] *N.Z. Djalilov, G.M. Damirov.* Spektri opticheskikh parametrov amorfnykh tverdikh rastvorov sistemi Se-S. Izv. NAN Azerb., seriya fiz.-mat. i tekhn., fiz. i astr., XXVIII, №5, 2008. (in Russian)
- [17] *N.Z. Djalilov, M.A. Makhmudova.* Opticheskie spektri YbBi<sub>2</sub>Te<sub>4</sub> i YbBi<sub>4</sub>Se<sub>7</sub>. Izv. NAN Azerb., seriya fiz.-mat. i tekhn., fiz. i astr., XXVIII, №2, 2010 (v pechati). (in Russian)
- [18] *N. Mott, E. Devis.* Elektronnije protsessi v nekristallicheskikh veshestvakh. Moskva «Mir», 1982. (in Russian)
- [19] *K.K. Shvarts, Yu.N. Shunin, Ya.A. Teteris.* Izv. AN Lat. SSR, ser. fiz. i tekhn. nauk. №4, 1987, 51-57. (in Russian)

Received: 04.04.2011

## SPATIAL STRUCTURE OF NEUROPEPTIDE ALLATOSTATIN-4

**L.I. VELIYEVA, E.Z. ALIYEV**

*Baku State University, Z. Khalilov str.23, AZ 1148, Baku, Azerbaijan*

*e-mail: Lala.Veliyeva@rambler.ru*

By method of conformational analysis there was determined the spatial structure of neuropeptide allatostatin -4 belonging to allatostatins family. On the basic of value of intramolecular conformational energy calculation was conducted quantitative assessment of the stability of molecule's possible conformational status in dipolar medium terms.

**Keywords:** Allatostatin, conformational analysis, structure.

**PACS:** 87.10.-e

### INTRODUCTION

The allatostatins form a family of bioactive neuropeptides which play key role in regulation of processes of synthesis and juvenile hormone release at various kinds of insects [1-4]. The important role in realization of allatostatin functions play their conformational characteristics and 3-dimensional spatial configuration, studying of which necessary for understanding the mechanisms of neuropeptides is functioning at molecular level. In present work by method of molecular mechanics on the basic of phased approach described in works [5,6] there was conducted investigation of structure and conformational dynamics of allatostatin-4 molecule. Primary molecule structure offered in work [4] is a linear sequence of eight aminoacid residuals H-Asp<sup>1</sup>- Arg<sup>2</sup>-Leu<sup>3</sup> - Tyr<sup>4</sup> -Ser<sup>5</sup>-Phe<sup>6</sup>-Gly<sup>7</sup>-Leu<sup>8</sup>-NH<sub>2</sub> and includes residuals with aromatic rings in positions 4 and 6 of neuropeptide chain. The molecule contains also two residuals with charged functional groups at the ends of own side-chains. This is negatively charged carboxylic group at the residual of asparagine acid (Asp<sup>1</sup>) and positively charged guanidine group at arginine (Arg<sup>2</sup>). Presence of volumetric side chain with branching at C<sup>γ</sup> – atom in leucine residuals (Leu<sup>3</sup>, Leu<sup>8</sup>) may influence fundamentally onto interaction of conformational condition of main and side chains of allatostatin-4 molecule.

### METHOD OF CALCULATION

On fig.1 is shown scheme of phased calculation of allatostatin-4 molecule fragments. Molecule structure modeling was conducted by methods of theoretical conformational analysis subject to polar atom environment on the basic of pack of applied computer programs [7]. They based on quantitative calculation of complete conformational energy of investigated fragment and search of its local minimums by method of conjugate gradients. Conformational energy ( $E_{\text{conf}}$ ) is represented as additive contributions sum from non-valence ( $E_{\text{nonval}}$ ), electrostatic ( $E_{\text{el}}$ ) atoms interactions, torsional rotational energy around valent connections ( $E_{\text{tors}}$ ) and energy of hydrogen bonds formation ( $E_{\text{h.b.}}$ ). Semiempirical potential functions and their parameterization used in work are taken from work [8]. Polar atom environment in calculation experiment was modeling by means of character  $\epsilon=10$  and parameter D describing depth of hydrogen bonds equal to -1,5 kcal/mole in Morse potential [5,6]. In work there also used standard system

of identifiers describing conformational conditions either separate aminoacid residuals (residual shapes – B, R, P and L) or fragments of various length. Aminoacid residual's shape (i.e. shape of its main chain) characterizes appliance of  $\varphi$  and  $\psi$  angles to peptide chain of one or another area of conformational space: R( $\varphi, \psi=-180^{\circ} \div 0^{\circ}$ ); B( $\varphi=-180^{\circ} \div 0^{\circ}, \psi=0^{\circ} \div 180^{\circ}$ ); L( $\varphi, \psi=0^{\circ} \div 180^{\circ}$ ) and P ( $\varphi=0^{\circ} \div 180^{\circ}, \psi=-180^{\circ} \div 0^{\circ}$ ).

Match of aminoacid residuals shapes in polypeptide chain forms a shape of chain itself. Folding method of two adjacent residuals of peptide chain in independent coordinate space X, Y, Z defines by two types of shapes: *e* and *f*. They describe unfolded and folded types of polypeptide chain structure accordingly. Structural types vary by angle  $\theta=\psi_i + \varphi_{i+1}$ , value of which at all possible shapes of residuals approximately to zero in shape *e* or equal  $180^{\circ}$  in shape *f*. Conformational conditions of side chain of aminoacid residuals indicate by symbols  $\chi_i$  where  $i=1, 2$  or  $3$  for  $\chi$  angle value in interval  $0^{\circ} \div 120^{\circ}$ ;  $-120^{\circ} \div 0^{\circ}$  and  $-120^{\circ} \div 0^{\circ}$ , accordingly. Counting of dihedral angle of rotation was conducted according to standard nomenclature [9].

### RESULTS OF CALCULATION AND THEIR DISCUSSION

Spatial structure of the molecule studied on the basic of stable conformations of methyl amides N- acetyl - $\alpha$ -aminoacids subject to various orientations of their side chains. Phased calculation of allatostatin – 4 spatial structures included studying of conformational conditions of sequentially expandable fragments due to scheme shown in fig.1. While calculating tripeptide fragment Asp<sup>1</sup>- Arg<sup>2</sup>-Leu<sup>3</sup> for asparagine acid taking account of R and B shapes of main chain because for the first residual of molecule B and L shapes are isoenergetic. For leucine residual in position 3 of peptide chain there had been took into account R, B and L shapes of its main chain, but values of dihedral angles of side chain ( $\chi_1, \chi_2$ ) before beginning of the conformational energy minimization procedure were taken as equal to 60, 180 and -60°. Angle value  $\chi_2$  in side chain of residuals Tyr and Phe took equal to 90°. Total number of low-energy conformational conditions calculated for fragments Asp<sup>1</sup>- Arg<sup>2</sup>-Leu<sup>3</sup>, Leu<sup>3</sup>-Tyr<sup>4</sup>-Ser<sup>5</sup>-Phe<sup>6</sup> and Phe<sup>6</sup>-Gly<sup>7</sup>-Leu<sup>8</sup> were accordingly 171, 1215 and 324. Values of relative energy of fragment conformations chosen for next calculation of overlapping section of allatostatin-4 molecule depending on peptide chain length vary in range of  $0^{\circ} \div 3$  kcal/mol. As

## SPATIAL STRUCTURE OF NEUROPEPTIDE ALLATOSTATIN-4

follows from calculation results, more than half of allowed conformations on tripeptide fragment Asp<sup>1</sup>-Arg<sup>2</sup>-Leu<sup>3</sup> (58, 9%) belong to shape *fe* with semifolded shape of peptide chain. Due to calculation results the conformations of shape *fe* almost for 2.0 kcal/mol energetically efficient than low-energetical conformations with fully open shape of the main chain (into interval of relative energy 0÷3 kcal/mole fits only 7,7 % of low-energetical conformations of shape *ee*). Preference of such structures stipulated by effective interactions of side chains of oppositely charged arginine

residues side chains and asparagine acid. Contribution from energy of interresidual interactions in *fe* shape conformations is maximal and makes -7,8 kcal/mol. Totally summary contribution from the energy of non-valence and electrostatic interactions of these residuals in low-energetically conformations vary in range of -5,1 ÷ -7,8 kcal/mol. In global conformation of *fe* shape there forms hydrogen bond between oxygen atom of carboxyl group Asp<sup>1</sup> and hydrogen atom of amid group of Arg<sup>2</sup> main chain. Total number of low-energy tripeptide conformations chosen for next calculations phase was 39.

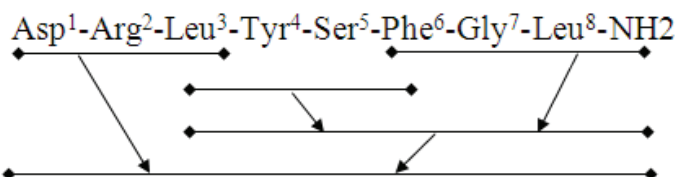


Fig. 1. Calculation scheme of stable conformations of allatostatin-4 molecule

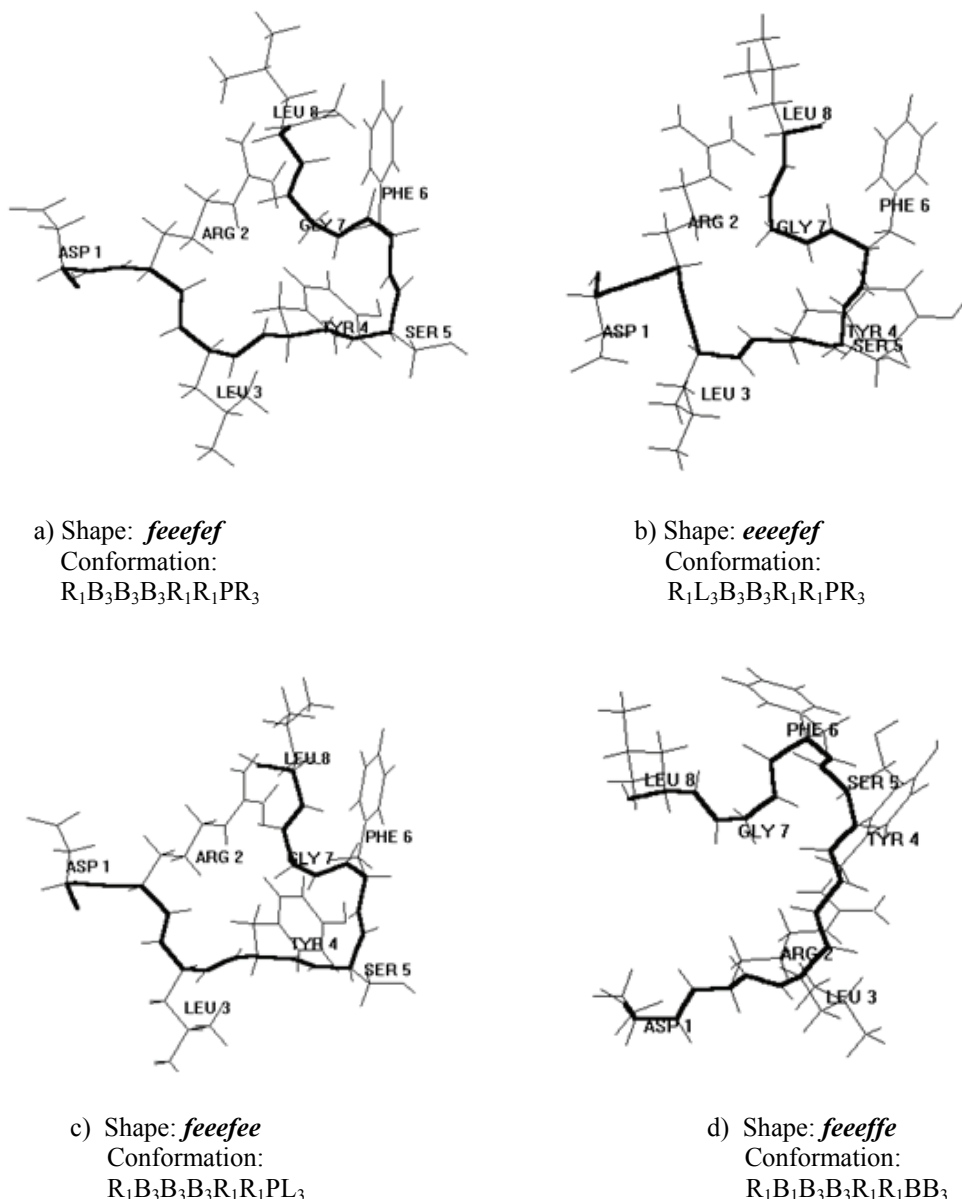


Fig. 2. Conformational conditions of allatostatin-4 molecule with  $E_{rel}=0.0$  (a), 1,6 kcal/mol (b), 1,8 kcal/mol (c), 2,1 kcal/mol (d)

For tetra peptide fragment Leu<sup>3</sup>-Tyr<sup>4</sup>-Ser<sup>5</sup>- Phe<sup>6</sup> energetically preferable are conformations of shapes *eef* and *eff* (27,9 and 18% from total number of calculated conformations with  $E_{rel} = 0 \div 5$  kcal/mol, accordingly). Stable structures with local energy minimums of this fragment is stabilized mainly by non- valence interactions of residuals with aromatic side chains Tyr<sup>4</sup> and Phe<sup>6</sup> (order – 5,0 kcal/mol). In low-energy conformation belonging to shape *eff* there forms  $\beta$ -bending in section Leu<sup>3</sup>-Phe<sup>6</sup>, where distance between C<sup>a</sup> – atoms of residuals Tyr<sup>4</sup> and Phe<sup>6</sup> equal to 5,4 Å. Such bending forwards approach and almost parallel location of rings residuals so that distance between rings centers of gravity vary in range of 4,2  $\div$  4,5 Å. Creating of  $\beta$ -bending in low-energy tetra peptide conformations and forming hydrogen bonds between atoms of residuals peptide links located in positions 3 and 6 of the main chain indicate forming of compact structure, stabilized by dispersive interactions which may stay kept at increase of peptide

chain length. Effective interresidual interactions between Tyr<sup>4</sup> and Phe<sup>6</sup> form also in conformations of shape *fee*, however, they on 1,7 kcal/mol yield to the fragment global conformation. General contribution into such structures stabilization bring dipeptide interactions Leu<sup>3</sup>-Tyr<sup>4</sup> (-5, 1 kcal/mol). Presence of serine residual containing hydroxyl group in side chain, defines specific of spatial building of given sector of allatostatin-4 molecule. It is known that at Ser owing to electrostatic interactions between its main and side chains brightly express tendency to participate in formation of  $\beta$  structures. In all calculated fragment conformations arrives hydrogen bond between OH group of side and NH group of main chain of serine, which length vary in very narrow interval of values 2,48  $\div$  2,51 Å. Thus, tetra peptide fragment closely packed into space and stabilized mainly by non- valence interactions introduced in next calculations mainly by conformations of shapes *eef*, *fee* and *eff*.

Table 1  
Energy distribution of allatostatin -4 conformations

| No | shape          | Relative energy, kcal/mol |     |     |     |     |    |  | Percentage correlation in conformations |
|----|----------------|---------------------------|-----|-----|-----|-----|----|--|---|
|    |                | 0÷1                       | 1÷2 | 2÷3 | 3÷4 | 4÷5 | >5 |  |   |
| 1  | <i>feeeef</i>  | 1                         | 6   | 3   | 7   | 6   | 26 |  | 28.1                                    |
| 2  | <i>feefee</i>  | -                         | 1   | -   | 2   | 1   | 22 |  | 15.3                                    |
| 3  | <i>feffff</i>  | -                         | -   | 1   | -   | 3   | 17 |  | 12.7                                    |
| 4  | <i>feeffe</i>  | -                         | -   | 1   | -   | 1   | 16 |  | 10.4                                    |
| 5  | <i>fefeee</i>  | -                         | -   | 1   | 1   | -   | 1  |  | 1.6                                     |
| 6  | <i>fffefff</i> | -                         | -   | -   | 1   | -   | 10 |  | 6.2                                     |
| 7  | <i>feeeeff</i> | -                         | -   | -   | 3   | 4   | 16 |  | 13.2                                    |
| 8  | <i>eeeeef</i>  | -                         | 1   | 2   | 1   | -   | 2  |  | 3.4                                     |
| 9  | <i>eeeffff</i> | -                         | -   | 1   | 1   | -   | 2  |  | 2.3                                     |
| 10 | <i>effefff</i> | -                         | -   | -   | -   | 1   | 4  |  | 2.8                                     |
| 11 | <i>eeeeffe</i> | -                         | -   | -   | -   | 1   | 2  |  | 1.7                                     |
| 12 | <i>eefeeee</i> | -                         | -   | -   | -   | 1   | 3  |  | 2.3                                     |

Table 2  
Energy parameters of allatostatin -4 low- energetical conformations

| No | Shape          | Conformation * |                |                |                |                |                |     | Energy contribution, (kJ/mol) |          |          |           |            |           |
|----|----------------|----------------|----------------|----------------|----------------|----------------|----------------|-----|-------------------------------|----------|----------|-----------|------------|-----------|
|    |                | Asp            | Arg            | Leu            | Tyr            | Ser            | Phe            | Gly | Leu                           | $E_{nb}$ | $E_{el}$ | $E_{tor}$ | $E_{conf}$ | $E_{rel}$ |
| 1  | <i>feefef</i>  | R <sub>1</sub> | B <sub>3</sub> | B <sub>3</sub> | B <sub>3</sub> | R <sub>1</sub> | R <sub>1</sub> | P   | R <sub>3</sub>                | -44,3    | 3,0      | 4,3       | -36,9      | 0,0       |
| 2  | <i>eeeeef</i>  | R <sub>1</sub> | L <sub>3</sub> | B <sub>3</sub> | B <sub>3</sub> | R <sub>1</sub> | R <sub>1</sub> | P   | R <sub>3</sub>                | -44,9    | 4,5      | 5,1       | -35,4      | 1,6       |
| 3  | <i>feefee</i>  | R <sub>1</sub> | B <sub>3</sub> | B <sub>3</sub> | B <sub>3</sub> | R <sub>1</sub> | R <sub>1</sub> | P   | L <sub>3</sub>                | -42,4    | 2,3      | 4,9       | -35,2      | 1,8       |
| 4  | <i>feeffe</i>  | R <sub>1</sub> | B <sub>1</sub> | B <sub>3</sub> | B <sub>3</sub> | R <sub>1</sub> | R <sub>1</sub> | B   | B <sub>3</sub>                | -42,9    | 3,1      | 4,9       | -34,9      | 2,1       |
| 5  | <i>fefeee</i>  | R <sub>1</sub> | B <sub>1</sub> | R <sub>2</sub> | B <sub>3</sub> | B <sub>2</sub> | B <sub>3</sub> | B   | R <sub>3</sub>                | -41,7    | 2,8      | 4,2       | -34,6      | 2,4       |
| 6  | <i>eeeffff</i> | R <sub>1</sub> | L <sub>3</sub> | B <sub>3</sub> | R <sub>3</sub> | R <sub>1</sub> | B <sub>3</sub> | P   | R <sub>3</sub>                | -42,4    | 3,9      | 4,1       | -34,3      | 2,6       |
| 7  | <i>feefff</i>  | B <sub>2</sub> | L <sub>3</sub> | B <sub>3</sub> | B <sub>3</sub> | R <sub>2</sub> | B <sub>3</sub> | P   | R <sub>3</sub>                | -40,0    | 2,5      | 3,8       | -33,7      | 3,3       |
| 8  | <i>fffefff</i> | R <sub>1</sub> | R <sub>3</sub> | R <sub>3</sub> | B <sub>3</sub> | R <sub>1</sub> | B <sub>3</sub> | P   | R <sub>3</sub>                | -40,0    | 3,2      | 3,4       | -33,4      | 3,5       |
| 9  | <i>feffff</i>  | R <sub>1</sub> | B <sub>1</sub> | B <sub>3</sub> | R <sub>3</sub> | R <sub>1</sub> | B <sub>3</sub> | P   | R <sub>3</sub>                | -40,1    | 2,6      | 5,8       | -32,8      | 4,1       |
| 10 | <i>eeeefff</i> | R <sub>1</sub> | L <sub>3</sub> | B <sub>3</sub> | B <sub>3</sub> | R <sub>2</sub> | B <sub>3</sub> | P   | R <sub>3</sub>                | -40,3    | 4,0      | 3,9       | -32,4      | 4,6       |
| 11 | <i>effefff</i> | B <sub>1</sub> | R <sub>3</sub> | R <sub>3</sub> | B <sub>3</sub> | R <sub>1</sub> | B <sub>3</sub> | P   | R <sub>3</sub>                | -40,9    | 5,3      | 2,6       | -32,2      | 4,8       |
| 12 | <i>eefeeee</i> | R <sub>1</sub> | L <sub>3</sub> | R <sub>2</sub> | B <sub>3</sub> | B <sub>1</sub> | B <sub>3</sub> | P   | R <sub>3</sub>                | -41,4    | 3,8      | 5,8       | -31,8      | 5,1       |

\* - conventional signs of local minimums of monopeptides see in text.

Onto tetra peptide fragment Phe<sup>6</sup>-Gly<sup>7</sup>-Leu<sup>8</sup> the number of calculated conformations belonging to 4 shapes and 16 forms of peptide chain is 324. In low-

energy fragment conformation yield to glycine residual playing the role of hinge in fragment structure does form effective interresidual interactions between Phe<sup>6</sup> and Leu<sup>8</sup>.

### SPATIAL STRUCTURE OF NEUROPEPTIDE ALLATOSTATIN-4

Thus conditions either with open or half-folded main chain shape realize with equal probability. About this stipulate both minimization results and analysis of contribution of interresidual interactions in low-energetical fragment conformational conditions. In

fragment global conformation there forms hydrogen bonds between atoms of residuals Phe<sup>6</sup> and Leu<sup>8</sup> main chain, which length vary due to main chain conformational condition from 2,03 to 2,07 Å.

Table 3  
Energy contributions (kcal/mole) of interresidual interactions in low- energetical conformations of allatostatin-4 molecule.

| Amino acid residues | $E_{\text{rel}} = 0 \text{ kcal/mol}$     |                                    | $E_{\text{rel}} = 1,6 \text{ kcal/mol}$   |                                    |
|---------------------|---|------------------------------------|---|------------------------------------|
|                     | Distance between C <sup>α</sup> atoms (Å) | $\sum_{i,j}^8 E_{i,j}$<br>(kJ/mol) | Distance between C <sup>α</sup> atoms (Å) | $\sum_{i,j}^8 E_{i,j}$<br>(kJ/mol) |
| Asp1-Arg2           | 3.8                                       | -7.5                               | 3.8                                       | -5.1                               |
| Arg2-Leu3           | 3.8                                       | -1.6                               | 3.8                                       | -1.6                               |
| Leu3-Tyr4           | 3.8                                       | -2.1                               | 3.8                                       | -2.1                               |
| Tyr4-Ser5           | 3.8                                       | -1.9                               | 3.8                                       | -1.9                               |
| Ser5-Phe6           | 3.8                                       | -2.2                               | 3.8                                       | -2.3                               |
| Phe6-Gly7           | 3.8                                       | 0.8                                | 3.8                                       | -0.8                               |
| Gly7-Leu8           | 3.8                                       | -1.5                               | 3.8                                       | -1.5                               |
| Asp1-Leu3           | 6.4                                       | -0.7                               | 5.6                                       | -4.8                               |
| Arg2-Tyr4           | 6.0                                       | -3.3                               | 5.9                                       | -2.8                               |
| Leu3-Ser5           | 7.2                                       | -0.2                               | 7.2                                       | -0.2                               |
| Tyr4-Phe6           | 5.4                                       | -5.0                               | 5.4                                       | -5.1                               |
| Ser5-Gly7           | 5.0                                       | -1.0                               | 5.0                                       | -1.0                               |
| Phe6-Leu8           | 5.7                                       | -3.3                               | 5.7                                       | -3.3                               |
| Asp1-Tyr4           | 9.5                                       | 0.5                                | 8.9                                       | 0.5                                |
| Arg2-Ser5           | 9.3                                       | -0.1                               | 9.3                                       | -0.1                               |
| Leu3-Phe6           | 8.7                                       | -0.1                               | 8.6                                       | -0.1                               |
| Tyr4-Gly7           | 4.3                                       | -2.5                               | 4.2                                       | -2.6                               |
| Ser5-Leu8           | 8.4                                       | -0.0                               | 8.3                                       | -0.0                               |
| Asp1-Ser5           | 12.9                                      | -0.1                               | 12.4                                      | 0.1                                |
| Arg2-Phe6           | 9.3                                       | -0.3                               | 9.2                                       | -0.2                               |
| Leu3-Gly7           | 6.1                                       | -0.2                               | 5.9                                       | -0.2                               |
| Tyr4-Leu8           | 7.4                                       | -0.2                               | 7.3                                       | -0.2                               |
| Asp1-Phe6           | 13.0                                      | 0.1                                | 12.9                                      | 0.1                                |
| Arg2-Gly7           | 6.1                                       | -1.3                               | 6.0                                       | -1.1                               |
| Leu3-Leu8           | 8.6                                       | -0.0                               | 8.4                                       | 0.0                                |
| Asp1-Gly7           | 9.5                                       | -0.1                               | 9.5                                       | -0.1                               |
| Arg2-Leu8           | 6.8                                       | -3.3                               | 6.6                                       | -2.3                               |
| Asp1-Leu8           | 9.8                                       | -0.0                               | 10.0                                      | 0.1                                |

Table 4  
Dihedral angles of side and main chains of aminoacid residuals in low- energetical allatostatin-4 conformations.

| Residue          | Dihedral angles  |  |  |
|------------------|--|--|--|
| Asp <sup>1</sup> | $\varphi = -89, \psi = -44, \omega = 178,$<br>$\chi_1 = 54, \chi_2 = 105$                | $\varphi = -73, \psi = -43, \omega = 178,$<br>$\chi_1 = 61, \chi_2 = 112$                | $\varphi = -89, \psi = -44, \omega = 180,$<br>$\chi_1 = 54, \chi_2 = 105$                |
| Arg <sup>2</sup> | $\varphi = -134, \psi = 97, \omega = 179,$<br>$\chi_1 = -67, \chi_2 = 174, \chi_3 = 161$ | $\varphi = 53, \psi = 57, \omega = 175,$<br>$\chi_1 = 57, \chi_2 = 179, \chi_3 = 181$    | $\varphi = -133, \psi = 98, \omega = 183,$<br>$\chi_1 = -67, \chi_2 = 174, \chi_3 = 182$ |
| Leu <sup>3</sup> | $\varphi = -99, \psi = 94, \omega = 183,$<br>$\chi_1 = 54, \chi_2 = 177, \chi_3 = 182$   | $\varphi = -100, \psi = 94, \omega = 183,$<br>$\chi_1 = -56, \chi_2 = 174, \chi_3 = 187$ | $\varphi = -99, \psi = 96, \omega = 182,$<br>$\chi_1 = -54, \chi_2 = 177, \chi_3 = 187$  |
| Tyr <sup>4</sup> | $\varphi = -150, \psi = 165, \omega = 177,$<br>$\chi_1 = -67, \chi_2 = 95, \chi_3 = 180$ | $\varphi = -148, \psi = 165, \omega = 178,$<br>$\chi_1 = -65, \chi_2 = 96, \chi_3 = 179$ | $\varphi = -148, \psi = 164, \omega = 178,$<br>$\chi_1 = -61, \chi_2 = 95, \chi_3 = 180$ |
| Ser <sup>5</sup> | $\varphi = -71, \psi = -52, \omega = 171,$<br>$\chi_1 = 56, \chi_2 = 177$                | $\varphi = -69, \psi = -52, \omega = 171,$<br>$\chi_1 = 57, \chi_2 = 179$                | $\varphi = -71, \psi = -53, \omega = 170,$<br>$\chi_1 = 57, \chi_2 = 180$                |
| Phe <sup>6</sup> | $\varphi = -60, \psi = -29, \omega = 178,$<br>$\chi_1 = 62, \chi_2 = 81$                 | $\varphi = -60, \psi = -29, \omega = 178,$<br>$\chi_1 = 62, \chi_2 = 81$                 | $\varphi = -61, \psi = -35, \omega = 179,$<br>$\chi_1 = 57, \chi_2 = 80$                 |
| Gly <sup>7</sup> | $\varphi = 80, \psi = -77, \omega = 182$   | $\varphi = 80, \psi = -77, \omega = 182$   | $\varphi = 72, \psi = -89, \omega = 181$   |
| Leu <sup>8</sup> | $\varphi = -104, \psi = -60, \omega = 179,$<br>$\chi_1 = 53, \chi_2 = 176, \chi_3 = 186$ | $\varphi = -104, \psi = -60, \omega = 179,$<br>$\chi_1 = 53, \chi_2 = 176, \chi_3 = 186$ | $\varphi = 50, \psi = 59, \omega = 180,$<br>$\chi_1 = -58, \chi_2 = 174, \chi_3 = 186$   |
| $E_{\text{rel}}$ | 0,0 kcal/mol   | 1,6 kcal/mol   | 1,8 kcal/mol   |

Table 5

Hydrogen bonds in low- energetical allatostatin-4 conformations.

| No | shape           | Conformation  | Hydrogen bond length (in Å)  |  |
|----|-----------------|---|--|--|
| 1  | <i>feefef</i>   | R <sub>1</sub> B <sub>3</sub> B <sub>3</sub> B <sub>3</sub> R <sub>1</sub> R <sub>1</sub> PR <sub>3</sub> | C <sup>γ</sup> O(Asp <sup>1</sup> )...HN(Arg <sup>2</sup> )<br>C' O(Tyr <sup>4</sup> )...HN(Gly <sup>7</sup> )<br>NH(Ser <sup>5</sup> )...OH (Ser <sup>5</sup> )<br>C' O (Phe <sup>6</sup> )...HN(Leu <sup>8</sup> )   | 2,83<br>2,75<br>2,50<br>2,12                 |
| 2  | <i>eeeeef</i>   | R <sub>1</sub> L <sub>3</sub> B <sub>3</sub> B <sub>3</sub> R <sub>1</sub> R <sub>1</sub> PR <sub>3</sub> | C <sup>γ</sup> O(Asp <sup>1</sup> )...HN(Leu <sup>3</sup> )<br>C' O(Tyr <sup>4</sup> )...HN(Gly <sup>7</sup> )<br>NH(Ser <sup>5</sup> )...OH (Ser <sup>5</sup> )<br>C' O (Phe <sup>6</sup> )...HN(Leu <sup>8</sup> )   | 2,26<br>2,67<br>2,51<br>2,13                 |
| 3  | <i>feefee</i>   | R <sub>1</sub> B <sub>3</sub> B <sub>3</sub> B <sub>3</sub> R <sub>1</sub> R <sub>1</sub> PL <sub>3</sub> | C <sup>γ</sup> O(Asp <sup>1</sup> )...HN(Arg <sup>2</sup> )<br>N <sup>ε</sup> H(Arg <sup>2</sup> )...OC'(Leu <sup>8</sup> )<br>NH(Ser <sup>5</sup> )...OH (Ser <sup>5</sup> )<br>C' O (Phe <sup>6</sup> )...HN(Leu <sup>8</sup> )  | 2,79<br>1,92<br>2,50<br>2,26                 |
| 4  | <i>feeeffe</i>  | R <sub>1</sub> B <sub>1</sub> B <sub>3</sub> B <sub>3</sub> R <sub>1</sub> R <sub>1</sub> BB <sub>3</sub> | C' O(Tyr <sup>4</sup> )...HN(Gly <sup>7</sup> )<br>NH(Ser <sup>5</sup> )...OH (Ser <sup>5</sup> )<br>C' O (Phe <sup>6</sup> )...HN(Leu <sup>8</sup> )  | 2,80<br>2,50<br>2,09                         |
| 5  | <i>fefehee</i>  | R <sub>1</sub> B <sub>1</sub> R <sub>2</sub> B <sub>3</sub> B <sub>2</sub> B <sub>3</sub> BR <sub>3</sub> | N <sup>ε</sup> H(Arg <sup>2</sup> )...OC'(Phe <sup>6</sup> )<br>C' O (Phe <sup>6</sup> )...HN(Leu <sup>8</sup> )   | 2,71<br>2,08                                 |
| 6  | <i>eeeeffff</i> | R <sub>1</sub> L <sub>3</sub> B <sub>3</sub> R <sub>3</sub> R <sub>1</sub> B <sub>3</sub> PR <sub>3</sub> | C <sup>γ</sup> O(Asp <sup>1</sup> )...HN(Leu <sup>3</sup> )<br>C' O (Arg <sup>2</sup> )...HN(Tyr <sup>4</sup> )<br>C' O(Tyr <sup>4</sup> )... NH <sub>2</sub><br>NH(Ser <sup>5</sup> )...OH (Ser <sup>5</sup> )<br>C' O(Ser <sup>5</sup> )...NH <sub>2</sub><br>C' O (Phe <sup>6</sup> )...HN(Leu <sup>8</sup> ) | 2,40<br>2,87<br>2,13<br>2,49<br>2,93<br>2,01 |
| 7  | <i>feeeffff</i> | B <sub>2</sub> L <sub>3</sub> B <sub>3</sub> B <sub>2</sub> R <sub>2</sub> B <sub>3</sub> PR <sub>3</sub> | C' O(Tyr <sup>4</sup> )...NH <sub>2</sub><br>C' O (Phe <sup>6</sup> )...HN(Leu <sup>8</sup> )  | 1,92<br>1,99                                 |
| 8  | <i>fffeffff</i> | R <sub>1</sub> R <sub>3</sub> R <sub>3</sub> B <sub>3</sub> R <sub>1</sub> B <sub>3</sub> PR <sub>3</sub> | NH(Asp <sup>1</sup> )...C' O(Tyr <sup>4</sup> )<br>C' O(Tyr <sup>4</sup> )...NH <sub>2</sub><br>NH(Ser <sup>5</sup> )...OH (Ser <sup>5</sup> )<br>C' O (Phe <sup>6</sup> )...HN(Leu <sup>8</sup> )   | 2,91<br>2,00<br>2,48<br>2,00                 |
| 9  | <i>fefffff</i>  | R <sub>1</sub> B <sub>1</sub> B <sub>3</sub> R <sub>3</sub> R <sub>1</sub> B <sub>3</sub> PR <sub>3</sub> | C <sup>γ</sup> O(Asp <sup>1</sup> )...HN(Arg <sup>2</sup> )<br>C' O(Arg <sup>2</sup> )...HN(Tyr <sup>4</sup> )<br>C' O(Tyr <sup>4</sup> )...NH <sub>2</sub><br>NH(Ser <sup>5</sup> )...OH (Ser <sup>5</sup> )<br>C' O(Ser <sup>5</sup> )...NH <sub>2</sub><br>C' O (Phe <sup>6</sup> )...HN(Leu <sup>8</sup> )   | 2,6<br>2,8<br>2,1<br>2,5<br>2,9<br>2,0       |
| 10 | <i>eeeeffff</i> | R <sub>1</sub> L <sub>3</sub> B <sub>3</sub> B <sub>3</sub> R <sub>2</sub> B <sub>3</sub> PR <sub>3</sub> | C <sup>γ</sup> O(Asp <sup>1</sup> )...HN(Leu <sup>3</sup> )<br>C <sup>γ</sup> O(Asp <sup>1</sup> )...HN(Arg <sup>2</sup> )<br>C' O(Tyr <sup>4</sup> )...NH <sub>2</sub><br>C' O (Phe <sup>6</sup> )...HN(Leu <sup>8</sup> )  | 2,4<br>2,6<br>2,1<br>2,0                     |
| 11 | <i>efffffff</i> | B <sub>1</sub> R <sub>3</sub> R <sub>3</sub> B <sub>3</sub> R <sub>1</sub> B <sub>3</sub> PR <sub>3</sub> | C' O(Tyr <sup>4</sup> )...NH <sub>2</sub><br>NH(Ser <sup>5</sup> )...OH (Ser <sup>5</sup> )<br>OH (Ser <sup>5</sup> )...NH(Phe <sup>6</sup> )<br>C' O (Phe <sup>6</sup> )...HN(Leu <sup>8</sup> )  | 2,0<br>2,5<br>2,3<br>2,0                     |
| 12 | <i>eefeeee</i>  | R <sub>1</sub> L <sub>3</sub> R <sub>2</sub> B <sub>3</sub> B <sub>1</sub> B <sub>3</sub> PR <sub>3</sub> | C <sup>γ</sup> O(Asp <sup>1</sup> )...HN(Leu <sup>3</sup> )<br>C' O(Tyr <sup>4</sup> )...NH <sub>2</sub><br>NH(Ser <sup>5</sup> )...OH (Ser <sup>5</sup> )<br>OH (Ser <sup>5</sup> )...NH(Phe <sup>6</sup> )<br>C' O(Ser <sup>5</sup> )...NH <sub>2</sub><br>C' O (Phe <sup>6</sup> )...HN(Leu <sup>8</sup> )    | 1,9<br>2,5<br>2,5<br>2,1<br>2,8<br>2,0       |

Total number 458 of primary variants composed for minimization procedure for whole molecule conformational energy correspond to 90 forms and 41 shapes of peptide chain. They are combinations of low-energy conformational conditions of fragments Arg<sup>1</sup>-Leu<sup>3</sup>, Leu<sup>3</sup>-Phe<sup>6</sup>, Phe<sup>6</sup>-Leu<sup>8</sup> and their overlapping sections, relative energy of which doesn't exceed 5 kcal/mol. Conformational analysis of phased scalable and overlapping fragments of allatostatin-4 molecule elicits significant portability of results while increasing of given

peptide chain length (table 1 and 2). As minimization result of energy of compiled structural variants there were found low-energetical conformations of allatostatin-4 molecule. In relative energy interval 0÷10 kcal/mol include conformations of 12 oktapeptide structural type.

Calculation showed that allatostatin-4 molecule in conditions of water environment may form several stable conformational conditions separated by low energetical barrier 5,0 kcal/mol.

## SPATIAL STRUCTURE OF NEUROPEPTIDE ALLATOSTATIN-4

In tote, 53 % of calculated structures contain open form of Arg<sup>2</sup>- Tyr<sup>4</sup> sector and differ only with conformational conditions of C- ended fragment Ser<sup>5</sup> - Leu<sup>8</sup>. In tables 2-3 there are given energy parameters of low- energetical conformations of allatostatin-4, and in table 4 – values of dihedral angles of molecule condition with global minimum of intramolecular conformational energy.

On fig. 2 there are given stereoisograms of the molecule in four conformations with global ( $E_{conf} = -36, 9$  kcal/mol) and local energy minimums ( $E_{conf} = -35,4; -35,2; -34,9$  kcal/mol). Here should be noted that great number of low- energetical conformations are characterized by folded structure of the peptide chain at C- end of molecule. These conformations differ mainly with the energy of dispersive interactions i.e. ultima analyse, packing density and stipulate limitation of conformational freedom of C- ended allatostatin-4 fragment. About it argues also significant differentiation of shapes, because from 41 examined shapes into the interval of relative energy fit only 12.

In global conformation of the molecule at Tyr<sup>4</sup> – Ser<sup>5</sup>- Phe<sup>6</sup>-Gly<sup>7</sup> sector there arrives  $\beta$ - rotation of peptide chain, what about argue the distance between C<sup>α</sup>- atoms of residuals Tyr<sup>4</sup> and Gly<sup>7</sup> (4,3 Å ; table 3) and hydrogen bonds between main chain atoms Tyr<sup>4</sup> and Gly<sup>7</sup> (table 5).

Next upon stability conformation is – R<sub>1</sub>L<sub>3</sub>B<sub>3</sub>B<sub>3</sub>R<sub>1</sub>R<sub>1</sub>PR<sub>3</sub>; belonging to shape *eeeefef*, at 1,6 kcal/mol yields upon stability to the global conformation of shape *eeeefef*. Upon summary contribution of tetra- and pentapeptide interactions (-2,6 kcal/mol) the global conformation appreciable

exceeds other stable conformations R<sub>1</sub>B<sub>3</sub>B<sub>3</sub>B<sub>3</sub>R<sub>1</sub>R<sub>1</sub>PL<sub>3</sub> (13,2 kcal/mol) and R<sub>1</sub>B<sub>3</sub>B<sub>3</sub>R<sub>1</sub>R<sub>1</sub>PL<sub>3</sub> (-10, 4 kcal/mol). In last conformation, however, due to closeness of distant onto chain residuals Arg<sup>2</sup> and Leu<sup>3</sup> there forms effective interaction between side chain of arginine residual and leucine main chain (-1,2 kcal/mol) and also tripeptide interaction between Phe<sup>6</sup> and Leu<sup>8</sup> (-2,7 kcal/mol).

In the global conformation there form hydrogen bonds between oxygen atoms of carbonyl group and hydrogen atoms of amid group of peptide links: CO (Tyr<sup>4</sup>)...HN (Gly<sup>7</sup>) and CO (Phe<sup>6</sup>)...HN (Leu<sup>8</sup>) (table 5). Hydrogen bonds form also in another conformations but most optimal conformations of oktaapeptide stabilize mainly by interactions, formed earlier in stable conformations of overlapping fragments- tripeptide Asp<sup>1</sup>-Arg<sup>2</sup>-Leu<sup>3</sup> and tetra peptide Leu<sup>3</sup>-Tyr<sup>4</sup>-Ser<sup>5</sup>-Phe<sup>6</sup>. In low-energetical conformations of oktaapeptide there form also interresidual interactions due to peptide chain elongation. Such new interactions in global conformation are contacts between Arg<sup>2</sup> - Gly<sup>7</sup> (-1,3 kcal/mol) and Arg<sup>2</sup>-Leu<sup>8</sup> (-3,3 kcal/mol). In conformation of shape *eeeffff* new contacts also form between Tyr<sup>4</sup> and NH<sub>2</sub> of C-ended group of the molecule (- 3,5 kcal/mol).

Generalizing research results it is possible to suppose that in conditions of water environment the allatostatin-4 molecule may realize series of low-energetical conformational conditions varying mainly with conformational conditions of C- ended fragment. Received results may serve as a base for task-oriented allatostatin-4 modification with aim of creating analogs of more selective and prolonged actions.

- 
- [1] G.E. Pratt, D.E. Farnsworth, N.R. Siegel, K.F. Fok, R. Feyereisen. Identification of an allatostatin from adult Diptera punctata. Biochem. Biophys. Res . Commun. 1990; 29:1243-1247.
  - [2] B. Stay, S. Fairbairn, C.G. Yu. Role of allatostatins in the regulation of juvenile hormone synthesis. Arch. Insect. Biochem. Physiol.. 1996; 32: 287-297.
  - [3] A.P. Woodhead, B. Stay, S.L. Seidel, M.A. Khan, S.S. Tobe. Primary structure of four allatostatins: neuropeptide inhibitors of juvenile hormone synthesis. Proc. Natl. Acad. Sci. USA. 1989; 85:5997-6001.
  - [4] A.P. Woodhead, M.A. Klan, B. Stay, S.S. Tobe. Two new allatostatins from the brains of Diptera punctata. Insect. Biochem. Mol. Biol. 1994; 24: 257-263.
  - [5] E.M. Popov. Quantitative approach to conformations of proteins. Int. J. Quantum Chem. 1979; 16:707-737
  - [6] E.M. Popov. The Structural Organization of Proteins (in Russian), Nauka, Moscow, 1989.
  - [7] N.M. Godjaev, I.S. Maksumov and L.I. Ismailova. The program for semiempirical calculation of conformations of the molecular complexes. J.Chem.Struct.(in Russian), 1983; 24:147-148.
  - [8] F.A. Momany, R.F. McGuire, A.W. Burgess, H.A. Scheraga. Energy parameters in polypeptides: Geometric parameters, partial atomic charges, nonbonded interaction for naturally occurring amino acid. Phys. Chem. 1975;79:2361-2381.
  - [9] IUPAC-IUB Commission on Biochemical Nomenclature Abbreviations and Symbols for Description of Conformation of Polypeptide Chains. Pure Applied Chem. 1974; 40:291-308.

Received: 08.04.2011

## INVESTIGATION OF CLARK-LAGERWALL EFFECT IN THE SMALL PARTICLES -LIQUID CRYSTAL SYSTEM

**T.D. IBRAGIMOV**

*H.M. Abdullayev Institute of Physics of Azerbaijan National Academy of Sciences  
AZ-1143, G. Javid Avenue, 33, Baku*

**G.M. BAYRAMOV, A.R. IMAMALIEV**

*Baku State University,  
AZ-1148, Z. Khalilov street, 23, Baku, Azerbaijan*

The smectic  $C^*$  based on a three-component mixture of liquid crystals (LC) with not mesogene chiral additive and showing ferroelectric properties has been developed. The physical parameters which are responsible for electrooptical effects are defined. The Clark-Lagerwall effect both in the pure smectic  $C^*$  and with the additive of small particles of the centrosymmetric substance  $Al_2O_3$  and the ferroelectric  $SrTiO_3$  is investigated. It has been shown that time characteristics of a cell with LC -  $Al_2O_3$  are a little bit worsened in comparison with a cell with the pure LC. It is caused by increase of the rotational viscosity of the ferroelectric liquid crystal with addition of small particles  $Al_2O_3$ . Time characteristics of the Clark – Lagerwall effect in the LC -  $SrTiO_3$  cell essentially surpass time characteristics of the cell with pure LC because the transition from the deformed UP-state to a DOWN-state demands overcoming much lower energy than the transition from the pure UP-condition to the DOWN-state.

**Key words:** small particles, liquid crystal, ferroelectricity, smectic phase.

**PACS:** 77.84Nh; 77.80bg; 61.30Eb; 61.30Gd

### INTRODUCTION

Devices based on liquid crystals (displays, light modulators, etc.) are characterized by low operating voltage and sufficiently high contrast ratio (100:1) [1-4]. Ferroelectric liquid crystals (FLC) have greater potential [5-7]. Having spontaneous polarization, FLCs much stronger interact with external electric field in comparison with a nematic LC. At typical values of an operating field ( $E = 2 \cdot 10^5$  V/m) the density of free interaction energy of nematic LC with electric field has an order

$$F_{el} = 1/2\Delta\epsilon\epsilon_0E^2 = 2 \text{ J/m}^3,$$

where for anisotropy of dielectric constant of nematic liquid crystal the  $\Delta\epsilon \approx 10$  is taken and for electric constant  $\epsilon_0 = 8.85 \text{ nF/m}$ . The typical value of  $\Delta\epsilon$  equals to 10.

At the same time the density of free interaction energy of FLC (typical values of spontaneous polarization has order of  $10^{-4} - 10^{-3} \text{ C/m}^2$ ) with electric field, at such values of field intensity has an order

$$F_{el} = P_S E \approx 20 - 200 \text{ J/m}^3.$$

As seen,  $F_{el}$  for FLC surpasses one for nematic LC on 1-2 orders. Therefore, the electrooptical effect in FLCs possesses the best time and threshold characteristics. Ferroelectric properties are observed in the chiral smectic  $C^*$  phase of LC. Spontaneous polarization in this phase arises as consequence of combination of layering and inclination of structure with chirality and polarity of molecules [6-8]. If there is transverse dipole group close to the chiral center then ordering of these dipoles are occurred along smectic layers perpendicularly to long axes of molecules, forming spontaneous polarization. Spontaneous polarization varies from  $1 \text{ nC} \cdot \text{cm}^{-2}$  to  $500 \text{ nC} \cdot \text{cm}^{-2}$

[5,7,8] in modern synthesized FLCs. One of consequences of chirality of LC molecules is twist of the smectic  $C^*$  phase (Fig. 1a). The planar structure of smectic  $C^*$  liquid crystal (smectic layers are perpendicular to substrates) in the crossed polarizers looks as a set parallel equal sited strips. The helical structure is deformed at field application because the electric field aspires to orientate the spontaneous polarization in parallel to its direction, and since some critical field defined by the formula ( $\theta \ll 1$ ) [6]

$$E_n = (\pi^4/4) K \theta^2 / P_S L^2$$

the helical structure is completely untwisted ( Fig. 1b). Value K in last formula is approximately equal to an elastic constant of a longitudinal bend. Applying a sign-variable field on the planar sample, for example, a rectangular bipolar impulse, and having directed one of the crossed polarizers in parallel to an axis of one switched states, we will obtain light modulation with high contrast, small operating voltage and switching time. A set of electro-optical effects is observed in FLCs such as effect of spin up of helical structure [6], effect of deformation of helical structure [2], etc. The most suitable effect for application in displays and light modulators is Clark-Lagerwall which is carried out in surface-stabilized ferroelectric liquid crystal (SSFLC) [9].

At thickness smaller than a pitch of smectic  $C^*$ , the helical structure is suppressed by surface forces. The twist states are formed at sufficiently strong polar coupling of FLC molecules with a substrate surface (Fig. 2) where spontaneous polarization turns along layers on  $180^\circ$  at advancement from one layer to another [10]. If polar coupling is insufficiently strong, the further reduction of a thickness leads to loss of stability of these states. In the work of Clark and Lagerwall [9], the cell thickness equaled to  $1.5 \mu\text{m}$ .

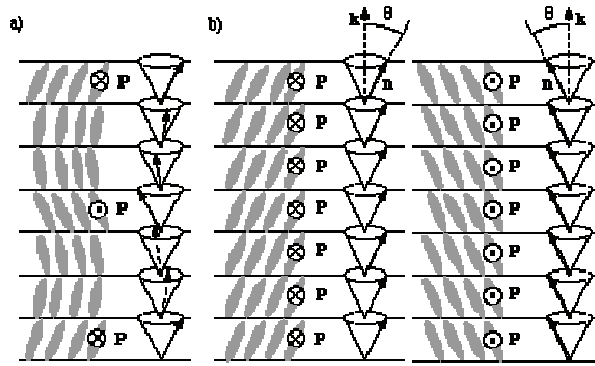


Fig.1. Distribution of director in the smectic  $C^*$  phase.

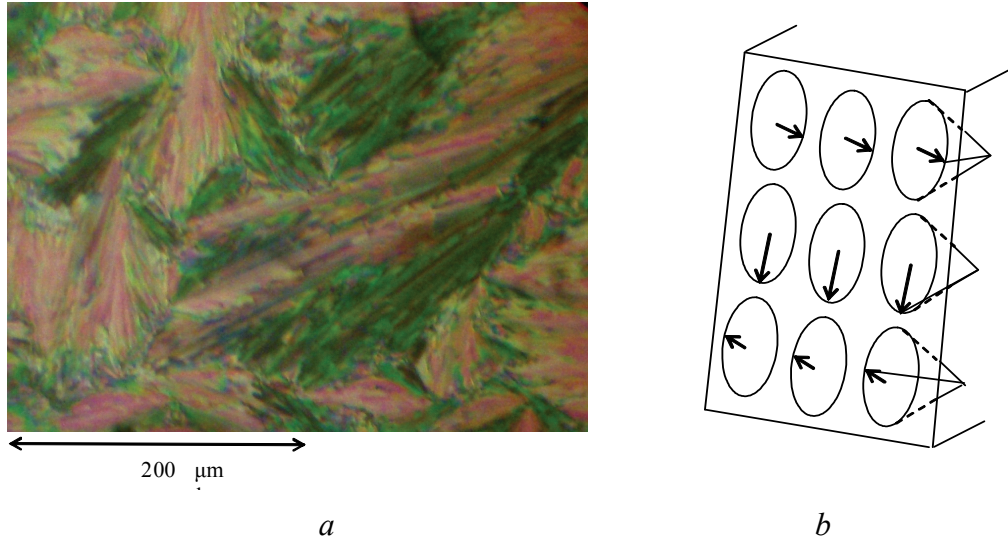


Fig.2. Twist states under polarizing microscope (a). Distribution of the director in the twist state (b).

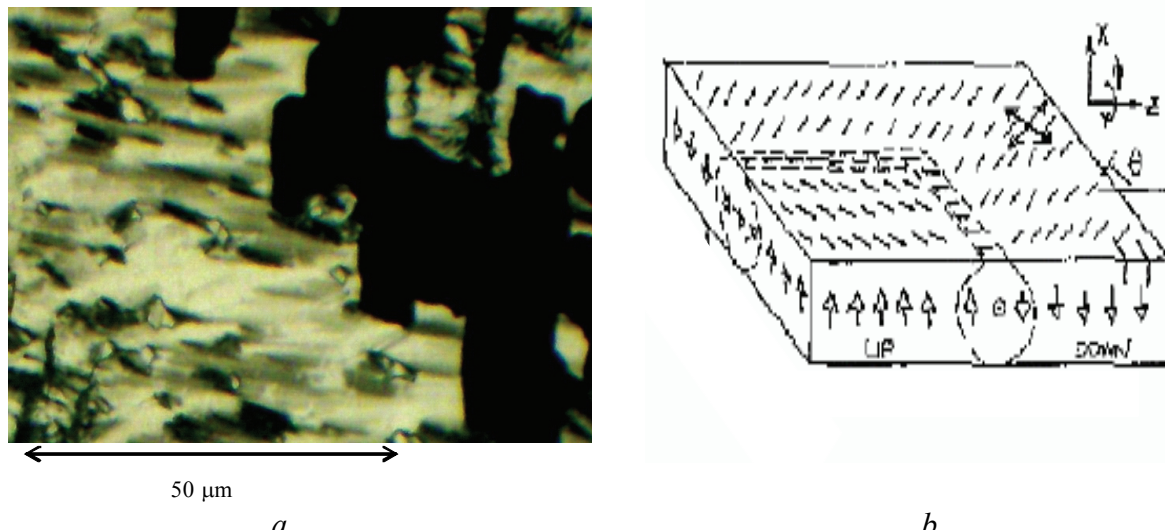


Fig.3. The form of surface-stabilized states under polarizing microscope (a). Distribution of the director and spontaneous polarization in UP and DOWN states of surface- stabilized ferroelectric liquid crystal (b).

Thus, instead of spiral structure there is two surface-stabilized states divided by accurate borders - (Fig. 3). It is possible to reach full absorption of each of these states by means of rotation of the sample that indicates to uniformity of distribution of the director in these states. The angular difference between directions

of the director in these states is equal to the doubled angle of inclination  $2\theta$ . These states are called UP and DOWN. Spontaneous polarization is directed upwards in one of these states and it is done downwards at another. At application of electric field in the form of a rectangular bipolar wave there is faster switching with memory between these states.

Dependence of switching time  $\tau$  on voltage at the Clark-Lagerwall effect has complex character [11]. At large values of electric field, we deal with a mode of bulk switching: the director turns near one of surfaces on all area of cell and this picture is stretched along a thickness before full turn of the director at other surface. The switching time is inversely proportional to applied voltage at regime of bulk switching.

It seemed, it is possible to obtain light modulation with frequency of tens and hundreds MHz increasing the voltage applied on the SSFLC-cell. However, it is interfered by two factors: electric breakdown of the cell: even at very careful clearing of FLC, it makes the way at values of intensity of electric field exceeding  $10^8$  V/m; as a rule, ferroelectric liquid crystals have a negative sign of anisotropy of dielectric permeability ( $\varepsilon_{\perp} > \varepsilon_{\parallel}$  or  $\Delta \varepsilon = \varepsilon_{\perp} - \varepsilon_{\parallel} < 0$ ) as transverse dipole group responsible for occurrence of spontaneous polarization simultaneously increases a transverse component of dielectric permeability. Quadratic interaction of anisotropy of dielectric permeability with electric field - which interferes with switching at great values of electric field intensity prevails over linear interaction of spontaneous polarization with electric field and a minimum is observed in dependence  $\tau(U)$  [12].

Such V-shaped form of dependence  $\tau(U)$  is characteristic for the overwhelming majority of ferroelectric liquid crystals, and it is recommended to

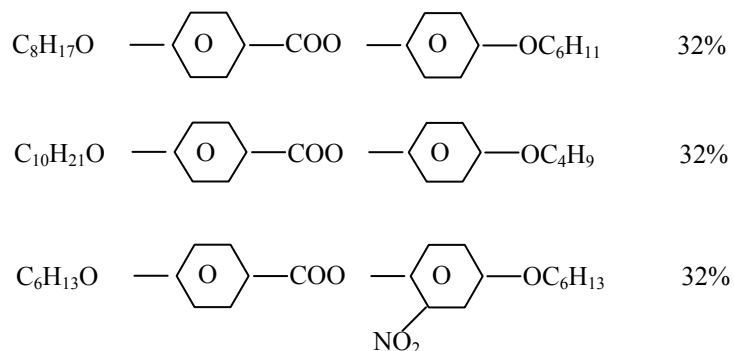
work in the field of voltages getting near this minimum at use of FLC in electrooptical devices. At low voltage the switching time is inversely as the square of voltage. It is connected by that at small values of electric field, the transition from one state to another occurs by movement of domain walls. Observation shows that the switching regime with movement of domain walls has nonthreshold character.

According to the Avrami model [10], the switching time depends not only on growth rate of domain walls but also on number of nuclei per an square unit. The more is the number of nuclei, the less is the proportionality factor between switching time and voltage. One of means of reduction of indicated factor is addition of small solid particles playing role of centers of nucleus formation.

In the present work, influence of the small solid particles embedded in FLC on time characteristics of the Clark – Lagerwall effect is investigated. At that case two types of particles are considered: the particles of centrosymmetric substance  $\text{Al}_2\text{O}_3$  and the particles of ferroelectric  $\text{SrTiO}_3$ .

## EXPERIMENTAL

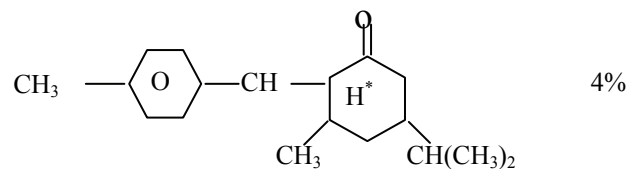
In order to stimulate ferroelectricity in liquid crystals one can doping achiral smectic liquid crystal by polar chiral addition [13]. As a basic smectic C, the mixture of liquid crystals was used



At molar ratio 1:1:1 with phase transitions

Cryst 16 °C SmC 59 °C SmA 72°C N 89°C Iso

Obtained mixture was doped by chiral addition with purpose to induce ferroelectricity [14]



As polar chiral addition is not mesogene, its addition narrows mesophases, especially temperature interval of existence of smectic  $C^*$  phase. Obtained liquid crystal possesses following phases:

Cryst 6.0°C SmC\* 43.5°C SmA 67.0 °C N 76.0 °C Iso

Monodominance of sample at small thickness it is reached by giving of low-frequency electric field  $f=20$  Hz,  $E=10$  V/ $\mu\text{m}$  with the subsequent application

concerning high-frequency ( $f=2$  kHz,  $E=10$  V/ $\mu\text{m}$ ) near the point of phase transition SmA - Sm  $C^*$  inside the smectic A phase.

The mixture was doped with 1.0 wt. % of the  $\text{Al}_2\text{O}_3$  particles with an average size of  $0.2 \mu\text{m}$  or the ferroelectric  $\text{SrTiO}_3$  (spontaneous polarization has order  $3000 \text{ nC}\cdot\text{cm}^{-2}$ ) particles with the average size of  $0.5 - 2.0 \mu\text{m}$ . Dispersion was spent by mechanical and ultrasonic methods in the isotropic phase of the matrix.

For measurement of parameters of obtained ferroelectric LC, the electrooptical cell with a thickness of  $30 \mu\text{m}$  and the area of  $200 \text{ mm}^2$  has been prepared. We will describe some technological subtleties of preparation of an electrooptical cell. First of all, cell substrates should be the optical glasses passing all the width of visible and near infra-red part of spectrum. Besides, for achievement of uniformity of a thickness on all area plainness should be high enough, i.e. surfaces of glasses should be polished with accuracy  $0.1 \lambda \approx 50 \text{ nm}$  ( $\lambda$ -wavelength of incident light). Drawing of current-carrying layer  $\text{In}_2\text{O}_3$  is spent by a method of sedimentation from a solution. Thus the thickness of layer  $\text{In}_2\text{O}_3$  also should be no more than  $0.2 \lambda \approx 100 \text{ nm}$ .

The planarly oriented layer is put by the following technology. The polyamide lacquer of 5 % is dissolved in dimethylacetamide and 40 nm are passed through the glass filter with the pore sizes of 40 nm. The drop of the obtained solution is fallen on glass plates and the system rotates in a centrifuge with frequency of 3000 rpm for a uniform covering. A plate is keep at temperature  $300^\circ\text{C}$  within 0.5 hours in the drying box. After that stage heat treatment (polymerization), working surfaces of plates is rubbed with a special fabric in one direction for the purpose of obtaining of homogeneous orientation.

The large thickness ( $d \geq 5 \mu\text{m}$ ) of LC layer are specified by dielectric gaskets in the form of sticky polymer in which solid balls of equal diameter are dispersed. At heating above  $200^\circ\text{C}$ , polymer melting sticks together plates to each other, and the backlash between them turns out in regular intervals. Thus heterogeneity of a thickness does not exceed  $0.5 \mu\text{m}$ . We will notice that at such selection of a thickness and orientant the strong planar coupling in absence of electric field takes place.

The small thickness turn out ( $d \leq 5 \mu\text{m}$ ) without gaskets. The droplet of the diluted lacquer in acetone is inserted in four corners of one of substrates. The second substrate is put on the first substrate after lacquer drying. Then this system is located in the special holder with four screws helping to press substrates to each other and to obtain the necessary gap. Non-uniformity of a thickness is shown in a kind of interference bands eliminated by these small screws. Thus it is possible to set a thickness of a gap between substrates with accuracy of  $0.1 \mu\text{m}$ . The average thickness of a cell is defined by measurement of capacity of the empty (blank) cell by means of the formula

$$d = \varepsilon_0 S/C$$

where  $S$  is the area spending sites of substrates,  $C$  is electric capacity of a cell,  $\varepsilon_0 = 8.85 \text{ nF/m}$  is an electric constant.

Cell filling was made by capillary forces at the isotropic phase. After filling, the cell is encapsulated by

special glue for the purpose of prevention of evaporation of a liquid crystal. Obtaining of homogeneous orientation is reached by slow cooling from the isotropic phase in the presence of sine electric field (50 V, 1 kHz).

Temperature interval of ferroelectric phase and pitch of spiral structure are defined visually under polarizing microscope. At transition of smectics A to smectic  $C^*$  homogeneous areas turn to striped areas (Fig. 4). Distance between these strips approximately equals to the helical pitch. Applying a bipolar impulse to the cell we may obtain switching between two homogeneous states. Thus optical axes of these states are turned from each other on  $2\theta$ . The inclination angle is defined by this condition. Spontaneous polarization and rotational viscosity has been defined by advanced Martinot - Lagard method [15].

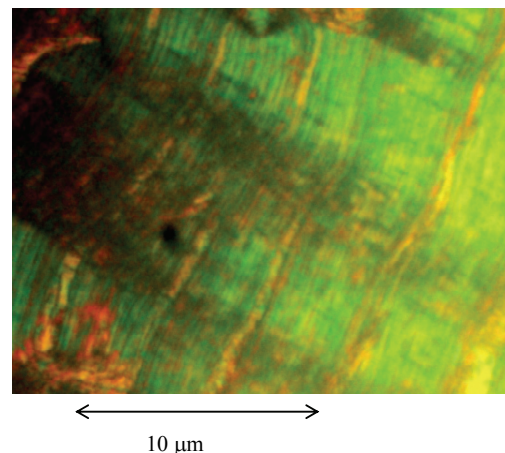


Fig.4. Chiral twisted planar texture of FLC at cell thickness of  $20 \mu\text{m}$ .

## RESULTS AND DISCUSSION

Measurements of some physical parameters of pure FLC show that they have following values: temperature interval of ferroelectric phase -  $6.0^\circ\text{C} - 43.5^\circ\text{C}$ ; pitch of helical structure at  $20^\circ\text{C}$  -  $3.5 \mu\text{m}$ ; inclination angle at  $20^\circ\text{C}$  -  $33^\circ$ ; spontaneous polarization at  $20^\circ\text{C}$  -  $3.5 \text{ nCl/cm}^2$ ; rotational viscosity at  $20^\circ\text{C}$  -  $85 \text{ mPa}\cdot\text{s}$ .

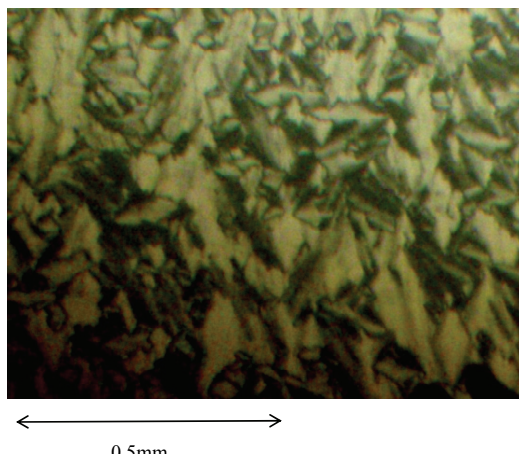
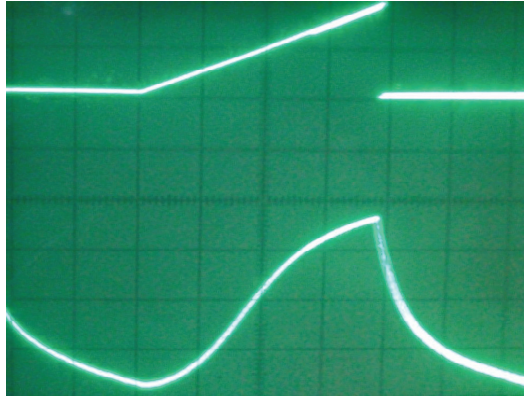


Fig. 5. The planar texture of ferroelectric liquid crystal dispersed by particles  $\text{Al}_2\text{O}_3$ .

Planar texture of ferroelectric liquid crystal dispersed by aluminum oxide particles is shown in Fig.5. Estimations show that at cell thickness of  $5 \mu\text{m}$  on  $1\text{mm}^2$  contain more than  $10^4$  particles of  $\text{Al}_2\text{O}_3$ . It is difficult to find out distortions of smectic C\* structure created by these particles visually under a polarizing microscope (Fig. 6). In our opinion, it is caused with extremely small sizes of these particles ( $r \leq 0.2 \mu\text{m}$ ).



*Fig.6.* The oscilloscope of the cell transmission with ferroelectric liquid crystal dispersed by particles  $\text{Al}_2\text{O}_3$  (the cell thickness of  $1.3 \mu\text{m}$ ), when sawtooth voltage is applied to the cell.

Characteristics of the Clark - Lagerwall effect in FLC + $\text{Al}_2\text{O}_3$  substantially do not differ from this effect observed in pure FLC. First of all, the effect has nonthreshold character as seen from the oscilloscope of cell transmission when sawtooth voltage is applied on the cell (Fig. 6).

Time characteristics of the cell with FLC + $\text{Al}_2\text{O}_3$  become little bit worsened in comparison with the cell with pure FLC (Fig. 9). It is connected by that rotary viscosity of ferroelectric liquid crystal increases with addition of small particles  $\text{Al}_2\text{O}_3$ . It proves to be true independent measurements under the form of a depolarizing current. As is known the area limited to the curve of a depolarizing current is equal to  $2P_S \cdot S$ , where

$P_S$  is spontaneous polarization and  $S$  is the working area of an electrooptical cell. The halfwidth  $U\tau_{1/2}$  of this curve gives the rotational viscosity on following formula [16]:

$$\gamma = P_S U \tau_{1/2} / 1.76 d$$

where  $U$  is voltage applied to an electrooptical cell.

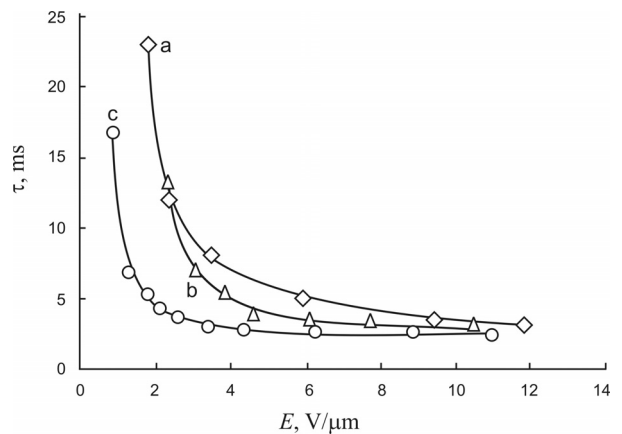


*Fig.7.* Dependence of switching time on applied electric field intensity: a – pure FLC (layer thickness of  $1.7 \mu\text{m}$ ); b-FLC dispersed by  $\text{Al}_2\text{O}_3$  particles (layer thickness of  $1.3 \mu\text{m}$ ); c-FLC dispersed by  $\text{SrTiO}_3$  particles (layer thickness  $2.3 \mu\text{m}$ ).

Unlike particles  $\text{Al}_2\text{O}_3$ , particles  $\text{SrTiO}_3$  are obviously visible under a polarizing microscope (Fig. 8). It is possible to see on the average  $10^3$  particles  $\text{SrTiO}_3$  in  $1 \text{ mm}^2$ . Full transition from one state to another occurs during time  $\tau$  called switching time. If action of the applied field takes place at smaller time  $t$  then transition is incomplete and the texture also differs (Fig.8).

The preliminary measurements spent in cells with thickness of  $30 \mu\text{m}$  and  $5 \mu\text{m}$  show that physical parameters of the composite essentially do not differ from parameters of pure ferroelectric LC.

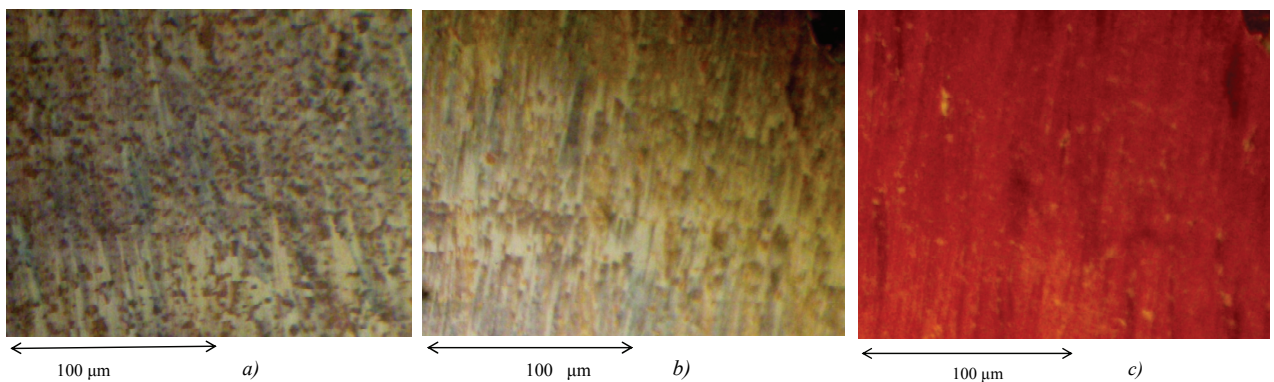


*Fig. 8.* A planar texture of ferroelectric liquid crystal dispersed by particles  $\text{SrTiO}_3$  (cell thickness of  $2.3 \mu\text{m}$ )  
a)  $U=0$ ; b)  $U = 10 \text{ V}$ ,  $t = 0.5 \text{ ms}$  c)  $U = 10 \text{ V}$ ,  $t = 5 \text{ ms}$ .

In comparison with centrosymmetric particles  $\text{Al}_2\text{O}_3$ , ferroelectric particles  $\text{SrTiO}_3$  strongly deform a field director of ferroelectric liquid crystal, i.e. play a role of the centers of declination. It is connected, firstly,

rather large sizes of these particles, secondly, presence of permanent polarizing charges on surface of these particles which co-operating with spontaneous polarization of ferroelectric liquid crystal deform the

spatial distribution of the director. The electrooptical effect in such cell also has nonthreshold character.

Time characteristics of the Clark – Lagerwall effect of FLC + SrTiO<sub>3</sub> at high voltage, i.e. in the bulk regime of switching essentially surpass time characteristics of a cell with pure FLC (Fig. 7) since transition from the deformed UP-state to a DOWN- state demands overcoming much smaller energy than transition from a pure UP-state to a DOWN-state.

Predictably, switching time of a cell with FLC + SrTiO<sub>3</sub> considerably is less than at a cell with pure FLC where the switching regime by movement of domain borders takes place at small voltage. It will be conform with Avrami model according to which the switching speed from UP – state to DOWN- state and on the contrary, except of electric field intensity, is defined also by number of the nucleus centers, where formation and growth of domains of an opposite sign begin. These centers serve as fortuitous defects in an electrooptical cell with the pure LC, and numerous small particles SrTiO<sub>3</sub> serve in a cell with FLC + SrTiO<sub>3</sub>. The FLC

structure is strongly deformed for two reasons: surfaces of these particles are strongly polarized and the sizes of these particles coincide with widths of domain walls. Therefore, switching rate of a cell with FLC + SrTiO<sub>3</sub> is more than at a cell with the pure FLC at low voltage.

## CONCLUSIONS

It has been shown that time characteristics of a cell with LC - Al<sub>2</sub>O<sub>3</sub> appear a little bit worsened in comparison with a cell with the pure LC. It is connected by that rotational viscosity of ferroelectric liquid crystal increases with addition of small particles Al<sub>2</sub>O<sub>3</sub>. While time characteristics of the Clark – Lagerwall effect in the LC - SrTiO<sub>3</sub> cell essentially surpass time characteristics of the cell with the pure LC since transition from the deformed a UP-state to a DOWN- state demands overcoming much smaller energy than transition from a pure UP-state to a DOWN-state.

The work has been supported by Scientific and Technology center in Ukraine (grant No 5352).

- 
- [1] V.G. Chigrinov. Liquid crystal Devices, 1999, Springer Verlag, 384 P.
  - [2] Handbook of Liquid Crystals, 1, Fundamentals, ed. By D.Demus, J.Goodby, John Wiley & Sons, 1998, 950 P.
  - [3] J.Ch. Khoo, Liquid Crystals, John Wiley & Sons, 2007, 387 P.
  - [4] Displays. Ed. G. Pankov. Moscow, Mir, 1982, 312 P. (In Russian).
  - [5] S.T. Lagerwall. Ferroelectrics and antiferroelectric liquid crystals, Willey VCH, 1999, 437 P.
  - [6] R.B. Meyer. Mol. Crystal.& Liq.Cryst. 40 (1977) 33-48.
  - [7] L.M. Blinov, L.A. Bresnev. Uspekhi Fiz. Nauk. 143, No2 (1984) 391- 248 (In Russian).
  - [8] D.M. Walba. Advances on the Synthesis and Reactivity of Solids. 1 (1991) 173-235.
  - [9] N.A. Clark, S.T. Lagerwall. Appl. Phys. Lett., 36 (1980) 899-901.
  - [10] J. Ouchi, H. Takezoe, A. Fukuda. Jap. J. Appl. Phys. 26, No 1 (1987)1-14.
  - [11] N.A. Clark, M.A. Handshy, S.T. Lagerwall. Mol. Cryst. Liq. Cryst., 94 (1983) 213-234.
  - [12] K. Nakamura, H. Orihara, Y. Ishibashi, Y. Yamada. Jap. J. Appl. Phys. 27, No 5 (1988) 705-709.
  - [13] W. Kukzhinsky, H. Stegemeyer. Chemical Physics Letters.70, No1 (1980)123-126.
  - [14] E.P. Pozhidaev, S.L. Smorgon, A.L. Andreev, I.N. Kompanets, V.Ya. Zyryanov, S.I. Kompanets. Ferroelectrics, 212 (1998)153-160.
  - [15] Ph. Martinot-Lagarde. Ferroelectrics. 84 (1988) 53-64.0
  - [16] I. Dahl, S.T. Lagerwall, K. Skarp. Phys. Rev. A. 36, No9 (1988) 4380-4389.

Received: 09.03.2011

## ELECTRONIC BAND STRUCTURE OF TlFeSe<sub>2</sub> IN FERROMAGNETIC PHASE

Z.A. JAHANGIRLI <sup>1,4</sup>, K. MIMURA<sup>2</sup>, K. WAKITA<sup>3</sup>,  
Y. SHIM<sup>2</sup>, G.S. ORUDZHEV<sup>4</sup>, N.T. MAMEDOV<sup>2</sup>

<sup>1</sup>*H.M. Abdullayev Institute of Physics, Azerbaijan National Academy of Sciences*

<sup>2</sup>*Osaka Prefecture University, Japan*

<sup>3</sup>*Chiba Institute of Technology, Japan*

<sup>4</sup>*Technical University, Azerbaijan*

Electronic band structure of crystalline TlFeSe<sub>2</sub> has been calculated using full-potential method of Linear Augmented Plane Wave (LAPW) in density-functional approach with exchange-correlation potential taken in Generalized Gradient Approximation (GGA). The chemical bond in TlFeSe<sub>2</sub> is shown to be metallic because energies of 3d-electrons localized at iron atoms are close to Fermi level energy.

**Keywords:** density functional theory, LDA, spintronics, ferromagnetic.

**PACS:** 75.50.Dd, 75.50 Ee, 75.50 Pp

Spintronics is a subfield of quantum electronics where particle's spin, or own mechanic momentum of a particle is used along with particle's charge to physically represent the information. In connection with this, magnetic materials such as magnetic semiconductors are of great interest. The electronic band structure of magnetic materials is tightly related to d- or f- shell electrons of the atoms of rare earth and transient elements. Because of the 3d<sup>6</sup>4s<sup>2</sup> ground state configuration of the valence electrons in Fe atoms, magnetic functionalities are naturally expected in Fe-contained materials. In particular, Fe-contained materials with lowered dimensionality are of special interest.

TlFeSe<sub>2</sub> with quasi-one-dimensional linear chain structure and space group  $C_{2/m}(C_{2h}^3)$  [1,2] has attracted our attention as one of such materials. Seidov *et al.* [3] have experimentally studied temperature dependences of

magnetic susceptibility and electric resistivity of TlFeSe<sub>2</sub>. The obtained results have been indicative of an anti-ferromagnetic ordering in semiconducting phase of TlFeSe<sub>2</sub>.

First calculations, performed in plane wave basis by using empiric pseudo-potential method [4, 5] could not provide a comprehensive view on electronic band structure of TlFeSe<sub>2</sub>, because of the emerged technical difficulties caused by necessity to take into account relativistic effects, electron correlation and electron magnetic ordering in the empty shells of Fe atoms.

We have then employed LAPW- based density functional method [6] to take into account spin polarization effects inherent in ground state of empty shell of Fe atom. By choosing spin direction (z) of d electrons of Fe atom, we have examined how the total energy per unit cell ( $E_{tot}$ ) depends on the total spin projection ( $S_z$ ) on this direction.

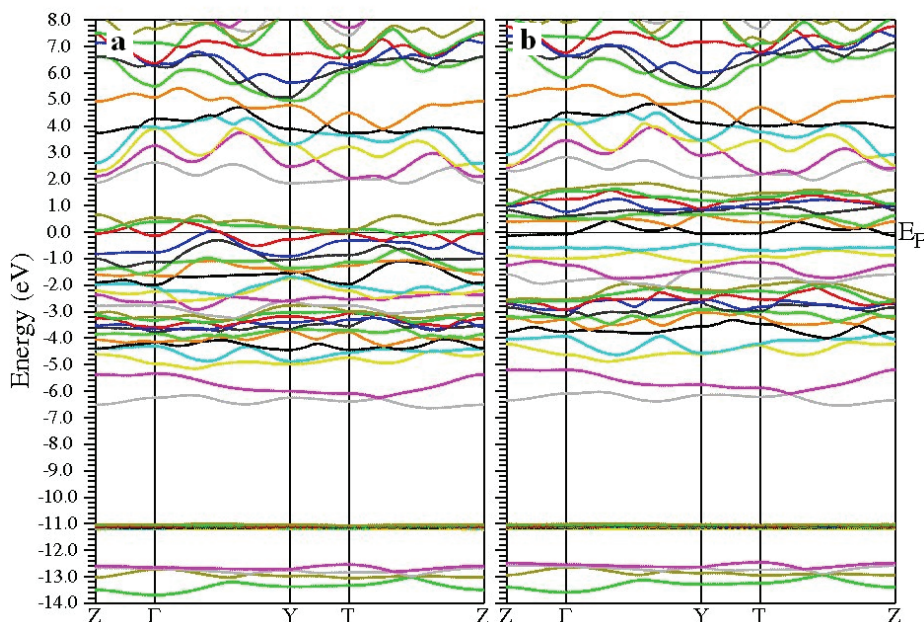


Fig. 1. Band structure of TlFeSe<sub>2</sub>: a- "spin-up", b- "spin-down". It also follows from the obtained results that coupling of six 3d electrons

## ELECTRONIC BAND STRUCTURE OF TlFeSe<sub>2</sub> IN FERROMAGNETIC PHASE

Calculations have been performed with the use of WIEN2k program packet [7]. The convergence of the iterations has been as high as 1meV for randomly chosen 436 k-points inside the reduced Brillouin zone of TlFeSe<sub>2</sub>. The states with energy less than -6 Ry have been treated as core states. Stable anti-ferromagnetic and unstable ferromagnetic phases have been found to be possible according to the obtained results. Here we present the results related to ferromagnetic phase of TlFeSe<sub>2</sub>.

In this phase, TlFeSe<sub>2</sub> is a metallic compound for both spin polarizations (Fig. 1).

In Table 1 we have given total energy per unit cell for six values of the total spin projection,  $S_z$ . As follows from the Table 1, the minimum energy per unit cell corresponds to the spin configuration with  $S_z=5$ .

The total and local DOS (density-of-state) distributions are shown in Fig. 2. Analysis of the obtained DOS drives to a conclusion that crystal orbitals occupied by 3 non-coupled electrons are 3d Fe orbitals with energies close to Fermi level energy. The contribution of the other atoms into total DOS is negligibly small.

$(S_z=0)$  is energetically non-favorable. At the same time, the energy difference between  $E_{tot}$  for  $S_z=5$  and  $S_z=4$  is rather small (0,001 Ry, Table. 1). Therefore it would be hardly correct to completely exclude electron configuration for which the total spin projection  $S_z$  equals 4.

Table 2 contains muffin-tin radii ( $R_{MT}$ ), distance to the nearest neighbor, sum of muffin-tin radii of the nearest neighbors, and charge in muffin-tin sphere (MT) for each atom in the unit cell.

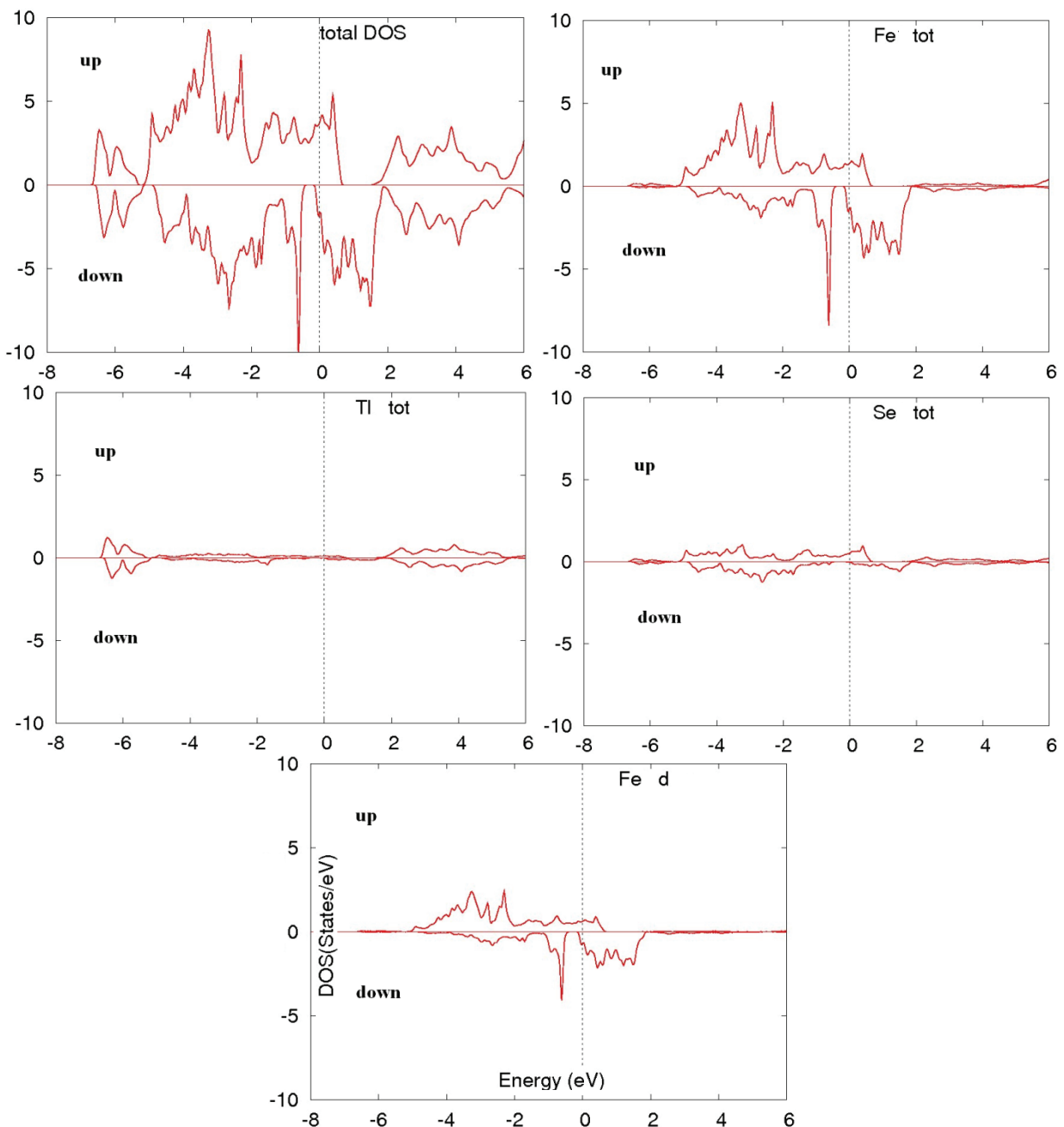


Fig. 2. Full and local DOS in TlFeSe<sub>2</sub> for “spin-up” и “spin-down” polarizations.

Table 1

Total spin projections ( $S_z$ ) and total energy per unit cell ( $E_{tot}$ )

| $S_z$     | 6           | 5           | 4           | 3           | 2           | 1           | 0           |
|-----------|-------------|-------------|-------------|-------------|-------------|-------------|-------------|
| $E_{tot}$ | -105688.854 | -105688.859 | -105688.858 | -105688.856 | -105688.854 | -105688.847 | -105688.838 |

Table 2

Muffin-tin radiuses, distance to the nearest neighbor, sum of  $R_{MT}$  of the nearest neighbors, charge in MT sphere.

| atom | $R_{MT}$ (a.u.) | nearest neighbor/distance (a.u.) | sum of $R_{MT}$ | charge in MT sphere |
|------|-----------------|----------------------------------|-----------------|---------------------|
| Tl   | 2.5             | Se1/ 6.11345                     | 4.57            | 5.4165              |
| Fe   | 2.33            | Se1/ 4.42953                     | 4.4             | 5.2246              |
| Se1  | 2.07            | Fe/ 4.42953                      | 4.4             | 6.7095              |
| Se2  | 2.07            | Fe/ 4.4506                       | 4.4             | 6.6992              |

It is seen from the Table 2 that muffin-tin spheres of Fe и Se atoms are adjoined. The charge that is concentrated in muffin-tin sphere of Se atom is noticeably larger than that in muffin-tin sphere of Tl or Fe. It is then possible to conclude that ionic constituent is yet appreciable and that chemical bonding in ferromagnetic phase of  $TlFeSe_2$  bears not only metallic but also ionic character.

The authors are thankful to Prof. F.M. Hashimzade for reading the manuscript and useful advises. This work was performed under the grant EIF-2011-1(1)-40/01-22 of Science Development Foundation under the President of Azerbaijan Republic.

- 
- [1]. A. Kutoglu, Naturwissenschaften, 1974, 61,125
  - [2]. K. Klepp, H. Boller, Monatshefte fur chemie, 1979, 110, 1045
  - [3]. Z. Seidov, H.-A. Krug von Nidda, J. Hemberger, A. Loidl, G. Sultanov, E. Kerimova, A. Panfilov, Phys. Rev B, 2001, v. 65, 014433.
  - [4]. F.M. Gashimzade, G.S. Orujev, Z.A. Jakhangirov. FTT, 1993, t.35, №7. (in Russian)
  - [5]. G.S. Orujev, N.A. Aliyeva, Z.A. Jakhangirov. Preprint №114, NPO KI, g. Baku, 1991. (in Russian)
  - [6]. David J. Singh, Plane Waves, Pseudopotentials and the LAPW, Method, Kluwer Academic Publishers, Boston, 1994, p. 225
  - [7]. P. Blaha, K. Schwarz, and J. Luitz, WIEN2k, A Full Potential Linearized Augmented Plane Wave Package for Calculating Crystal Properties Karlheinz Schwarz, Techn. Universitat Wien, Austria, 1999, ISBN 3-9501031-0-4.

Received: 19.04.2011

## EFFECT OF THE LIGHT ON CHARGE CARRIERS MOBILITY IN GALLIUM MONOSELENIDE CRYSTALS

**A.SH. ABDINOV, R.F. BABAYEVA, R.M. RZAYEV**

*Baku State University, Az 1145, Baku, Z. Khalilov str., 23*

*Тел.: (994 12) 4397373, e-mail: [abdinov\\_axmed@yahoo.com](mailto:abdinov_axmed@yahoo.com)*

*[Babaeva-Rena@yandex.ru](mailto:Babaeva-Rena@yandex.ru)*

The effect of light from the different region of spectrum (from the intrinsic and impurity absorption region of spectrum) on the mobility if charges in pure and alloyed by gadolinium atoms crystals of p-GaSe have been investigated at temperature of  $T=77\pm350$ K.

It is established that the value and course of dependence of mobility on the temperature changes at influence of light. In addition there is residue mobility effect. All this effect of light on the mobility depends both on the dark resistivity of pure and on the doping level and on the spectrum composition of light.

It is find out that observed effect of the light on the mobility in both group of crystals due to the optical smooching of potential barrier free energetically zone (optical erasing of drift barriers).

**Keywords:** layered structure, effect of light, charge carrier mobility.

**PACS:** SQ 621.315.592

### 1. INTRODUCTION

Semiconducting  $A^{III}B^{VI}$  compounds with layered structure, in particular gallium monoselenide crystals with high photosensitivity, as well as unusual photoelectric properties attract attention of the researchers [1-3].

In this paper results received by us at research of the effect of light from different region of optical spectrum on mobility of charge carriers (study of "mobility photoeffects") in pure (non-doped specially) and doped by gadolinium atoms gallium monoselenide crystals are reported.

### 2. EXPERIMENT

The research objects were pure (with  $\rho_d \approx 10^3; 10^4; 2 \cdot 10^5; 9 \cdot 10^5; 4 \cdot 10^6; 9 \cdot 10^6; 2 \cdot 10^7; 1,5 \cdot 10^8 \Omega \cdot \text{cm}$  at 77 K) and doped ( $N_{Gd} \approx 10^{-5}; 10^{-4}; 10^{-3}; 10^{-2}$  and  $10^{-1}$  at.%) gallium monoselenide crystals (p-GaSe). Dark specific resistance of the doped crystals at 77 K depending on  $N_{Gd}$  varied within  $10^2 \div 10^9 \Omega \cdot \text{cm}$  limits and had its maximal value for  $N_{Gd} \approx 10^{-4}$  at.% and minimal one for  $N_{Gd} \approx 10^{-1}$  at.%.

Samples of rectangular parallelepiped shape were cut off from large ingots which were grown by a method of slow cooling at constant temperature gradient along the ingot. Doping was carried out from a solid phase [4].

In pure crystals at 300 K for different samples dark specific resistance ( $\rho_d$ ), mobility ( $\mu$ ) and concentration of the majority charge carriers ( $p_0$ ) were  $\sim 10^2 \div 10^3 \Omega \cdot \text{cm}$ ,  $90 \div 100 \text{ cm}^2/\text{V} \cdot \text{s}$  and  $\sim 10^{14} \div 10^{15} \text{ cm}^{-3}$  accordingly. With decreasing of temperature down to 77 K the concentration of the charge carriers in investigated crystals decreased only by one-two order of magnitude (at 77K  $p_0 \approx 10^{13} \div 10^{14} \text{ cm}^{-3}$ ) and change (growth) of  $\rho_d$  value sometimes reached up to several orders of magnitude. This fact testifies that in p-GaSe crystals under certain conditions at low temperatures besides concentration, mobility of the charge carriers also strongly (than by  $\mu \sim T^{3/2}$  or  $\mu \sim T^{3/2}$  low [5]) varies with temperature. At discussion before received on  $\mu(T)$  results, it was supposed that it may be conditioned by dominant role of

drift barriers [6-8] in current transit. For check of this version one of suitable ways may be study of influence of illumination on  $\mu$ .

With this purpose we recorded dependences of  $\mu$  from temperature ( $T$ ), time ( $t$ ), intensity ( $\Phi$ ) and wave length ( $\lambda$ ) of the light in p-GaSe samples with different dark specific resistance ( $\rho_d$ ) and doping level ( $N_{Gd}$ ) under different conditions.

### 3. RESULTS

It have been established that under other identical conditions, under effect of white or monochromatic light from fundamental absorption region mobility of the charge carriers in high-resistance pure (Fig. 1), as well as doped with  $N_{Gd} \leq 10^{-4}$  at.% (Fig. 2) crystals at first (at low intensities) nearly, under the linear law increases and further (at high large intensities) the dependence  $\mu(\Phi)$  goes to saturation. In so doing the index of power ( $k_o$ ) for low temperature part of  $\mu(T)$  dependence decreases with increasing of the light intensity ( $\Phi$ ) (Fig. 3). In p-GaSe<Gd> crystals effect of light on value and the course of temperature dependence of  $\mu$  has appeared dependent also on doping level ( $N_{Gd}$ ). With growth of  $N_{Gd}$  at first (for  $N_{Gd} \leq 10^{-4}$  at. %) the effect of light appears more strongly and then (for  $N_{Gd} > 10^{-4}$  at. %) (Fig. 4) is considerably weakly.

Thus both dependence  $\mu(T)$  and value of  $\mu$  and the temperatures  $T_M$ , at which the recession of charge carrier mobility under the law  $\mu \sim T^{3/2}$  begins, appear dependent also from prehistory of the investigated sample. If a sample previously at low temperatures ( $T < 120 \div 150$  K for different samples depending on  $\rho_d$  and  $N_{Gd}$ ) to expose for a long time to white or monochromatic light from fundamental absorption region, values of  $\mu$ ,  $T_M$  as well as  $\kappa_o$  (at  $T \leq T_M$ ) after termination the effect of the light, during the certain interval of time (10-15 minutes, depending on  $\rho_d$ ) significantly differ from available parameters both in the dark and at direct effect of the light (Fig. 5).

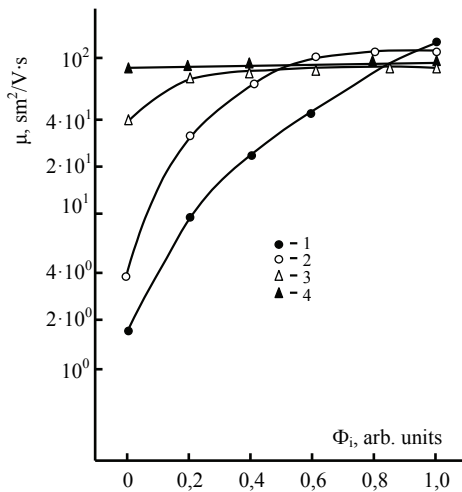


Fig. 1. Dependence of charge carrier mobility on intensity of monochromatic light from fundamental absorption region in  $p$ -GaSe crystals with different specific dark resistance:

$$T = 77 \text{ K}; \lambda_i = 0.58 \text{ mcm}$$

$$\rho_d^{(77K)}, \text{Ohm} \cdot \text{cm} : 1 - 1.5 \cdot 10^8; 2 - 2 \cdot 10^7;$$

$$3 - 9 \cdot 10^5, 4 - 10^3$$

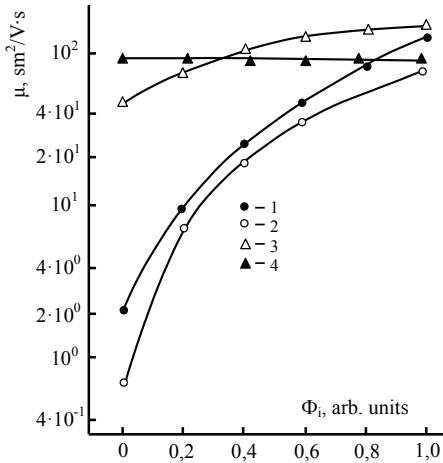


Fig. 2. Dependence of the charge carrier mobility on intensity of monochromatic light from fundamental absorption region in  $p$ -GaSe crystals with different doping levels.  $T = 77 \text{ K}; \lambda_i = 0.58 \text{ mcm}$

$$N_{Gd}, \text{at.\%} : 1 - 0; 2 - 10^{-4}; 3 - 10^{-2}, 4 - 10^{-1}$$

$$\rho_d^{(77K)}, \text{Ohm} \cdot \text{cm} : 1 - 1.5 \cdot 10^8$$

Under other identical conditions  $\mu$  has appeared dependent also on wavelength of the light (Fig. 6). It is established that under the effect of white or monochromatic light from fundamental absorption region,  $\mu$  increases relative to its dark value ( $\mu_0$ ) and after termination of the effect of the light only in  $\sim 100 \div 120$  s reaches its initial dark value - "positive mobility memory" is observed.

Under the effect of the light from impurity absorption region creating negative photoconductivity, or IR erasing of intrinsic photoconductivity the mobility of

free charge carriers decreases relative to  $\mu_0$  (Fig. 5, curves 2 and 4) and after termination of the effect of the illumination  $\mu$  reaches its initial value in  $\sim 40 \div 60$  s - "negative mobility memory" is observed (Fig. 8).

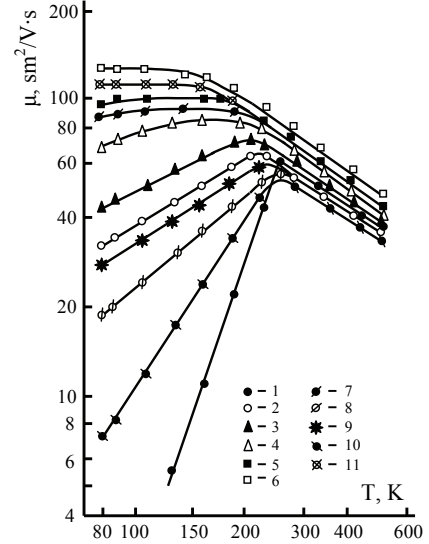


Fig. 3. Temperature dependence of the charge carrier mobility in  $p$ -GaSe crystals under illumination by monochromatic light from fundamental absorption region with different intensity:

$$T = 77 \text{ K}; \rho_d, \text{Ohm} \cdot \text{cm} : 1, 2, 3, 4, 5, 6 - 1.5 \cdot 10^8,$$

$$7, 8, 9 - 2 \cdot 10^7, 10, 11 - 9 \cdot 10^5. \lambda_i = 0.58 \text{ mcm}.$$

$$\Phi_i = \text{arb. units} : 1, 4, 9 - 0.0; 2, 8, 10 - 0.2; 4 - 0.6;$$

$$5 - 0.8; 6 - 1.0; 3, 9, 11 - 0.4$$

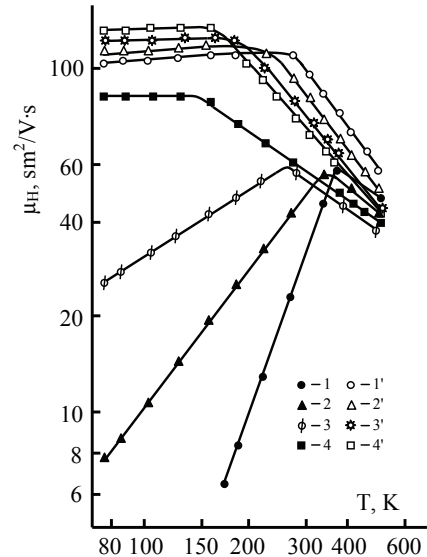


Fig. 4. Temperature dependence of the charge carrier mobility in  $p$ -GaSe<Gd> crystals illuminated by monochromatic light from fundamental absorption region with different intensity:

$$T = 77 \text{ K}; N_{Gd}, \text{at.\%} : 1, 2 - 10^{-1};$$

$$3, 4, 5, 6, 7 - 10^{-4}, \lambda_i = 0.58 \text{ mcm}$$

$$\Phi_i = 1, 3 - 0.1; 4 - 0.3; 5 - 0.6; 6 - 0.8; 2, 7 - 0.9$$

## EFFECT OF THE LIGHT ON CHARGE CARRIERS MOBILITY IN GALLIUM MONOSELENIDE CRYSTALS

In case of “positive mobility memory” initial dark value of mobility ( $\mu_0$ ) can be restored more quickly (almost instantly).

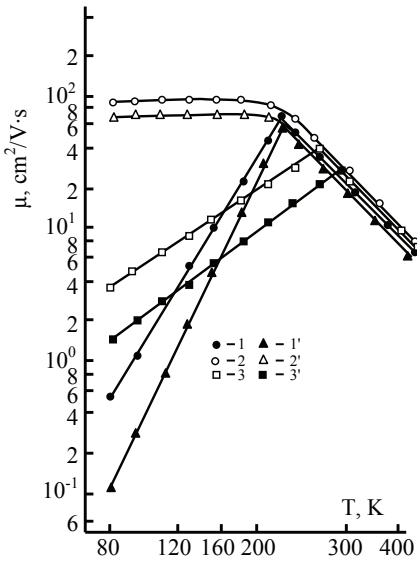


Fig. 5. Temperature dependence of the charge carrier mobility in  $p$ -GaSe (curves 1-3) and  $p$ -GaSe<Gd> (curves 1'-3') crystals in initial dark condition (1 and 1'), under effect of the light (2 and 2') and after the termination of the effect of the light (3 and 3'):  $T = 77 \text{ K}$ ;  $\lambda_i = 0.58 \text{ mcm}$

$$\Phi_i = 0.3 \text{ arb. units}; \Delta t = 5 \text{ sec}$$

$$\rho_d^{(77 \text{ K})}, \text{Ohm} \cdot \text{cm} : 1, 2, 3 - 1.5 \cdot 10^8;$$

$$N_{Gd}, \text{at.\%} : 1, 2, 3 - 0; 1', 2', 3' - 10^{-4}$$

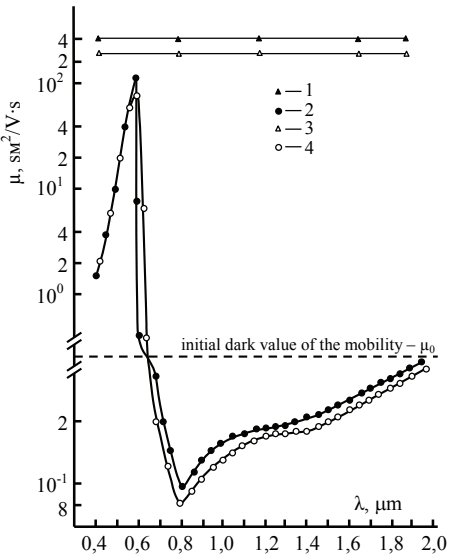


Fig. 6. Dependence of the charge carrier mobility on light wavelength in  $p$ -GaSe (curves 1 and 2) and  $p$ -GaSe<Gd> (curves 3 and 4) crystals:

$$T = 77 \text{ K}; \Phi_c = 0.7 \Phi_m;$$

$$\rho_d^{(77 \text{ K})}, \text{Ohm} \cdot \text{cm} : 1 - 10^3; 2 - 1.5 \cdot 10^8;$$

$$N_{Gd}, \text{at.\%} : 3 - 10^{-1}; 4 - 10^3$$

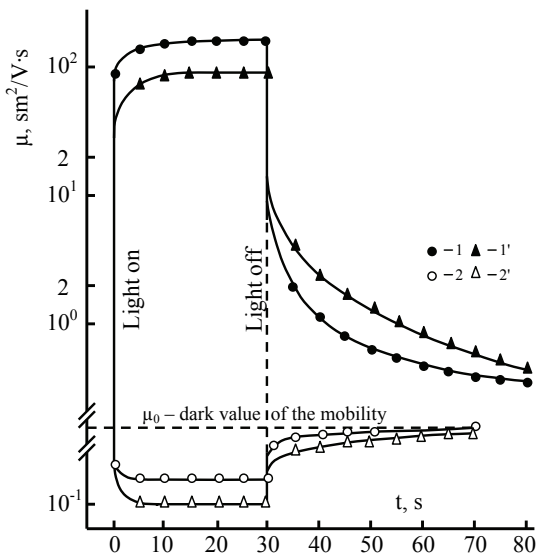


Fig. 7. Dependence of the charge carrier mobility on time in  $p$ -GaSe (curves 1 and 2) and  $p$ -GaSe<Gd> (curves 1' and 2') crystals under illumination by light from fundamental (curves 1 and 1') and impurity (curves 2 and 2') absorption region.

$$T = 77 \text{ K}; N_{Gd}, \text{at.\%} : 1, 2 - 0; 1', 2' - 10^{-4};$$

$$\rho_d^{(77 \text{ K})}, \text{Ohm} \cdot \text{cm} : 1, 2 - 2 \cdot 10^7$$

$$\Phi_i = 0.3 \text{ arb. units} : 1, 1' - 0.3; 2, 2' - 1.0.$$

$$\lambda, \text{mcm} : 1, 1' - 0.58; 2, 2' - 0.80$$

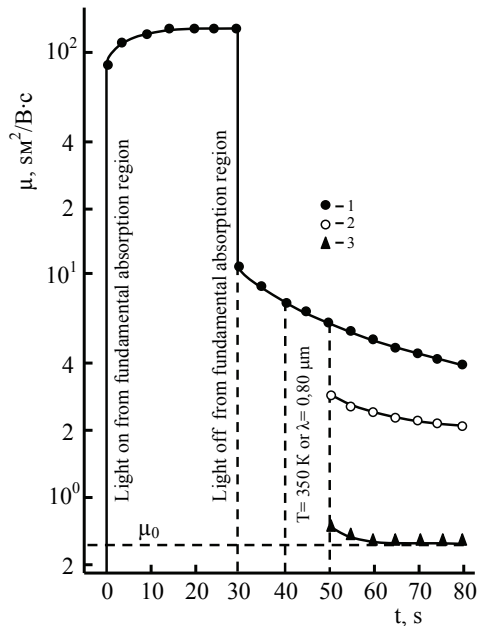


Fig. 8. Kinetics of the charge carriers mobility after termination of illumination by the light from fundamental absorption region without additional effect (curve 1) and in case of short-term effect of thermal (curve 2) and light (curve 3) pulse from impurity absorption region:  $T = 77 \text{ K}$ ;

$$\lambda_i = 0.58 \text{ mcm} \quad \lambda_i = 0.80 \text{ mcm} \quad \Phi = 0.9 \Phi_m$$

$$\rho_d = 1.5 \cdot 10^8 \text{ Ohm} \cdot \text{cm}; \Delta t = 10 \text{ sec}$$

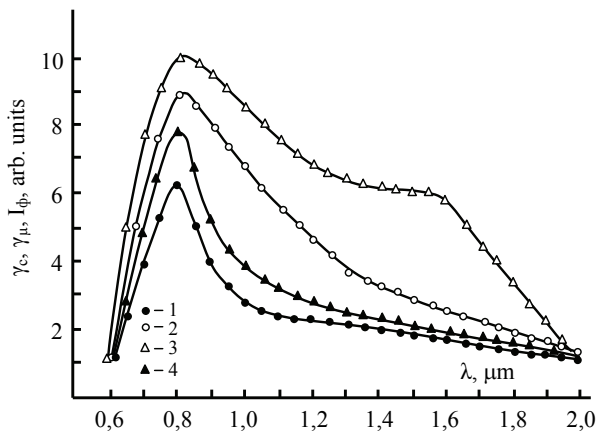


Fig. 9. Spectral distribution of negative photoconductivity (curve 4), IR erasing of the “mobility memory” (curve 1), IR erasing of residual (curve 2) and intrinsic (curve 3) photoconductivity:

$$T = 77 \text{ K}; \rho_d^{(77 \text{ K})} = 1.5 \cdot 10^8 \text{ Ohm} \cdot \text{cm}$$

For this purpose it is enough to heat a sample up to  $T \geq 350\text{K}$  with the subsequent sharp cooling by immersing it in liquid nitrogen or to expose it to the light from impurity absorption region during 10-15 s (by temperature or IR-erasing accordingly) (Fig. 9). With increase of the temperature effect of the light, as well as prehistory of the sample on mobility of the charge carriers decreases and at  $T > 150\text{K}$  these effects completely disappear.

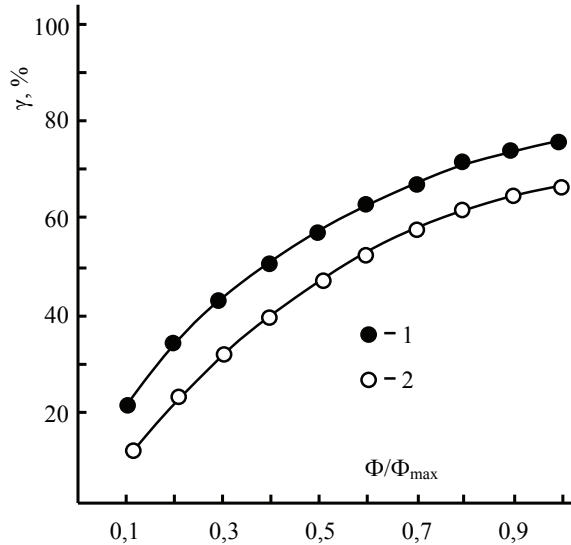


Fig. 10. Dependence of depth of IR erasing of the “mobility memory” in  $p$ -GaSe (curve 1) and  $p$ -GaSe<Gd> (curve 2) crystals on erasing light intensity:

$$T = 77 \text{ K}; \rho_d^{(77 \text{ K})} = 1.5 \cdot 10^8 \text{ Ohm} \cdot \text{cm}; \\ N_{\text{Gd}} = 10^{-3} \text{ at.\%}; \lambda_i = 0.80 \text{ mcm} \Delta t = 10 \text{ sec}$$

As opposed to thermal erasing, in case IR-erasing the absolute restoration of  $\mu_0$  does not occur. In the latter case under optimum conditions (under optimum wavelength, intensity and duration of the effect of IR

light) a depth of IR-erasing of the “mobility memory”

$$(\gamma = \frac{\mu_{pc} - \mu_{po}}{\mu_{po}} \cdot 100\%) \text{ does not exceed } 60\text{-}70\%.$$

It is established that spectral distribution of IR-erasing of the “mobility memory” in both crystals groups good correlated with spectra of IR-erasing of residual and intrinsic photoconductivity, as well as spectrum of negative photoconductivity (Fig. 9). It is necessary to note that the depth of IR-erasing of the “mobility memory” ( $\gamma$ ) in the investigated crystals has appeared dependent also on intensity of erasing light ( $\Phi_{\text{er}}$ ). With increasing  $\Phi_{\text{er}}$  a value of  $\gamma$  at first increases approximately under the linear law and further (at high  $\Phi_{\text{er}}$ ) the dependence  $\gamma(\Phi_{\text{er}})$  approximate to saturation (Fig. 10).

#### 4. DISCUSSION

Passing to discussion of the received results, first of all it is necessary to note that the established dependences of the charge carriers mobility on effect of the light at different temperatures, value of dark specific resistance and doping level for crystals, as well as on the time from the point of view of existing conceptions in the scientific literature for features of the charge carriers mobility in quasi-homogeneous semiconductors are abnormal. More correctly, these results do not converge with criteria of the specified theory and it appears inexplicable on their basis. In our opinion, therewith it is necessary to take into account also effect of factors caused by specificity of a potential relief of free energy bands of gallium monoselenide crystals [6]. In particular, it is supposed that because of presence of vacancies of the gallium atoms (or ions), and/or displacement of the adjacent layers relative to each other, as well as areas consisting of other modifications [9], in separate microareas of the investigated sample exist chaotic (on distribution and on the dimensions) large-scale defects. Therefore, the gallium monoselenide crystals under certain conditions (at low temperatures, in the dark and at low illuminations) behave as the partially disorder semiconductors in whole consisting of low resistance matrix (LRM) with chaotic high-resistance inclusions (HRI) [6, 7]. As opposed to non-crystalline semiconductors (for example, vitreous, amorphous semiconductors, etc.), therewith though as a whole prevails integrated order caused by single crystallinity, however its some local microareas behave similarly to disorder. A degree of the irregularity of such (partially disordered) semiconductor is determined by quantity and dimensions of the macroscopic defects. Such partial irregularity in turn determines value of the dark specific resistance and causes detection of a number of anomalies in electronic, including transport properties of the investigated material. In such structure recombination barriers on LRM-HRI borders and drift barriers between adjacent HRI areas arises [7, 8]. Naturally, the larger a degree of such partial irregularity the larger be value of specific dark resistance of the crystal. With increase of temperature or intensity of the light from fundamental absorption area falling on a sample occurs gradual thermal or optical ordering (smoothing of a potential relief of free areas) of the crystal accordingly.

At low doping of  $p$ -GaSe<Gd> crystals gadolinium ions under the effect of internal electric field existing in LRM-HRI borders are accumulated around HRI and increase the dimensions of HRI and irregularity degree of the crystal. At last, at those contents of the entered gadolinium atoms, when LRM-HRI border already is gradually saturated by *Gd* ions, begins their entry also in inside of HRI. Thus they partially replacing absent gallium ions result in reduction of irregularity degree of the crystal. At more high doping levels growing part of gallium vacancies are filled by gadolinium ions and the investigated crystal approximate to quasi-ordered state. On the other hand, because of covalent bonds between gadolinium ions situated in adjacent layers, considerably increases interlayer bonds in the crystal. Further (at more higher doping levels) introduced gadolinium atoms already begin regularly distribute on all volume of the crystal and investigated crystal gradually approximate to condition of regularly doped quasi-ordered semiconductor. And in such  $p$ -GaSe<Gd> crystal bonds between the adjacent layers becomes rather strong than in pure  $p$ -GaSe crystals. Therefore  $p$ -GaSe<Gd> single crystals with  $N_{Gd} \approx 10^2 \div 10^3$  at.% have more stable, high reproducible parameters and characteristics than low doped crystals.

Within the framework of the above described model it is possible to assume that in high-resistance gallium monoselenide crystals at low temperatures in the dark besides scattering on different dot defects [5], current transit (accordingly mobility of the charge carriers) is determined also by presence of the drift barriers in the appropriate free bands with height  $\Delta\epsilon_{dr}$ . And the effect of drift barriers on current transit is dominant and the charge carriers for overcoming these barriers should expend energy  $\Delta\epsilon = \Delta\epsilon_{dr}$ . For this reason with increase of temperature, at first (at low temperatures) the mobility of the charge carriers increases more strongly (under the law  $\mu \sim \exp(-\Delta\epsilon_{dr}/kT)$ ) than at domination scattering of the charge carriers on impurity ions ( $\mu \sim T^{3/2}$ ).

As with growth of  $\Delta\epsilon_{dr}$  increases also  $\rho_d$ , under other identical conditions with growth of  $\rho_d$  an index of power in  $\mu(T)$  dependence at low temperatures ( $k_o$ ) increases. More correctly, in crystals with high  $\rho_d$  the course of  $\mu(T)$  curves appears more abrupt.

In  $p$ -GaSe<Gd> crystals an irregularity degree of the crystal and value of  $\Delta\epsilon_{dr}$  with  $N_{Gd}$  vary not monotonously and with growth of  $N_{Gd}$  at first (at  $N_{Gd} < 10^{-4}$  at. %) both they increase and further (at  $N_{Gd} > 10^{-4}$  at. %) passing through a maximum begin to decrease. Thereof, at low temperatures the steepness of  $\mu(T)$  curves varies with a doping level non-monotonously.

Under illumination with white or monochromatic light from fundamental absorption region owing to optical smoothing of the potential relief of free energy bands of the crystal [10] an index of power in  $\mu(T)$  dependence at low temperatures decreases.

Under illumination with light from impurity absorption region owing to change of the recombination channel (replacement of slow recombination through r-centers to fast S-centers [11]) concentration of the charge carriers in free bands decreases and the height of the potential barriers, including drift barriers, increases. This in turn results in reduction of the charge mobility.

As to detection of "positive and negative mobility effect", as well as "mobility memory", both of them in frameworks of aforesaid may be connected to presence of recombination barriers in investigated crystals. Significantly interfering on recombination of non-equilibrium free charge carriers, these barriers slow down process of restoration of initial (existing before illumination) state of the drift barriers.

Within the framework of the offered model observable in high-resistance pure and weak doped crystals "the effect of residual mobility" can be explained by partial compensation of the bulk charge on LRM-HRI border by a charge of the superfluous concentration of charge carriers [11] created by light. After termination of the effect of the light, because of an obstacle recombination barriers this superfluous concentration of non-equilibrium charge carriers recombine non-instantly, but much more slowly. Therefore initial value of  $\Delta\epsilon_{dr}$  mobility for the charge carriers also establishes slowly - the "effect of mobility memory" is observed.

At  $T > T_M$  and high  $N_{Gd}$  owing to temperature and impurity smoothing of the potential relief of free energy bands the role of drift (including recombination) barriers in mobility of charge carriers sharply decreases. Therefore decays (or disappears) both dependence of  $\mu$  on effect of light, the "effect of memory mobility" and effect of prehistory of the sample on the charge carrier mobility.

## 5. CONCLUSION

Thus one can say that the found out features of the effect of the light on mobility of charge carriers in high-resistance, as well as in low-doped by gadolinium atoms gallium monoselenide crystals, first of all, are stipulated by partial irregularity of this material.

With application of the model of the semiconductor with two energy barriers and different local energy levels (traps, capture levels, slow and fast recombination centers) in the band-gap it is possible satisfactorily to explain the received results.

- 
- [1] A.Sh. Abdinov, A.G. Kyazimzadeh. Fiz. i Tekh. Poluprovodnikov, 1975, V. 9, No. 11, PP. 2135-2138 (in Russian).
  - [2] A.Sh. Abdinov, A.M. Guseynov. Residual IR-quenching of intrinsic photoconductivity in indium and gallium selenide single crystals. Doklady AN Az. SSR, 1989, V. 45, No. 4, PP. 11-16 (in Russian).
  - [3] A.Sh. Abdinov., R.F. Babayeva, R.M. Rzayev, Sh.A. Allahverdiyev. Sensitized impurity photoconductivity in  $p$ -GaSe single crystals, doped with rare-earth elements. Bulletin of Baku University, ser. fiz. mat. nauk, 2006, No.3, PP. 156-161 (in Russian).
  - [4] A.M. Guseynov, T.I. Sadykhov. Reception of indium selenide single crystals doped with rare-earth elements. In collection: Electrophysical properties of semiconductors and gas-discharge plasma. Baku, ASU, 1989, PP. 42-44 (in Russian).

- [5] *V.L. Bonch-Bruyevich, S.G. Kalashnikov.* Physics of semiconductors, Moscow, "Science", 1990, 668 p. (in Russian).
- [6] *R.F. Babayeva.* Izvestiya NAN Azerb., ser. fiz. mat. i tekhn. nauk., Fizika i Astronomiya, 2009, V. XXIX, No. 5, PP. 202-205 (in Russian).
- [7] *M.K. Sheynkman, A. Ya. Shik.* Fiz. i Tekh. Poluprovodnikov, 1976, V. 10, No.2, PP. 209-232 (in Russian).
- [8] *V.B. Sandomirskiy, A.G. Zhdan, M.A. Messerer, I.B. Gukyayev.* The mechanism of the frozen (residual) conductivity of semiconductors. Fiz. i Tekh. Poluprovodnikov, V. 7, No.6, 1973, PP. 1314-1321(in Russian).
- [9] *Z.S. Medvedeva.* Chalcogenides of elements of III subgroups of periodic system. Moscow, "Science", 1968, 215 p. (in Russian).
- [10] *S.M.Ryvkin.* Photoelectric phenomena in semiconductors. M. "Science", 1963, 494 p. (in Russian).
- [11] *V.I. Tahirov, A.G. Kyazymzadeh, M.M. Panakhov.* Izvestiya Vuzov, Fizika, 1981, V. 24, No.6, PP. 28-31. (in Russian).

*Received: 18.05.11*

## THEORETICAL INVESTIGATION OF VIBRATIONAL FREQUENCIES AND MOLECULAR STRUCTURE OF SOME $[M(Cl)_6]^{2-}$ IONS

**GÜRKAN KEŞAN AND CEMAL PARLAK**

*Department of Physics, Dumlupınar University,  
43100, Kütahya, Turkey*

The normal mode frequencies and corresponding vibrational assignments and structural parameters of  $[M(Cl)_6]^{2-}$  ions ( $M = Ti$ , Ge or Zr) have been theoretically examined by means of B3LYP density functional method with Lanl2dz basis sets. The thermodynamics functions, atomic charges, the highest occupied and lowest unoccupied molecular orbitals (HOMO or LUMO) of these ions were also predicted at the same level of theory. Theoretical results have been successfully compared against available experimental data in the literature.

**Keywords:**  $[Ti(Cl)_6]^{2-}$ ,  $[Ge(Cl)_6]^{2-}$ ,  $[Zr(Cl)_6]^{2-}$ , B3LYP, Lanl2dz.

**PACS:** 31.15. E, 33.20.Ea, 33.20.Tp

### 1. INTRODUCTION

Octahedral halide complexes,  $[M(Cl)_6]^{2-}$  which is called hexahalogeno compounds, of  $O_h$  symmetry have been extensively studied for many years [1-3]. Experimental data of the vibrational spectra of  $[M(Cl)_6]^{2-}$  ions ( $M = Ti$ , Ge or Zr) ions exist in the literature [1, 4-6]. The B3LYP density functional model exhibits good performance on electron affinities, excellent performance on bond energies and reasonably good performance on vibrational frequencies and geometries of inorganic or ion compounds [7] as well as organic and neutral compounds [8]. The Lanl (Los Alamos National Laboratory) basis sets, also known as Lanl2dz (Lanl-2-double zeta) and developed by Hay and Wadt [9-11], have been widely used in quantum chemistry, particularly in the study of compounds containing heavy elements.

The goal of present study is to aid in making assignments to the fundamental normal modes of  $[M(Cl)_6]^{2-}$  ( $M=Ti$ , Ge, Zr) and in clarifying the experimental data available for these ions. In this study, the vibrational spectra of  $[M(Cl)_6]^{2-}$  ions are performed using the DFT/B3LYP method with Lanl2dz basis set and compared to available experimental data. Geometric parameters, thermodynamic properties, atomic charges and HOMO-LUMO molecular orbitals were also calculated for these ions with same level.

### 2. CALCULATION

For the vibrational calculation, molecular structure of  $[M(Cl)_6]^{2-}$  ions were first optimized by B3LYP model with Lanl2dz basis set. The optimized geometric structure concerning to the minimum on the potential energy surface was provided by solving self-consistent field (SCF) equation iteratively. The absence of imaginary frequencies confirmed that the optimized structure is a local minimum. The graphics of optimization steps for these ions were carried out by the ChemCraft program [12]. After the optimization, the vibrational frequencies of  $[M(Cl)_6]^{2-}$  were calculated using the same method and the basis set under the keyword Freq = Raman and then scaled to generate the corrected frequencies. Correction factors for selected regions or vibrational modes were

calculated using  $\sum (v^{exp} / v^{calc}) / n$  [7, 13]. The thermodynamics properties, HOMO and LUMO energies and atomic charges of related ions were also provided by B3LYP/Lanl2dz level. The calculation utilized the  $O_h$  symmetry of  $[M(Cl)_6]^{2-}$  (Figure 1) was performed using the Gaussian 09.A.1 program package [14]. Each of the vibrational modes was assigned by means of visual inspection using the GaussView 5.0.8 [15]. GaussSum 2.2.5 program was also used for visualization of the structure and simulated vibrational spectra [16].

### 3. RESULTS AND DISCUSSION

The optimized geometrical parameters of  $[M(Cl)_6]^{2-}$  calculated by DFT/B3LYP method with Lanl2dz basis set show that depending on the title ionic radii of the compounds, M – Cl bond lengths are different. According to calculated geometric parameters, M – Cl bond lengths are 2.40, 2.43 and 2.54 Å, respectively. The Cl – M – Cl bond and torsion angles are same for these ions as 90 ° and 180°, respectively, due to their geometrical layout resembles.

Optimizations realized three steps. The each of title ions is stable state in step number 3. These steps are shown in Fig. 2.

The  $[Ti(Cl)_6]^{2-}$  ion is more stable than  $[Ge(Cl)_6]^{2-}$  and  $[Zr(Cl)_6]^{2-}$  ions. These compare can be also seen Table 1.

Several thermodynamics parameters, capacity, zero point energy, entropy etc., calculated by DFT/B3LYP method Lanl2dz basis set are presented in Table 1.

The variation in the Zero Point Vibrational Energy, ZPVE, seems to be insignificant. The total energy and change in total entropy of  $[M(Cl)_6]^{2-}$  ( $M=Ti$ , Ge, Zr) are at room temperature.

Each of  $[M(Cl)_6]^{2-}$  ions consist of 7 atoms, so it has 15 normal mode frequencies and belongs to the  $O_h$  point group. Fig. 1. demonstrates the six normal modes for these ions. The calculated vibrational frequencies for  $[M(Cl)_6]^{2-}$  ions at B3LYP with Lanl2dz basis set are given in Table2 2-4, together with experimental data, for comparison. Vibration modes  $v_4$ ,  $v_{5,6}$  and  $v_{10,11,12}$  are Raman active, whereas  $v_{1,2,3}$  and  $v_{7,8,9}$  are infrared active.

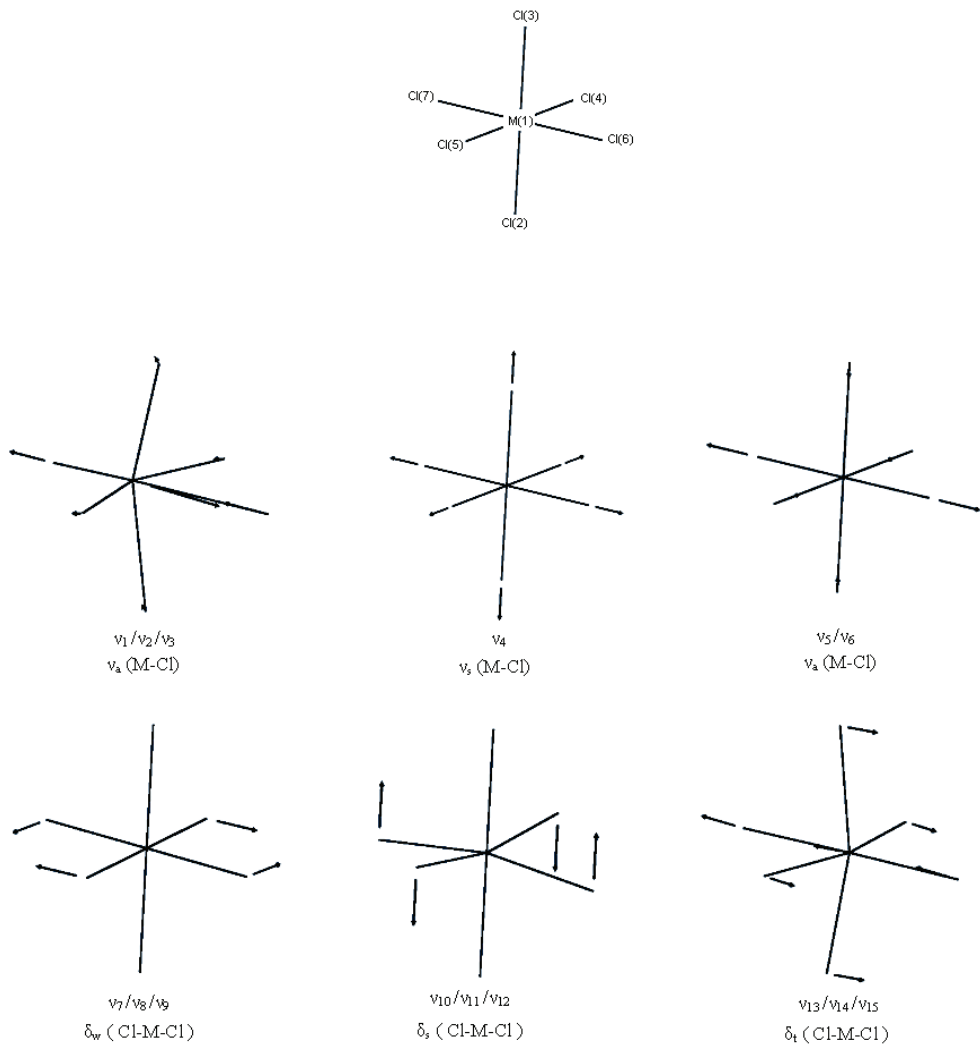


Fig. 1. Vibrational modes of  $[M(Cl)_6]^{2-}$  ( $M = Ti, Ge, Zr$ )

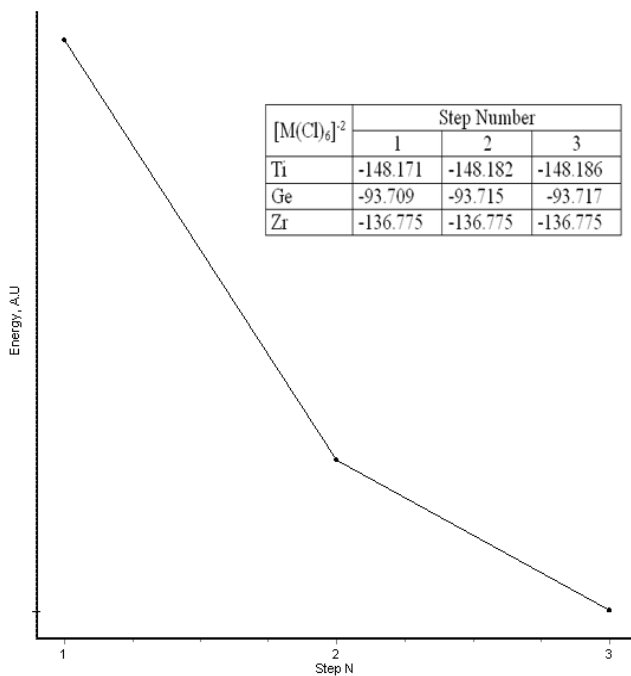


Fig. 2. Optimization steps for  $[M(Cl)_6]^{2-}$  ( $X=Ti, Ge$  and  $Zr$ ).

**THEORETICAL INVESTIGATION OF VIBRATIONAL FREQUENCIES AND MOLECULAR STRUCTURE OF SOME  $[M(Cl)_6]^{2-}$  IONS**

Table 1.

The thermodynamic parameters of  $[M(Cl)_6]^{2-}$  ( $M=Ti$ , Ge and Zr) calculated by B3LYP/Lanl2dz level.

| Parameters                                | B3LYP/ Lanl2dz $[M(Cl)_6]^{2-}$ |          |           |
|---|---------------------------------|----------|-----------|
|   | Ti                              | Ge       | Zr        |
| Optimal global minimum energy, (Hartree)  | -148.1863                       | -93.7167 | -136.7750 |
| Thermal total energy, (kcal/mol)          | 11.400                          | 11.342   | 11.314    |
| Heat capacity, (kcal/mol k)               | 0.034                           | 0.034    | 0.034     |
| Entropy, (kcal/mol k)                     |                                 |          |           |
| <i>Total</i>                              | 0.010                           | 0.010    | 0.011     |
| <i>Translational</i>                      | 0.043                           | 0.043    | 0.043     |
| <i>Rotational</i>                         | 0.025                           | 0.025    | 0.026     |
| <i>Vibrational</i>                        | 0.035                           | 0.035    | 0.039     |
| Vibrational energy, (kcal/mol)            | 9.622                           | 9.564    | 9.537     |
| Zero point vibrational energy, (kcal/mol) | 4.167                           | 4.082    | 3.830     |
| Rotational constants (GHz)                | 0.626                           | 0.611    | 0.558     |
| Dipole moment (Debye)                     | 0.541                           | 0.376    | 0.508     |

Table 2.

Normal modes of  $[Ti(Cl)_6]^{2-}$  calculated at the B3LYP/Lanl2dz level of theory.

| Mode / Assignment               | Calculated Frequency | Infrared Intensity <sup>a</sup> | Raman Activity <sup>b</sup> | Experimental Frequency <sup>c</sup> | Corrected Frequency <sup>d</sup> |
|---------------------------------|----------------------|---------------------------------|-----------------------------|-------------------------------------|----------------------------------|
| $v_1 / v_a$ (M-Cl)              | 316                  | 231.08                          | 0                           | 316                                 | 354                              |
| $v_2 / v_a$ (M-Cl)              | 316                  | 231.08                          | 0                           |                                     | 354                              |
| $v_3 / v_a$ (M-Cl)              | 316                  | 231.08                          | 0                           |                                     | 354                              |
| $v_4 / v_s$ (M-Cl)              | 285                  | 0                               | 34.13                       | 320                                 | 320                              |
| $v_5 / v_a$ (M-Cl)              | 196                  | 0                               | 6.00                        | 271                                 | 220                              |
| $v_6 / v_a$ (M-Cl)              | 196                  | 0                               | 6.00                        |                                     | 220                              |
| $v_7 / \delta_w$ ( Cl-M-Cl )    | 178                  | 0.26                            | 0                           | 183                                 | 200                              |
| $v_8 / \delta_w$ ( Cl-M-Cl )    | 178                  | 0.26                            | 0                           |                                     | 200                              |
| $v_9 / \delta_w$ ( Cl-M-Cl )    | 178                  | 0.26                            | 0                           |                                     | 200                              |
| $v_{10} / \delta_s$ ( Cl-M-Cl ) | 161                  | 0                               | 7.75                        | 173                                 | 181                              |
| $v_{11} / \delta_s$ ( Cl-M-Cl ) | 161                  | 0                               | 7.75                        |                                     | 181                              |
| $v_{12} / \delta_s$ ( Cl-M-Cl ) | 161                  | 0                               | 7.75                        |                                     | 181                              |
| $v_{13} / \delta_t$ ( Cl-M-Cl ) | 90                   | 0                               | 0                           | -                                   | 101                              |
| $v_{14} / \delta_t$ ( Cl-M-Cl ) | 90                   | 0                               | 0                           |                                     | 101                              |
| $v_{15} / \delta_t$ ( Cl-M-Cl ) | 90                   | 0                               | 0                           |                                     | 101                              |
| Correction factor               | 1.1216               |                                 |                             |                                     |                                  |
| Average factor                  | 1.1213               |                                 |                             |                                     |                                  |

<sup>a</sup> and <sup>s</sup> asymmetric and symmetric, respectively. <sup>a</sup> Units of infrared intensity are km/mol. <sup>b</sup> Units of Raman activity are  $\text{A}^4/\text{amu}$ . <sup>c</sup> References [4]. <sup>d</sup> Frequency multiplied by the average correction factor by 1.1213.

Table 3.

Normal modes of  $[Ge(Cl)_6]^{2-}$  calculated at the B3LYP/Lanl2dz level of theory.

| Mode / Assignment               | Calculated Frequency | Infrared Intensity <sup>a</sup> | Raman Activity <sup>b</sup> | Experimental Frequency <sup>c</sup> | Corrected Frequency <sup>d</sup> |
|---------------------------------|----------------------|---------------------------------|-----------------------------|-------------------------------------|----------------------------------|
| $v_1 / v_a$ (M-Cl)              | 284                  | 176.34                          | 0                           | 310                                 | 318                              |
| $v_2 / v_a$ (M-Cl)              | 284                  | 176.34                          | 0                           |                                     | 318                              |
| $v_3 / v_a$ (M-Cl)              | 284                  | 176.34                          | 0                           |                                     | 318                              |
| $v_4 / v_s$ (M-Cl)              | 254                  | 0                               | 71.22                       | 318                                 | 285                              |
| $v_5 / v_a$ (M-Cl)              | 205                  | 0                               | 10.60                       | 213                                 | 230                              |
| $v_6 / v_a$ (M-Cl)              | 205                  | 0                               | 10.60                       |                                     | 230                              |
| $v_7 / \delta_w$ ( Cl-M-Cl )    | 185                  | 11.31                           | 0                           | 213                                 | 207                              |
| $v_8 / \delta_w$ ( Cl-M-Cl )    | 185                  | 11.31                           | 0                           |                                     | 207                              |
| $v_9 / \delta_w$ ( Cl-M-Cl )    | 185                  | 11.31                           | 0                           |                                     | 207                              |
| $v_{10} / \delta_s$ ( Cl-M-Cl ) | 160                  | 0                               | 10.30                       | 191                                 | 179                              |
| $v_{11} / \delta_s$ ( Cl-M-Cl ) | 160                  | 0                               | 10.30                       |                                     | 179                              |
| $v_{12} / \delta_s$ ( Cl-M-Cl ) | 160                  | 0                               | 10.30                       |                                     | 179                              |
| $v_{13} / \delta_t$ ( Cl-M-Cl ) | 101                  | 0                               | 0                           | -                                   | 113                              |
| $v_{14} / \delta_t$ ( Cl-M-Cl ) | 101                  | 0                               | 0                           |                                     | 113                              |
| $v_{15} / \delta_t$ ( Cl-M-Cl ) | 101                  | 0                               | 0                           |                                     | 113                              |
| Correction factor               | 1.1712               |                                 |                             |                                     |                                  |
| Average factor                  | 1.1213               |                                 |                             |                                     |                                  |

<sup>a</sup> and <sup>s</sup> asymmetric and symmetric, respectively. <sup>a</sup> Units of infrared intensity are km/mol. <sup>b</sup> Units of Raman activity are  $\text{A}^4/\text{amu}$ . <sup>c</sup> References [5]. <sup>d</sup> Frequency multiplied by the average correction factor by 1.1213.

Normal modes of  $[Zr(Cl)_6]^{2-}$  calculated at the B3LYP/Lanl2dz level of theory.

| Mode / Assignment               | Calculated Frequency | Infrared Intensity <sup>a</sup> | Raman Activity <sup>b</sup> | Experimental Frequency <sup>c</sup> | Corrected Frequency <sup>d</sup> |
|---------------------------------|----------------------|---------------------------------|-----------------------------|-------------------------------------|----------------------------------|
| $v_1 / v_a$ (M-Cl)              | 297                  | 195.59                          | 0                           | 290                                 | 333                              |
| $v_2 / v_a$ (M-Cl)              | 297                  | 195.59                          | 0                           |                                     | 333                              |
| $v_3 / v_a$ (M-Cl)              | 297                  | 195.59                          | 0                           |                                     | 333                              |
| $v_4 / v_s$ (M-Cl)              | 285                  | 0                               | 25.97                       | 327                                 | 320                              |
| $v_5 / v_a$ (M-Cl)              | 224                  | 0                               | 2.73                        | 237                                 | 251                              |
| $v_6 / v_a$ (M-Cl)              | 224                  | 0                               | 2.73                        |                                     | 251                              |
| $v_7 / \delta_w$ ( Cl-M-Cl )    | 142                  | 5.47                            | 0                           | 150                                 | 159                              |
| $v_8 / \delta_w$ ( Cl-M-Cl )    | 142                  | 5.47                            | 0                           |                                     | 159                              |
| $v_9 / \delta_w$ ( Cl-M-Cl )    | 142                  | 5.47                            | 0                           |                                     | 159                              |
| $v_{10} / \delta_s$ ( Cl-M-Cl ) | 137                  | 0                               | 6.91                        | 153                                 | 154                              |
| $v_{11} / \delta_s$ ( Cl-M-Cl ) | 137                  | 0                               | 6.91                        |                                     | 154                              |
| $v_{12} / \delta_s$ ( Cl-M-Cl ) | 137                  | 0                               | 6.91                        |                                     | 154                              |
| $v_{13} / \delta_t$ ( Cl-M-Cl ) | 73                   | 0                               | 0                           | -                                   | 82                               |
| $v_{14} / \delta_t$ ( Cl-M-Cl ) | 73                   | 0                               | 0                           |                                     | 82                               |
| $v_{15} / \delta_t$ ( Cl-M-Cl ) | 73                   | 0                               | 0                           |                                     | 82                               |
| Correction factor               | 1.0710               |                                 |                             |                                     |                                  |
| Average factor                  | 1.1213               |                                 |                             |                                     |                                  |

<sup>a</sup> and <sup>s</sup> asymmetric and symmetric, respectively. <sup>a</sup> Units of infrared intensity are km/mol. <sup>b</sup> Units of Raman activity are  $\text{A}^4/\text{amu}$ . <sup>c</sup> References [6]. <sup>d</sup> Frequency multiplied by the average correction factor by 1.1213.

Vibrational modes of  $v_{13,14,15}$  are inactive in both, so it can be said that its frequencies are combination and overtone bands. The correction factors are obtained by taking the average of the ratios between the computed and experimental frequencies for all modes of a particular motion type [7, 13]. The computed correction factors for the B3LYP/Lanl2dz are presented in under the each tables and their average is 1.1213 for Lanl2dz basis set. Check et al.'s average correction factor was 1.1670 of B3LYP method for Lanl2dz basis set on a set of 36 metal halide molecules [7]. Determined correction factor in this study is close to previously reported value.

In order to make a comparison between the experimental and theoretical wavenumbers, we have calculated root mean square deviation (RMSD) which is a frequently used measure of the differences between values predicted by a model and actually observed from the thing being modeled. RMSD is given by

$$RMSD = \sqrt{\sum_i^N (\lambda w_i^{th} - w_i^{exp})^2 / N}$$

where N is the total number of vibrational modes,  $\lambda$  is scaling factor,  $w^{th}$  and  $w^{exp}$  are the theoretical and experimental frequencies ( $\text{cm}^{-1}$ ), respectively [13]. In this study, RMSD value has been obtained as  $33 \text{ cm}^{-1}$  for  $[Ti(Cl)_6]^{2-}$ ,  $20 \text{ cm}^{-1}$  for  $[Ge(Cl)_6]^{2-}$  and  $23 \text{ cm}^{-1}$  for  $[Zr(Cl)_6]^{2-}$ . The calculated Infrared and Raman spectra of the title ions are given in Figure 3.

The calculated Mulliken charges of  $[M(Cl)_6]^{2-}$  ( $M = Ti, Ge$  and  $Zr$ ) ions are shown in Table 5. Mulliken charge of M1 in each ion is 0.15, 0.89 and 0.55,

respectively. The charge distributions of Cl atoms are similar value. Regarding the calculations, there is considerable positive charge on metal atom with a corresponding negative charge on each Cl atoms. This suggests that the ion is held together in part by electrostatic forces.

Table 5.  
Atomic charges distributions of  $[M(Cl)_6]^{2-}$   
( $M = Ti, Ge$  and  $Zr$ )

|     | B3LYP/Lanl2dz<br>$M = Ti, Ge$ and $Zr$ |       |       |
|-----|--|-------|-------|
| M1  | 0.15                                   | 0.89  | 0.55  |
| Cl2 | -0.38                                  | -0.50 | -0.44 |
| Cl3 | -0.38                                  | -0.48 | -0.42 |
| Cl4 | -0.36                                  | -0.48 | -0.42 |
| Cl5 | -0.34                                  | -0.46 | -0.40 |
| Cl6 | -0.36                                  | -0.48 | -0.42 |
| Cl7 | -0.36                                  | -0.48 | -0.42 |

The HOMO and LUMO orbitals are the main orbital take part in chemical stability. The HOMO describes the ability to donate an electron and LUMO as an electron acceptor. The absorption of the electronic transition is defined from the ground to the first excited state. In other words, the transitions can be described from HOMO to LUMO. The HOMO is located over Cl atoms in  $[M(Cl)_6]^{2-}$ . The atomic compositions of the frontier molecular orbital and their orbital energies are shown in Fig. 4.

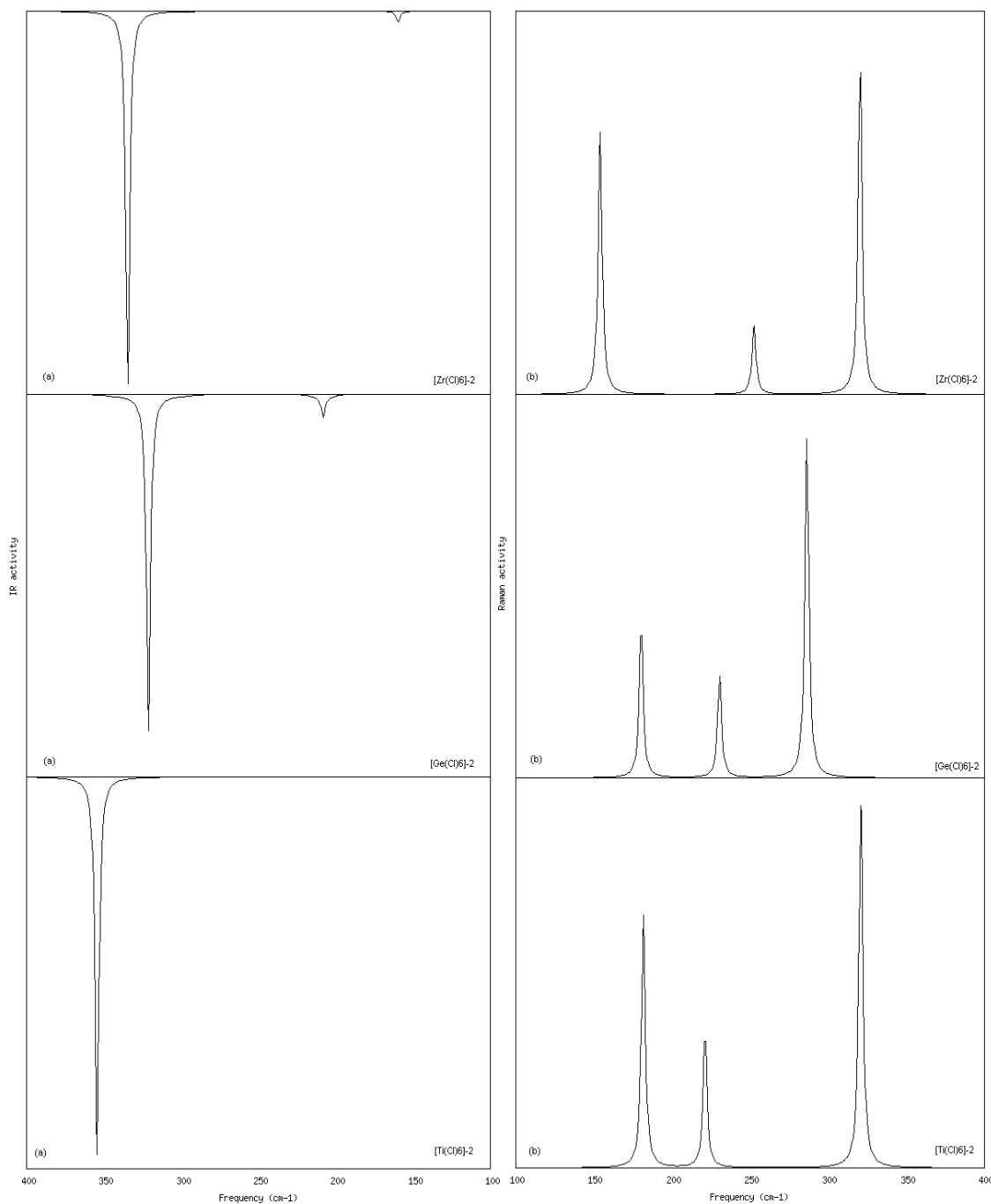


Fig. 3. Infrared (a) and Raman (b) spectra of  $[M(Cl)_6]^{2-}$  ( $M=Ti$ , Ge and Zr)

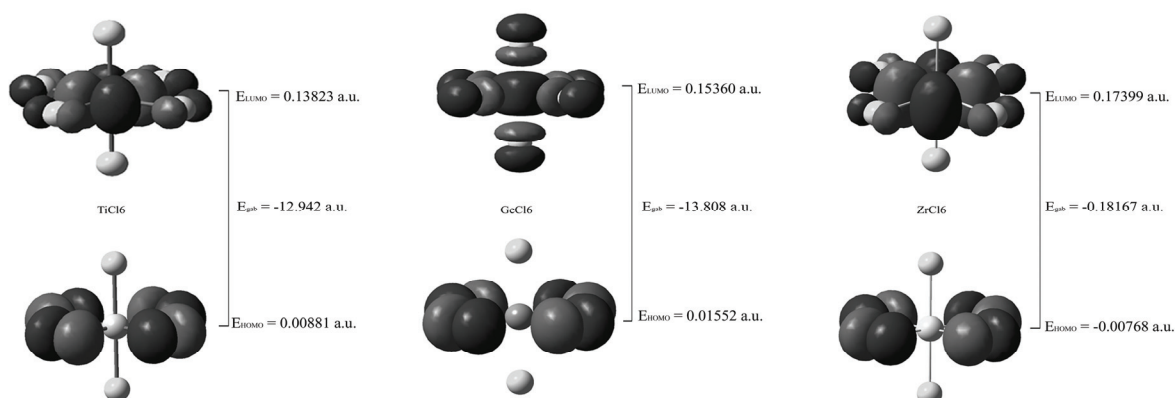


Fig. 4. Atomic orbital compositions of the frontier molecular orbital for  $[M(Cl)_6]^{2-}$  ( $M = Ti$ , Ge and Zr).

#### 4. CONCLUSION

In present investigation, molecular structure, vibrational frequencies, thermodynamics parameters and HOMO-LUMO orbitals have been studied using DFT/B3LYP method with Lanl2dz basis set. The

$[\text{Ti}(\text{Cl})_6]^{2-}$  ion is more stable than others. The RMSD between the experimental and calculated frequencies is very similar for each ions. The HOMO is located over Cl atoms for all ions.

- 
- [1] K. Nakamoto, "Infrared and Raman spectra of inorganic and coordination compounds" Wiley, New York, (1986).
  - [2] K. Horiuchi, H. Iwafune, T. Asaji and D. Nakamura, "Lattice stability in  $\text{A}_2\text{MCl}_6$  ionic crystals (A identical to  $\text{C}_5\text{H}_5\text{NH}$  or  $\text{CH}_3\text{C}_5\text{H}_4\text{NH}$ ; M identical to Sn or Te)" J. Phys.: Condens. Matter, 6 (1994) 9075-9078
  - [3] G. Anand, Fadnis and Terence J. Kemp, "Photo-oxidation of alcohols by hexachlorometalate(IV) ions (M = Pt, Pd, or Ir): spin trapping and matrix isolation electron spin resonance studies" J. Chem. Soc., Dalton Trans., 7 (1989) 1237-1240.
  - [4] R.J.H. Clark, L. Maresca, R.J. Puddephatt, "Preparation and vibrational spectra of the MX62- and MX4Y22- ions (M =titanium or tin; X =chlorine, bromine, or iodine)" Inorg. Chem., 7 (1968) 1603-1606.
  - [5] I.R. Baettie, T. Gilson, K. Livingston, V. Fawcett, and, G.A. Ozin, "The vibrational spectra of some chloro-complexes of germanium, tin, phosphorus, arsenic, and antimony" J. Chem. Soc. A, (1967) 712-718
  - [6] D.M. Adams and D.C. Newton, "Vibrational spectra of halides and complex halides. Part VI. The ions  $[\text{MCl}_6]^{2-}$ , M = Ti, Zr, Hf" J. Chem. Soc. A, (1968) 2262-2263,
  - [7] C.E. Check, T.O. Faust, J.M. Bailey, B.J. Wright, T.M. Gilbert, L.S. Sunderlin, Journal of Physical Chemistry A, "Addition of Polarization and Diffuse Functions to the LANL2DZ Basis Set for P-Block Elements" 105 (2001) 8111-8116.
  - [8] C. Parlak, "Theoretical and experimental vibrational spectroscopic study of 4-(1-Pyrrolidinyl)piperidine" Journal of Molecular Structure, 966 (2010) 1-7.
  - [9] P.J. Hay, W.R. Wadt, "Ab initio effective core potentials for molecular calculations. Potentials for the transition metal atoms Sc to Hg" J. Chem. Phys., 82 (1985) 270-283.
  - [10] W.R. Wadt, P.J. Hay, "Ab initio effective core potentials for molecular calculations. Potentials for main group elements Na to Bi" J. Chem. Phys., 82 (1985) 284-295.
  - [11] P.J. Hay, W.R. Wadt, "Ab initio effective core potentials for molecular calculations. Potentials for K to Au including the outermost core orbitals" J. Chem. Phys., 82 (1985) 299-310.
  - [12] G.A. Zhurko, D.A. Zhurko, ChemCraft 1.6, <http://www.chemcraftprog.com>, 2011.
  - [13] I. Bytheway, M.W. Wong, "The prediction of vibrational frequencies of inorganic molecules using density functional theory" Chem. Phys. Lett., 282 (1998) 219-226.
  - [14] M.J. Frisch, G.W. Trucks, H.B. Schlegel, G.E. Scuseria, M.A. Robb, J.R.Cheeseman, G. Scalmani, V. Barone, B. Mennucci, G.A. Petersson, H. Nakatsuji, M. Caricato, X. Li, H.P. Hratchian, A.F. Izmaylov, J. Bloino, G. Zheng, J.L. Sonnenberg, M. Hada, M.Ehara, K.Toyota, R.Fukuda, J.Hasegawa, M. Ishida, T. Nakajima, Y. Honda, O. Kitao, H. Nakai, T.Vreven, J.A.Montgomery, Jr., J.E.Peralta, F.Ogliaro, M.Bearpark, J.J.Heyd, E.Brothers, K.N.Kudin, V.N.Staroverov, R. Kobayashi, J. Normand, K.Raghavachari, A. Rendell, J.C. Burant, S.S. Iyengar, J. Tomasi, M. Cossi, N. Rega, J.M. Millam, M. Klene, J.E. Knox, J.B. Cross, V. Bakken, C. Adamo, J.Jaramillo, R.Gomperts, R.E. Stratmann, O. Yazyev, A. J. Austin, R. Cammi, C. Pomelli, J. W. Ochterski, R. L. Martin, K. Morokuma, V.G. Zakrzewski, G. A. Voth, P. Salvador, J.J. Dannenberg, S. Dapprich, A.D. Daniels, Ö. Farkas, J.B. Foresman, J.V. Ortiz, J. Cioslowski and D.J. Fox, Gaussian 09, Revision A.1, Gaussian Inc., Wallingford CT, 2009.
  - [15] R.D. Dennington, T.A. Keith, J.M. Millam, GaussView 5.0.8, Gaussian Inc., 2008.
  - [16] N.M. O'Boyle, A.L. Tenderholt, K.M. Langner, J. "cclib: A library for package-independent computational chemistry algorithms" Comp. Chem. 29 (2008) 839-845.

Received: 12.05.2011

## THE CRYSTAL STRUCTURE OF $\text{Ga}_{0.83}\text{In}_{0.83}\text{Fe}_{0.34}\text{S}_3$

**J. HASANI BARBARAN, G.G. GUSEINOV, R.B. VELIYEV, A.B. MAGERRAMOV**

*G.M. Abdullayev Institute of Physics National Academy of Sciences,*

*G. Javid ave., 33, Baku, AZ-1143, Azerbaijan*

*e-mail: [jhasani2000@yahoo.com](mailto:jhasani2000@yahoo.com)*

*[g.guseinov@rambler.ru](mailto:g.guseinov@rambler.ru)*

The single crystals of the  $\text{Ga}_{0.83}\text{In}_{0.83}\text{Fe}_{0.34}\text{S}_3$  have been grown. It is established that the unit cell parameters of the hexagonal lattice are:  $a=3.7813 \text{ \AA}$ ,  $c=12.1888 \text{ \AA}$ ,  $V=151.04 \text{ \AA}^3$ ,  $\rho_{\text{rent}}=3.84 \text{ g/cm}^3$ , sp.gr.  $P3m1$ ,  $Z=1.33$ .

**Keywords:** crystal structure, hexagonal lattice.

**PACS:** 548.571; 548.4

### INTRODUCTION

The phase diagram of  $\text{Ga}_2\text{S}_3\text{-In}_2\text{S}_3$  quasi-binary sections were investigated by the authors of [1-2]. They found that only one compound of  $\text{GaInS}_3$  composition with constants of hexagonal lattice:  $a=3.810 \text{ \AA}$ ,  $a=17.241 \text{ \AA}$ , sp. gr.  $P3m1$ ,  $Z=2$  forms in this system.

The formation phases of quasi-binary sections ( $\text{Ga}_2\text{S}_3\text{-In}_2\text{S}_3$ ) of Ga-In-S system are studied, the growth number of single crystals with the general formula  $(\text{Ga}, \text{In})_2\text{S}_3$  and crystal structures of all these polymorphous phases are defined by us earlier with taking into consideration the presence of different polymorphous modifications and polytypic forms of  $\text{Ga}_2\text{S}_3$  and  $\text{In}_2\text{S}_3$  at Ga change by X-ray diffraction method [3-18]. For growth of these single crystals the previously synthesized crystal powders of the following compositions:  $\text{GaInS}_3$ ,  $\text{Ga}_{0.75}\text{In}_{1.25}\text{S}_3$  and  $\text{Ga}_{0.5}\text{In}_{1.5}\text{S}_3$  are used. The temperature ranges of crystal growing are:

- |   |                        |                        |
|---|------------------------|------------------------|
| 1. $\text{GaInS}_3$                             | $T_1=973 \text{ K}$ ,  | $T_2=873 \text{ K}$ ;  |
| 2. $\text{Ga}_{0.75}\text{In}_{1.25}\text{S}_3$ | $T_1=1073 \text{ K}$ , | $T_2=973 \text{ K}$ ;  |
| 3. $\text{Ga}_{0.5}\text{In}_{1.5}\text{S}_3$   | $T_1=1173 \text{ K}$ , | $T_2=1073 \text{ K}$ ; |

Time of growth was selected between 250-320 hours and the dimensions of the quartz ampoules, used for crystals growth, were  $L=200 \text{ mm}$ ,  $d=12 \text{ mm}$ , transporter agency  $I_2=6.7 \text{ mg/cm}^3$ , mass example 0.5 gr.

All of the mentioned single crystals were produced by CVD (Chemical Vapor Deposition) and analyzed by detailed X-ray analysis. The selected crystals, tested by X-ray Laue and rotation precession methods, were employed to define the unit cell constants and the following results were obtained:

All grown single crystals obtained from gas phase with participation of  $I_2$  are investigated by X-ray analysis, the lattice parameters, their symmetry and crystallographic structures are defined. The big amount of publication data [3-18] is dedicated to the analysis of structural-crystallochemical characteristics and one can formulate that the different layered structures the characteristics of which are the following form at the change of relation of In atoms to Ga ones:

- The bulk yellow crystals obtained from  $\text{GaInS}_3$  and  $\text{Ga}_{0.75}\text{In}_{1.25}\text{S}_3$  crystallize in hexagonal system with lattice parameters:  $a=6.53 \text{ \AA}$  and  $c=17.90 \text{ \AA}$  [3].

- The red layered single crystals grown up in temperature interval  $T_1=1073 \text{ K}$  and  $T_2=973 \text{ K}$  are related to hexagonal system with lattice parameters:  $a=3.80 \text{ \AA}$  and  $c=30.50 \text{ \AA}$  [4].
- Among the red crystals with layered structure, there are slightly blonde layered single crystals with triangular forms. These crystals belong to polytypical forms of  $\text{GaInS}_3$  with cell parameters  $a=3.80 \text{ \AA}$  and  $c=45.90 \text{ \AA}$  [5].
- The layered yellow crystals obtained from the  $\text{Ga}_{0.5}\text{In}_{1.5}\text{S}_3$  composition in temperature interval  $T_1=973 \text{ K}$  and  $T_2=873 \text{ K}$ , are rhombic ones with the lattice parameters:  $a=19.11$ ,  $b=6.20$  and  $c=3.81 \text{ \AA}$  [6].
- The oval shaped layered yellow crystals obtained from the  $\text{Ga}_{0.75}\text{In}_{1.25}\text{S}_3$  composition in the temperature  $T_1=1173 \text{ K}$  and  $T_2=1073 \text{ K}$  have hexagonal structure and crystallize in two polytypic forms. Their cell parameters are  $a=3.81 \text{ \AA}$ ,  $c=18.20 \text{ \AA}$  and  $a=3.81 \text{ \AA}$ ,  $c=54.92 \text{ \AA}$ , correspondingly [7].
- The layered blackish crystals obtained from  $\text{Ga}_{0.5}\text{In}_{1.5}\text{S}_3=\text{GaIn}_3\text{S}_6$  and  $\text{Ga}_{0.75}\text{In}_{1.25}\text{S}_3$  compositions at  $T_1=1073 \text{ K}$  and  $T_2=973 \text{ K}$  are hexagonal with  $a=3.8 \text{ \AA}$  and  $c=21.1 \text{ \AA}$  lattice parameters [8].
- The octahedron shaped crystals were grown at high temperatures and belong to cubic spinel with  $a=10.61 \text{ \AA}$  [9].

The present work is devoted to the growth of  $\text{Ga}_{0.83}\text{In}_{0.83}\text{Fe}_{0.34}\text{S}_3$  single crystals obtained by partial exchange of tetrahedral cations of Ga, In by Fe atoms in hexagonal structure  $\text{GaInS}_3$  ( $a=3.81 \text{ \AA}$  and  $c=18.20 \text{ \AA}$ ) and the clarification of its crystal lattice.

### SYNTHESIS AND GROWTH OF $\text{GA}_{0.83}\text{IN}_{0.83}\text{FE}_{0.34}\text{S}_3$ SINGLE CRYSTALS

Growth of the  $\text{Ga}_{0.83}\text{In}_{0.83}\text{Fe}_{0.34}\text{S}_3$  single crystals was started by the synthesis through the direct fusion of the initial elements with stoichiometric ratio. The element purity grade was no less than 99.998%. Iron was preliminarily purified from the oxide layer by hydrogen passing at temperature range of 820-880K. The necessary

amounts of elements of corresponding compositions were placed into the glassy-carbonic Su-2500 crucibles and then in quartz tubes. The synthesis in the glassy-carbonic crucibles prevents the interaction between metal compound and quartz, which may contaminate the synthesized material by oxides. Then the preliminarily evacuated ampoules were filled with argon gas and evacuation was done again to achieve a residual pressure of  $10^{-4}$  torr. The  $\text{Ga}_{0.83}\text{In}_{0.83}\text{Fe}_{0.34}\text{S}_3$  crystals were obtained by heating the ampoule content in a declined furnace at 1250–1275K for 2.0–2.5 hrs. Then the melted masses were cooled down to 973K and kept at this temperature for 15 days [18]. The crystal growth method has been described by Memo [10]. The structural analysis was

carried out by the powder X-ray diffractometer (D8 ADVANCE,  $\text{CuK}\alpha$ -radiation,  $\lambda=1.5406 \text{ \AA}$ , mode-40 kV, 40 mA,  $0.5^\circ < 2\theta < 80^\circ$ ,  $T=300\text{K}$ ). The experimental data processing was done by the software EVA and TOPAS.

### THE STRUCTURE INVESTIGATION

Comparison of the diffraction data of this work with appropriate data of the polymorphic and polytypic forms of  $\text{Ga}_2\text{S}_3\text{-In}_2\text{S}_3$  system showed that they are fully consistent with the crystals grown from the  $\text{Ga}_{0.5}\text{In}_{1.5}\text{S}_3$  gas phase [11]. Also Table 1 presents all the X-ray diffraction data indexed by TOPAS (tab.1; fig.1) software.

Table 1.

X-ray diffraction data for  $\text{Ga}_{0.83}\text{In}_{0.83}\text{Fe}_{0.34}\text{S}_3$

| Nº | $2\theta$ | $d_{exc}$ | $I/I_0$ | $h$ | $k$ | $l$ |
|----|-----------|-----------|---------|-----|-----|-----|
| 1  | 7.247     | 12.1888   | 577     | 0   | 0   | 1   |
| 2  | 14.523    | 6.0944    | 50.6    | 0   | 0   | 2   |
| 3  | 21.858    | 4.0629    | 5929    | 0   | 0   | 3   |
| 4  | 23.334    | 3.8091    | 402     | 1   | 0   | 2   |
| 5  | 28.195    | 3.1625    | 83.8    | 1   | 0   | 1   |
| 6  | 29.753    | 3.0004    | 412     | 0   | 1   | 3   |
| 7  | 29.285    | 3.0472    | 9.7     | 0   | 0   | 4   |
| 8  | 30.976    | 2.8846    | 54.5    | 1   | 0   | 2   |
| 9  | 36.841    | 2.4377    | 107     | 0   | 0   | 5   |
| 10 | 40.401    | 2.2307    | 101     | 1   | 0   | 4   |
| 11 | 44.566    | 2.0314    | 132     | 0   | 0   | 6   |
| 12 | 46.398    | 1.9554    | 36.9    | 1   | 0   | 5   |
| 13 | 48.087    | 1.8906    | 64.8    | 1   | 1   | 0   |
| 14 | 48.699    | 1.8683    | 10      | 1   | 1   | 1   |
| 15 | 52.512    | 1.7412    | 94.2    | 0   | 0   | 7   |
| 16 | 53.003    | 1.7262    | 69.9    | 1   | 0   | 6   |
| 17 | 53.408    | 1.7141    | 9.48    | 1   | 1   | 3   |
| 18 | 56.128    | 1.6373    | 3.39    | 2   | 0   | 0   |
| 19 | 56.677    | 1.6227    | 8.66    | 2   | 0   | 1   |
| 20 | 58.305    | 1.5812    | 7.77    | 2   | 0   | 2   |
| 21 | 60.137    | 1.5374    | 4.54    | 1   | 0   | 7   |
| 22 | 60.74     | 1.5236    | 16.7    | 0   | 0   | 8   |
| 23 | 62.075    | 1.4939    | 2.46    | 1   | 1   | 5   |
| 24 | 67.639    | 1.3839    | 4.75    | 1   | 1   | 6   |
| 25 | 67.783    | 1.3814    | 3.84    | 1   | 0   | 8   |
| 26 | 69.044    | 1.3592    | 6.8     | 2   | 0   | 5   |
| 27 | 69.33     | 1.3543    | 3.77    | 0   | 0   | 9   |
| 28 | 73.943    | 1.2808    | 6.14    | 1   | 1   | 7   |
| 29 | 74.349    | 1.2748    | 5.24    | 2   | 0   | 6   |
| 30 | 75.976    | 1.2515    | 14.3    | 1   | 0   | 9   |
| 31 | 76.977    | 1.2377    | 12.3    | 2   | 1   | 0   |
| 32 | 78.392    | 1.2188    | 43.1    | 0   | 0   | 10  |
| 33 | 78.849    | 1.2129    | 4.27    | 2   | 1   | 2   |

**THE CRYSTAL STRUCTURE OF  $\text{Ga}_{0.83}\text{In}_{0.83}\text{Fe}_{0.34}\text{S}_3$**

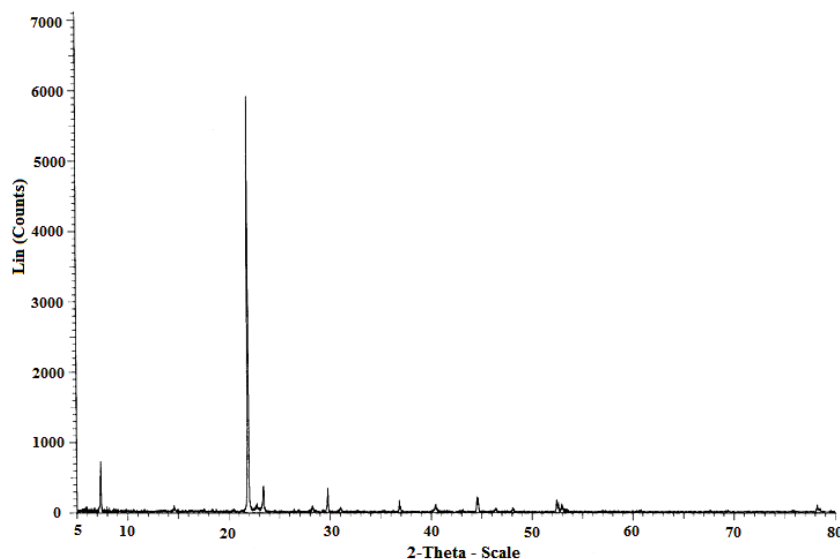


Fig. 1. X-ray diffraction for  $\text{Ga}_{0.83}\text{In}_{0.83}\text{Fe}_{0.34}\text{S}_3$

The process of indexing shows that the studied phase crystallizes in the trigonal symmetry with the lattice constants of  $a=3.7813 \text{ \AA}$ ,  $c=12.1888 \text{ \AA}$ ,  $V=151.04 \text{ \AA}^3$ ,  $\rho_{\text{XRD}}=3.84 \text{ g/cm}^3$ , in hexagonal position, sp. gr. P3m1,  $Z=1.33$ . As mentioned above, one of polytypic of  $\text{Ga}_{0.5}\text{In}_{1.5}\text{S}_3$  was characterized by similar crystallographic data. The differences between this crystal and those obtained in present research are because of the presence or absence of the inversion symmetry: the structure in the first crystal consists of the inversion symmetry, but the studied crystals of  $\text{Ga}_{0.83}\text{In}_{0.83}\text{Fe}_{0.34}\text{S}_3$  have no such symmetry. According to the atomic positions of  $\text{Ga}_{0.5}\text{In}_{1.5}\text{S}_3$  crystal, the atomic positions of  $\text{Ga}_{0.83}\text{In}_{0.83}\text{Fe}_{0.34}\text{S}_3$  were defined easily. In this case, the main issue was finding the position of the Fe atoms. It is important to know that in such layered structures, the octahedral voids are always filled with In atoms. Hence, it appears the atoms of iron must be statically located in the tetrahedral positions of In or Ga atoms. Among the three possible options for distribution of Fe atoms, the best result was obtained in the version, which is shown in figure 2.

Thus, this structure is isostructural one with  $\text{Ga}_{0.5}\text{In}_{1.5}\text{S}_3$ , and  $\text{ZnIn}_2\text{S}_3$  [20]. The layered one-packet structure was defined in the isotropic approximation to  $R=0.072$ . The final atomic coordinates are given in table 2.

Interatomic distances are S-S=3.70 $\text{\AA}$ , In-S=2.60 $\text{\AA}$  (in octahedron), (Ga,Fe)-S=2.30–2.34 $\text{\AA}$ ; (In,Ga)-S=2.34–2.36 $\text{\AA}$ . Since the package involved four layers of S atoms, the structural formula for one package corresponds to  $\text{Ga}_{1.11}\text{In}_{1.11}\text{Fe}_{0.44}\text{S}_4$ . Also the visual inspection of the crystals under the microscope showed a red color mass consisting of free oriented plates.

Thus, we can conclude that by direct melting of the initial elements was synthesized the single crystals of magnetic semiconductor of  $\text{Ga}_{0.83}\text{In}_{0.83}\text{Fe}_{0.34}\text{S}_3$  composition.

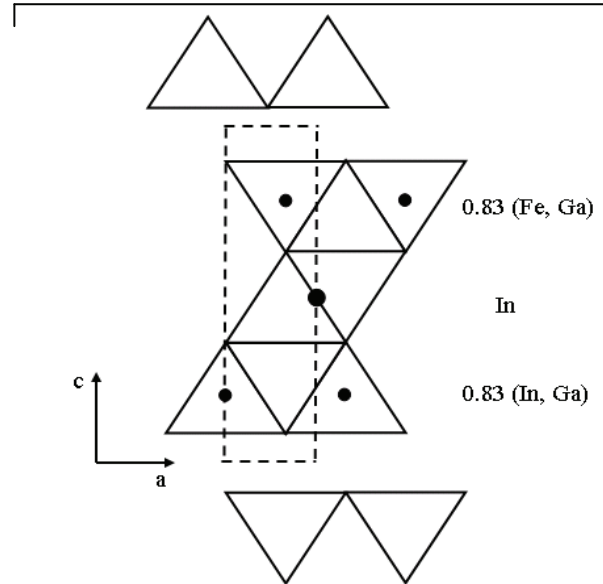


Fig. 2. The projection of  $\text{Ga}_{0.83}\text{In}_{0.83}\text{Fe}_{0.34}\text{S}_3$  crystal structure on the (010) plane.

Table. 2.  
Atomic coordinates and isotropic temperature displacement factors of  $\text{Ga}_{0.83}\text{In}_{0.83}\text{Fe}_{0.34}\text{S}_3$ .

| Atom           | $x$ | $y$ | $z$   | $B_i$ |
|----------------|-----|-----|-------|-------|
| In             | 0   | 0   | .5000 | 2.533 |
| Ga, In         | 2/3 | 1/3 | .8100 | 1.820 |
| Ga, Fe         | 1/3 | 2/3 | .1900 | 1.679 |
| S <sub>1</sub> | 2/3 | 1/3 | .6126 | 1.721 |
| S <sub>2</sub> | 1/3 | 2/3 | .3874 | 2.653 |
| S <sub>3</sub> | 1/3 | 2/3 | .8757 | 1.574 |
| S <sub>4</sub> | 2/3 | 1/3 | .1243 | 1.721 |

- [1] M. I. Zargarov, R. S. Gadimov, Izv. AN. USSR. Non-org. mater. 5(1969)317.
- [2] V.P. Ambors, I.Ya. Andronik, V.P. Mushinskiy. Nekotorie voprosi khimii i fiziki poluprovodnikov

- slojnogo sostava. Ujgorod: Izd-vo UGU, 1970, s. 238-241.(in Russian)
- [3] I. R. Amiraslanov, R. B. Valiyev, G. G. Guseinov et al., Rep. of Azerb. SSR AS 44(1990)33.

- [4] *G. G. Guseinov, M. G. Kazimov, A. S. Guliyev et al.*, Rep. of Azerb. SSR AS 44(1990)26.
- [5] *I. R. Amiraslanov, G. G. Guseynov, H. S. Mamedov et al.*, Crstallogr. Rep. 33(1988)767.
- [6] *G. G. Guseinov, I. R. Amiraslanov, A. S. Guliyev et al.*, Izv. AS. SSSR. Non-org. Mater. 23(1987)854.
- [7] *G. G. Guseinov, I. R. Amiraslanov, A. S. Guliyev et al.*, Crstallogr. Rep. 32(1987)243.
- [8] *M.G. Kazimov, G.G. Guseinov, A.B. Magerramov et al.*, J. Fiz. 5(1999)18-19.
- [9] *I. R. Amiraslanov, G. G. Guseinov, A. S. Guliyev et al.*, Azerb. IPAS Baku 183(1986)39.
- [10] *W. Wong-Ng., H. McMurdie, B. Paretzkin., et.al.*, NBS (USA), ICDD Grant-in Aid, (1988).
- [11] *I. R. Amiraslanov, Yu. F. Asadov, B. A. Maksimov, et.al.*, Sov.Phys.Crystallogr. (Engl.Transl.), 35(1990)187.
- [12] *M. Schulte-Kelinghaus, V. Kramer, Z. Naturforsch., B:Anorg. Chem., Org.Chem.*, 37(1982)390.
- [13] *I.R. Amiraslanov, T.Kh. Azizov, G.G. Guseinov i dr.* Neorganicheskie materiali, 24(1988)723.(in Russian)
- [14] *M.G. Kazimov, G.G. Guseinov, A.B. Magerramov i dr.* J.Fizika, 5(1999)18. (in Russian)
- [15] *M.G. Kazimov, G.G. Guseinov, E.A. Isaeva i dr.* AMEA-nin Xəbərləri, 2( 2003)139. (in Russian)
- [16] *M.G. Kazimov, G.G. Guseinov M.G. Kazimov i dr.* AMEA-nin Xəbərləri, 5(2005)129. (in Russian)
- [17] *M.G. Kazimov, I.B. Asadov, G.G. Guseinov.* AMEA-nin Məruzələri, 58(2002)113. (in Russian)
- [18] *A. Memo, H. Haeuseler,* Z. Naturforsch, 57 b(2002)509-511.
- [19] *I. R. Amiraslanov, R. B. Veliyev, A. A. Musaev et al.*, DAS Acad. Sci. of Azerb. 46(1990)33.
- [20] *F. G. Donika, S. I. Radautsan, G. A. Kiosse et al.*, Crstallogr. Rep. 16(1971)235.

*Received: 28.02.2011*

## A MICROSCOPIC THEORY OF SPIN EXCITATIONS IN A RECTANGULAR FERROMAGNETIC NANOWIRES

V.A. TANRIVERDIYEV, V.S. TAGIYEV

*G.M. Abdullayev Institute of Physics of NAS of Azerbaijan,*

*Baku, Az -1143, G. Javid ave., 33*

*E-mail : solstphs @physics.ab.az.*

A Green function analysis is used to study spin-waves excitations in ferromagnetic nanowires. The expression of Green function for different spins of ferromagnetic nanowires is derived. The nanowire is modeled as having a cubic cross section. The results are illustrated numerically for a particular choice of parameters

**Keywords:** A. Magnetic material

**PACS:** 75.70. Ak

Materials with magnetic properties periodically modulated at the nanometer scale have potential for applications in magneto-electronic devices, and new physical phenomena. In fact, concurrent progress in these various branches of science and technology has made possible a comprehensive understanding of the properties of materials at the nanoscale, and in particular of small magnetic elements. [1-3].

Fundamental interest in ferromagnetic nanowire lies in the emergence of novel magnetic and transport properties as the dimension approaches the length scale of a few nanometers to a few tens of nanometers. Conductance and flux quantization have been observed for ferromagnetic nanowire arrays and giant magnetoresistance is realized in multilayer-structured nanowires. Current interest in research on ferromagnetic

nanowires is stimulated by the potential application to future ultra-high-density magnetic recording media and electronic devices. In light of the increasing interest in using magnetic nanostructured materials for device applications, a complete understanding of their static and dynamic magnetic properties is required [2-4].

Spin-wave phenomena in cylindrical ferromagnetic nanowires have recently been studied by a number of authors [5,6]. For example, T.M. Nguyen and M.G. Cottam developed a microscopic theory for spin waves in ferromagnetic nanowires with approximately circular cross section [7,8]. A nanowire can be modeled as having a chosen shape and size cross section (in the x-y plane) with a finite number spins arranged. These layers are stacked vertically to form a long nanowire extending in the z direction from  $-\infty$  to  $\infty$ .

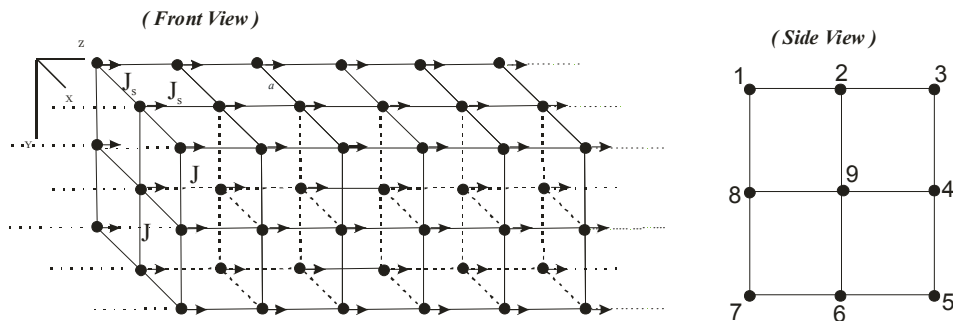


Fig. 1. Model of rectangular ferromagnetic nanowires. The nanowires are infinite in the direction perpendicular to the axes z.

The system will be represented by the Hamiltonian

$$H = -\frac{1}{2} \sum_{i,j} J_{ij} \left\{ S_i^z S_j^z + S_i^+ S_j^- \right\} - \sum_i g_i \mu_0 H_0 S_i^z - \sum_i D_i (S_i^z)^2 \quad (1)$$

where  $J_{ij}$  is the exchange coupling between sites labeled  $i$  and  $j$ . As indicated in fig. 1 we consider in this article a ferromagnetic nanowire which having a cubic cross section. The exchange coupling between surface and bulk spin, and between surface spins is assumed to be  $J$  and  $J_s$ , respectively. The second term of Eq. (1) describes the Zeeman interaction of the spins with an externally

applied field  $H_0$ , the last contribution is a single-ion anisotropy term.

The Hamiltonian may be written in terms of boson operators using the Holstein-Primakoff transformation. The non-interaction (linear) spin-waves are described by the quadratic term  $H^{(2)}$  that has the following form

$$H^{(2)} = \sum_{i,j} J_{ij} \left\{ S_j a_i^+ a_i - \sqrt{S_i S_j} a_i a_j^+ \right\} + \sum_i g_i \mu H_0 a_i^+ a_i + 2 \sum_i D_i S_i a_i^+ a_i \quad (2)$$

Spectrum of magnons, the temperature dependence of magnetization of ferromagnetic nanowires under consideration are obtained using GF method [9,10] Employing the equation of motion for the GF  $G_{i,j}(t,t') = \langle\langle a_i(t); a_j^-(t') \rangle\rangle$  one obtains the following equation

$$\begin{aligned} & (\omega - g\mu H_0 - 2DS - 4J_s S)G_{n,m}^{1,\tau} + J_s S(G_{n,m}^{2,\tau} + G_{n,m}^{8,\tau}) + J_s S G_{n+1,m}^{1,\tau} + J_s S G_{n-1,m}^{1,\tau} = \delta_{n,m}^{1,r} \\ & (\omega - g\mu H_0 - 2DS - 4J_s S - JS)G_{n,m}^{2,\tau} + J_s S(G_{n,m}^{1,\tau} + G_{n,m}^{3,\tau}) + JS G_{n,m}^{9,\tau} + J_s S G_{n+1,m}^{2,\tau} + J_s S G_{n-1,m}^{2,\tau} = \delta_{n,m}^{2,r} \\ & (\omega - g\mu H_0 - 2DS - 4J_s S)G_{n,m}^{3,\tau} + J_s S(G_{n,m}^{2,\tau} + G_{n,m}^{4,\tau}) + J_s S G_{n+1,m}^{3,\tau} + J_s S G_{n-1,m}^{3,\tau} = \delta_{n,m}^{3,r} \\ & (\omega - g\mu H_0 - 2DS - 4J_s S - JS)G_{n,m}^{4,\tau} + J_s S(G_{n,m}^{3,\tau} + G_{n,m}^{5,\tau}) + JS G_{n,m}^{9,\tau} + J_s S G_{n+1,m}^{4,\tau} + J_s S G_{n-1,m}^{4,\tau} = \delta_{n,m}^{4,r} \\ & (\omega - g\mu H_0 - 2DS - 4J_s S)G_{n,m}^{5,\tau} + J_s S(G_{n,m}^{4,\tau} + G_{n,m}^{6,\tau}) + J_s S G_{n+1,m}^{5,\tau} + J_s S G_{n-1,m}^{5,\tau} = \delta_{n,m}^{5,r} \\ & (\omega - g\mu H_0 - 2DS - 4J_s S - JS)G_{n,m}^{6,\tau} + J_s S(G_{n,m}^{5,\tau} + G_{n,m}^{7,\tau}) + JS G_{n,m}^{9,\tau} + J_s S G_{n+1,m}^{6,\tau} + J_s S G_{n-1,m}^{6,\tau} = \delta_{n,m}^{6,r} \\ & (\omega - g\mu H_0 - 2DS - 4J_s S)G_{n,m}^{7,\tau} + J_s S(G_{n,m}^{6,\tau} + G_{n,m}^{8,\tau}) + J_s S G_{n+1,m}^{7,\tau} + J_s S G_{n-1,m}^{7,\tau} = \delta_{n,m}^{7,r} \\ & (\omega - g\mu H_0 - 2DS - 4J_s S - JS)G_{n,m}^{8,\tau} + J_s S(G_{n,m}^{7,\tau} + G_{n,m}^{1,\tau}) + JS G_{n,m}^{9,\tau} + J_s S G_{n+1,m}^{8,\tau} + J_s S G_{n-1,m}^{8,\tau} = \delta_{n,m}^{8,r} \\ & (\omega - g\mu H_0 - 2DS - 6JS)G_{n,m}^{9,\tau} + JS(G_{n,m}^{2,\tau} + G_{n,m}^{4,\tau} + G_{n,m}^{6,\tau} + G_{n,m}^{8,\tau}) + JS G_{n+1,m}^{9,\tau} + JS G_{n-1,m}^{9,\tau} = \delta_{n,m}^{9,r} \end{aligned} \quad (3)$$

Here  $n$  and  $m$  are layer indices, while  $1, \dots, 9$  and  $\tau$  label the position of the spins in layers  $n$  and  $m$ , respectively.

The system is also periodic in the  $z$  direction, which lattice constant is  $a$ . According to Bloch's theorem has been employed for plane waves in order to receive the system equations [11, 12]

$$G_{n\pm l,m}^{(1,2,3,4,5,6,7,8,9),\tau} = \exp[\pm ika] G_{n,m}^{(1,2,3,4,5,6,7,8,9),\tau} \quad (4)$$

Using (4) the Green function are obtained by solving the equations (3).

$$\begin{aligned} G_{n,n}^{\tau,\tau} &= \sum_{l=1 \atop l \neq 4}^7 \frac{a(\omega_{kl})}{\omega - \omega_{kl}}; \quad \tau = (1,3,5,7) \\ a(\omega_{kl}) &= \frac{-2J_s^4 S^4 (\omega_{kl} - \Omega_b) - 4J_s^2 S^2 (\omega_{kl} - \Omega_t) (J^2 S^2 + \alpha(\omega_{kl})) - (4J^2 S^2 + \alpha(\omega_{kl})) (\omega_{kl} - \Omega_t)^2 (JS - \omega_{kl} + \Omega_t)}{\prod_{j \neq l \atop j \neq 4} (\omega_{kl} - \omega_{kj})} \\ \alpha(\omega_{kl}) &= (\omega_{kl} - \Omega_b)(JS - \omega_{kl} + \Omega_t) \\ G_{n,n}^{\tau,\tau} &= \sum_{l=1 \atop l \neq 5}^7 \frac{b(\omega_{kl})}{\omega - \omega_{kl}}; \quad \tau = (2,4,6,8) \\ b(\omega_{kl}) &= \frac{-2J_s^4 S^4 (\omega_{kl} - \Omega_b) + 2J_s^2 S^2 (\omega_{kl} - \Omega_t) (J^2 S^2 + 2\alpha(\omega_{kl})) - (3J^2 S^2 + \alpha(\omega_{kl})) (\omega_{kl} - \Omega_t)^2 (JS - \omega_{kl} + \Omega_t)}{\prod_{j \neq l \atop j \neq 5} (\omega_{kl} - \omega_{kj})} \\ \alpha(\omega_{kl}) &= (\omega_{kl} - \Omega_b)(JS - \omega_{kl} + \Omega_t) \\ G_{n,n}^{9,9} &= \sum_{l=1}^3 \frac{c(\omega_{kl})}{\omega - \omega_{kl}}; \quad a(\omega_{kl}) = -\frac{4J_s^2 S^2 + (\omega_{kl} - \Omega_t)(JS + \omega_{kl} + \Omega_t)}{\prod_{j \neq l} (\omega_{kl} - \omega_{kj})} \end{aligned} \quad (5)$$

where  $\Omega_t = g\mu H_0 + DS + 2J_s S(2 - \cos k)$ ;  $\Omega_b = g\mu H_0 + DS + 2JS(3 - \cos k)$

The poles of the Green functions occur at energies, which are the roots of the spin wave dispersion equation for the nanowires under consideration. Note that it was expected to receive in the considering system of the nine

freqencies. But the expression for seven different freqencies are obtained, because of degenerate in freqencies of  $\omega_{k6}$  and  $\omega_{k7}$ .

$$\begin{aligned}
 \omega_{k1} &= -2r \cos(\varphi/3) + (JS + 2\Omega_t + \Omega_b)/3, \\
 \omega_{k2} &= 2r \cos((\pi - \varphi)/3) + (JS + 2\Omega_t + \Omega_b)/3, \\
 \omega_{k3} &= 2r \cos((\pi + \varphi)/3) + (JS + 2\Omega_t + \Omega_b)/3, \\
 \omega_{k4} &= \Omega_t + JS \\
 \omega_{k5} &= \Omega_t \\
 \omega_{k6} &= 0.5(JS + 2\Omega_t) + 0.5S\sqrt{J^2 + 8J_s^2} \\
 \omega_{k7} &= 0.5(JS + 2\Omega_t) + 0.5S\sqrt{J^2 + 8J_s^2}
 \end{aligned} \tag{6}$$

where

$$\begin{aligned}
 r &= \sqrt{|3\psi - (JS + 2\Omega_t + \Omega_b)^2|}/3, \quad \varphi = \arccos\left(\frac{q}{r^3}\right) \\
 q &= (JS + 2\Omega_t + \Omega_b)^3/27 - \psi(JS + 2\Omega_t + \Omega_b)/6 - 2S^2(J_s^2\Omega_b + J^2\Omega_t) + \Omega_t\Omega_b(JS + \Omega_t)/2 \\
 \psi &= -4J_s^2S^2 - 4J^2S^2 + JS\Omega_b + 2\Omega_t\Omega_b + JS\Omega_t + \Omega_t^2
 \end{aligned}$$

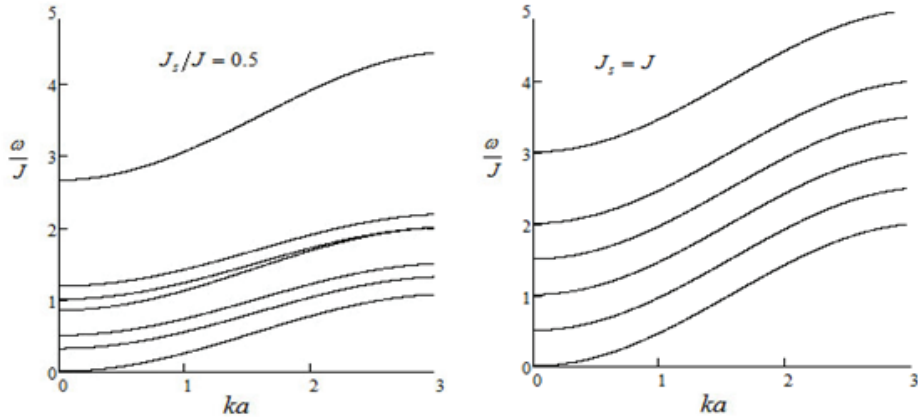


Fig. 2. Spin wave frequency versus wave number  $ka$  for the nanowires under consideration with parameters  $g\mu H_0/J = 0.2$ ,  $D/J = 0.1$ ,  $S = 0.5$ .

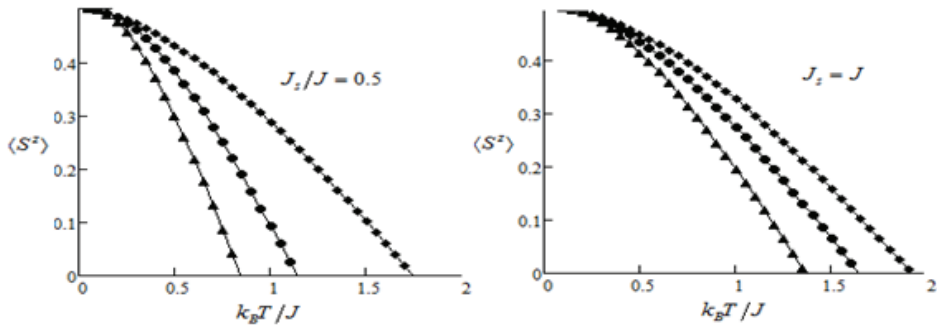


Fig. 3. Temperature dependence of the local- spin magnetization for the same parameters as in figure 2.

Solving the average spin, we derive the correlation function  $\langle S^- S^+ \rangle$  using the spectrum theorem [11,13]

$$\langle S^- S^+ \rangle = -\frac{2S}{N\pi} \sum_k \int_{-\infty}^{\infty} d\omega \frac{\text{Im} G(k, \omega + i\varepsilon)}{e^{\beta\omega} - 1} \tag{7}$$

Here  $\beta = 1/k_B T$ ,  $k_B$  is the Boltzmann constant,  $T$  is the temperature. Using (5) and the relation  $I/(x + i\varepsilon) = P(1/x) - i\pi\delta(x)$  to obtain the imaginary part of the Green functions, one finally obtains [11]

$$\begin{aligned}\langle S_{n,9}^- S_{n,9}^+ \rangle &= -\frac{2S}{N} \sum_k \sum_{l=1}^3 \frac{c(\omega_{kl})}{e^{\beta\omega_{kl}} - 1} \\ \langle S_{n,\tau}^- S_{n,\tau}^+ \rangle &= -\frac{2S}{N} \sum_k \sum_{\substack{l=1 \\ l \neq 4}}^7 \frac{a(\omega_{kl})}{e^{\beta\omega_{kl}} - 1} \quad \tau = 1,3,5,7 \quad (8) \\ \langle S_{n,\tau}^- S_{n,\tau}^+ \rangle &= -\frac{2S}{N} \sum_k \sum_{\substack{l=1 \\ l \neq 5}}^7 \frac{b(\omega_{kl})}{e^{\beta\omega_{kl}} - 1} \quad \tau = 2,4,6,8\end{aligned}$$

According to the theory of Callen [14] the average spin can be calculated using the following equation

$$\langle S^z \rangle = \frac{(S+1+\Phi)\Phi^{2S+1} + (S-\Phi)(1+\Phi)^{2S+1}}{\Phi^{2S+1} - (1+\Phi)^{2S+1}} \quad (9)$$

where  $\Phi = \frac{\langle S^- S^+ \rangle}{2\langle S^z \rangle}$ . Now the equation (8) and (9) can be solved self consistently to obtain the average spin at any given temperature. If  $S = 1/2$   $\langle S^z \rangle = \frac{1}{2} - \langle S^- S^+ \rangle$ .

Fig. 2 shows the frequencies of the spin-wave branches plotted versus  $ka$  for nanowires under consideration. The frequencies for the lowest branches are zero at  $ka = 0$ . The spin wave frequencies increase with increasing wave vectors and exchange coupling between spins.

The temperature dependence of magnetization in the nanowires under consideration is demonstrated in fig. 3. The spontaneous magnetization of the spins at zero temperature is  $\langle S^z \rangle = 0.5$ . Magnetization of the surface spins labeled  $\tau = 1, 3, 5, 7$  are smaller than that of the spins labeled  $\tau = 2, 4, 6, 8$ . The bulk spin magnetization is stronger than that of surface spins.

- 
- [1] *V.S. Tkachenko, V.V. Kruglyak, A.N. Kuchko*, Phys.Rev. B 81, 024425 (2010).
  - [2] *Z.K. Wang, M.H. Kuok, S.C. Ng, D.J. Lockwood, M.G. Cottam, K. Nielsch, R.B. Wehrspohn, and U. Gösele*, Phys. Rev. Lett. v.89, n.2, 027201 (2002).
  - [3] *O.A. Tretiakov and Ar. Abanov*, Phys. Rev. Lett. 105, 157201 (2010).
  - [4] *A. Ghaddar, F. Gloaguen, J. Gieraltowski*, Jurnal of Physics: Conference Series 200, 072032 (2010).
  - [5] *H. Leblond, V. Veerakumar, M. Manna*, Physical Review B 75, 214413 (2007).
  - [6] *E.V. Tartakovskaya*, Phys. Rev. B 71, 180404(R) (2005).
  - [7] *T.M. Nguyen and M.G. Cottam*, Phys.Rev. B 71, 094406 (2005).
  - [8] *T.M. Nguyen and M.G. Cottam*, Journal of Magnetism and Magnetic Materials 272-276, p.1672-1673, (2004).
  - [9] *M.Ye. Zhuravlev, J.D. Burton, A.V. Vedyayev and E.Y. Tsymbal*, J. Phys. A: Math. Gen. 38 5547–5556, (2005).
  - [10] *V.A. Tanrıverdiyev, V.S. Tagiyev*, Superlattices and Microstructures, Volume 43, Issue 3, p. 190-194. (2008).
  - [11] *H.T. Diep*, Phys.Lett. A 138, 69 (1989).
  - [12] *V.A. Tanrıverdiyev, V.S. Tagiyev, S.M. Seyid-Rzayeva*, FNT 12 (2003).
  - [13] *R. Schiller and W. Nolting*, Phys. Rev. B 60, 462–471 (1999).
  - [14] *H.B. Callen*, Phys. Rev. 130 890 (1963).

*Received: 27.05.2011*

## FORBIDDEN ROTATIONAL TRANSITIONS OF TRANS-CONFORMER OF MOLECULE CH<sub>3</sub>CH<sub>2</sub>OH

**S.B. KAZIMOVA, A.S. GASANOVA, E.Ch. SAIDOV**

*H.M. Abdullayev Institute of Physics of NASA, Azerbaijan,*

*Baku, AZ-1143. H. Javid pr., 33*

*E-mail: samusaev@mail.az. tel: 4324268*

The microwave rotational spectrum of trans-conformer of molecule CH<sub>3</sub>CH<sub>2</sub>OH in 26000-78000 MHz range is investigated. 72 forbidden transitions in main vibrational state are identified. The spectrum theoretical treatment is carried out by rotational Watson Hamiltonian-A reduction in I' axial representation. The rotational and centrifugal constants are specified.

**Keywords:** vibrational-rotational spectrum, forbidden transition, centrifugal disturbance.

**PACS:** 537.86.029.65/.79

The rotational spectrum of trans-conformer of molecule CH<sub>3</sub>CH<sub>2</sub>OH is investigated in [1,2]. The identification and interpretation of rotational spectrum of this molecule in microwave range of wave length for more high values of rotational quantum number J [3] are continued by us.

The spectrometer sensitivity increase [4] allows us to observe the forbidden centrifugal transitions appearing because of “guided” dipole moment  $\mu_C$ .

The calculation on rotational and centrifugal constants of rotational spectrum defined in [3] shows that

many such  $\mu_a$ -transitions can be in the investigated range. The task solving of search and identification of these transitions is our aim.

The identifications carried out step-by-step. Firstly, the rotational transition frequencies being in the investigated range and errors of their definition using Watson Hamiltonian - A reduction including quartic, sextic and octic centrifugal constants have been calculated on known spectroscopic constants:

$$\tilde{H} = \tilde{H}^{(1)} + \tilde{H}^{(2)}$$

where:

$$\begin{aligned} \tilde{H}^{(1)} &= \frac{1}{2}(\tilde{X} - \tilde{Y})J^2 + [\tilde{Z} - \frac{1}{2}(\tilde{X} + \tilde{Y})]J^2 - \Delta_J J^4 - \\ &- \Delta_{JK} J^2 J_z^2 - \Delta_R J_z^4 + H_J J^6 + H_{JK} J^4 J_z^2 + H_{KJ} J^2 J_z^4 + \\ &+ H_K J_z^6 + L_J J^8 + L_{JK} J^6 J_z^2 + L_{JK} J^4 J_z^4 + L_{KK} J^2 J_z^6 + L_K J_z^8 \\ \tilde{H}^{(2)} &= \frac{1}{2}(\tilde{X} - \tilde{Y})J^2 J_{XY}^2 - 2\delta_J J^2 J_{XY}^2 - \delta_K (J_z^2 J_{XY}^2 + \\ &+ J_{XY}^2 J_z^2) + 2h_J J^4 J_{XY}^2 + h_{JK} J^2 (J_z^2 J_{XY}^2 + J_{XY}^2 J_z^2) + \\ &+ h_K (J_z^4 J_{XY}^2 + J_{XY}^2 J_z^4) + 2l_J J^6 J_{XY}^2 + l_{JK} J^4 (J_z^2 J_{XY}^2 + \\ &+ J_{XY}^2 J_z^2) + l_J J^2 (J_z^4 J_{XY}^2 + J_{XY}^2 J_z^4) + l_K (J_z^6 J_{XY}^2 + J_{XY}^2 J_z^6) \end{aligned}$$

Here:  $\tilde{X}, \tilde{Y}, \tilde{Z}$  are rotational constants;

$\Delta_J, \Delta_{JK}, \Delta_K, \delta_J, \delta_K$  are quartic centrifugal constants;

$H_J, H_{JK}, H_{KJ}, H_K, h_J, h_{JK}, h_K$  are sextic centrifugal constants;

$L_J, L_{JK}, L_{KJ}, L_K, l_J, l_{JK}, l_K$  are octic centrifugal constant;

$J_X, J_Y, J_Z$  are principal moments of inertia.

Table 1  
The frequencies (MHz) of doublet transitions of trans-conformer of molecule CH<sub>3</sub>CH<sub>2</sub>OH

| «c» transitions                    | $\nu_{exp}$ | $\nu^a - \nu^c$ | «b» transitions                    | $\nu_{exp}$ |
|------------------------------------|-------------|-----------------|------------------------------------|-------------|
| 12 <sub>66-</sub> 13 <sub>58</sub> | 58889.529   | 11.838          | 12 <sub>66-</sub> 13 <sub>59</sub> | 58901.367   |
| 12 <sub>6-</sub> 13 <sub>59</sub>  | 58901.347   | -11.818         | 12 <sub>6-</sub> 13 <sub>58</sub>  | 58889.529   |
| 11 <sub>65-</sub> 12 <sub>57</sub> | 76662.796   | 0.224           | 11 <sub>66-</sub> 12 <sub>57</sub> | 76663.020   |
| 7 <sub>4_3-</sub> 8 <sub>35</sub>  | 42052.601   | -2.821          | 7 <sub>4_4-</sub> 8 <sub>35</sub>  | 42049.780   |
| 6 <sub>4_3-</sub> 7 <sub>35</sub>  | 60135.900   | 0.678           | 6 <sub>4_2-</sub> 7 <sub>35</sub>  | 60136.578   |
| 4 <sub>3_2-</sub> 5 <sub>24</sub>  | 43539.100   | 6.40            | 4 <sub>3_1-</sub> 5 <sub>24</sub>  | 43545.500   |

Table 2  
Forbidden transitions of trans-conformer of ethyl alcohol molecule

| transitions |    |    |   |    |    |    | $\nu_{exp}$ | $\nu_{calc}$ | $\Delta\nu$ |
|-------------|----|----|---|----|----|----|-------------|--------------|-------------|
| 3           | 2  | 2  | - | 3  | 1  | 2  | 74824.900   | 74824.685    | 0,215       |
| 4           | 3  | 2  | - | 5  | 2  | 4  | 43539.100   | 43539.132    | -0,032      |
| 4           | 4  | 0  | - | 3  | 3  | 0  | 252951.382  | 252951.206   | 0,176       |
| 5           | 4  | 1  | - | 6  | 3  | 3  | 77690.866   | 77690.689    | 0,177       |
| 6           | 6  | 0  | - | 6  | 5  | 2  | 287382.475  | 287382.472   | 0,003       |
| 6           | 6  | 1  | - | 6  | 5  | 1  | 287382.475  | 287382.472   | 0,003       |
| 6           | 4  | 3  | - | 7  | 3  | 5  | 60135.900   | 60135.732    | 0,168       |
| 7           | 6  | 2  | - | 7  | 5  | 2  | 287354.965  | 287355.055   | -0,09       |
| 7           | 6  | 1  | - | 7  | 5  | 3  | 287354.965  | 287355.073   | -0,108      |
| 7           | 4  | 3  | - | 8  | 3  | 5  | 42052.601   | 42052.589    | 0,012       |
| 8           | 6  | 3  | - | 8  | 5  | 3  | 287312.560  | 287312.592   | -0,032      |
| 8           | 6  | 2  | - | 8  | 5  | 4  | 287312.653  | 287312.670   | -0,017      |
| 8           | 1  | 7  | - | 7  | 2  | 5  | 76577.318   | 76577.400    | -0,082      |
| 8           | 5  | 3  | - | 9  | 4  | 5  | 77213.651   | 77213.819    | -0,168      |
| 9           | 6  | 4  | - | 9  | 5  | 4  | 287250.607  | 287250.569   | 0,038       |
| 9           | 6  | 3  | - | 9  | 5  | 5  | 287250.607  | 287250.642   | -0,035      |
| 9           | 7  | 2  | - | 8  | 6  | 2  | 497087.701  | 497087.750   | -0,049      |
| 9           | 7  | 3  | - | 8  | 6  | 3  | 497087.701  | 497087.750   | -0,049      |
| 9           | 5  | 5  | - | 10 | 4  | 7  | 59511.436   | 59511.283    | 0,153       |
| 10          | 6  | 5  | - | 10 | 5  | 5  | 287163.970  | 287163.826   | 0,144       |
| 10          | 6  | 4  | - | 10 | 5  | 6  | 287164.871  | 287164.642   | 0,229       |
| 10          | 10 | 1  | - | 10 | 9  | 1  | 495876.650  | 495876.401   | 0,249       |
| 10          | 10 | 0  | - | 10 | 9  | 2  | 495876.650  | 495876.401   | 0,249       |
| 11          | 6  | 6  | - | 11 | 5  | 6  | 287046.549  | 287046.470   | 0,079       |
| 11          | 6  | 5  | - | 11 | 5  | 7  | 287048.546  | 287048.657   | -0,111      |
| 11          | 10 | 2  | - | 11 | 9  | 2  | 495864.736  | 495864.741   | -0,005      |
| 11          | 10 | 1  | - | 11 | 9  | 3  | 495864.736  | 495864.741   | -0,005      |
| 11          | 6  | 5  | - | 12 | 5  | 7  | 76662.796   | 76662.790    | 0,006       |
| 11          | 6  | 6  | - | 12 | 5  | 8  | 76668.139   | 76668.067    | 0,072       |
| 12          | 6  | 7  | - | 12 | 5  | 7  | 286891.864  | 286891.738   | 0,126       |
| 12          | 6  | 6  | - | 12 | 5  | 8  | 286896.986  | 286897.044   | -0,058      |
| 12          | 10 | 3  | - | 12 | 9  | 3  | 495847.411  | 495847.314   | 0,097       |
| 12          | 10 | 2  | - | 12 | 9  | 4  | 495847.411  | 495847.314   | 0,097       |
| 12          | 6  | 6  | - | 11 | 5  | 6  | 497275.420  | 497275.439   | -0,019      |
| 12          | 6  | 7  | - | 11 | 5  | 7  | 497277.560  | 497277.524   | 0,036       |
| 12          | 6  | 6  | - | 13 | 5  | 8  | 58889.529   | 58889.586    | -0,057      |
| 12          | 6  | 7  | - | 13 | 5  | 9  | 58901.347   | 58901.221    | 0,126       |
| 13          | 6  | 8  | - | 13 | 5  | 8  | 286692.043  | 286691.781   | 0,262       |
| 13          | 6  | 7  | - | 13 | 5  | 9  | 286703.529  | 286703.701   | -0,172      |
| 13          | 10 | 4  | - | 13 | 9  | 4  | 495823.016  | 495822.893   | 0,123       |
| 13          | 10 | 3  | - | 13 | 9  | 5  | 495823.016  | 495822.893   | 0,123       |
| 14          | 10 | 5  | - | 14 | 9  | 5  | 495790.280  | 495790.147   | 0,133       |
| 14          | 10 | 4  | - | 14 | 9  | 6  | 495790.280  | 495790.147   | 0,133       |
| 14          | 3  | 12 | - | 13 | 4  | 10 | 62985.368   | 62985.384    | -0,016      |
| 14          | 7  | 8  | - | 15 | 6  | 10 | 76072.461   | 76072.370    | 0,091       |
| 15          | 10 | 6  | - | 15 | 9  | 6  | 495747.775  | 495747.645   | 0,13        |
| 15          | 10 | 5  | - | 15 | 9  | 7  | 495747.775  | 495747.645   | 0,13        |
| 15          | 7  | 8  | - | 16 | 6  | 10 | 58279.900   | 58279.985    | -0,085      |
| 15          | 7  | 9  | - | 16 | 6  | 11 | 58282.707   | 58282.605    | 0,102       |
| 16          | 7  | 9  | - | 17 | 6  | 11 | 40432.150   | 40432.356    | -0,206      |
| 16          | 7  | 10 | - | 17 | 6  | 12 | 40437.650   | 40437.788    | -0,138      |
| 16          | 10 | 7  | - | 16 | 9  | 7  | 495693.899  | 495693.848   | 0,051       |
| 16          | 10 | 6  | - | 16 | 9  | 8  | 495693.899  | 495693.848   | 0,051       |
| 17          | 10 | 8  | - | 17 | 9  | 8  | 495627.037  | 495627.115   | -0,078      |
| 17          | 10 | 7  | - | 17 | 9  | 9  | 495627.037  | 495627.115   | -0,078      |
| 17          | 8  | 9  | - | 18 | 7  | 11 | 75455.124   | 75455.016    | 0,108       |
| 17          | 8  | 10 | - | 18 | 7  | 12 | 75455.124   | 75455.281    | -0,157      |
| 18          | 4  | 14 | - | 19 | 1  | 18 | 45785.232   | 45785.240    | -0,008      |
| 18          | 10 | 9  | - | 18 | 9  | 9  | 495545.444  | 495545.696   | -0,252      |
| 18          | 10 | 8  | - | 18 | 9  | 10 | 495545.444  | 495545.696   | -0,252      |
| 19          | 4  | 15 | - | 20 | 1  | 19 | 38797.497   | 38797.702    | -0,205      |
| 19          | 8  | 12 | - | 20 | 7  | 14 | 39803.320   | 39803.272    | 0,048       |
| 22          | 9  | 14 | - | 23 | 8  | 16 | 39167.778   | 39167.614    | 0,164       |
| 23          | 5  | 18 | - | 24 | 0  | 24 | 492226.553  | 492226.387   | 0,166       |
| 26          | 10 | 17 | - | 26 | 9  | 17 | 494119.119  | 494118.673   | 0,446       |
| 26          | 10 | 16 | - | 26 | 9  | 18 | 494119.119  | 494118.726   | 0,393       |
| 30          | 12 | 19 | - | 31 | 11 | 21 | 55062.000   | 55062.031    | -0,031      |
| 30          | 12 | 18 | - | 31 | 11 | 20 | 55062.000   | 55062.032    | -0,032      |
| 31          | 4  | 28 | - | 31 | 3  | 28 | 33910.940   | 33910.751    | 0,189       |
| 32          | 4  | 29 | - | 32 | 3  | 29 | 27599.312   | 27599.253    | 0,059       |
| 32          | 5  | 27 | - | 31 | 6  | 25 | 329992.513  | 329993.180   | -0,667      |
| 33          | 6  | 28 | - | 34 | 3  | 32 | 250796.619  | 250796.015   | 0,604       |

Here  $\Delta\nu = \nu_{exp} - \nu_{calc}$

Table 3.

Rotational and centrifugal constants, errors and correlation matrix of these parameters of trans-conformer of ethyl alcohol molecule.

| Parameters             | Values          | Correlation matrix |         |         |                  |                     |                  |                  |                  |                     |                      |                      |                     |                     |                      |                     |                      |                       |                       |                        |                      |                       |                        |                      |  |
|------------------------|-----------------|--------------------|---------|---------|------------------|---------------------|------------------|------------------|------------------|---------------------|----------------------|----------------------|---------------------|---------------------|----------------------|---------------------|----------------------|-----------------------|-----------------------|------------------------|----------------------|-----------------------|------------------------|----------------------|--|
|                        |                 | A (MHz)            | B (MHz) | C (MHz) | $\Delta_J$ (kHz) | $\Delta_{JK}$ (kHz) | $\Delta_K$ (kHz) | $\delta_J$ (kHz) | $\delta_K$ (kHz) | H <sub>J</sub> (Hz) | H <sub>JK</sub> (Hz) | H <sub>KJ</sub> (Hz) | H <sub>K</sub> (Hz) | h <sub>J</sub> (Hz) | h <sub>JK</sub> (Hz) | h <sub>K</sub> (Hz) | L <sub>J</sub> (mHz) | L <sub>JK</sub> (mHz) | L <sub>KJ</sub> (mHz) | L <sub>KKJ</sub> (mHz) | L <sub>K</sub> (mHz) | l <sub>JK</sub> (mHz) | l <sub>LKJ</sub> (mHz) | l <sub>K</sub> (mHz) |  |
| A (MHz)                | 9 350,6771(11)  | 1,0                |         |         |                  |                     |                  |                  |                  |                     |                      |                      |                     |                     |                      |                     |                      |                       |                       |                        |                      |                       |                        |                      |  |
| B (MHz)                | 8 135,2361(9)   | 0,7                | 1,0     |         |                  |                     |                  |                  |                  |                     |                      |                      |                     |                     |                      |                     |                      |                       |                       |                        |                      |                       |                        |                      |  |
| C (MHz)                | 34 891,7916(31) | 0,5                | 0,9     | 1,0     |                  |                     |                  |                  |                  |                     |                      |                      |                     |                     |                      |                     |                      |                       |                       |                        |                      |                       |                        |                      |  |
| $\Delta_J$ (kHz)       | 8,546(4)        | -0,4               | -0,8    | -0,3    | 1,0              |                     |                  |                  |                  |                     |                      |                      |                     |                     |                      |                     |                      |                       |                       |                        |                      |                       |                        |                      |  |
| $\Delta_{JK}$ (kHz)    | - 28,566(23)    | 0,3                | 0,7     | 0,3     | 0,9              | 1,0                 |                  |                  |                  |                     |                      |                      |                     |                     |                      |                     |                      |                       |                       |                        |                      |                       |                        |                      |  |
| $\Delta_K$ (kHz)       | 253,004(71)     | -0,4               | -0,9    | -0,4    | -0,9             | 0,9                 | 1,0              |                  |                  |                     |                      |                      |                     |                     |                      |                     |                      |                       |                       |                        |                      |                       |                        |                      |  |
| $\delta_J$ (kHz)       | 1,7367(9)       | 0,3                | 0,8     | 0,2     | 0,9              | -0,9                | 0,9              | 1,0              |                  |                     |                      |                      |                     |                     |                      |                     |                      |                       |                       |                        |                      |                       |                        |                      |  |
| $\delta_K$ (kHz)       | 6,70(5)         | 0,4                | 0,8     | 0,3     | 0,9              | -0,9                | 0,9              | -0,9             | 1,0              |                     |                      |                      |                     |                     |                      |                     |                      |                       |                       |                        |                      |                       |                        |                      |  |
| H <sub>J</sub> (Hz)    | 0,0009(65)      | -0,3               | -0,7    | -0,3    | -0,9             | 0,9                 | -0,9             | 0,9              | -0,9             | 1,0                 |                      |                      |                     |                     |                      |                     |                      |                       |                       |                        |                      |                       |                        |                      |  |
| H <sub>JK</sub> (Hz)   | 1,31(9)         | 0,3                | 0,7     | 0,2     | 0,9              | -0,9                | 0,9              | -0,9             | 0,9              | 0,9                 | 1,0                  |                      |                     |                     |                      |                     |                      |                       |                       |                        |                      |                       |                        |                      |  |
| H <sub>KJ</sub> (Hz)   | - 9,6(4)        | -0,3               | -0,7    | -0,2    | -0,9             | 0,9                 | -0,9             | 0,9              | -0,9             | 0,9                 | 1,0                  |                      |                     |                     |                      |                     |                      |                       |                       |                        |                      |                       |                        |                      |  |
| H <sub>K</sub> (Hz)    | 37,5(10)        | -0,3               | -0,8    | -0,3    | -0,9             | 0,9                 | -0,9             | 0,9              | -0,9             | -1,0                | 0,9                  | -0,9                 | 1,0                 |                     |                      |                     |                      |                       |                       |                        |                      |                       |                        |                      |  |
| h <sub>J</sub> (Hz)    | - 0,005(1)      | 0,3                | 0,7     | 0,2     | 0,9              | -0,9                | 0,9              | -0,9             | 0,9              | -1,0                | 1,0                  | -0,9                 | 1,0                 |                     |                      |                     |                      |                       |                       |                        |                      |                       |                        |                      |  |
| h <sub>JK</sub> (Hz)   | 0,29(12)        | -0,3               | -0,7    | -0,2    | -0,2             | 0,9                 | -0,9             | 0,9              | -0,9             | 0,9                 | -0,9                 | 0,9                  | 0,9                 | 0,9                 | 0,9                  | 0,9                 | 0,9                  | 0,9                   | 0,9                   | 0,9                    | 0,9                  | 0,9                   | 0,9                    | 0,9                  |  |
| h <sub>K</sub> (Hz)    | 67,3(36)        | -0,3               | -0,2    | 0,1     | -0,5             | 0,7                 | -0,5             | 0,5              | -0,5             | -0,9                | 0,9                  | -0,8                 | 0,7                 | 0,9                 | 0,9                  | 0,9                 | 0,9                  | 0,9                   | 0,9                   | 0,9                    | 0,9                  | 0,9                   | 0,9                    | 0,9                  |  |
| L <sub>J</sub> (mHz)   | - 0,004(3)      | 0,3                | 0,0     | -0,2    | 0,1              | -0,6                | 0,6              | -0,3             | 0,5              | 0,6                 | -0,9                 | 1,0                  | -0,7                |                     |                      |                     |                      |                       |                       |                        |                      |                       |                        |                      |  |
| L <sub>JK</sub> (mHz)  | -0,15(9)        | -0,2               | 0,1     | 0,1     | -0,1             | 0,5                 | -0,5             | 0,2              | -0,5             | -0,5                | 0,9                  | -0,9                 | 0,5                 | 0,5                 | 0,5                  | 0,5                 | 0,5                  | 0,5                   | 0,5                   | 0,5                    | 0,5                  | 0,5                   | 0,5                    | 0,5                  |  |
| L <sub>KJ</sub> (mHz)  | - 51,4(59)      | 0,2                | -0,1    | -0,1    | 0,0              | -0,4                | 0,4              | -0,1             | 0,4              | 0,4                 | -0,7                 | 0,9                  | 0,9                 | 0,9                 | 0,9                  | 0,9                 | 0,9                  | 0,9                   | 0,9                   | 0,9                    | 0,9                  | 0,9                   | 0,9                    | 0,9                  |  |
| L <sub>KKJ</sub> (mHz) | 64(17)          | -0,1               | -0,2    | -0,2    | -0,2             | 0,1                 | -0,1             | 0,2              | -0,2             | 0,2                 | -0,2                 | -0,7                 | 0,7                 | 0,4                 | 0,4                  | 0,4                 | 0,4                  | 0,4                   | 0,4                   | 0,4                    | 0,4                  | 0,4                   | 0,4                    | 0,4                  |  |
| L <sub>K</sub> (mHz)   | - 86(11)        | 0,3                | 0,7     | 0,3     | 0,9              | -0,8                | 0,8              | -0,9             | 0,8              | 0,9                 | -0,8                 | 0,9                  | -0,8                | 0,9                 | 0,9                  | 0,9                 | 0,9                  | 0,9                   | 0,9                   | 0,9                    | 0,9                  | 0,9                   | 0,9                    | 0,9                  |  |
| L <sub>LJ</sub> (mHz)  | 0,0002(8)       | -0,3               | -0,7    | -0,2    | -0,8             | 0,8                 | -0,9             | -0,8             | -0,8             | -0,9                | 0,8                  | -0,9                 | 0,8                 | 0,8                 | 0,8                  | 0,8                 | 0,8                  | 0,8                   | 0,8                   | 0,8                    | 0,8                  | 0,8                   | 0,8                    | 0,8                  |  |
| l <sub>JK</sub> (mHz)  | - 0,29(8)       | 0,3                | 0,6     | 0,2     | 0,8              | -0,8                | 0,7              | -0,8             | 0,7              | 0,9                 | -0,9                 | 0,8                  | 0,8                 | 0,8                 | 0,8                  | 0,8                 | 0,8                  | 0,8                   | 0,8                   | 0,8                    | 0,8                  | 0,8                   | 0,8                    | 0,8                  |  |
| l <sub>LKJ</sub> (mHz) | 7(2)            | 0,3                | 0,6     | 0,2     | 0,8              | -0,8                | 0,7              | -0,8             | 0,7              | 0,9                 | -0,9                 | 0,8                  | 0,9                 | 0,9                 | 0,9                  | 0,9                 | 0,9                  | 0,9                   | 0,9                   | 0,9                    | 0,9                  | 0,9                   | 0,9                    | 0,9                  |  |
| l <sub>K</sub> (mHz)   | - 722(104)      | 0,3                | 0,7     | 0,3     | 0,9              | -0,8                | 0,8              | -0,9             | 0,8              | 0,9                 | -0,8                 | 0,9                  | 0,9                 | 0,9                 | 0,9                  | 0,9                 | 0,9                  | 0,9                   | 0,9                   | 0,9                    | 0,9                  | 0,9                   | 0,9                    | 0,9                  |  |
| h <sub>K</sub> (Hz)    | 67,3(36)        | 1,0                |         |         |                  |                     |                  |                  |                  |                     |                      |                      |                     |                     |                      |                     |                      |                       |                       |                        |                      |                       |                        |                      |  |
| L <sub>J</sub> (mHz)   | - 0,004(3)      | -0,8               | 1,0     |         |                  |                     |                  |                  |                  |                     |                      |                      |                     |                     |                      |                     |                      |                       |                       |                        |                      |                       |                        |                      |  |
| L <sub>JK</sub> (mHz)  | -0,15(9)        | 0,9                | -0,8    | 1,0     |                  |                     |                  |                  |                  |                     |                      |                      |                     |                     |                      |                     |                      |                       |                       |                        |                      |                       |                        |                      |  |
| L <sub>KJ</sub> (mHz)  | - 51,4(59)      | -0,8               | 0,8     | 0,8     | 1,0              |                     |                  |                  |                  |                     |                      |                      |                     |                     |                      |                     |                      |                       |                       |                        |                      |                       |                        |                      |  |
| L <sub>KKJ</sub> (mHz) | 64(17)          | 0,7                | -0,8    | -0,7    | 0,9              | 1,0                 |                  |                  |                  |                     |                      |                      |                     |                     |                      |                     |                      |                       |                       |                        |                      |                       |                        |                      |  |
| L <sub>K</sub> (mHz)   | - 86(11)        | -0,6               | 0,7     | 0,6     | -0,8             | 0,5                 | 1,0              |                  |                  |                     |                      |                      |                     |                     |                      |                     |                      |                       |                       |                        |                      |                       |                        |                      |  |
| L <sub>LJ</sub> (mHz)  | 0,0002(8)       | 0,9                | -0,8    | -1,0    | 1,0              | -0,8                | 0,9              | 1,0              |                  |                     |                      |                      |                     |                     |                      |                     |                      |                       |                       |                        |                      |                       |                        |                      |  |
| l <sub>JK</sub> (mHz)  | - 0,29(8)       | -0,9               | 0,8     | 0,9     | -1,0             | 0,9                 | -0,9             | 0,4              | 1,0              |                     |                      |                      |                     |                     |                      |                     |                      |                       |                       |                        |                      |                       |                        |                      |  |
| l <sub>LKJ</sub> (mHz) | 7(2)            | 0,8                | -0,8    | -0,8    | 0,9              | -0,9                | 0,9              | -0,4             | -1,0             | 1,0                 |                      |                      |                     |                     |                      |                     |                      |                       |                       |                        |                      |                       |                        |                      |  |
| l <sub>K</sub> (mHz)   | - 722(104)      | 0,8                | -0,8    | -0,8    | 0,9              | -0,9                | 0,9              | -0,4             | -0,9             | -1,0                | 1,0                  |                      |                     |                     |                      |                     |                      |                       |                       |                        |                      |                       |                        |                      |  |

Further, the experimentally defined frequencies of forbidden transitions beginning from transitions with small  $J$  the calculative errors of which are minimum ones are introduced in the solution of reversal spectroscopic task and it is solved. Later, the parameter clarification, spectrum calculation on which gives the possibility to identify the new group of lines of forbidden transitions with bigger  $J$  and etc is carried. The direct spectroscopic task is solved every time after introduction of new frequencies in the calculation and for further treatment the transitions the frequencies of which are calculated with minimum error are chosen.

The decomposition of transitions series in microwave spectrum of CH<sub>3</sub>CH<sub>2</sub>OH is caused by vibrational-torsional-rotational interactions. The series of doublet transitions the identification of which would be evidence of the presence of "weak" transitions in the observed rotational spectrum are observed. According to calculations, the decompositions of these doublet transitions decrease with the increase of quantum number

$J$  up to zero. At definite value of quantum number  $J$  the decomposition isn't bigger than 2MHz. The identification of these series we begin especially from these transitions.

The presence of such doublets is the best proof of spectrum identification rightness and the relation of doublets to forbidden transitions. The frequencies of such doublets are given in table 1.

The calculation carried out by such way gives the possibility to identify 72μ<sub>c</sub> forbidden transitions 28 from which lie in millimeter and 44 lie into submillimeter range of wave lengths.

The frequencies of these transitions with values of experimentally measured frequencies, their differences with calculated values of transition frequencies in first axial representation are given in the table 2.

The values of rotational and centrifugal constants, errors of their calculation and also correlation matrix of these parameters in the second axial representation are given in table 3.

- 
- [1] Ch.O. Gajar, S.A. Musayev, S.B. Kazimova, A.A. Abdullayev, M.E. Aliyev, A.S. Hasanova. Etanol ve izopropanol molekullarinin submillimetrik tejrubi udulma spektrlerinin kataloqlari. AMEA Fizika Instituti. Preprint № 002. Baki: Elm. 2004, 25 s.
  - [2] Ch.O. Gajar, S.A. Musayev, E.Ch. Saidov, S.B. Kazimova, A.A. Abdullayev, M.E. Aliyev. Etil spirti molekulunun santimetirik, millimetrik tejrubi udulma spektrlerinin tezlikleri kataloqlari. AMEA Fizika Instituti. Preprint №003. Baki:Elm,2004,25 s.
  - [3] Ch. Gajar, S. Musayev, A. Abdullayev, S. Kazimova. Fizika, 2006, v. 12, N 1-2, p. 41-45.
  - [4] J. Pearson, K.V.L.N. Sastry, M. Winnewisser et al. J. Mol. Spectrosc., 1995, v. 24, N 1, p. 246-261.
  - [5] Ch. Gajar, S. Musayev, A. Abdullayev, and M. Aliyev. Instruments and Experimental Techniques (IET). 2005, v 48, No.2, p. 222-224.
  - [6] T. Millar, G. Macdonald, and R. Habing. "The detection of hot ethanol in G34,3+0,15," Mon. Not. R. Astron. Soc, 25, 273. (1995).
  - [7] S.A. Musayev. Dokl. NAN Azerbaijana, 2001, t. 57, № 4-6, s. 111-119. (in Russian)
  - [8] S.A. Musayev. Dissertatsiya d.f.-m. nauk "Tsentronejnoe vozmushenie i vnutrennee vrashenie v molekulakh etilovogo i izopropilovogo spirtov". BAKU – 2003. (in Russian)
  - [9] O.I. Baskakov, Ch.O. Gajar, S.A. Musayev, D.A. Rzayev, E.Yu. Salayev. Submillimetroviy spektr molekuli *trans*-etanola. Trudi VII Vsesoyuznogo simpoziuma po molekulyarnoy spektroskopii visokogo i sverkhvisokogo razresheniya. Tomsk, 1986, chast 3, s. 84. (in Russian)

Received: 01.03.2011

## IR-SPECTROSCOPIC INVESTIGATION OF HIGH-SILICEOUS ZEOLITE-CLYNOPTILOLIT

**T.Z. KULIYEVA, E.A. AGAYEVA\*, G.M. EYVAZOVA, N.N. LEBEDEVA**

*Baku State University, SII of Physical Problems*

*\*Institute of chemical problems of Azerbaijan NAS*

The absorption spectra of natural zeolite-clynoptilolit from mineral resources of Azerbaijan subsoil have been investigated in the present work. IR spectra are measured on Varian-3600 FT-IR spectrophotometer in wide frequency range from 4000 up to 400  $\text{cm}^{-1}$ . According to literature data the identification of absorption band has been carried out.

**Keywords:** absorption spectra, clynoptilolit.

**PACS:** 78.30

### INTRODUCTION

The zeolites are the big group of natural hydrated aluminium silicates being non-stoichiometrical compounds the compositions of which change in wide intervals forming the series of solid solutions. Nowadays more than 45 structural types of natural zeolites widely spread of which are mordenite and klinoptilolit used by us, are well known. The zeolite worth is caused by usual for these minerals scroll aluminosilicate frame forming the system of cavities and channels the dimension of entrance windows of which is big enough in order that molecules and ions of majority organic and inorganic compounds can penetrate into them. The zeolite frames are formed by silicon and aluminium anionites. Because of frame construction it has the negative charge and this charge is compensated by alkaline and earth metal cations and water molecules being in frame pores and cavities weakly connected with it. The water can be eliminated at heating or zeolite vacuumization that doesn't influence on bracket frame. Its structure practically doesn't change. The zeolite pores of right form connecting between each other by "windows" form the set of through channels inside crystals. That's why the zeolites can be considered as the object on which one can investigate the electron pore-emission, the electron multiplication and gas discharge in the pores, dielectric and electric properties at pore saturation by different gases and liquids besides already well known phenomena (adsorption, ion-exchanging phenomena). In Azerbaijan Republic 14 varieties of zeolite mineral family which mainly are connected with volcanism revealing throughout Azerbaijan geological history have been established. The geological peculiarity of zeolitic regions gives us the reason to consider that Azerbaijan territory is the one of most perspective regions on natural zeolites [1], especially on high-siliceous ones the wide use of which in many regions is established. The belonging of natural zeolite investigated by us to high-siliceous ones of klinoptilolit type [2] on the base of X-ray and spectral analyses has been established. The clynoptilolit crystal structure belongs to monoclinic syngony with parameters:  $a=17.74\text{A}$ ,  $b=17.9\text{A}$ ,  $c=7.4\text{A}$ , space group is  $C2/m$ ,  $\beta=117^\circ$ .

The structure consists of alternate negatively charged aluminosilicate oxygen tetrahedrons  $\text{AlO}_4$  and  $\text{SiO}_4$  which connecting between each other by tops form the pores-nano-channels of two types A and B with dimensions  $0.6 \times 0.4\text{nm}$  (A type) and  $0.4 \times 0.4\text{ nm}$  (B type).

The content of these channels present itself the extra-frame subsystem which is positively charged ions-cations  $\text{Na}^+$ ,  $\text{K}^+$ ,  $\text{Mg}^+$ ,  $\text{Ca}^+$  compensating the frame negative charge and also the big number of coordinating water molecules  $\text{H}_2\text{O}$ . The water plays the important role for supplying the clynoptilolit frame stability because the hydrogen bond forms between frame oxygen atoms posititing in the positively charged ion coordination and  $\text{H}_2\text{O}$  molecules posititing in cation coordination that leads to increase of ion mobility in pore space as it is shown in [3].

It is known that IR-spectra are sensitive ones to the changes both hydrogen and coordination bonds in the crystal, that causes our interest to the measurement of absorption spectra in long-distance IR-region.

### EXPERIMENT

We have the monoblock of natural zeolite from which the lamellar samples for physical experiment are cut out. The fine-crystalline powder obtained at this operation is the investigation object of present work. The spectra are taken on Varian-3600 FT-IR spectrophotometer in the frequency interval of average (4000 up to 400  $\text{cm}^{-1}$ ) IR region.

### THE RESULTS AND THEIR DISCUSSION

The two wide absorption bands: from 3400 up to 3500  $\text{cm}^{-1}$  and wide band from 1000 up to 1060  $\text{cm}^{-1}$  are clearly expressed on spectrogram (fig.1) taken in frequency interval 3500 up to 400  $\text{cm}^{-1}$ . The frequency 3470  $\text{cm}^{-1}$  shows on the presence of coordinating water and its big width evidences on localization of (OH) groups in the channels connected with each other by hydrogen bonds. However, the discrete bands in this frequency region caused by valence oscillations of dipole groups (O-H) in nano-pores don't reveal in the spectrum.

At investigation of IR zeolite absorption spectra it is necessary to note that all observable absorption bands relate to two oscillation types: 1 are oscillations inside  $\text{AlO}_4$  and  $\text{SiO}_4$  tetrahedrons being the primary structural units not reflecting the peculiarities of zeolite structure; 2 are oscillations on tetrahedron external bonds. The oscillation second type depends on zeolite structure, coupling character of tetrahedrons into secondary structural units forming the inlets in zeolite cavity. Besides it the observable oscillations indicate on the

mixed composition of tetrahedrons and can't be related to oscillations only of  $\text{AlO}_4$  or  $\text{SiO}_4$ .

The more strong absorption bands observed in spectra of all zeolites at  $1250\text{-}950 \text{ cm}^{-1}$ , frequency is  $1053 \text{ cm}^{-1}$  belonging to this interval is caused by oscillations ( $\text{T-O}_i$ ) inside tetrahedrons and is related to first type oscillation, i.e. isn't sensitive to zeolite structure. The frequency  $1638 \text{ cm}^{-1}$  can be related to deformation oscillations  $\text{H-O-H}$  relating to second type oscillations, i.e. is sensitive to

zeolite structure; the frequency  $796 \text{ cm}^{-1}$  is caused by symmetrical valence oscillations inside tetrahedrons ( $\text{T-O}_i$ ), i.e. is related to first type oscillations; the frequency  $461 \text{ cm}^{-1}$  is related to deformation valence oscillation inside tetrahedrons and also belongs to first type oscillation; the frequency  $605 \text{ cm}^{-1}$  is responsible for oscillations of duplex rings and depends on connection character of tetrahedrons which form the nano-channel inlets.

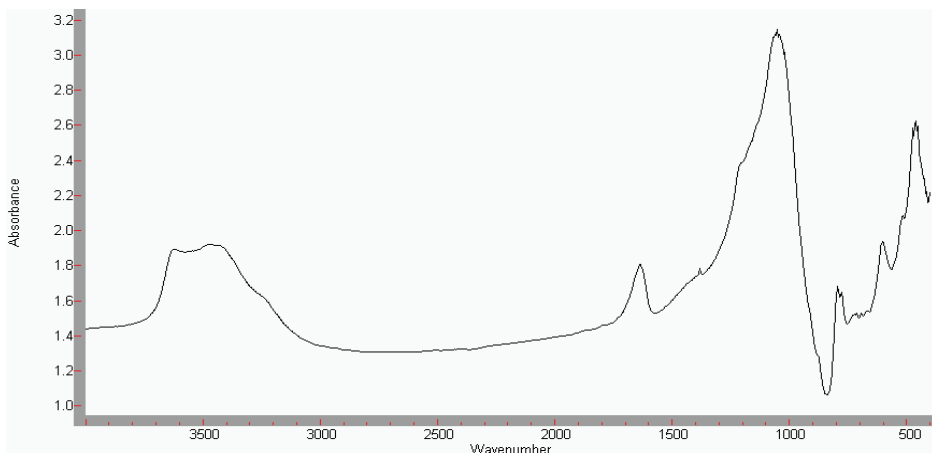


Fig. 1. The absorption spectrum of natural zeolite in average IR-region.

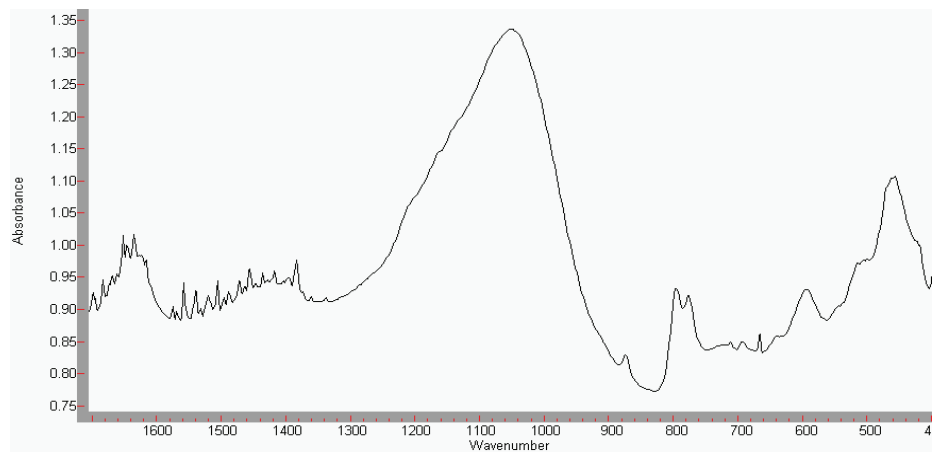


Fig. 2. The absorption band of natural zeolite-clynoptilolite.

The spectrogram written with big resolution (fig.2) allows us to carry out the identification of absorption bands in  $1600\text{-}600 \text{ cm}^{-1}$  interval. The band  $1558 \text{ cm}^{-1}$  relating to deformation oscillations of  $\text{H-O-H}$  group depending on zeolite structure and is sensitive to its changes is emphasized. The  $875 \text{ cm}^{-1}$ ,  $778 \text{ cm}^{-1}$ ,  $713 \text{ cm}^{-1}$ ,

$694 \text{ cm}^{-1}$ ,  $668 \text{ cm}^{-1}$  bands which can be related to symmetrical valence oscillations inside tetrahedrons ( $\text{T-O}_i$ ) are identified.

All values of absorption bands observed by us in IR-spectra are in well agreement with literature data on IR-spectra of high-siliceous compounds.

- [1] S.T. Amirov. "Tseoliti Azerbajijana", Baku, "Elm", 2004. (in Russian)
- [2] T.Z. Kuliyeva, N.N. Lebedeva, V.I. Orbukh, Ch.A. Sultanov. Fizika, XV, №3, 2009, 43.
- [3] V.G. Solovyov. "Eksperimentalnie issledovaniya fizicheskikh svoystv regulyarnikh matrichnikh kompozitov i sloistikh system s

- nanostruktuirovannimi neorganicheskimi i organiceskimi veshestvami", Avtoreferat dissertatsii, Sankt-Peterburg, 2005. (in Russian)
- [4] K. Nakamoto. "IK-spektri neorganicheskikh i koordinatsionnikh soedineniy", Moskva, 1966. (in Russian)

Received: 09.02.2011

## TO FRACTAL GEOMETRY OF NANOOBJECTS ON VAN DER WAALS SURFACE IN $A_2^V B_3^{VI}$ SYSTEM

**F.K. ALESKEROV<sup>1</sup>, K.Sh. KAKHRAMANOV<sup>1</sup>, A.Sh. KAKHRAMANOV<sup>2</sup>**

<sup>1</sup>*SPU «Selenium» of Azerbaijan NAS, G. Javid ave., 29A, Baku, Azerbaijan*

<sup>2</sup>*Baku State University, Z. Khalilov str., 23, Baku*

The practical application of Weershtrass and Van-der-Varden functions at morphology evaluation of nanoobject surface on (0001)  $A_2^V B_3^{VI}$  surface has been found. Taking into consideration this fact the analyses of different scales of nanostructured elements in  $A_2^V B_3^{VI}$  systems taking into account Van-der-Varden function graph are carried out.

**Keywords:** fractals, morphology, layered crystals.

**PACS:** 61.43.Hv; 64.60.al; 68.65.Ac

### INTRODUCTION

The investigation of the fractal geometry for application in different fields of solid-state electronics presents the special interest. The self-similarity is the main property of fractal structures. These structures seem similarly in the different spatial scales.

By the form of the separate fragment one can make the conclusion on the structure of the whole object. The systems characterized by fractional dimension [1] are called fractals. At the study of fractal aggregates the computer modeling plays the special role so the possibility to consider the different modes of particle aggregation and their scale appears.

The numerical simulation leads to real to real aggregate structural organization on small scales. The analysis of works dedicated to this direction is presented in monograph [1].

The fractal models are usually constructed on the base of different mathematical algorithms with use of modern computer graphics [2].

In [1-2] the well known classic fractal functions: Bolzano, Weershtrass, Hankel, Kover Serpinsky, Bezikovich, Rimann, Darbu, Kantor, Salfetka Serpinsky and Van-der-Varden have been considered.

Bezikovich function is the sample of continuous function which hasn't neither final nor infinite derivative in any point. The effective iterative process containing the several stages exists for the construction of the given function.

The aim of the work is to search of self-similar regions on Van der Waals surfaces of layered crystals and the revealing the fractality properties in them.

### THE RESULTS ON FRACTAL APPLICATION FOR ANALYSIS OF INTERFACE NANO-STRUCTURED ELEMENTS (INSE)

The nanoobjects on (0001)  $A_2^V B_3^{VI}$  surface are necessary to consider on the base of ideas and algorithms with the use of fractal elements. It allows us to locate INSE on the crystal base surface taking under consideration the percolation processes between layers of semiconductor thermoelectric crystals.

The fractal conceptions in physical and natural structures have been earlier studied in [3]. It is shown that fractal systems form the series of objects which can be

described by functions introduced by Weershtrass and Van-der-Varden [3].

Let's  $f_0(x)$ , absolute difference between x value and nearest to it integral value

$$f_0(x) = \begin{cases} x & \text{at } 0 \leq x \leq \frac{1}{2} \\ 1-x & \text{at } \frac{1}{2} \leq x \leq 1 \end{cases}$$

This  $f_0(x)$  function is linear on each interval  $\left[\frac{S-1}{2}, \frac{S}{2}\right]$  where s is integral number; continuous one

on the whole number axis, periodic one with period 1. Function graph is polygonal line the separate sections of which have the angular coefficient  $\pm 1$ . Let's define the

functions  $f_n(x) = \frac{f_o(4^n \cdot x)}{4^n}$ ,  $n=1,2,\dots$ . These

functions are linear in interval  $\left[\frac{S}{2 \cdot 4^n}, \frac{S+1}{2 \cdot 4^n}\right]$ . They are

continuous also and have the period  $\frac{1}{4^n}$ . The Van-der-

Varden function graph is shown on the fig.1. The developed iterative formula of Van-der-Varden function calculation has the form:

$$V(x) = \lim_{m \rightarrow \infty} \sum_{i=0}^m \sum_{j=0}^{i-1} F(4^i, x - \frac{j}{i})$$

$$F(a, x) = \begin{cases} x & 0 \leq ax < \frac{1}{2} \\ \frac{1}{a} - x, \frac{1}{2} \leq ax \leq 1 \end{cases}$$

Note than the further iterations without change of diagram scale made by us show the fit of function graph to  $ox$  axis (fig.1, c).

The base surface in  $Sb_2Te_3$  ( $Bi_2Te_3$ ) is irregular; however there are locally situated regions with more or less regular structure. Looking the series of electronically microscopic images of Van der Waals surface of  $A_2^V B_3^{VI}$

obtained on AFM one can see hierarchies of nanoformations on (0001)  $Sb_2Te_3$  surface (fig.2).

The analysis shows the whole regions of separate blocks of aggregated nanoparticles in the form of hierarchies of “mountain ranges”. The self-similar fractal structures in the different scales evidence about the fact that they can be described by Van-der-Varden functions. The nanoobjects on surface (0001)  $Bi_2Te_3$  (fig.3) are necessary to study with the help of fractal physics. The obtained results are compared by the construction method with the help of system of iterated functions. Cutting the small part from the structure having the signs of fractality we can consider it in some increase and reveal that it

similar to the whole structure. Such operation we can make continuously and then even microscopic nanoobjects will be similar to the structure as a whole. In reality we have some maximum and minimum scales of section heights and foundations (they are mentioned by pointers on the fig.2 and 3).

Thus, the considered structures have the determined fractal character. The self-similarity caused by the method peculiarities of their generation is their distinguishing characteristic. The self-similarity reveals on all levels. The determined fractals form in iteration process. They can be described by Van-der-Varden function.

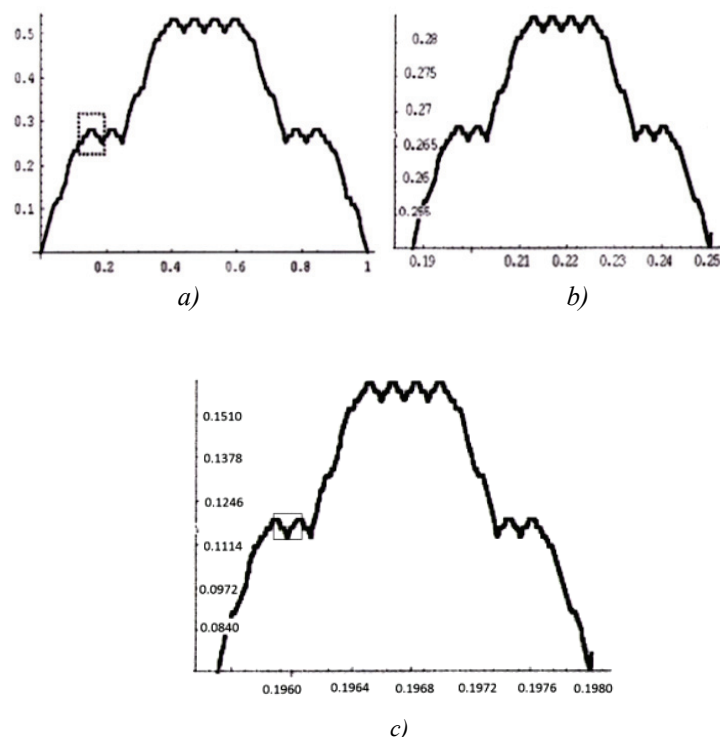


Fig. 1. (a,b,c) Van-der-Varden function; a) 3-rd iteration, b) 5-th iteration, c)7-th iteration

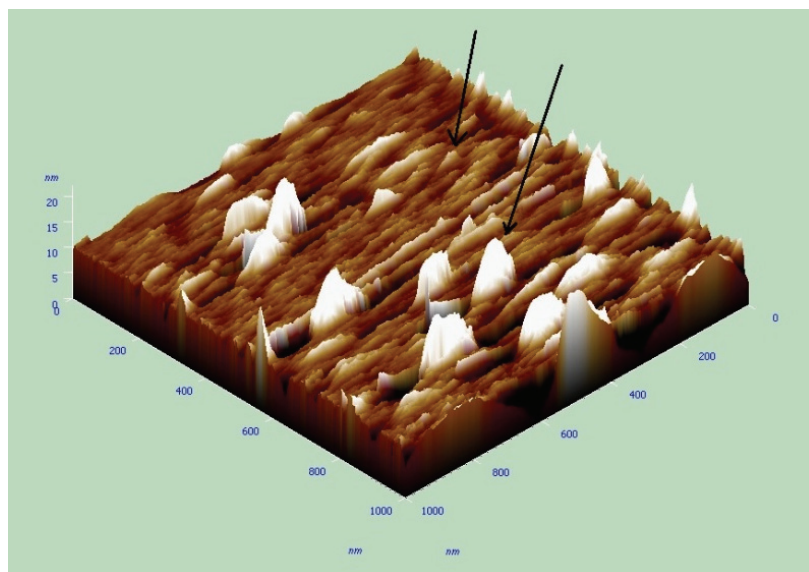


Fig. 2. AFM image in b 3D-dimension of interface nanoobjects in  $Sb_2Te_3<Te>$

**TO FRACTAL GEOMETRY OF NANOOBJECTS ON VAN DER WAALS SURFACE IN  $A_2^V B_3^{VI}$  SYSTEM**

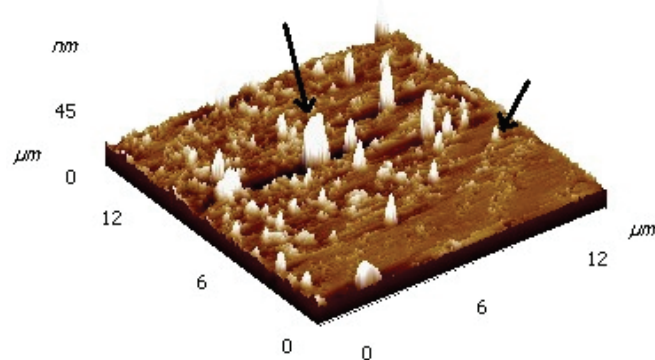


Fig. 3. AFM image in 3D-dimension of interface nanoobjects in  $\text{Bi}_2\text{Te}_3\langle\text{Te}\rangle$ .

- [1] P. Meakin, Fractals, Scaling and Growth Far from Equilibrium. Cambridge University Press. Cambridge, 1998, p.101.
- [2] R.M. Kronover. Fraktali i khaos v dinamicheskikh sistemakh. Per. s angl., M.: Postmarket, 2000.
- [3] A.Sh. Kakhramanov, F.K. Aleskerov, K.Sh. Kakhramanov. Fizika, 2009, v. XV, №4, p.98-101.

Received: 14.02.2011

## SELENIUM OPTICAL SPECTRA OBTAINED UNDER DIFFERENT CONDITIONS (PART II)

N.Z. JALILOV

*H.M. Abdullayev Institute of Physics of Azerbaijan NAS  
AZ-1143, H. Javid, 33, Baku*

The reflection coefficients  $R(E)$  of amorphous (massive and film) and polycrystalline (massive) selenium in beam energy interval 1–6 eV normally incident on the surface are measured in the work. The spectral dependences of their optical constants and dielectric functions are calculated by Kramers-Kronig method. It is shown that the different conditions of selenium sample preparation lead to the change of short range ordering in atom configuration. This changes the electronic structure and consequently, the optic parameters of these materials.

**Keywords:** reflection, Se, spectrum, annealing, condition, film.

**PACS:** 535.3; 539.2/6:539./.04

### INTRODUCTION

The selenium as the elementary conductor in polycrystalline and amorphous states [1] is widely used in electronography, infrared technology, electrooptical converters. Many fundamental works are devoted to its investigation. However, the supposed separate models used for the explanation of electron processes taking part in it and nowadays they are need the new data. This is connected with the fact that selenium has the different structural peculiarities. Being the inorganic superpolymer, the selenium has the amorphous,  $\alpha$  and  $\beta$  monoclinic, hexagonal modifications with ring-shaped, chain molecules which have the different atom number. In wide temperature interval all its modifications can exist in the sample simultaneously and in different quantities. Moreover, many selenium properties will be depend on the relation of these modifications in the sample and on the condition of their preparation.

The formation conditions and peculiarities of this or that selenium layer structure prepared by the molecular steam condensation in vacuum have been revealed and established in ref [2]. It is shown that the selenium layer structure prepared by the evaporation in vacuum is defined by the temperature of condensing molecular steam, structure of near-surface layer and temperature substrate. Moreover, the layer structure can present itself the supercooled state, first, second amorphous forms or intermediate amorphous state. In the given work it is established that structure of first amorphous form consists of ring-shaped molecules of  $Se_8$  type polymerized in accumulations the dimensions of which are equal to some hundreds nano-meters. The structure of second amorphous form consists of continuous polymerized chain molecules of lattice structural units of selenium hexagonal modification type. Such amorphous state is the long-chain polymer of homogeneous density with initial softening temperature 299K about. Such structure in the comparison with the structure of selenium first amorphous form is more stable one. In the process of the transition from first amorphous form to the second one the intermediate amorphous state forms. This state is constructed from structural elements of first and second amorphous forms and is enriched by atomic selenium.

The samples prepared at different conditions that gives the possibility of selenium obtaining with different

structures in order to investigate its optical properties with the help of measurement of reflection coefficient  $R(E)$  and calculations of optical parameters on Kramers-Kronig relation are studied in the given work. As it is known the crystalline selenium has the chain structure, the bond between atoms has the covalent character and between chain atoms has Van-der-Waals character. It has the complex electronic structure. Its electronic structure depends also on sample structural changes.

The study of their properties with structure change in amorphous or glass-forming systems presents the interest as at this the possibility of correlation study between the structure and material properties (molar volume, viscosity, glass-transition temperature, thermal expansion coefficient and others) is appeared.

The semiconductor optical spectra are connected with their electronic structures. The material energy level defining their many physicochemical parameters is the one of its main parameters. The knowing of material dispersion allows us to predict the principal possibilities of definite property realization and its application in semiconductor electronics.

The reflection coefficients  $R(E)$  of some materials: amorphous and monocrystalline Se, monocrystalline  $InSnTe_2$ ,  $TlIn_{0.9}Ce_{0.1}Se_2$ ,  $TlInSe_2Ce_{0.04}$ ,  $TlInSe_2$ ,  $Cu_3GdTe_3$ ,  $Cu_5GdTe_4$ ,  $CuGdTe_2$ , amorphous  $Se_{95}As_5$  (with Sm impurity), monocrystalline  $Bi_2Te_3$  (with Ni, Cu, Zn, Tb, Cl impurities), polycrystalline ( $Bi_2Te_3$ - $Bi_2Se_3$ ) (with Tb, Cl impurities),  $YbBi_2Te_4$ ,  $YbBi_4Se_7$  have been measured by us. Also their optical parameters:  $\theta$  reflected light phase, absorption  $\kappa$  and refraction  $\kappa$  indexes,  $\varepsilon_1$  real and  $\varepsilon_2$  imaginary parts of dielectric constant,  $\alpha$  absorption coefficient, the function of characteristic  $-Im\epsilon^{-1}$  volume and  $-Im(\epsilon+1)^{-1}$  surface electron losses, electrooptical differential functions ( $\alpha, \beta$ ),  $\varepsilon_2E$  optical conduction,  $\varepsilon_2E^2$  integral function of bound density of states,  $\varepsilon_0(E)$  effective static dielectric constant,  $n_{ef}(E)$  effective number of valence electrons taking part in transitions up to the given energy  $E$ . The results on optical spectra of amorphous selenium obtained at the different conditions are given in the article.

The measurement of selenium reflection coefficient  $n_{ef}(E)$  prepared at the different conditions and the definition of their optical spectra on its base is the aim of the given work.

## THE INVESTIGATION TECHNIQUE

$B_5$  which is melted and endured at temperature  $280^\circ C$  during three hours is taken for the obtaining of the amorphous sample and further the ampoule with selenium is put in cool water. The samples for the measurements are prepared from this amorphous selenium mass. The amorphous films by  $2\text{--}8 \mu m$  thickness are obtained by thermal evaporation in vacuum and by the hot wall method on the substrates from the cover glass. The selenium polycrystalline samples are obtained by slow cooling of melted selenium.

The reflection coefficient  $R(E)$  of amorphous massive, film and polycrystalline selenium are measured by the method of double-beam spectroscopy at room temperature in radiation energy interval  $1\text{--}6$  eV normally falling on the surface.

As it is mentioned in [3] the semiconductor optical functions in wide region of fundamental absorption are effectively studied by the method of almost normal mirror reflection. Other optical methods have the essential principal methodical limits and give the information in limited spectral regions. They add the results of normal reflection at the definition of optical transition values.

The interaction of light with the substance is described by refractive  $n$  and absorption  $k$  indexes which characterize the plane wave phase and attenuation in the substance. These values can be defined on  $R(E)$  from Kramers-Kronig formula:

$$\theta(E_0) = \frac{E_0}{\pi} \int_0^{\infty} \frac{\ln R(E)}{E_0^2 - E^2} dE. \quad (1)$$

The computer program applied in refs [4-14] is written by us for the calculation of the optical parameters of the investigated materials on the base of experimental data on  $R(E)$ .

## RESULTS AND THEIR DISCUSSION

In the present work  $R(E)$  reflection is measured and the optical functions of  $\text{YbBi}_2\text{Te}_4$  and  $\text{YbBi}_4\text{Se}_7$  are defined on its base. Their such parameters as: reflected light phase  $\theta$ , absorption  $k$  and refractive  $n$  indexes, real  $\varepsilon_1$  and imaginary  $\varepsilon_2$  parts of dielectric constants, absorption coefficient  $\alpha$ , the functions of characteristic volume –  $\text{Img } \varepsilon^{-1}$  and surface –  $\text{Img } (\varepsilon+1)^{-1}$  electron losses, electrooptical differential functions ( $\alpha, \beta$ ), optical conduction  $\varepsilon_2 E$ , integral function of bound state density  $\varepsilon_2 E^2$ , dielectric constant  $\varepsilon_0(E)$ , effective number of valence electrons  $n_{ef}(E)$  taking part in optical transitions up to the given energy  $E$ . From the obtained results:  $R(E)$  function, electrooptical differential functions ( $\alpha, \beta$ ), optical conduction  $\varepsilon_2 E$ , integral function of bound state density  $\varepsilon_2 E^2$ , dielectric constant  $\varepsilon_0(E)$ , effective number of valence electrons  $n_{ef}(E)$  taking part in optical transitions up to the given energy  $E$  are presented on fig.1-8 and the values of band-to-band optical transitions defined on  $\varepsilon_2(E)$  base in photon energy region  $1\text{--}6$  eV are given in the table.

As it is mentioned in [15] the study of absorptive transitions on the materials is impossible because of big absorption value in the region of interband transition energies  $E > E_g$  ( $E_g$  is minimum energy of interband

transitions). The reflection method is the unique effective method. The analytical singularities of imaginary part of the complex dielectric constant  $\varepsilon_2(E)$  and the functions bound by densities of states  $dN/dE$  almost coincide. The gradient of interband states makes the main contribution into the analytical singularity of  $dN/dE$  function:

$$\frac{dN_{ij}}{dE} \sim \int \frac{dS_k}{|\nabla_k E_{ij}|}, \quad (2)$$

where  $E_{ij}(k) = E_j(k) - E_i(k)$  is the distance between conduction and valence bands. The values  $dN/dE$  near critical points in  $k$  – space defined by  $|\nabla_k E_{ij}|=0$  expression and also the positions of critical points and transition type can be theoretically calculated from band structure.

The analysis of  $\varepsilon_2(E)$ ,  $dN/dE$  functions and  $R(E)$  reflection coefficient show that the position in the energy spectrum and peak character are similar or they are close enough for these parameters. That's why one can define the values of corresponding interband intervals and band nature with the help of direct comparison of experimental data of crystal reflection in  $E > E_g$  region.

It is known that the least energy  $E_g$  between occupied and free states is the one of the important parameters. The high transparency in wide energy region  $E < E_g$  is character for non-crystalline materials. There are some methods of its definition and the values on  $\alpha(E)$  absorption coefficient level of long-wave edge. The exact value  $E_g$  for non-crystalline semiconductors is discussion one and usually the discussion of spectrum character  $\alpha(E)$  in Urbakh and Tauz models is carried out without evaluations of  $E_g$  [16].  $E_g$  is defined from Tauz model by the value of absorption coefficient  $\alpha(E) = 10^3 \text{ cm}^{-1}$ .

As it is mentioned in [16]  $N(E)$  density of states is the similarly suitable for crystalline and non-crystalline substances. According to results of experimental data the path of density of states in non-crystalline substance isn't strongly differ from corresponding one in the crystal. In the first case the thin structure can be lubricated and the local states can appear in the forbidden band, the band structure saves as it is defined by atomic short ordering order in materials.

The hexagonal crystalline selenium consists of helical chains formed parallel to each other. The chemical bond inside the chains has the covalent character and it is very strong, but the bond between the chains is the weak bond of Van-der-Waals type. At rapid melt cooling the viscosity becomes very high and the glassy state appears before the chains had time to reorientate. The decomposition of ideal structure of non-crystalline solid state is in the systems including the atoms with unshared electron couples. Very often at bond opening the electron couple is on the one of fragments, i.e. the heterolytic bond opening takes place. The one positive and one negative charged defect centers in the regions of the short range ordering appear. The energy necessary for bond opening is partly compensated because of unshared electron couple of atoms being in nearest surrounding and the number of chemical bonds doesn't change in total. Thus, there is the structural disordering along with density

oscillations and existing topological disordering in homogenous glasses of stoichiometric composition. The last one reveals in the form of positive and negative charged defect centers as in the case of point defect in the crystals. As a result the reaction defect the formation of which is characterized by the least change of free energy, dominated.

As it is mentioned in [17] it is impossible to make the principal boundary between monocrystalline, polycrystalline and amorphous states of the substances. The presence of the band structure: forbidden and conduction bands can be obtained from the fact of atom short range ordering existence and there is no need to require the periodic atom disposition for this conclusion. These questions for amorphous and crystalline selenium have been studied in [18-26], their electronic structures

have been defined and compared. As a rule, the sharpness of selenium thin structure decreases at its amorphization.

The disposition and the form of semiconductor bands are defined by crystal chemical composition, its symmetry and atom properties forming the crystal [27]. The atom-like wave functions are used in all band calculations in the capacity of initial ones and the character of chemical bonds between atoms forming it is taken under consideration along with crystal symmetry properties.

The optical properties in the semiconductors are directly connected with their band structure [28]. The expression of imaginary dielectric constant  $\varepsilon_2(\omega)$  is calculated by bond structure by the following formula:

$$\varepsilon_2(\omega) = \frac{4\pi^2 e^2}{m^2 \omega^2} \sum_{v,c} \int_{\text{c},\text{A}} \frac{2dk}{(2\pi)^3} |eM_{cv}(k)|^2 \delta(E_c(k) - E_v(k) - \hbar\omega). \quad (3)$$

This expression is the main one which shows the bond between bond structure and optical constants. This expression is often used in comparison with expressions for other optical constants as it doesn't include the refraction index. The spectra for  $\varepsilon_1(\omega)$  one can find with the help of dispersion relation of Kramers-Kronig substituting the expression (3) in it:

$$\varepsilon_1(\omega) = 1 + \frac{8\pi e^2}{m^2} \sum_{v,c} \int_{\text{c},\text{A}} \frac{2dk}{(2\pi)^3} \frac{|eM_{cv}(k)|^2}{[E_c(k) - E_v(k)]/\hbar} \frac{1}{[E_c(k) - E_v(k)]^2 / \hbar^2 - \omega^2}. \quad (4)$$

One can calculate all optical constants if the bond structure is known by  $\varepsilon_2(\omega)$  and  $\varepsilon_1(\omega)$ . The calculations of such type have been carried out in [28].

The optical parameter functions represented on fig.1-8 are connected between each other, but the each from them presents the definite interest.  $\varepsilon_2(\omega)$  function on which the optical transitions of the investigated samples are defined, is directly connected with their electronic structure.

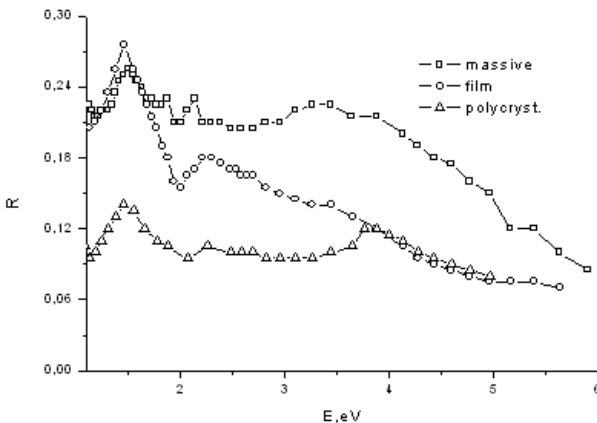


Fig.1. The reflection spectra  $R(E)$ : of amorphous, massive, film and polycrystalline selenium.

These transitions are given in the table. They can be divided into two groups: intra- and interband transitions, i.e. the transitions having the less values of forbidden band width (1,88; 2,21; 1,88 eV for amorphous massive,

film and polycrystalline selenium correspondingly) that is seen from the table.

Nowadays it is established that one can change the optical, photoelectric and electric properties of chalcogenide and chalcogene glassy semiconductors with the change of chemical composition and also with introduction of impurities. Moreover, the change of concentration of charged defect centers  $D^+$  и  $D^-$  ( $U^1$  are centers) of these materials takes place because of change of coordination number in the region of short range ordering. These defects form from the initial neutral defects  $D^0$  by the reaction:



which can be intrinsic or impurity and mixed defects that gives us the possibility to control their physical properties.

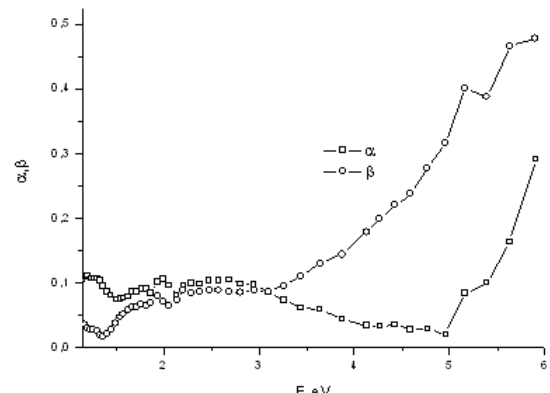


Fig.2. The spectra of electrooptical differential functions ( $\alpha, \beta$ ) of amorphous massive selenium.

## SELENIUM OPTICAL SPECTRA OBTAINED UNDER DIFFERENT CONDITIONS (PART II)

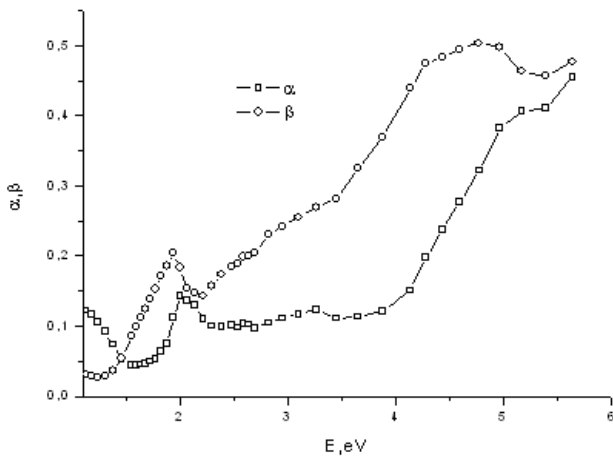


Fig.3. The spectra of electrooptical differential functions ( $\alpha$ ,  $\beta$ ) of film amorphous selenium.

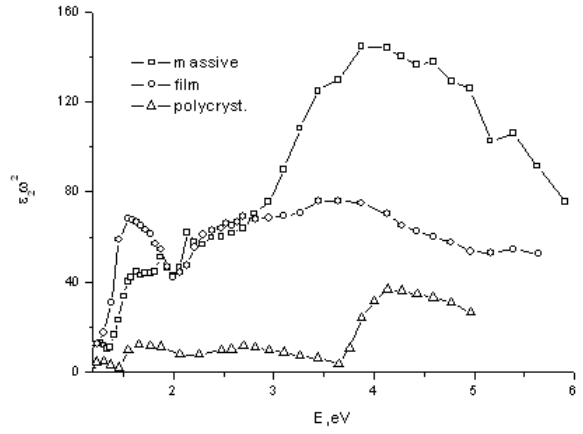


Fig.6. The spectra of integral function of bound state density  $\epsilon_2 E^2$  of amorphous, film and polycrystalline selenium.

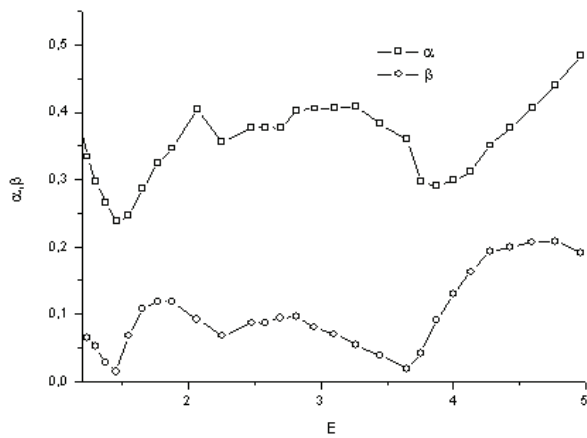


Fig.4. The spectra electrooptical differential functions ( $\alpha$ ,  $\beta$ ) of polycrystalline selenium.

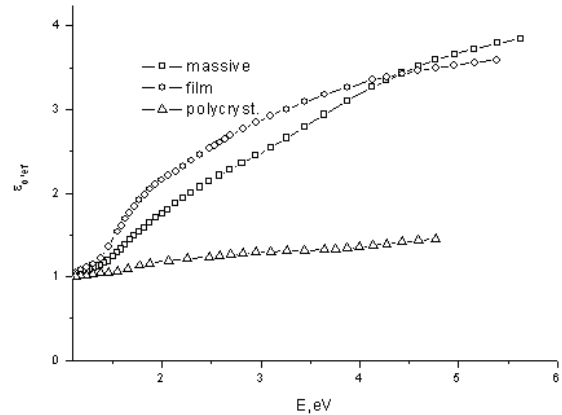


Fig.7. The effective statistic dielectric constant  $\epsilon_0(E)$  of amorphous massive, film and polycrystalline selenium.

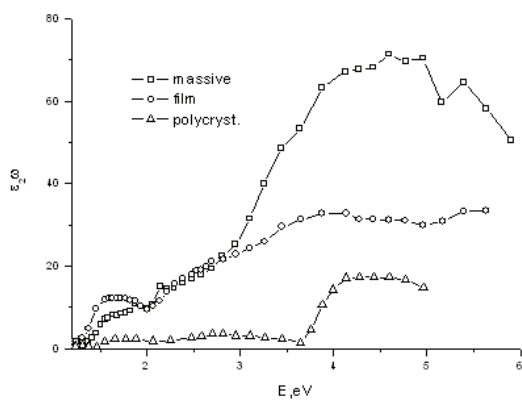


Fig.5. The spectrum of optical conduction  $\epsilon_2 E$  of amorphous massive, film and polycrystalline selenium.

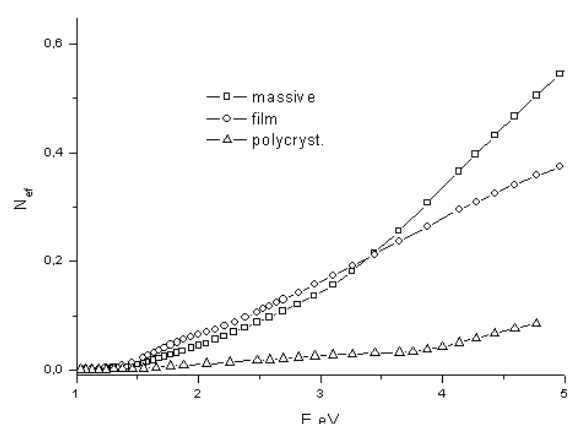


Fig.8. The effective number of valence electrons  $n_{ef}(E)$  participating in the transitions up to the given energy  $E$  of amorphous massive, film and polycrystalline selenium.

| Samples           | The optical transitions defined by $\epsilon_2(E)$ maxima in 1÷6 eV energy interval |      |      |      |      |      |      |      |      |      |
|-------------------|---|------|------|------|------|------|------|------|------|------|
| Amorphous massive | 1,24  | 1,3  | 1,55 | 1,88 | 1,99 | 2,21 | 2,29 | 2,26 | 3,64 | 4,77 |
| Film              | 1,13  | 1,46 | 1,55 | 2,21 | 2,29 | 2,38 | 2,53 | 2,69 | 3,44 | 5,19 |
| Polycrystalline   | 1,24  | 1,55 | 1,65 | 1,88 | 2,48 | 2,69 | 4    | 4,13 | -    | -    |

From fig. 1-8 and the table it is seen that spectra of optical parameters of amorphous (massive, film) and polycrystalline (massive) selenium reveal the differences that is connected with their structural differences. This is related to optical transitions in these materials that it is seen from the table.

## CONCLUSION

Thus, the selenium reflection coefficient prepared at different conditions and having the different structures

has been measured in the work in the beam energy interval 1-6 eV incident normally on the surface. The optical parameters of the investigated samples are calculated on its base with the help of Kramers-Kronig relations. It is established that these parameters are different for different selenium samples prepared at different conditions. This fact reveals in the values of optical transitions in these materials. The obtained results are explained by the change of short range ordering in them in the dependence on sample preparation conditions.

- 
- [1] *G.B. Abdullaev, D.Sh. Abdinov, Fizika selena, Izd. ELM, Baku , (1975) 403.*(In Russian)
  - [2] *I.D. Nabitovic, Dis. Dokt. fiz.-mat. Nauk, Lvov, (1970) 328.* (In Russian)
  - [3] *V.V. Sobolev, V.V. Nemoshkalenko, Elektronnaya struktura poluprovodnikov, Kiev, nauk. Dumka (1988).* (In Russian)
  - [4] *N.Z. Jalilov, S.I. Mextieva, N.M. Abdullaev, AMEA Xəbərlər, fizika-riyaziyyat və texnika elmləri seriyası fizika və astronomiya, XXVII, №5 (2007) 114.*
  - [5] *N.Z. Jalilov, S.I. Mextieva, N.M. Abdullaev, Fizika, XIII №4 (2007) 89.*
  - [6] *N.Z. Jalilov, G.Z. Damirov, AMEA Xəbərlər, fizika-riyaziyyat və texnika elmləri seriyası fizika və astronomiya, XXVII №5 (2009) 125.*
  - [7] *N.Z. Jalilov, S.I. Mextieva, N.M. Abdullaev, M.I. Veliev, II Ukrainskaya nauc. kon. po poluprovod, (2004) 140.* (In Russian)
  - [8] *N.Z. Jalilov, S.I. Mextieva, N.M. Abdullaev, M.I. Veliev, AMEA Xəbərlər, fizika-riyaziyyat və texnika elmləri seriyası fizika və astronomiya, XXIV №5(I) (2004).* (In Russian)
  - [9] *S.I. Mextieva, N.M. Abdullaev, N.Z. Jalilov, N.R. Mamedov, Dokladi NAN Azerb., LXIII №4 (2007) 48.* (In Russian)
  - [10] *N.Z. Jalilov, N.M. Abdullaev, N.R. Mamedov, Amorfnie i Mikrokristalliceskoe Poluprovodniki, Sb. Trudov VI Mejd. Konf., Sankt-Peterburg, (2008) 238.* (In Russian)
  - [11] *N.Z. Jalilov, N.M. Abdullaev, N.R. Mamedov, G.M. Askerov, Fizika, XIV №3 (2008) 144.* (In Russian)
  - [12] *N.Z. Jalilov, G.M. Damirov, Trudi X Mejd. Konf. «Opto-nanoelektronika, nanotexnologie i mikrosistemi», Ulyanovsk, (2008) 45.* (In Russian)
  - [13] *N.Z. Jalilov, G.M. Damirov, FTPFTPI, 45, №4 (2011) 500-505.* (In Russian)
  - [14] *N.Z. Jalilov, G.M. Damirov, AMEA Xəbərlər, fizika-riyaziyyat və texnika elmləri seriyası fizika və astronomiya, XXVIII №5 (2008) 134.*
  - [15] *J.C. Phillips, Phys. Rev. 125 (1962) 1931; 133 (1964) A452.*
  - [16] *N. Mott, E. Devis, Elektronnije processi v nekristalliceskix veshestvax, Moskva «MiR» (1982).* (In Russian)
  - [17] *A. Rouz, A.Poyz, Osnovi teorii fotoprovimosti, Izd., Mir, Mockva, (1966).* (In Russian)
  - [18] *N.J. Shevchik, M. Cardona and J. Tejeda, Physical Review B, 8 №6 (1973) 2833-2841.*
  - [19] *J.D. Joannopoulos, M. Schlüter and L. Cohen Marvin, Physical Review B, 11 №6 (1975) 2186-2199.*
  - [20] *A. Vaidyanathan, S.S. Mitra and Y.F. Tsay, Physical Review B, 21 №6 (1980) 2475-2481.*
  - [21] *R.H. Williams and J.I. Polanco, J. Phys C: Solid State Phys., 7 (1974) 2745-2759.*
  - [22] *L.D. Laude and Fitton, B. Kramer and K. Maschke, Physical Review Letters, 27 №16 (1971) 1053-1056.*
  - [23] *B. Kramer, Phys. Stat. sol., 41 (1960) 725-733.*
  - [24] *J.L. Hartke and Paul J. Regensburger, Physical Review, 139 №3A (1965) A970-A980.*
  - [25] *G. Weiser and J. Stuke, Phys. Stat. sol., 35 (1969) 747-753.*
  - [26] *I.M. Cidilkovskiy. Zonnaya struktura poluprovodnikov. M. Nauka, 1978, 328 c.* (In Russian)
  - [27] *F. Bassani, J. Pastori Parravicini. Elektronnije sostayaniya i opticeskie perexodi v tverdix telax, M..Nauka, 1982, 391 c.* (In Russian)
  - [28] *E.M. Godjaev, G.S. Orudjev, D.M. Kafarov, FTT, 46, №5 (2004) 811.* (In Russian)

Received: 04.03.2011

## THE ANNEALING INFLUENCE ON SPECTRA OF OPTICAL PARAMETERS OF Bi<sub>2</sub>Te<sub>3</sub>- Bi<sub>2</sub>Se<sub>3</sub> FILM SAMPLES IN 1÷6 eV RANGE

**N.Z. JALILOV, G.M. DAMIROV<sup>†</sup>**

*H.M. Abdullayev Institute of Physics of NAS, AZ-1143, G. Javid ave., 33, Baku*

<sup>†</sup>[gafil@physics.ab.az](mailto:gafil@physics.ab.az)

The reflection spectra  $R(E)$  of film samples Bi<sub>2</sub>Te<sub>3</sub> - Bi<sub>2</sub>Se<sub>3</sub> of *n*-and *p*-types without and with annealing in the beam energy interval 1÷6 eV incident normally on the surface are measured. The spectra of their optical parameters and values of optical transitions are defined by Kramers-Kronig method. It is shown that the character of the spectrum change of optical parameters and electron transition values change with annealing.

**Keywords:** optical spectra, thermoelectric materials, Bi<sub>2</sub>Te<sub>3</sub>, Bi<sub>2</sub>Se<sub>3</sub>.

**PACS:** 535.3; 539.2/6:539./.04

### 1. INTRODUCTION

The bismuth telluride and solid solutions on its base are applied at the preparation of different energy converters [1]. The experimental investigations of optical properties of solid solutions Bi<sub>2</sub>Te<sub>3</sub> - Bi<sub>2</sub>Se<sub>3</sub> and Bi<sub>2</sub>Te<sub>3</sub> are published in the series of works [2-5]. The data on thermoelectric materials on the base of Bi<sub>2</sub>Te<sub>3</sub> are given in the ref [2]. The results on the study of Bi<sub>2</sub>Te<sub>3</sub> band structures are given in [3-5].

The bismuth telluride presents itself the semiconductor having the good thermoelectric properties. It belongs to crystal group of  $A_2^V B_3^{VI}$  type. Its crystalline structure is formed by the repetitions of five-level packets which are quintets consisting of atoms disposed in the following sequence ... - Te<sup>(1)</sup> - Bi - Te<sup>(2)</sup> - Bi - Te<sup>(1)</sup> ... .

Bi<sub>2</sub>Te<sub>3</sub> is well known as effective material for thermoelectric converters and it is easier to prepare it by the way of doping, obtain the both *n*- and *p*-types [1,2]. The both mono- and polycrystalline Bi<sub>2</sub>Te<sub>3</sub> and its solid solutions with Bi<sub>2</sub>Se<sub>3</sub> are mainly used in converters. The band structure of Bi<sub>2</sub>Te<sub>3</sub> crystal is theoretically calculated in [3]. The absence of experimental data on the value of spin-orbital interaction ( $\Delta$ ) is the main difficulty.

Bi<sub>2</sub>Te<sub>3</sub> crystals have the packet structure and the bond between neighbor packets has the mixed Van-der-Waals-covalent character [6]. The additional bond because of the transition of one p-electron on d-levels and the overlapping of some d-levels with valence band exists between packets. All this causes the essential metallic properties and comparatively small values of forbidden band energies in 0,15÷0,35 eV range.

In relation to optics Bi<sub>2</sub>Te<sub>3</sub> and its analogues are the uniaxial crystals. The dielectric constant in them is the tensor of second order and depends on the direction of incident wave in respect of optical axis *C*. The optical properties of bismuth telluride in the region of higher frequencies are investigated in [4].

The polycrystalline film samples Bi<sub>2</sub>Te<sub>3</sub> - Bi<sub>2</sub>Se<sub>3</sub> of *n*- and *p*-type are representatives of disordered system in which the change of their physical properties is explained by the influence of different external factors including the temperature on the change of short range ordering in atom configuration. In our case the change of optical parameters with annealing can be explained by the change of short range ordering in them.

The study of the influence of annealing on the reflection coefficients of film polycrystalline samples Bi<sub>2</sub>Te<sub>3</sub> - Bi<sub>2</sub>Se<sub>3</sub> of *n*- and *p*-type and the spectrum definition of their optical parameters on its base is the task of the given work.

### 2. EXPERIMENT TECHNIQUE

The Bi<sub>2</sub>Te<sub>3</sub> - Bi<sub>2</sub>Se<sub>3</sub> films of *n*- and *p*-type technology is described in [2,7,8]. The films by width 0,3μm of Bi<sub>2</sub>Te<sub>3</sub> - Bi<sub>2</sub>Se<sub>3</sub> polycrystalline of *n*- and *p*-type are obtained. The crystals doped by Cl impurities have *n*-type conduction and crystals doped by Tb impurities have *p*-type conduction.

The reflection spectra of normally incident radiation on surface of Bi<sub>2</sub>Te<sub>3</sub> - Bi<sub>2</sub>Se<sub>3</sub> film samples of *n*- and *p*-type without annealing in the radiation energy range 1÷6 eV are investigated in the this work. The reflection coefficient is measured by two-beam method.

The interaction of the light with the substance is described by refraction index *n* and absorption index *k* which character the phase and damping the plane wave in the substance. These values can be defined by the measurements of reflection coefficient  $R(E)$  and by Kramers-Kronig formula:

$$\theta(E_0) = \frac{E_0}{\pi} \int_0^\infty \frac{\ln R(E)}{E_0^2 - E^2} dE. \quad (1)$$

The definition methods of optical parameters are given in [9,10]. The optical parameters of the investigated materials are calculated by the programs constructed by the author of [11] ref which are applied at calculation of optical parameters of series of materials [12-16].

### 3. THE RESULTS AND THEIR DISCUSSION

The reflection coefficient  $R(E)$  of film polycrystalline samples Bi<sub>2</sub>Te<sub>3</sub> - Bi<sub>2</sub>Se<sub>3</sub> of *n*- and *p*-type are measured and the spectra of their optical parameters:  $\alpha$  absorption coefficient,  $\epsilon_2$  imaginary and  $\epsilon_1$  real parts of dielectric constant, *n* refraction and *k* absorption indexes, effective number of valence number  $n_{\text{ef}}(E)$  taking part in transitions up to the given energy *E*, effective static dielectric constant  $\epsilon_{0,\text{eff}}(E)$ , the functions of characteristic -  $\text{Img } \epsilon^{-1}$  volume and  $-\text{Img}(\epsilon+1)^{-1}$  surface electron losses,

$\theta$  phase of reflected light, the optical conduction  $\varepsilon_2 E$ , integral function of bound density of states  $\varepsilon_2 E^2$  and electrooptical differential functions ( $\alpha, \beta$ ).

The spectra of  $R(E)$  reflection coefficients, the spectra of  $k$  and  $n$  coefficients,  $\varepsilon_2$  imaginary and  $\varepsilon_1$  real parts of dielectric constant, spectra of density of states  $J(\varepsilon_2 E^2)$  correspondingly are presented on fig.1-4 and in the table the values of interband optical transitions defined on  $\varepsilon_2$  maximums is given.

The presented data gives the possibility gives us the possibility to compare the optical spectra in  $\text{Bi}_2\text{Te}_3 - \text{Bi}_2\text{Se}_3$  film samples of  $n$ - and  $p$ -type with and without annealing, that is seen from fig.1-4 and table.

Table

| The optical transitions in $\text{Bi}_2\text{Te}_3 - \text{Bi}_2\text{Se}_3$ film samples of $n$ - and $p$ -type with and without annealing, defined by $\varepsilon_2$ peaks in 1-6 eV beam energy interval |                          |                             |                          |
|--|--------------------------|-----------------------------|--------------------------|
| $n$ -type without annealing  | $n$ -type with annealing | $p$ -type without annealing | $p$ -type with annealing |
| 1.15   | 1.49                     | 1.49                        | 1.19                     |
| 1.41   | 1.60                     | 1.69                        | 1.31                     |
| 1.54   | 2.58                     | 1.99                        | 1.94                     |
| 1.77   | 2.90                     | 2.39                        | 2.19                     |
| 1.87   | 3.20                     | 2.49                        | 2.39                     |
| 2.08   | 3.90                     | 2.59                        | 2.50                     |
| 3.26   | 4.69                     |                             | 4.00                     |
| 3.76   |                          |                             | 4.49                     |
| 4.77   |                          |                             | 4.80                     |
| 5.15   |                          |                             | 5.30                     |

As it is seen from fig.1 in case of  $p$ -type the annealing of  $\text{Bi}_2\text{Te}_3 - \text{Bi}_2\text{Se}_3$  leads to essential growth of reflection coefficient and in case of  $n$ -type it doesn't change significantly. Probably, this is connected with improvement of  $\text{Bi}_2\text{Te}_3 - \text{Bi}_2\text{Se}_3$  structure of  $n$ - and  $p$ -type.

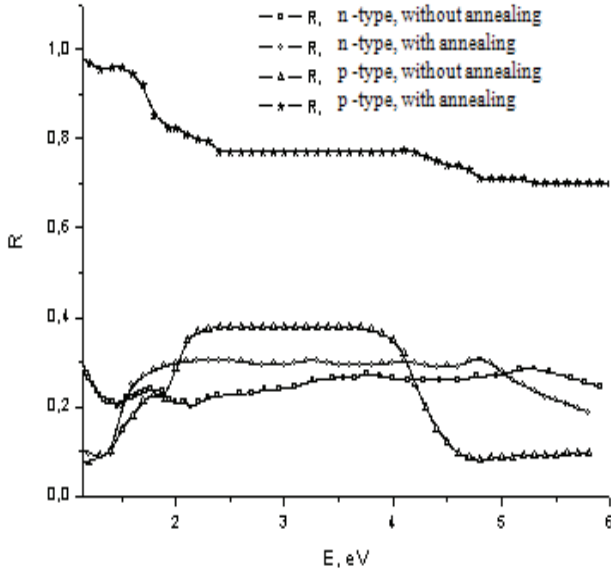


Fig.1. The reflection coefficients ( $R$ ) of film samples of  $n$ - and  $p$ -type with and without annealing.

The spectra  $k$  and  $n$  defined on  $R(E)$  and reflection phase where  $\theta$  reflection phase is defined by formula (1) are presented on fig. 2. It is necessary to mention that one

can define all other optical parameters on corresponding relations on these parameters.

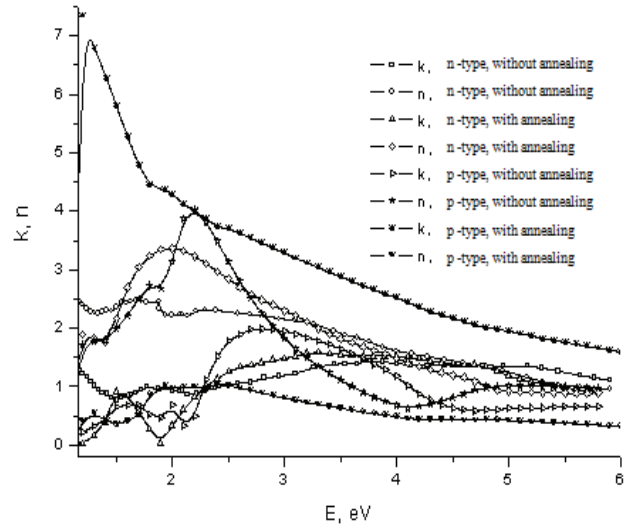


Fig.2. The spectra of  $k$  and  $n$  coefficients of  $\text{Bi}_2\text{Te}_3 - \text{Bi}_2\text{Se}_3$  film samples of  $n$ - and  $p$ -type with and without annealing.

The spectra of  $\varepsilon_1$  and  $\varepsilon_2$  coefficients of  $n$ - and  $p$ -type with and without annealing are given in fig. 3. As it is above mentioned, the optical transitions are usually defined on  $\varepsilon_2$  peaks. As it is seen from the figure the annealing changes the change character and its values.

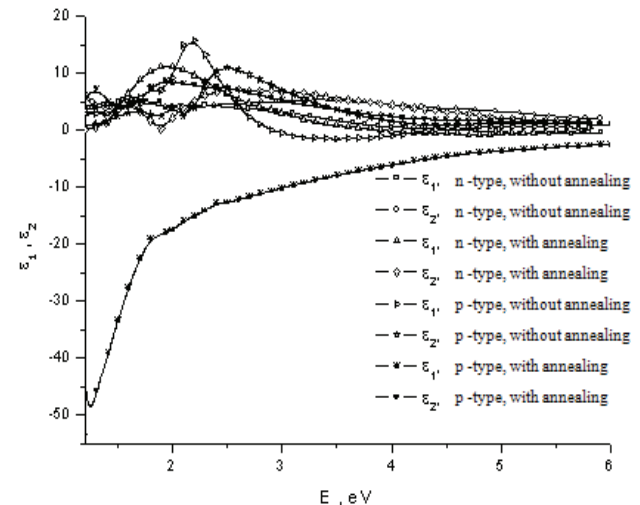


Fig.3. The spectra of  $\varepsilon_1$  and  $\varepsilon_2$  coefficients of  $\text{Bi}_2\text{Te}_3 - \text{Bi}_2\text{Se}_3$  film samples of  $n$ - and  $p$ -type with and without annealing.

The change with annealing of density of states  $J = \varepsilon_2 E^2$  of  $\text{Bi}_2\text{Te}_3 - \text{Bi}_2\text{Se}_3$  film polycrystalline samples of  $n$ - and  $p$ -type is given on fig.4. It is seen that the annealing strongly influences on change of density of states of  $\text{Bi}_2\text{Te}_3 - \text{Bi}_2\text{Se}_3$  film polycrystalline samples of  $n$ - and  $p$ -type.

According to table one can trace the changes of optical transition values in  $\text{Bi}_2\text{Te}_3 - \text{Bi}_2\text{Se}_3$  of  $n$ - and  $p$ -type with annealing.

As it is mentioned in ref [17] the study of absorbing transitions in materials is impossible because of big

absorption value in the region of interband transition energies  $E > E_g$  ( $E_g$  is forbidden band width). The reflection is unique effective method.

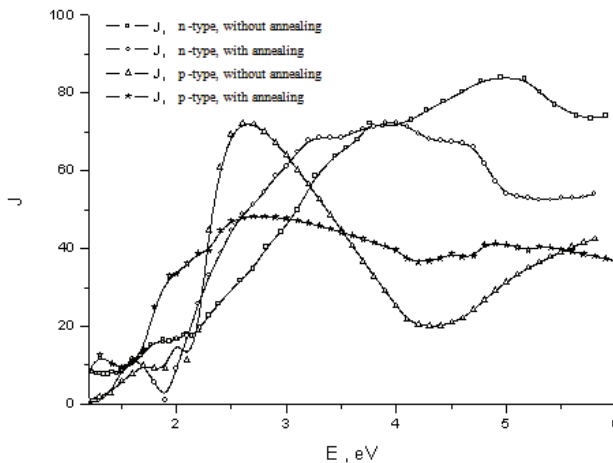


Fig. 4. The spectra of density of states of Bi<sub>2</sub>Te<sub>3</sub> - Bi<sub>2</sub>Se<sub>3</sub> film samples of *n*- and *p*-type with and without annealing.

The analytical singularities of imaginary part of complex dielectric constant  $\varepsilon_2(E)$  and functions connected by density of states  $dN/dE$  almost coincide and the gradient of interband distances makes the main contribution in  $dN/dE$  functions:

$$\frac{dN_{ij}}{dE} \sim \int \frac{dS_k}{|\nabla_k E_{ij}|}, \quad (2)$$

where  $E_{ij}(k) = E_j(k) - E_i(k)$  is distance between conduction and valence bands. Theoretically  $dN/dE$  values near critical points in k-space defined by  $|\nabla_k E_{ij}| = 0$  expression and also the position of critical points and transition type are calculated from band structure.

The analysis of  $\varepsilon_2(E)$ ,  $dN/dE$  functions and reflection coefficient  $R(E)$  show that position and peak character in their spectra are similar or very close to each other. That's why one can define the values of corresponding energy gaps and band nature with the help of direct comparison of experimental data in  $E > E_g$  region with theoretical calculations of  $dN/dE$  function. As it is mentioned in [18] the resonance frequency  $E_0$  presents itself the frequency at which the conduction  $2nk \cdot E$  achieves the maximum.

Thus, the reflection coefficient  $R(E)$  of Bi<sub>2</sub>Te<sub>3</sub> - Bi<sub>2</sub>Se<sub>3</sub> of film samples of *n*- and *p*-type with and without annealing in beam energy range 1÷6 eV incident normally on the surface are measured in the work. The spectra of optical parameters of the investigated samples and the electron transitions in them are defined. It is shown that change character of optical parameter spectra and the values of electron transitions in these samples changes with annealing, i.e. change of the short range ordering in them.

The authors are grateful to leader research scientist N.M. Abdullayev for submission of Bi<sub>2</sub>Te<sub>3</sub> - Bi<sub>2</sub>Se<sub>3</sub> samples.

- 
- |     |   |      |  |
|-----|---|------|--|
| [1] | V.L. Gurevich. Kinetika fononnikh sistem (M.: Nauka, 1980) 14.(in Rusiian)  | [10] | Opticheskie svoystva poluprovodnikov, <i>pod. red. Bira</i> (IL, M, 1970). (in Rusiian)  |
| [2] | B.M. Goltsman, V.A. Kudinov, I.A. Smirnov. Poluprovodnikovie termoelektricheskie svoystva materialov na osnove Bi <sub>2</sub> Te <sub>3</sub> (M.: Hayka, 1972), c.216. (in Russian) | [11] | N.Z. Jalilov. Trudi X Mejd. konf. «Opto-nanoelektronika, nanotekhnologii i mikrosistemi» (Ulyanovsk, 2008) 46-47. (in Rusiian)                   |
| [3] | P.M. Lee, L.Pincerle. Pros. Phys. Soc. 81, 461 (1963).  | [12] | N.Z. Jalilov, G.M. Damirov. Trudi X Mejd. konf. «Opto-nanoelektronika, nanotekhnologii i mikrosistemi» (Ulyanovsk, 2008) 45. (in Rusiian)        |
| [4] | D.I. Greenaway and G.Harbeke. I. Phys. Chem. Solids Pergamon Press, 26, 1585 (1965).  | [13] | N.Z. Jalilov, G.M. Damirov. FTP, 45, 500 (2011). (in Rusiian)  |
| [5] | E.V. Oleshko, V.N. Korolishin. FTT, 27, 2856 (1985). (in Rusiian)   | [14] | N.Z. Jalilov, G.M. Damirov. . Izvestiya NAN Azerb., ser. fiz.-mat. i tekhn., fiz i astr., XXVIII, №5, 134 (2008); XXIX, 125 (2009). (in Rusiian) |
| [6] | E.Mooser, W.C.Pearson, Phys. Chem. Solids 7, 5 (1958).  | [15] | N.Z. Jalilov, M.A. Makhmudova. . Izvestiya NAN Azerb., ser. fiz.-mat. i tekhn., fiz i astr., XXX, 71 (2010). (in Rusiian)                        |
| [7] | B.M. Goltsman, Z.M. Dashevskiy, V.I. Kaydanov, N.V. Kolomoets. Plyonochnie termoelementi: fizika i primenie (M.: Nauka, 1985) s.233. (in Rusiian)                                     | [16] | N.Z. Jalilov, S.I. Mekhtieva, N.M. Abdullayev. Izvestiya NAN Azerb., ser. fiz.-mat. i tekhn., fiz i astr., XXVII, 114 (2007). (in Rusiian)       |
| [8] | S.A. Semiletov. Trudi institute kristallografi, 10, 74 (1954). (in Rusiian)   | [17] | J.C. Phillips. Phys. Rev. 125, 1931 (1962), 133, A452 (1964).  |
| [9] | V.V. Sobolev, V.V. Nemoshkalenko. Elektronnaya struktura poluprovodnikov (Kiev, Nauk. Dumka, 1988). (in Rusiian)  | [18] | T. Moss, G. Barrel, B. Ellis. Poluprovodnikovaya optoelektronika (M.: Mir, 1976). (in Rusiian)   |

Received: 17.03.11

## THE ABSORBING COVERING OF VHF RADIATION

**S.T. AZIZOV**

*H.M. Abdullayev Institute of Physics Azerbaijan NAS,  
AZ 1143, G.Javid ave., 33, Baku*

The possibility of covering formation on the base of composition materials utilizing the residual electromagnetic radiation has been investigated. The coverings can be used for the defense of living organisms from VHF ill effect of given frequency radiation.

**Keywords:** VHF absorber, microwave spectroscopy.

**PACS:** 537.86, 537.87

### INTRODUCTION

The electromagnetic radiation absorbers carried out on the base of composition materials containing the thin metallic wires or high-dispersion metallic particles, the electromagnetic radiation absorption which carried out in filler surface layer because of skin-effect [1, 2].

The deficiency of these fillers is in the fact that efficiency of electromagnetic radiation absorption weakens with increase of its frequency that makes difficult the formation of high-frequency absorbers of electromagnetic radiation on the base of existing conducting materials. The improvement of selectivity and sensitivity of coverings absorbing the electromagnetic radiation is the task of investigation.

The carried out investigations of reflective characteristics of the systems consisting of quarter-wave layer of absorbing dielectric marked on metallic substrate, show the obtaining possibility of wave non-reflective absorption in them. The last one forms because of wave interference reflected from medium interface. Moreover, the required ratios of amplitudes and phases of reflected waves are achieved by the way of selection of corresponding values of dielectric constants, dielectric losses  $\epsilon''$  and the covering material thickness. The existence reality of non-reflecting wave absorption phenomenon in layered systems and in particular, in two-layered system dielectric-metal is theoretically and experimentally proved on the example of reflective characteristic investigation of polar molecule solutions in microwave range [3,4]. The selective absorption in such systems takes place at small thicknesses of covering layer and can be realized in wider wave range including the short-wave region of wave millimeter range. The existence of frequency spectrum and discrete thicknesses of substance layer in wave, at which the conditions of non-reflecting absorption of incident radiation are carried out, is the character peculiarity of wave selective absorption in the layer of polar dielectrics. They are individual ones for each substance and dependent on their dielectric static and dynamic characteristics.

The accessibility of dielectric materials makes perspective their use at the formation the cheap microwave absorbing systems on their base with application of simple technology of their preparation. Moreover, for improvement of absorber mechanical strength, they can be prepared from solid-state non-absorbing dielectric material with inclusion of high-

dispersion absorbing solid or capsule liquid dielectric materials in it.

### EXPERIMENT

For the purpose of checking of these statements the experimental investigations of solid state micro-wave radiation absorbers on the base of composition materials are carried out. The solid-state absorber consists of the covering with the liquid phase included in it with dispersion near the given wave range of incident radiation. The covering layer is made from the homogeneous solid-state material, the polar liquid is used in the capacity of absorbing filler, moreover, the concentration of mixture polar component and the covering layer thickness are chosen from the equality condition to zero of coefficient module of wave reflection.

The measurements of reflective characteristics of the investigated objects are carried out with the use of panoramic measurer of standing wave ratio and measuring waveguide cell short-circuited on the edge connected with it. The last one is thermostated and has the device for the smooth regulation of solution layer thickness. The minimum values of  $R_{min}$  are defined on experimentally taken dependences of  $R$  wave reflection coefficient module and  $l$  solution layer thickness in the cell. Simultaneously the quantitative evaluation of dielectric properties of investigated objects with the application of measurement method described in [5] is carried out. This method is based on the definition of  $\epsilon'$  dielectric constant and  $\epsilon''$  dielectric losses of investigation objects on measurement data of standing wave ratio and solution layer thickness in the point of the first minimum of  $R$  on  $l$  dependence. The acetonitrile and epoxide resin are used in the capacity of investigation.

### THE MEASUREMENT RESULTS

The polar liquids having the high values of both  $\epsilon'$  dielectric constants and  $\epsilon''$  dielectric losses are used in the capacity of microwave fillers. For technical realization of similar absorbing coverings the polar liquid can be used in the capacity of filler of any solid-state material. At low volume of such capsulated inclusions, the obtained absorbers could have the necessary constructive liquid and to provide the realization of the total absorption condition of incident radiation in them at definite selection of inclusions.

THE ABSORBING COVERING OF VHF RADIATION

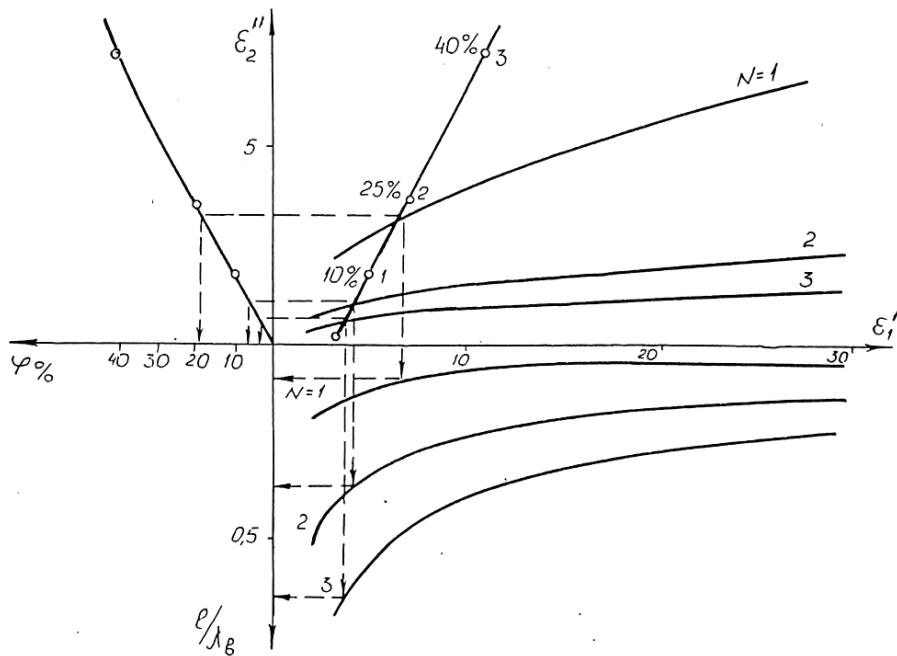


Fig. 1. The electromagnetic radiation absorber on the base of composition materials.

The inclusions themselves are carried in the form of liquid polar substance capsules put in defensive polymer film membranes. As non-polar matrix substance of the absorbers has  $\epsilon'' = 0$  and  $\epsilon'$  doesn't depend on frequency then at the given temperature  $T$  and  $\lambda$  wave length of incident electromagnetic wave, the choice of resonanse values  $\epsilon'_0$  and  $\epsilon''_0$  absorbers is achieved by variation of its liquid phase concentration [6,7].

The measurement results obtained at different concentrations of polar component, the dependence of  $\epsilon''$  dielectric losses on dielectric constant  $\epsilon'$  of marerial covering at the given frequency of incident electromagnetic radiation are shown on the fig.1.

The family of theoretically calculated  $\epsilon''$  on  $\epsilon'$  dependences corrsponding to the case of non-reflecting wave absorption in composition materials are presented here. With the help of the given technique the occurrence of optimal parameters of non-reflecting absorbers of SHV radiation containing the polar liquids in their content and havinf the wave dispersion in corresponding chosen frequency range, is possible.

The realization possibility at given  $T$  and  $\lambda$  electromagnetic radiation absorbers on the base of composition materials containing the high-dispersion capsulated polar liquids is illustrated by the following example. The smallness of liquid capsule dimensions in the comparison with emission wavelength is proposed in them for the comfort of result presentation.

According with data of works [8,9] the conditions of total or non-reflecting electromagnetic radiation absorption in two-layer system dielectric-metal is described by the following equations:

$$\pi(2N-1) + \operatorname{arctg} \frac{2\pi y}{n^2(1+y^2)-1} = \frac{1}{y} \ell n \sqrt{\frac{(1+n)^2 + (ny)^2}{(1-n)^2 + (ny)^2}} \quad (1)$$

$$\frac{\ell_o}{\lambda_o} = \frac{1}{4\pi n} \left[ \pi(2N-1) + \operatorname{arctg} \frac{2\pi y}{n^2(1+n^2)-1} \right] \quad (2)$$

where  $l_o$  is layer thickness,  $N$  is zeroth minimum number of the dependence of wave reflection coefficient on the substance layer thickness.

The wave refaction index  $n$  and dielectric loss factor  $y$  of material covering including into (1) and (2) equations are connected with its  $\epsilon'$ ,  $\epsilon''$  by known relations:

$$\epsilon' = n^2(1-y^2); \epsilon'' = 2n^2y \quad (3)$$

$\epsilon'$  and  $\epsilon''$  values including into (3) equation are connected with  $\epsilon'_1$  dielectric constant and  $\epsilon''_1$  dielectric loss of liquid phase and  $\epsilon_2$  of matrix substance by the equations:

$$\epsilon' = \epsilon'_1(\varphi_o) + \epsilon_2(1-\varphi_o) \quad \epsilon'' = \epsilon''_1 \varphi_o \quad (4)$$

where  $\varphi$  is liquid phase concentration in substance covering.

The joint solution of (1) – (4) equations allows us to calculate the chosen values of liquid phase concentration  $\varphi$  and covering layer thickness  $l_o$  at the given  $N$  values,  $\lambda$  incident radiation wavelength and dielectric coefficients of the used liquid phase  $\epsilon', \epsilon''$  and matrix material.

The realization possibility on the base of polar mixtures at the given electromagnetic radiation absorbers  $\lambda$  and  $T$  is illustrated by the following examples. The results of the calculation of  $\varphi$  and  $l$  by (1) – (4) equations of microwave absorbers at  $\lambda=1,5$  cm formed on the base of epoxide resin introduced in it in the capacity of capsulated acetonitrile filler are given below.

The epoxide resin has the dielectric constant  $\epsilon = 2.7$ . The acetonitrile has  $\epsilon' = 36.8$ ,  $\epsilon'' = 3.64$  at  $\lambda = 1.5$ cm

and  $T = 20^{\circ}\text{C}$  [10,11]. From the joint solution of the equation system (1) – (4) it is followed that the conditions of non-reflecting radiation absorption are carried out at the volume concentration of liquid phase at  $\varphi = 0.077$  and absorber layer thickness  $l = 0.173\text{sm}$  close to  $\lambda_g / 4$  (at  $N=1$ ).

## CONCLUSION

The practical possibility of covering formation on the base of composition materials utilized the residual and

often undesirable electromagnetic radiation which can be used for the defense of living organisms from SHV harmful influence, in location technique and also in other technique regions where the necessity in electromagnetic radiation absorption of the given frequency appears, has been considered in the given work. Besides, the possibility of covering selectivity and sensitivity improvement absorbing the electromagnetic radiation is considered.

- 
- [1] *I. Preissner*. NTZ Arch., 1989, 4, p. 175.
  - [2] *R.M. Kasimov*. Izmeritel'naya tekhnika. 1970, 10, s. 48.
  - [3] *R.M. Kasimov, M.A. Kalafit, E.R. Kasimov, Ch.O. Qajar, E.Yu. Salayev*. JTF, t. 66, №5, 1996, s. 167-171.
  - [4] *R.M. Kasimov, M.A. Kalafit, Ch.O. Qajar*. Fizika, t. 1, №2, 1995, s. 37-44.
  - [5] *R.M. Kasimov*. Metrologiya, 1987, 7, 45.
  - [6] *Mayer Ferdy*. Structures absorbentes hantes fréquences large bande. Patent N2665291, France, 1992.
  - [7] *E.R. Kasimov, S.T. Azizov, R.M. Kasimov, Ch.O. Qajar*. Patent № i 2000 0070, Azerbaijan, 2000 g.
  - [8] *R.M. Kasimov*. Injenerno-fizicheskiy jurnal. Moskva. 1994, t.6, №5-6, s.489.
  - [9] *R.M. Kasimov, M.A. Kalafit, E.R. Kasimov, Ch.O. Qajar*. Injenerno-fizicheskiy jurnal. t. 71, № 2, 1998, s. 282-285.
  - [10] *E.R. Kasimov, S.T. Azizov, R.M. Kasimov, Ch.O. Qajar*. Izvestiya AN Azerbaijana, ser. fiz.-tekhn. i mat. nauk, 1995, t.16, № 5-6, s. 22-29.
  - [11] *Ya.Yu. Akhadov*. Dielektricheskie parametri chistikh jidkostey. M., Izd. MAY, 1999, s. 285.

Received: 17.03.2011

**CONTENTS**

|     |  |    |
|-----|--|----|
| 1.  | Current-voltage (I-V) and capacitance-voltage (C-V) characteristics of $\text{Bi}_4\text{Ti}_3\text{O}_{12}$ amorphous films<br><b>Şemşettin Altindal, Adem Tataroğlu, A.A. Agasiyev, M.Z. Mamedov, E.M. Magerramov, J.G. Jabbarov, Kh.O. Qafarova</b>                                   | 3  |
| 2.  | Picosecond distributed feedback dye laser excited with diode-pumped solid-state micro laser<br><b>T.Sh. Efendiev, V.M. Katarkevich, Ch.O. Qajar, R.A. Karamaliyev</b>  | 7  |
| 3.  | Luminescent properties of $(\text{Ba},\text{Ca})\text{Ga}_2(\text{S},\text{Se})_4$ chalcogenide semiconductors doped with rare earths<br><b>V.Z. Zubialevich, E.V. Lutsenko, M.S. Leanenia, E.V. Muravitskaya, G.P. Yablonskii, A.M. Pashaev, B.G. Tagiev, O.B. Tagiev, S.A. Abushov</b> | 11 |
| 4.  | $SU(3)_C \times SU(3)_L \times U(1)_X$ model of electroweak interaction and electric charge quantization<br><b>O.B. Abdinov, F.T. Khalil - zade, S.S. Rzaeva</b>   | 20 |
| 5.  | Growth InGaN diode structure and double emission $(\text{Ca}_{1+x-y}\text{Eu}_y)\text{Ga}_2\text{S}_{4+x}$ phosphor for white LEDs<br><b>R. Jabbarov, N. Musayeva, S. Abdullayeva, F. Scholz, T. Wunderer, P. Benalloul, C. Barthou, C. Laurent</b>                                      | 28 |
| 6.  | Dispersion of optical parameters of $\text{YbBi}_2\text{Te}_4$ and $\text{YbBi}_4\text{Se}_7$<br><b>M.A. Makhmudova, N.Z. Jalilov</b>  | 32 |
| 7.  | Spatial structure of neuropeptide allatostatin-4<br><b>L.I. Veliyeva, E.Z. Aliyev</b>  | 36 |
| 8.  | Investigation of clark-lagerwall effect in the small particles - liquid crystal system<br><b>T.D. Ibragimov, G.M. Bayramov, A.R. Imamaliev</b>   | 42 |
| 9.  | Electronic band structure of $\text{TlFeSe}_2$ in ferromagnetic phase<br><b>Z.A. Jahangirli, K. Mimura, K. Wakita, Y. Shim, G.S. Orudzhev, N.T. Mamedov</b>  | 48 |
| 10. | Effect of the light on charge carriers mobility in gallium monoselenide crystals<br><b>A.Sh. Abdinov, R.F. Babayeva, R.M. Rzayev</b>   | 51 |
| 11. | Theoretical investigation of vibrational frequencies and molecular structure of some $[\text{M}(\text{Cl})_6]^{2-}$ ions<br><b>Gürkan Keşan and Cemal Parlak</b>   | 57 |
| 12. | The crystal structure of $\text{Ga}_{0.83}\text{In}_{0.83}\text{Fe}_{0.34}\text{S}_3$<br><b>J. Hasani Barbaran, G.G. Guseinov, R.B. Veliyev, A.B. Magerramov</b>   | 63 |
| 13. | A microscopic theory of spin excitations in a rectangular ferromagnetic nanowires<br><b>V.A. Tanrıverdiyev, V.S. Tagiyev</b>   | 67 |
| 14. | Forbidden rotational transitions of trans-conformer of molecule $\text{CH}_3\text{CH}_2\text{OH}$<br><b>S.B. Kazimova, A.S. Gasanova, E.Ch. Saidov</b>   | 71 |
| 15. | IR-spectroscopic investigation of high-siliceous zeolite - klynoptilolit<br><b>T.Z. Kuliyeva, E.A. Agayeva, G.M. Eyvazova, N.N. Lebedeva</b>   | 75 |
| 16. | To fractal geometry of nanoobjects on Van der Waals surface in $A_2^VB_3^{VI}$ system<br><b>F.K. Aleskerov, K.Sh. Kakhramanov, A.Sh. Kakhramanov</b>   | 77 |
| 17. | Selenium optical spectra obtained under different conditions (part II)<br><b>N.Z. Jalilov</b>  | 80 |
| 18. | The annealing influence on spectra of optical parameters of $\text{Bi}_2\text{Te}_3$ - $\text{Bi}_2\text{Se}_3$ film samples in 1÷6 eV range<br><b>N.Z. Jalilov, G.M. Damirov</b>  | 85 |
| 19. | The absorbing covering of VHF radiation<br><b>S.T. Azizov</b>  | 88 |



[www.physics.gov.az](http://www.physics.gov.az)